Politecnico di Milano

Dipartimento di Chimica, Materiali e Ingegneria Chimica "Giulio Natta"

A proposal of AC corrosion mechanism of carbon steel in cathodic protection condition

Andrea Brenna

Supervisor and Tutor: Prof. Luciano Lazzari

Coordinator: Prof. Chiara Castiglioni

Ph.D. Thesis in Materials Engineering – XXIV Course

2009 – 2011

Content

Preface

Buried pipelines used to transport hydrocarbons and dangerous fluids are provided with corrosion prevention systems, consisting of an insulating coating and a cathodic protection (CP) system. CP reduces (or halts) corrosion rate so that corrosion damage cannot occur during the designed lifetime of the structure. The presence of stray currents interference (DC or AC) may cause serious corrosion damages on a metallic structure, even under CP condition. While for DC interference there is large agreement on protection criteria for corrosion mitigation and international standards are available, AC induced corrosion represents a controversial subject and several aspects should be clarified.
AC interference can occur when a buried metallic pipe runs parallel to an interference source, as high-voltage transmission lines (HVTL) and AC traction systems, typically fed by a high voltage line at 50 or 16.7 Hz frequency. AC interference can take place by a conduction or induction mechanism and cause corrosion of the pipeline corresponding to coating defects, due to high local AC densities. Uncertainties still exist on CP criteria in the presence of AC interference and on the mechanism by which AC causes corrosion of carbon steel in CP condition.

This work is part of a two-phases project started in 2002 in the research group PoliLaPP ("Laboratorio di Corrosione dei Materiali Pietro Pedeferri") of Dipartimento di Chimica, Materiali e Ingegneria Chimica "Giulio Natta" of Politecnico di Milano. The research project deals primarily with the study of the effects of AC interference on steel in free corrosion and CP condition.
The first phase of the experimental research was initially granted by MIUR (Italian Ministry of School, University and Research); then, from June 2006, research activities were sponsored by Italian companies. During this phase, the influence of the simultaneous presence of AC and DC on steel corrosion in different environments was studied by means of a proper electrical circuit designed in order to measure and to apply separately the DC and AC signal.
The effects of AC interference on kinetics parameters (anodic and cathodic polarization curves) and on corrosion rate were widely investigated in various environments (e.g. soil-simulating solution, artificial sea water) for different metals (as carbon steel, galvanized steel, zinc and copper) varying interference conditions. Experimental tests showed that AC has a strong influence on corrosion kinetics (anodic and cathodic overpotentials) and on corrosion and equilibrium potential. A general decrease of both anodic and cathodic overpotentials and an increase of exchange current density were observed.
As regards AC corrosion of steel in CP condition, laboratory tests were carried out varying protection and interference conditions, in order to determine AC corrosion critical parameters and to assess CP criteria in the presence of AC interference. Actually, the research group is cooperating in the European Technical Committee CEN/TC 219 "Cathodic protection" in order to draw up a revised form of the Technical Specification (CEN/TS) on the evaluation of AC corrosion likelihood of cathodically protected buried pipelines, especially regarding protection criteria assessment, the identification of AC corrosion main influencing parameters and the monitoring of protection conditions.

This work is part of the second phase of the project (currently ongoing) which aims to propose a corrosion mechanism of cathodically protected carbon steel in the presence of AC interference, also on the basis of the experimental results obtained during the first phase of the research.

Different AC corrosion mechanisms of carbon steel in free corrosion as well as in CP condition have been proposed, although no one is able to fully explain the phenomenon. This doctoral thesis discusses a proposal of AC corrosion mechanism of carbon steel in CP condition. The hypothesized model represents an absolute novelty in the AC corrosion mechanism description. Electrochemical tests were carried out on carbon steel in simulated soil condition varying protection and interference conditions. Moreover, the effect of AC on protection potential and protection current and AC corrosion propagation were investigated.

This work refers to three years Ph.D. activities. Experimental tests were carried out in the laboratories of the research group PoliLaPP of Politecnico di Milano and, during an internship period of four months, in collaboration with the AC corrosion group of the Metallurgical and Materials Engineering Department of Colorado School of Mines (Golden, CO, USA).
The first part of the thesis (Chapter 1) provides a state of the art on AC corrosion characteristics and a wide description of the corrosion mechanisms proposed in literature for carbon steel in free corrosion as well as in CP condition. Chapter 2 reports a description of the experimental test conditions.
In the last part of the thesis, results are discussed as follows:

- Chapter 3 deals with the study of the effect of AC interference on protection potential and protection current density;
- Chapter 4 provides the description of the proposed AC corrosion mechanism;
- Chapter 5 discusses AC corrosion propagation on cathodically protected carbon steel and describes AC corrosion morphology. AC effect on magnesium anodic consumption is also discussed.

AC corrosion
State of the Art

Corrosion by alternating current (AC) of pipelines in cathodic protection (CP) condition is not well understood, despite discussion about it dates back to the late 19th century. Nowadays, there is agreement that at commercial AC frequencies (50 or 60 Hz) corrosion is possible, even on pipelines in CP condition and that AC corrosion is less than that caused by the equivalent direct current (DC). In the past 30 years, AC corrosion has become recognized as a threat to the integrity of underground structures, especially buried pipelines which share the way with high-tension electrical lines. The late 'wake-up' of the industry is due to factors as the following [1]: (1) the growing number of high-voltage transmission lines, (2) more applications using high-voltage power lines, as the high-speed railway in Europe, (3) the use of high-quality coatings that allows to increase the insulation conditions of the metal but results in high AC densities at the coating faults along the pipeline, and (4) poor or no awareness and knowledge of the phenomenon by pipeline operators. For these reasons, some aspects of AC corrosion are still under study.
Before discussing AC corrosion characteristics, a background of CP principles is presented. This overview is not exhaustive but recalls the main concepts about CP that could be helpful to understand the following discussion.

1.1 CATHODIC PROTECTION BACKGROUND [2]

CP is an electrochemical method of corrosion prevention and protection which can be applied to metals exposed to conductive environments. As shown in Figure 1.1, this technique is based on the circulation of a DC between an electrode (anode) placed in the environment and the metallic structure (cathode). The cathodic current lowers the potential of the metal and reduces (or halts) its corrosion rate.

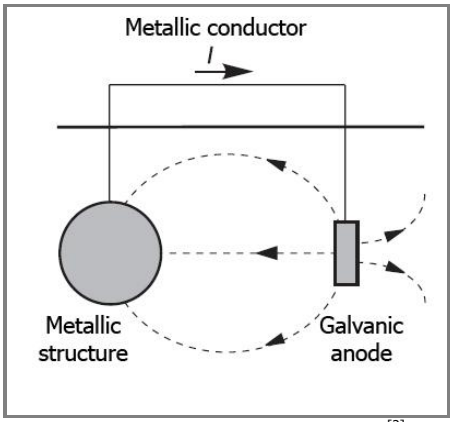

Figure 1.1*a* – CP by galvanic anode [2]

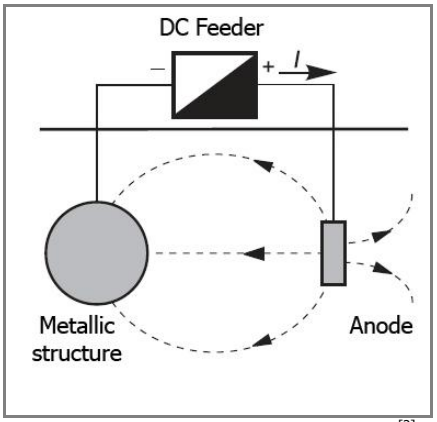

Figure 1.1*b* – CP by impressed currents [2]

The circulating current is obtained either by galvanic anodes (also called sacrificial anodes) or by an impressed current system. In the first case, CP is achieved through the galvanic coupling with a less noble metal (Figure 1.1*a*). Aluminium and zinc are used for steel protection in sea water while magnesium is employed in soil and fresh water; pure iron is usually used for stainless steel and copper alloys protection. The impressed current system makes use of a DC feeder (Figure 1.1*b*), with the positive pole connected to the anode, generally an insoluble metal (for example graphite, activated titanium) and the negative pole connected to the structure. CP is commonly applied to structures exposed to natural environments by means of both systems. Galvanic anodes are typically used in high conductivity environments (as sea water) and when a low current is required even in environments with low conductivity, as soil and concrete. Impressed current systems are adopted in high resistivity environments, typically soil and concrete, and are preferred when extended structures must be protected, due to the higher flexibility in the current supply.

1.1.1 The equilibrium potential

A metal (M) in an electrolyte is in equilibrium with its ions in accordance with the reaction:

(Eq. 1.1) $M = M^{z+} + ze^{-}$

The equilibrium potential (E_{eq}) is given by Nernst's equation:

(Eq. 1.2) $$E_{eq} = E_0 + K \cdot \mathrm{Log}\left(\frac{a_{M^{z+}}}{a_M}\right)$$

where E_0 is the metal standard potential, K is a constant, $a_M{}^{z+}$ is the metallic ions activity and a_M is the metal activity in the electrolyte. The reaction in Eq. 1.1 proceeds towards the right (anodic process) depending on the metal's potential (E) compared to E_{eq}:

- if $E > E_{eq}$, the metal dissolves (anodic behavior);
- if $E < E_{eq}$, the metallic ions deposit (cathodic behavior).

Potential moves from equilibrium when a current is exchanged between the metal and the electrolyte (electrons must be taken from or supplied to the metal). The relationship between potential (E) and current density (i) is described by the Butler-Volmer equation:

(Eq. 1.3) $$i = i_0\left\{\exp\left[\frac{(1-\alpha)\cdot zF}{RT}(E - E_{eq})\right] - \exp\left[-\frac{\alpha zF}{RT}(E - E_{eq})\right]\right\}$$

where i_0 is the exchange current density, T is the absolute temperature, z is the number of electrons involved in the reaction, F is the Faraday constant (96,500 C/mol), R is the universal gas constant (8.314 J/mol·K) and α is the so-called charge transfer coefficient. The difference ($E - E_{eq}$) is usually defined as the driving voltage and measures the metal's tendency to oxidize: a metal can corrode only if its potential is higher than the equilibrium potential. This may happen when a cathodic process has an equilibrium potential more noble than the metal equilibrium potential or by means of an external current source that takes electrons from the metal: this is the case of stray currents interference.

Generally, a corrosion reaction is the result of two semi-reactions: the oxidation reaction (anodic process) that releases electrons and the reduction reaction (cathodic process) that consumes electrons. For carbon steel, corrosion semi-reactions are:

(Eq. 1.4) $Fe = Fe^{2+} + 2e^{-}$ anodic process

(Eq. 1.5*a*) $2H^+ + 2e^- = H_2$ cathodic process in acid environment

(Eq. 1.5*b*) $O_2 + H_2O + 2e^- = 2OH^-$ cathodic process in neutral or alkaline environment

The number of electrons consumed (cathodic current, I_c) and produced (anodic current, I_a) is necessarily the same ($I_c = I_a$) and equal to the corrosion current (I_{corr}). The potential of the metal in free corrosion condition (E_{corr}) is obtained by plotting anodic and cathodic curves (Evans' diagram) and is given by their intersection point.

1.1.2 The protection potential

CP effectiveness depends on two distinct effects of the potential lowering: a *thermodynamic effect* which reduces (or brings to zero) the corrosion driving voltage, and a *kinetic effect* that depends on the increase of reaction resistances.
If the metal potential is below the equilibrium potential ($E < E_{eq}$), the anodic process cannot take place and, if metallic ions are present, they are reduced to metal. This condition is called *thermodynamic immunity*, i.e. the driving voltage is zero or negative. When potential lowering is not sufficient to set to zero the driving voltage (i.e., $E_{corr} > E > E_{eq}$), *quasi-immunity* condition is established and the potential is brought to values close enough to the equilibrium potential to make corrosion rate negligible or acceptable. Carbon steel structures in soil with potentials below -0.850 V CSE[1] (or -0.950 V CSE in the presence of sulphate reducing bacteria) operate in protection condition [2, 3]. As mentioned before, the potential lowering can increase the anodic resistance for active-passive metals, as in the case of stainless steels in pitting corrosion condition (protection by passivity).

1.1.3 The protection current density

In order to apply CP, an adequate current must be supply to the structure. This current is determined by the so-called *protection current density* (i_{CP}), which depends on cathodic processes that take place on the metal surface. With reference to Figure 1.2, if I_e is the current supplied to the structure by an anode, all electrons provided by the external current and by the anodic process (I_a), are consumed by the cathodic process (I_c). Accordingly, the potential of the metal is brought to the value that verifies the following equilibrium (Kirchhoff's law):

(Eq. 1.6) $I_e = I_c - I_a$

The external current (I_e), which sets to zero the anodic process ($I_a = 0$), is called *protection current.* Cathodic processes are typically oxygen reduction and hydrogen evolution, depending on the environment and on corrosion potential (E_{corr}). For carbon steel in the presence of oxygen (Figure 1.2*a*), the cathodic current is fixed to a limiting value determined by the amount of oxygen that reaches steel surface through diffusion process. This current (referred to a unit area) is called *oxygen limiting diffusion current density* (i_L) and depends on oxygen content, local turbulence, temperature and on the presence of scaling. Protection current density in soil varies from about 1 mA/m^2 in clayey soils, where oxygen is almost absent, to 150 mA/m^2 in sandy soils which are well aerated [2]. When potential is lower than hydrogen equilibrium potential, hydrogen evolution adds to oxygen reduction and the cathodic current density increases by decreasing potential.

[1] CSE, copper-copper sulphate electrode, +0.318 V SHE

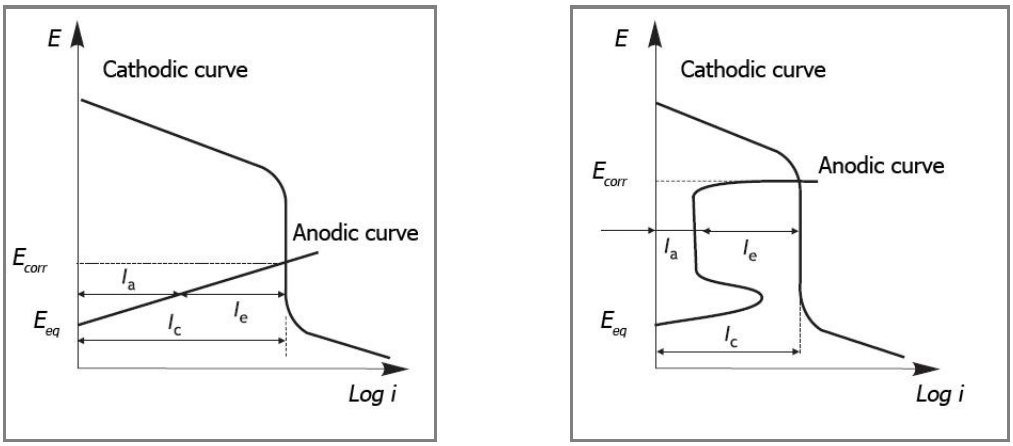

Figure 1.2 – CP electrochemical conditions for: a) an active material and b) a passive material [2]

1.1.4 Coating and scaling

In the presence of an insulating coating, the protection current becomes a small percentage of that required by a bare structure, since only uncoated areas as pores, defects and faults of the coating must be protected. Accordingly, the protection current density (i_{CP}) of a coated structure is proportional to the fraction of uncoated surface, through the relationship:

(Eq. 1.7) $$i_{CP} = i_B(1-\varepsilon)$$

where i_B is protection current density of the bare metal structure and ε is coating efficiency, defined as the unitary fraction of covered area. Coating efficiency changes with time: for a buried pipeline, it may change from 99.99% at installation to 90% after 10-20 years.
In sea water, the cathodic current causes the growth of a mix of calcium carbonate and magnesium hydroxide scale, commonly known as *calcareous deposit* which is particularly beneficial because reduces the protection current by acting as a barrier that limits oxygen diffusion and maintains alkalinity at the metal surface.
The protective behavior of deposits depends on sea water composition, current density and mechanical action (abrasion and vibration) that determine thickness, porosity and adherence of the scale. Once protection is interrupted, the calcareous deposit starts to dissolve.

1.1.5 Cathodic protection monitoring

CP criteria are generally based on the value of the structure-to-electrolyte potential. Potential measurement is therefore necessary in order to assess CP effectiveness [4].
The potential of a buried structure should be measured using a reference electrode placed in the immediate vicinity of the bare metal of the structure (e.g. corresponding to a coating defect) and a high impedance voltmeter whose positive pole is connected to the structure and its negative one to the reference electrode.
Since in most cases it's not possible to place the reference electrode so close to the structure (location 1 in Figure 1.3), the potential is measured by a reference electrode positioned far from the structure (location 2 in Figure 1.3). Nevertheless, in the presence of currents in the soil the potential measured at location 2 differs from the potential measured at location 1. The difference between the two potential measurements is equal to the algebraic sum of the ohmic voltage drops (IR drops) in the soil between the two positions (1 and 2).

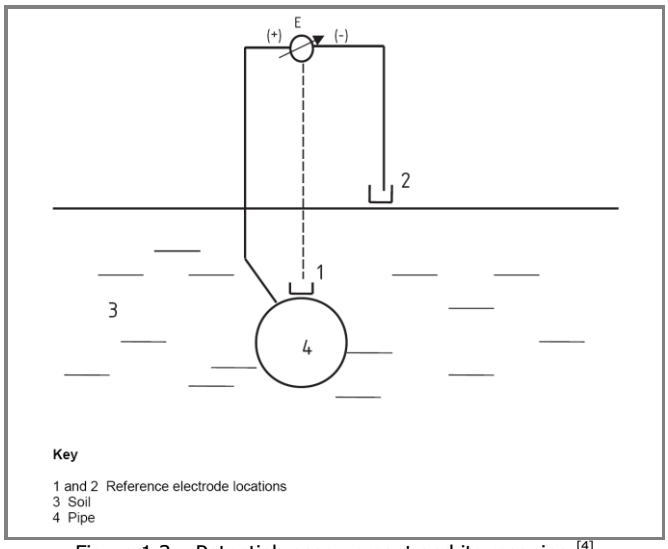

Figure 1.3 – Potential measurement and its meaning [4]

Generally, the measured potential (E) is the sum of three contributions [2]:

(Eq. 1.8) $E = E_{eq} + \eta + IR$

where E_{eq} is equilibrium potential with respect the reference electrode used, η is the overpotential contribution with respect to the equilibrium potential and IR is the ohmic drop in the electrolyte, that depends on the reference electrode and metal distance, environment resistivity and the circulating current (second Ohm's law). The sum (E_{eq} + η) is called true potential, also indicated as IR-free potential.
In the presence of protection currents in the soil, the potential measured at location 2 is generally more negative than the potential measured at location 1 due to the IR drop contribution. In the presence of DC stray currents, the potential measured at location 2 may be either more negative or more positive than the potential at location 1, according to the sense of currents.
The ohmic contribution (IR in Eq. 1.8) contaminates the potential measurement. It decreases when the reference electrode is placed close to the pipeline and, therefore, the simplest technique to minimize IR drop consists in placing the reference electrode as close as possible to the structure. Of the three parameters determining ohmic drop (resistivity, current and distance), resistivity plays the most important role. Potential is more negative than the true potential when stray current is cathodic and more positive when stray current is anodic; as a result, cathodic or anodic interference may indicate overprotection or severe corrosion, respectively. For a correct potential measurement, ohmic drop must be evaluated or eliminated by means of suitable techniques [2, 4] available but not discussed in this work.

1.2 ELECTRIC INTERFERENCE

Corrosion due to DC or AC interference could cause severe damage on buried structures, even in CP condition. As a general definition, interference is any alteration of the electric field caused by a foreign structure. If the foreign body is a conductor, the current is intercepted; if it is an insulator, the current is withdrawn. In both cases, there is a redistribution of current and potential lines within the electrolyte.

1.2.1 Stationary and non-stationary interference

Interference can be stationary or non-stationary [2]. *Stationary interference* occurs when the structure is immersed in a stationary electric field generated, for instance, by a CP system, and the effect is great if the structure is close to the groundbed. Figure 1.4 reports two general cases of DC stationary interference. In the first case (Figure 1.4*a*), the interfered pipeline crosses the protected one. The zone close to the groundbed tends to gather current from the soil, which is released at the crossing point causing corrosion. In the second case (Figure 1.4*b*), the two pipelines are parallel and the current is released more extensively, typically in zones in contact with low resistivity soil. In both cases, if the interfered structure is provided with an integral coating, interference cannot take place, but when the coating has faults, corrosion could be very severe since current concentrates in them.

Non-stationary interference takes place when the electric field is variable, as in the typical case of stray currents dispersed by traction systems, illustrated in Figure 1.5 in the case of a DC traction system. Interference takes place only during the transit of the train in the anodic zone corresponding to the substation and, in spite of the limited duration, the effects may be severe due to the high circulating current.

Electric interference could be due to DC or AC stray currents. While for DC interference corrosion there is large agreement on protection criteria for corrosion mitigation and international standards are available for several years [5-7], AC induced corrosion represents a controversial subject and many aspects need to be clarified, especially with respect to the mechanism by which AC causes corrosion of carbon steel in CP condition. An extensive discussion about the criteria of DC interference acceptance and corrosion prevention is provided in [2] and is not reported here.

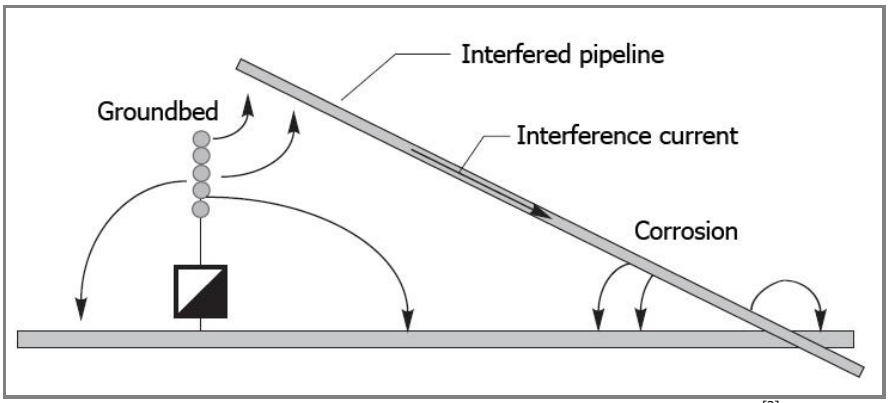

Figure 1.4*a* – Stationary interference between two crossing pipelines [2]

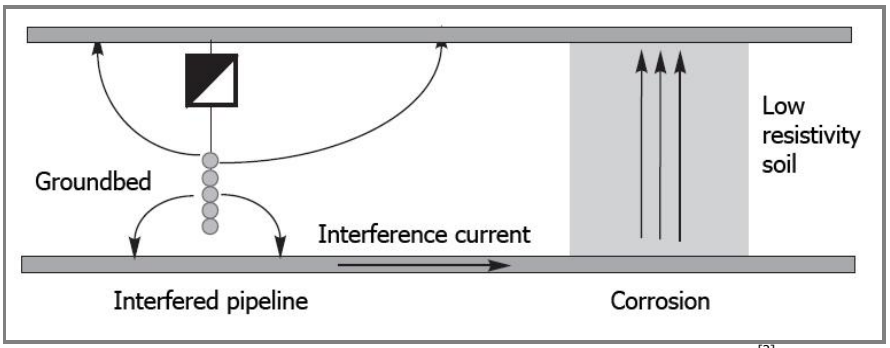

Figure 1.4*b* – Stationary interference between two parallel pipelines [2]

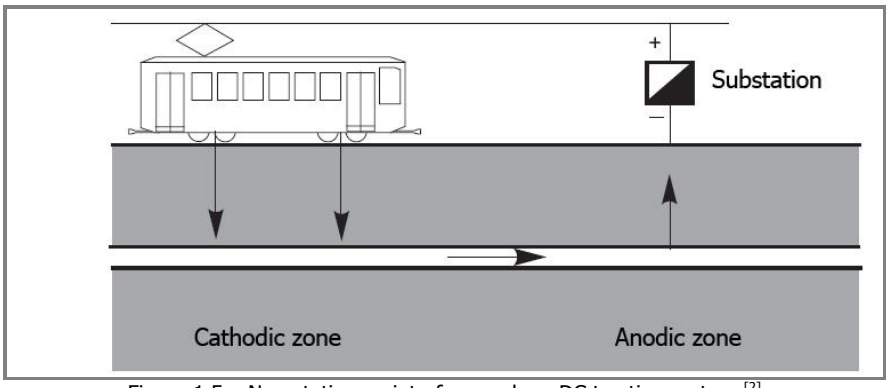

Figure 1.5 – Non-stationary interference by a DC traction system [2]

1.3 AC INTERFERENCE

Generally, electric interference requires the existence of a source of disturbance, a coupling mechanism and a receptor. In the case of AC interference, the source of disturbance is the power line, the receptor is the metallic structure (as a pipeline) and the coupling between the power line and the pipeline occurs by a capacitive, resistive or an inductive mechanism [1, 2]. Typically, AC interference sources are high-voltage overhead or underground power lines and AC traction systems (usually fed by a parallel high voltage line at 50 Hz or 16.7 Hz). AC interfering sources are described in further details in Paragraph 1.3.1. The increased number of AC corrosion-related failures is associated to the parallelism between buried pipelines and AC high voltage transmission lines which use the same right of way. The severity of interference is directly related to the pipeline's electrically continuous length that runs parallel to the source and to its external insulation from ground.

1.3.1 AC interference sources

The main AC interference sources are high-voltage transmission lines (HVTL) and AC traction systems.

1.3.1.1 High-voltage transmission lines

HVTL are used to transmit electric power over relatively long distances, usually from a central station to substations. They are also used for electric power transmission from one central station to another for load sharing. HVTL are made of high voltage (between 138 and 765 kV) overhead or underground conducting lines of either copper or aluminium. A transmission line can refer either to a single cable carrying electricity over a transmission system, or to the physical path that distributes electricity from producer to consumer. However, a distribution line is normally considered as a line that carries less than 69 kV and is used to distribute power from HVTL to end-use customers. Transmission lines, when interconnected each other, become the high voltage transmission network. The electric power distribution circuit is usually represented as two wires that bring electricity to users. In AC circuits, the two wires take turns with the frequency of the applied AC voltage.
Transmission lines mostly use a three-phase AC system, although single phase AC is sometimes used in railway electrification systems. High-voltage DC line is used only for very long distances (typically greater than 400 miles, or 600 km), for submarine power cables (typically longer than 30 miles, or 50 km) or to connect two non-synchronized AC networks. Electrical power is transmitted at high voltages to reduce energy lost in long distance transmission, through overhead power lines (Figure 1.6). High-voltage overhead conductors are not covered by insulator.

Figure 1.6 – Example of HVTL

Figure 1.7 – Italian high-speed railway [8]

The conductor material is usually an aluminum alloy, reinforced with steel strands. Copper is sometimes used for overhead transmission but aluminum is lower in weight and cost. Voltages of 66 kV and 33 kV are usually considered subtransmission voltages but are occasionally used on long lines with light loads. Voltages less than 33 kV are usually used for distribution. Voltages above 230 kV are considered extra high voltage and require different design compared to equipment used at lower voltages to maintain safety requirement. Transmission substations decrease the voltage of incoming electricity by means of voltage transformers, allowing the connection of HVTL and the lower voltage distribution network. Finally, at the point of use, the energy is transformed to low voltage (varying by country and customer requirements).

1.3.1.2 AC high-speed railway lines

There is a wide variety of electric traction systems around the world, which have been built according to the type of railway, its location and the available technology at the time of installation. Electric railway network can use either alternating or direct current. AC systems always use overhead wires; DC systems can use either an overhead wire or a third rail. The contact between the traction system and the power supply is guaranteed by a pantograph; the return circuit to the electric substation is given by the rails, connected to the substation. AC power transmission system along the line is used mainly for long distance; DC, on the other hand, is the preferred option for shorter lines, urban systems and tramways. It is easier to increase AC voltage than DC voltage, so it is easier to supply more power with an AC power system. The 25 kV AC railway electrification system is commonly used in railways worldwide, especially on high-speed lines. The choice of 25 kV is related to the efficiency of power transmission as a function of voltage and cost. A 25 kV AC system uses only one phase of the normal three-phases power supply. Electric power from a generating station is transmitted by overhead high voltage lines to substations, where a transformer lowers the voltage to 25 kV which has become an international standard.
The Italian high-speed railway (Rete Alta Velocità - Alta Capacità (AV/AC), RFI – Rete Ferroviaria Italiana, Gruppo Ferrovie dello Stato Italiane Spa [8], Figure 1.7) uses in non-urban sections a single-phase 25 kV AC electrification system at 50 Hz frequency. This system is innovative compared to 3 kV DC system used in the railway network and is the most used in Europe for high-speed/high-capacity lines. The power system is connected directly to the national grid at 380 kV and adopts the ring system that provides both efficacy and safety. In this system, power substations are connected each other with the first and the last substation connected to two central national grids at 380 kV by means of transformers that reduce the voltage to 150 or 132 kV (depending on the Italian geographic area). Electrical substations reduce AC voltage by means of transformers with the primary at 150 or 132 kV and the

secondary connected to two terminals at +25 kV (contact line) and -25 kV (feeder). The resulting system is the so-called 2x25 kV–50 Hz AC electrical system.
As mentioned before, in the case of AC interference, the coupling between the power line and the pipeline can occur by a capacitive, resistive or an inductive mechanism [1, 2, 9-11].

1.3.2 Capacitive coupling

The capacitive coupling is due to the influence of two or more circuits upon one another, through a dielectric medium as air, by means of the electric field acting between them [9]. The electric field associated with power conductors causes a current flow between a nearby aboveground metallic structure and earth. Since the capacitance between the pipeline and earth is negligible, the electric field normally doesn't induce an AC voltage on buried pipelines, even when dielectric coatings are used, but only on aboveground sections of the pipeline. The magnitude of the total stray current is a function of the size of the structure, its proximity to power conductors, the voltage of power conductors and their geometrical arrangement.

1.3.3 Resistive coupling

The resistive coupling is due to the influence of two or more circuits on one another by means of conductive paths (metallic, semi-conductive, or electrolytic) between the circuits [9]. This is the case of grounded structures of an AC power system that share the earth with other buried structures. Coupling effects may transfer AC to a metallic buried structure in the form of alternating current or voltage.
Whenever a grounded power system has unbalanced condition, current may flow to the earth. Indeed, resistive coupling is primarily a concern during a short-circuit condition on an AC power system, for instance when a large part of the current in a power conductor flows to the earth by means of foundations and grounding system of a tower or a substation. The current flow raises the electric potential of the earth near the structure, often to thousands of Volts with respect to remote earth, and can result in a considerable AC voltage across the coating of a metallic structure, as a pipeline. This can damage the coating, or even the structure itself. The potential difference between the earth and the structure can represent an electric shock hazard. Under some circumstances, the electric potential of the structure may be raised enough to transfer hazardous voltages over considerable distances, particularly if the structure is well coated. Resistive coupling effects are strongly dependent on a large number of factors, as the total short-circuit current, the power line overhead ground wire type, the size of foundations and grounding systems of towers or substations, the electrical resistivity of the soil as a function of depth and the distance between the power system and the affected metallic structure.
Lightning strikes to the power system can also initiate fault current conditions [9]. Lightning strikes to a structure or to earth in the vicinity of a structure can produce electrical effects similar to those caused by AC fault currents. If a lightning strike occurs between the tower structure and an overhead cloud, the potential of the tower could be raised to an extremely high voltage, with a current flow from the tower structure to the earth. The current flows to the earth through the grounding system and spreads uniformly through the earth (assuming a homogenous soil resistivity) in all radial directions. Therefore, the ground around the pipeline will be at a relatively high potential with respect to the pipeline potential and this could result in the coating damage. Fault currents can create a hole in the coating or can enlarge it by removing the previously adherent coating due to heating effect.

1.3.4 Inductive coupling

The inductive coupling is due to the influence of two or more circuits upon one another by means of the magnetic flux that links them [9]. AC flow in a power conductor produces an

alternating magnetic field around it which induces an AC in the coated pipeline, i.e. the power line and the pipeline behave as two coils of an auto-transformer. The current flow in the conductor creates an electromagnetic field which lies at right angles to the current that produces it. The magnetic field expands away from the conductor and then collapses towards the metallic structure.
If a pipeline is close enough and parallel to the electrical transmission line, the magnetic field will cross the pipeline with the induction of an AC voltage on the pipeline (Figure 1.8). In the case of a three-phases AC system where the current magnitudes in the three phases are equal and the three overhead conductors are equally distant from the axis of the pipeline, no voltage will be induced on the pipeline. However, the more frequently configuration (in which there is no symmetry between the three-phases conductors and the pipeline) will result in a measurable induced AC voltage [11] (Figure 1.9).
In conclusion, in the case of a buried pipeline, inductive and resistive coupling must be considered.

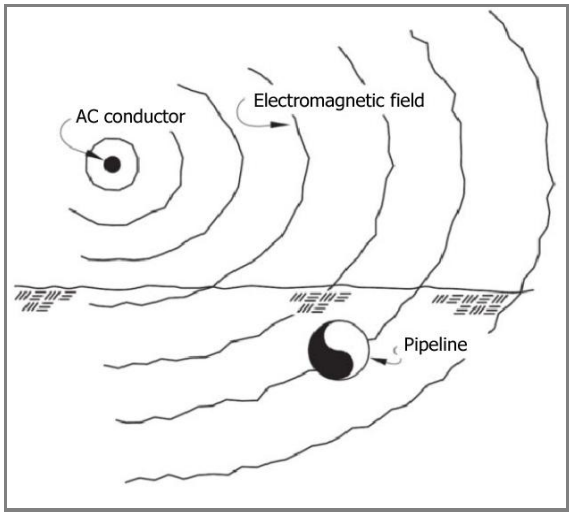

Figure 1.8 – Inductive coupling between an AC conductor and a buried pipeline [11]

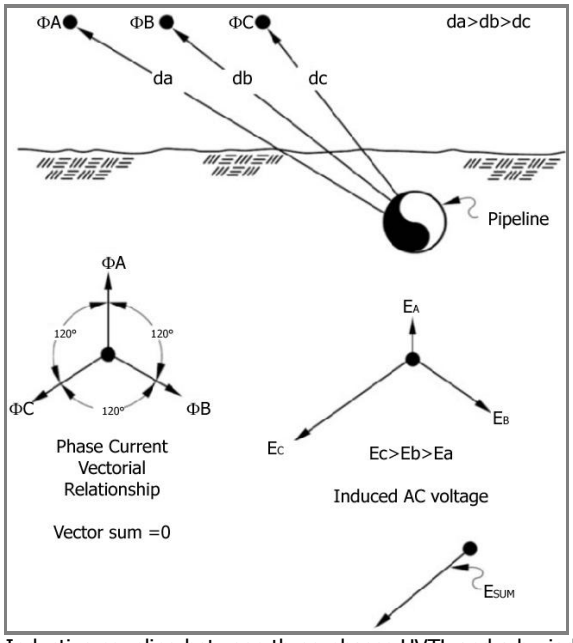

Figure 1.9 – Inductive coupling between three-phases HVTL and a buried pipeline [11]

1.4 CHARACTERISTICS OF AC CORROSION

As discussed before, a buried pipeline which shares a common path with AC transmission lines may be interfered by magnetic and electric fields generated by the power system (interference source). In the presence of AC interference, corrosion of the pipeline can occur.
The technical specification CEN/TS 15280:2006 [12] (currently under review) reports that factors which mainly influence AC corrosion phenomena are:

- induced alternating voltage;
- AC density on the exposed metal;
- DC polarization level;
- size of coating faults;
- local soil resistivity;
- local soil chemical composition.

A brief description of AC corrosion characteristics is reported below. Part of the discussion refers to the technical committee report "AC corrosion State-of-the-Art: Corrosion Rate, Mechanism, and Mitigation Requirements" [13] prepared in January 2010 by NACE International Task Group 327. NACE International (NACE, National Association of Corrosion Engineers) is the leader in the corrosion engineering and is recognized around the world as the premier authority for corrosion control solutions.
As mentioned in the preface, this work is part of a research project carried out by the group PoliLaPP ("Laboratorio di Corrosione dei Materiali Pietro Pedeferri") of Politecnico di Milano on the study of AC effects on metals corrosion, even in CP condition. The research group has participated to the preparation of the aforementioned report published by NACE International.

1.4.1 Alternating voltage (AV)

The technical specification CEN/TS 15280:2006 [12] reports alternating voltage (AV) of an interfered structure as the most important parameter to take into account in order to evaluate AC corrosion likelihood. AV can either be calculated or directly measured on the structure itself. AV measurement should be performed on pipelines or sections of them where unacceptable AC interference is suspected (or may be expected) based on map observation, calculation, or routine measurements.
AV measurement should be performed in a first instance on all test points, CP control stations, insulating joints, wherever an accessible measuring cable is connected to the pipeline. At a later stage, these measurements may be restricted to a few particular positions, chosen along the most influenced areas. For routine measurements, short duration AV measurements are sufficient and are carried out by means of a high impedance AC voltmeter between the metal structure and the reference electrode placed over the pipe; for a more correct measurement, the electrode should be located at the remote earth. For long-term evaluation, a data recorder instead of a voltmeter should be used.
The technical specification CEN/TS 15280:2006 [12] reports that, in order to reduce AC corrosion likelihood, the pipeline AV should not exceed at any time:

- 10 V where the local soil resistivity is greater than 25 Ω·m;
- 4 V where the local soil resistivity is lower than 25 Ω·m.

These values should be considered as threshold limits which significantly reduce AC corrosion likelihood. It should be pointed out that these values are based on long term practical experience of European operators and not on a scientific approach.
At present in the U.S., AV threshold is mostly driven by safety considerations. The standard NACE SP0177-2007 [9] reports that AV on structures must be reduced and maintained at safe levels to prevent shock hazards to personnel. The shock hazard degree depends on several factors, as the voltage level and duration of human exposure, human body and skin conditions, and the path and magnitude of any current conducted by human body. The U.S.

standard [9] reports that a steady-state touch AV of 15 V or more with respect to local earth constitutes a shock hazard. AV measurements should be compared with the threshold limits specified above. These AV limits are sometimes considered too restrictive for pipelines parallel to 50 or 60 Hz overhead HVTL without a corrosion failures history. Furthermore, the assessment of AC corrosion threat only on the basis of AV may be misleading and different factors, as AC density, the ratio between AC and DC densities, metal IR-free potential should take into account to define corrosion likelihood.

1.4.2 AC density

AC corrosion of steel is lower than DC corrosion, being in the range between 0.1 and 5% with respect to corrosion caused by the same amount of DC, as reported for instance by Pookote and Chin as from 1978 [14]. By laboratory test results on carbon steel in soil-simulating solution, Goidanich et al. [15] reported that AC corrosion is lower than 4% with respect to DC corrosion and decreases by increasing AC density.
Although several authors report the existence of a critical AC density threshold below which AC corrosion doesn't occur, the magnitude of this critical value is debated and large data variability can be found depending on interference condition and environment. In 1986, a corrosion failure on a high-pressure gas pipeline in Germany was attributed to AC corrosion. Field and laboratory investigations indicated that AC corrosion can occur on coated steel pipelines even if protection criteria are met. The main conclusions of German investigators can be summarized as follows [16]:

- AC corrosion doesn't occur if AC density is lower than 20 A/m^2;
- AC corrosion is unpredictable if AC density is between 20 and 100 A/m^2;
- AC corrosion occurs if AC density is greater than 100 A/m^2;
- the highest corrosion rates occur corresponding to coating holidays with a surface area between 100 and 300 mm^2.

Chin and Fu [17] reported that at 2,000 A/m^2 AC density the passive layer formed on mild steel in passivating sodium sulphate solution appears completely destroyed. On the basis of laboratory tests, Carpentiers and Pourbaix [18] concluded that AC corrosion is not related to any particular critical AC density value. Jones [19] observed that corrosion rate of carbon steel specimens in de-aerated sodium chloride solution exposed to 300 A/m^2 AC density increases of four to six times. Yunovich and Thompson [20] state that AC density in the order of 20 A/m^2 can significantly increase steel corrosion, with high penetration corrosion rate and general attack. Further, the authors stated that probably a theoretical 'safe' AC density (a threshold below which corrosion doesn't occur) doesn't exist. However, a practical AC density below which the corrosion rate increase is not considerable may exist.
The technical specification CEN/TS 15280:2006 [12] reports that a pipeline is considered protected by AC corrosion if the root mean square AC density is lower than 30 A/m^2. In practice, the evaluation of AC corrosion likelihood on the basis of AC density is:

- AC density lower than 30 A/m^2: no or low corrosion likelihood;
- AC density between 30 and 100 A/m^2: medium corrosion likelihood;
- AC density higher than 100 A/m^2: very high corrosion likelihood.

1.4.3 AC density/DC density ratio (i_{AC}/i_{DC})

The technical specification CEN/TS 15280:2006 [12] discusses AC corrosion likelihood also in terms of the ratio between AC and DC densities, providing the following supplementary indications:

- i_{AC}/i_{DC} lower than 5: low corrosion likelihood;
- i_{AC}/i_{DC} between 5 and 10: corrosion likelihood can exist and further investigation is typically necessary;

- i_{AC}/i_{DC} greater than 10: high corrosion likelihood and mitigation measures are normally taken.

The i_{AC}/i_{DC} ratio doesn't depend on the area of the metal exposed to the electrolyte. Nevertheless, it should be pointed out that the only use of i_{AC}/i_{DC} ratio is not recommended to assess AC corrosion risk, because of the misleading meaning that could be associated to it. For instance, a i_{AC}/i_{DC} ratio of 10 can represent different interference conditions, e.g. 30 A/m^2 AC density in the presence of 3 A/m^2 DC density or 3 A/m^2 AC density in the presence of 0.3 A/m^2 DC density. Even if the i_{AC}/i_{DC} ratio is the same, the interference condition (and the related corrosion risk) is different, i.e. 3 A/m^2 AC density is not recognized as a critical value, differently from 30 A/m^2 (Paragraph 1.4.2).

1.4.4 Soil characteristics

AC density (i_{AC}) at a coating defect depends on induced AV on the pipeline and on soil resistivity by the following equation:

(Eq. 1.9) $$i_{AC} = \frac{8AV}{\rho \pi d}$$

where ρ is soil resistivity and d the diameter of a circular holiday having a surface area equal to that of the real holiday. AC density varies linearly with AV and depends on soil characteristics by its resistivity, i.e. AC density is greater in soil with low electrical resistivity. Moreover, AC density increases by decreasing the dimension of the coating defect (for a fixed AV value). The local soil resistivity is controlled by the amount of soluble salts and by water content and is strongly influenced by the electrochemical processes occurring on the metal surface in CP condition. Indeed, the presence of a cathodic current results in the migration of cations towards the cathodically protected metal and in the pH increase of the electrolyte close to the metal, due to the cathodic reactions that occur on the metal surface (Eq. 1.5). Depending on soil composition, the electrical resistance of the soil near the coating defect can either increase or decrease with time due to chemical modifications according to the pH increase. In particular, earth-alkaline ions (as Ca^{2+} and Mg^{2+}) form hydroxides with relatively low solubility. The pH increase shifts the carbonate-bicarbonate equilibrium towards the precipitation of carbonates, with the formation of a calcareous deposit [2]. If a compact deposit is formed on the metal surface, the coating defect resistance can significantly increase up to a factor of 100. Otherwise, alkaline cations (as Na^+, K^+ or Li^+) form highly soluble hygroscopic hydroxides. As a consequence, a low electrical resistance due to the high ions concentration is observed. This process can decrease the electric resistance at the coating defect up to a factor of 60. According to this description, AC density on a coating defect is therefore dependant on [12]:

- the size of the holiday;
- the specific soil resistivity;
- the ratio of alkali and earth-alkali ions;
- the amount of hydroxyl ions produced, due to the cathodic current.

Furthermore, the presence of earth-alkaline ions (such as Ca^{2+} and Mg^{2+}) extends the passivity region expected from Pourbaix diagram of iron [21].

1.4.5 Corrosion rate

Large corrosion rate data variability can be found in literature, due to the presence of several factors that contribute to AC corrosion. Moreover, there is scarcity of data about the time-dependence of AC corrosion of carbon steel in CP condition. Some AC corrosion rate data referred to cathodically protected steel structures as well as to structures in free corrosion

condition are reported in this section. Ragault [22] carried out on-site experiments on a polyethylene coated steel gas transmission buried pipeline cathodically protected and parallel for 3 km with a 400 kV HVTL. The pipeline showed corrosion with corrosion depths equal to 0.1 up to 0.8 mm after one year of installation. On-site experiments were carried out as close as possible to field conditions. 12 coupons were installed for 18 months close to the test posts where the worst cases of corrosion were found. Results showed that corrosion depth was comprised between 0.3 and 0.5 mm with AC density from 30 and 4000 A/m^2 and on-potential between -2.0 and -2.5 V CSE. The author states that there is no clear relation between AC density level and corrosion penetration depth, but high level of AC density may be an indication of high AC corrosion risk. Wakelin et al. [23] discussed some cases of cathodically protected steel pipeline failures in Ontario (Canada), where AC corrosion was suspected.
Authors report that an AC density of approximately 100 A/m^2 or more provokes corrosion, even if the DC potential indicated that corrosion should not occur. Maximum corrosion rates calculated were found to increase with AC density. The authors report also that, with the exception of AC density, there were no other common denominators which linked all of the case histories together, even though there were a number of factors which may be important indicators of AC corrosion activity. Authors compare their results with some previous corrosion rate data taken from literature of cathodically protected steel in the presence of AC interference (Figure 1.10).

Song et al. [24] studied AC corrosion of cathodically protected buried pipeline by means corrosion coupons and ER (electrical resistivity) probes. Corrosion coupons simulate a coating defect and are usually made of a steel plate having a known bare surface area. In ER probes, corrosion rate is obtained by measuring the electric resistance change of a steel plate integrated in a coupon, due to the metal loss caused by corrosion. Details about this monitoring technique will be given in Paragraph 1.8.2.
Where pipeline was cathodically protected below –1.0 V CSE (on-potential, including IR drop contribution), AC corrosion rate was affected not by AV but by both frequency and AC density. Authors obtained an experimental relation between corrosion rate and AC density: corrosion rate increases linearly with AC density with slope of 0.619 if measured by corrosion coupon (Figure 1.11*a*) and 0.885 if measured with ER probes (Figure 1.11*b*).
Nielsen and Galsgaard [25] reported field test corrosion rates measured by means of corrosion ER coupons connected to a buried pipeline in CP condition. Two periods with different DC on-potential (including IR drop contribution) were established. In the first period, on-potential was kept quite negative to give excessive CP (-1.5 V CSE). In the second period, on-potential was -1.25 V CSE. The first condition produced the highest corrosion rates: authors recorded corrosion rate peaks as high as 10 mm/y during a period of two weeks (Figure 1.12).

A laboratory study of Yunovich and Thompson [20] reports corrosion rates of carbon steel specimens cathodically protected in the presence of 20 A/m^2 (low) and 500 A/m^2 (high) AC densities. Applied cathodic potential shifts were 0 mV (no CP), 100 mV (low) and 300 mV (high). The highest corrosion rates were measured in the presence of high CP and high AC densities (Figure 1.13). Goidanich et al. [15] reported results of weight loss tests on carbon steel specimens in aerated and de-aerated soil-simulating solution in the absence of CP. In the presence of 10 A/m^2 AC density, corrosion rate is nearly twice with respect to that measured for specimens in free corrosion condition. In the presence of AC densities higher than 30 A/m^2, corrosion rate increase can be considered unacceptable. The discussed literature data show that there is controversy about AC corrosion rate; furthermore, the relation between corrosion rate and AC parameters (as AC density) is not well understood.

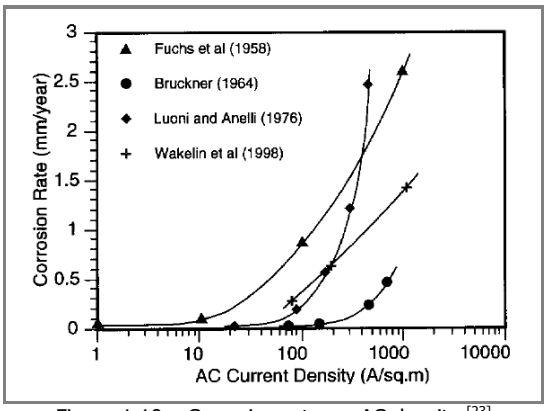

Figure 1.10 – Corrosion rate vs. AC density [23]

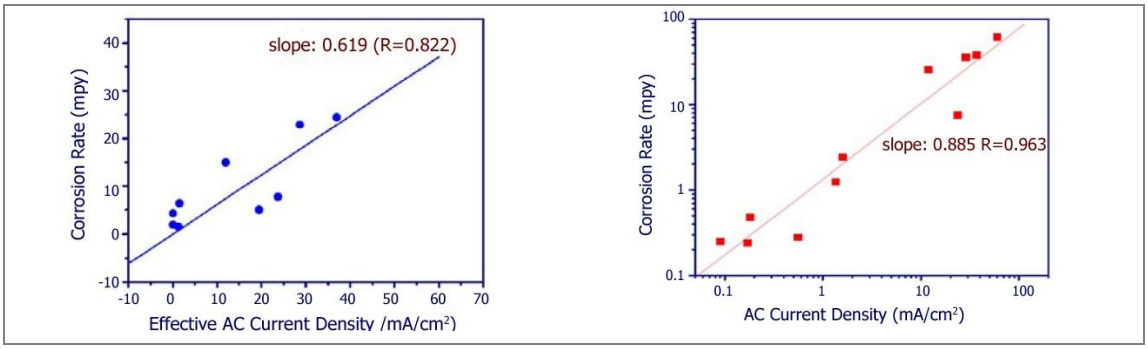

a) b)

Figure 1.11 – Corrosion rate vs. AC density measured by: a) corrosion coupons and b) ER probes [24]

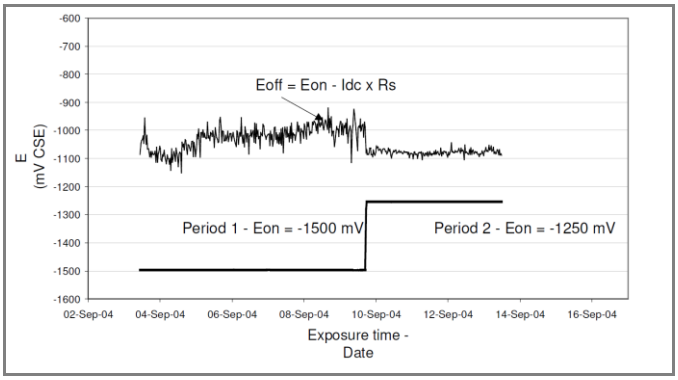

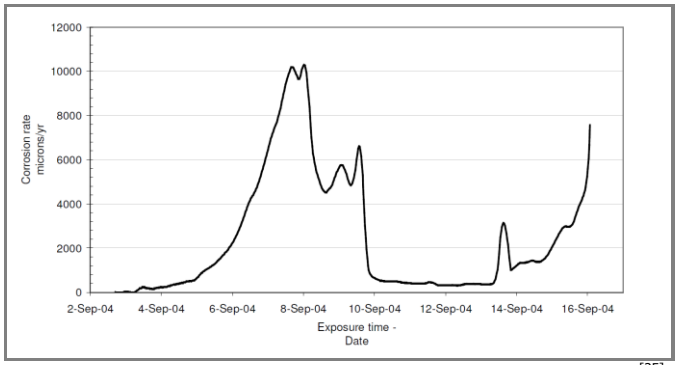

Figure 1.12 – Field test corrosion rate varying protection potential [25]

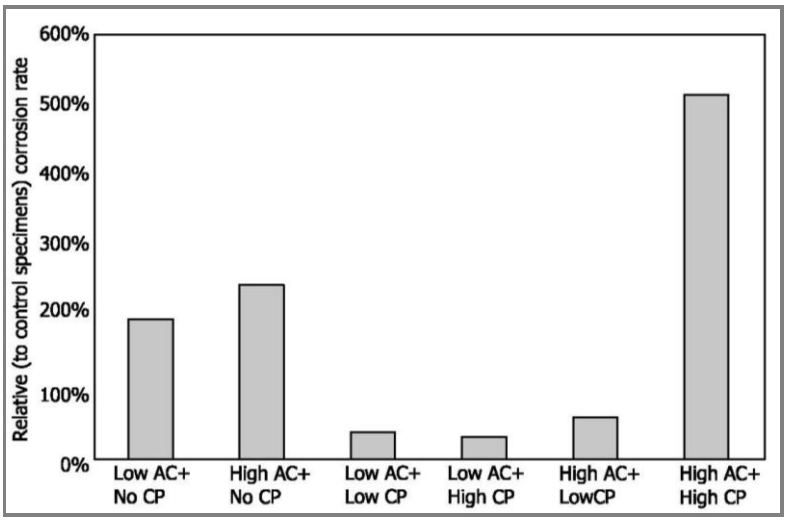

Figure 1.13 – Relative corrosion rate varying test conditions [20]

1.4.6 Frequency effect

There is agreement about the effect of the frequency of the signal on AC corrosion: corrosion rate decreases by increasing frequency [14, 17, 26-32]. Nevertheless, AC at power frequencies of 50 or 60 Hz can cause corrosion.
Fernandes [26] discussed a kinetic effect of frequency on corrosion: with the increase of frequency, the interval between successive anodic and cathodic half-cycles becomes shorter and the metallic ions formed in the anodic cycle would be available for the immediate redeposition in the cathodic cycle. In addition, the author states that at high frequencies hydrogen atoms formed during the cathodic cycle haven't enough time to coalesce and form hydrogen gas molecules. In this way, in the next anodic half-cycle, a layer of hydrogen atoms covers the metal surface and prevents the metal dissolution reaction.
The example reported below is taken from a Yunovich and Thompson study [32]. Authors calculated the current flow (corrosion current) through a steel specimen exposed to soil using an equivalent analog circuit (Randle's model, Figure 1.14). The circuit consists of a double layer capacitance (C1), the solution resistance (R_s) and the "effective resistance" (R_{eff}) that represents the combination of the charge-transfer and Warburg (diffusion-related) impedances. The circuit also includes an AC power source (HVTL). The analysis allows to simulate the electric behavior of the metal and to calculate the current passing through each component of an electric circuit varying the imposed AC frequency. AV is 24 V and AC density on the specimen is approximately 400 A/m^2.

Figure 1.15 shows the current passing through R_{eff} (related to corrosion process) and the current passing through R_s (the total current in the circuit) varying the frequency of the AV applied by the AC source. The impedance of the capacitor (C1) and the current through R_{eff} decreases with increasing frequency (and become zero if the frequency is infinite). Nevertheless, although most of the current at 60 Hz passes through the capacitor (C1) and thus does not affect corrosion reactions, there is an amount of AC (approximately 0.3% of the total current) that flows through R_{eff} at 60 Hz frequency [32].

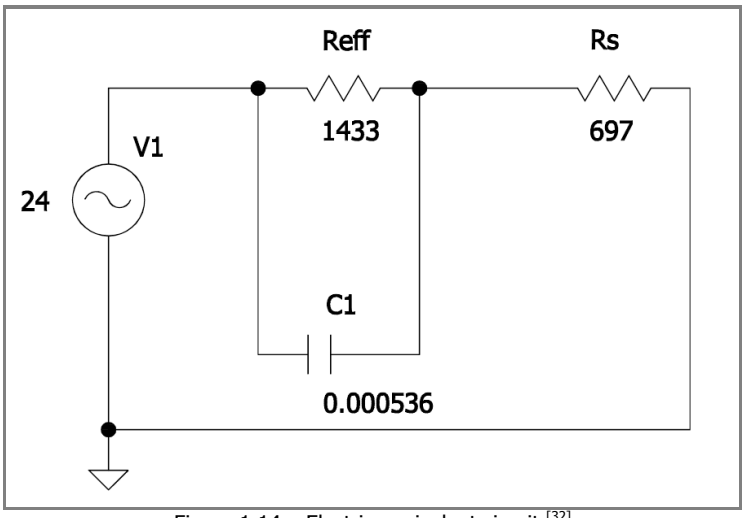

Figure 1.14 – Electric equivalent circuit [32]

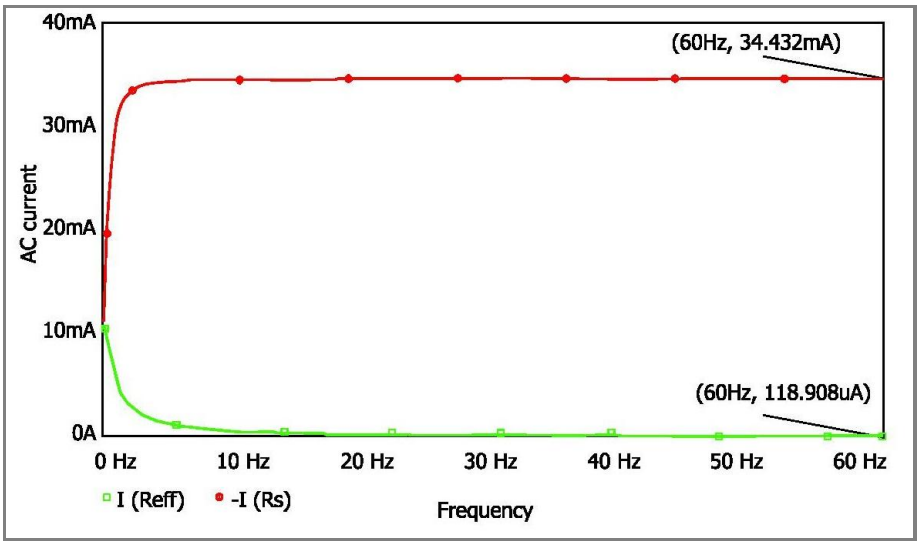

Figure 1.15 – Electrical response of the circuit in Figure 1.14: the red line is the total AC, the green line is the AC passing through R_{eff} [32]

1.5 MORPHOLOGICAL CHARACTERISTICS

AC corrosion is localized. Camitz et al. [33] studied AC corrosion in field on steel test coupons in CP condition and exposed to different AC densities. Two series of tests were performed, one at 10 V AC for almost two years, and another one at 30 V AC for 1.5 years. Authors recorded the IR-free potential (off-potential) of the test coupons with an oscilloscope: the potential varied according to the AV signal and, during the positive half cycle, off-potential shifted in the anodic direction to values less negative than the limit value for CP, meaning that CP was periodically lost due to AC interference. In several cases, the potential shifted to values even less negative than free corrosion potential. The authors report that corrosion attacks could be divided into three groups:

- small point-shaped attacks evenly distributed across the surface (uneven surface);
- large point-shaped attacks evenly distributed across the surface (rough surface);
- few large, deep local attacks on an un-corroded surface ("pocked" surface).

Nielsen and Cohn [34] described a corrosion tubercle of "stone hard soil" comprising a mixture of corrosion products and soil often observed to grow on the coating defect surface in the presence of AC interference.

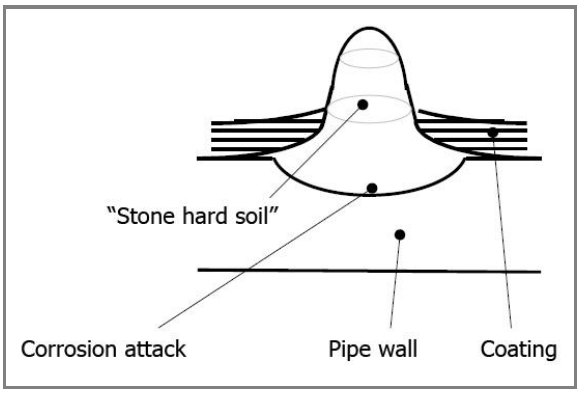

Figure 1.16 – Schematic illustration of the tubercle of "stone hard soil" that grows at the coating defect in connection with AC corrosion [34]

Figure 1.16 shows a schematic illustration [34]. The specific resistivity of the tubercle is expected to be significantly lower than the specific resistivity of the surrounding soil.
In addition, the effective area of the tubercle is considerably greater than the original coating defect. Both processes tend to decrease the spreading resistance of the associated coating defect during the corrosion process, making the corrosion process autocatalytic. Ragault [22], describing 31 AC corrosion cases on a polyethylene-coated gas transmission line, reports that corrosion products consisted mostly of magnetite mixed with soil. Williams [35] also indicates that the main corrosion product on steel interfered by AC is magnetite. Wakelin et al. [23], reported that the aspect of the pit site (i.e. hard hemisphere of soil surrounding the pit site, smooth round dish-shaped pits having a minimum diameter of 1 cm, hard tubercles covering the pit, etc.) could help to determine if AC corrosion is the primary cause of the failure. In order to provide supplementary information, a case study of failure analysis carried out by Linhardt and Ball [36] is reported.

1.5.1 A corrosion case study adapted from literature [36]

During a routine inspection of a natural gas transmission pipeline (pressure 25 bar, 150 mm inner diameter, 4.5 mm wall thickness, 45 years in service), a leak was identified by discoloration of plants. The area was excavated and the leaking section of the pipe (1.5 m long) was transferred to a laboratory for examination, together with samples from the surrounding soil. The leak was covered by a large cap (approximately 200 mm diameter) of hard, agglomerated soil.
The pipeline runs parallel to a railway (16.7 Hz system) for approximately 10 km, and the leak occurred at the end of this section. The pipe was coated with bitumen, and CP was checked every three years by extensive measurements. The protection criterion was met at all times, and the last check did not indicate the presence of a defect. The influence of AC wasn't considered critical. Measurements after the failure indicated AV peaks of 20 to 30 V in the affected region. Figure 1.17 shows the hard cap of soil adhering to the pipe that covers the leak. Polyester resin was used to impregnate the surface of the cap to stabilize its structure. After that, the bituminous coating around the cap was peeled off, and the whole cap was carefully removed from the pipe (Figure 1.18). The bituminous coating was brittle. In the area surrounding the leak, the coating was rather soft and sticky, well-adherent to the steel. After cleaning, localized attacks with deep cavities in a generally passive surface were found (Figure 1.19). The cap was cut perpendicular to the pipe's axis, in the plane of the leak position. Figure 1.20 shows the cross section of the soil cap removed from the pipe. Above the corroded area, the original layer of the coating is no longer visible. Instead, the bitumen formed a bubble-like black structure (Material A). Regions of soil material (Material B) and a white substance (Material C) separated by thin layers of material A were found. Samples of

materials A, B, and C were characterized by wet chemical analysis and by energy dispersive X-ray analysis (EDX). Results are summarized as follows:

- Material A: the black material was based on bitumen with different amounts of iron oxide (mainly magnetite) and a sodium compound, presumably carbonate. Inorganic components were finely dispersed in the bituminous matrix;
- Material B: the grey material was based on the soil material, a silicate incorporating minor amounts of alkali (Na, K) and earth-alkali (Ca, Mg) ions. The pH of the aqueous extract of the soil (1 g/10 mL) taken far from the corrosion site was 8.2. Soluble sodium content increases by decreasing the distance from the corrosion site and was found as high as 12,500 mg/kg inside the cap;
- Material C: the white substance was identified as a mixture of $NaHCO_3$ and Na_2CO_3 in a molar ratio of 1:1, without any significant impurities. The pH of a solution of 1 g in 10 mL distilled water was 9.6.

This case of pipeline corrosion was characterized by localized attack similar to pitting. The bituminous coating was found to be deformed like a bubble and magnetite was found as the major corrosion product; however, it didn't form a protective layer and was dispersed in the bituminous material. The large volumes of sodium carbonate embedded in the bubble indicate a high cathodic activity in the leak area. Failure analysis indicates that corrosion may be compatible with AC corrosion. These specific features are:

- strongly localized, pitting-like attack;
- finely dispersed magnetite as the predominant corrosion product;
- accumulation of large amounts of sodium carbonate;
- indications of local temperature excursions to values softening bitumen;
- mechanical forces mixing soil, bitumen, and sodium carbonate as could be achieved by slowly evolving gas bubbles.

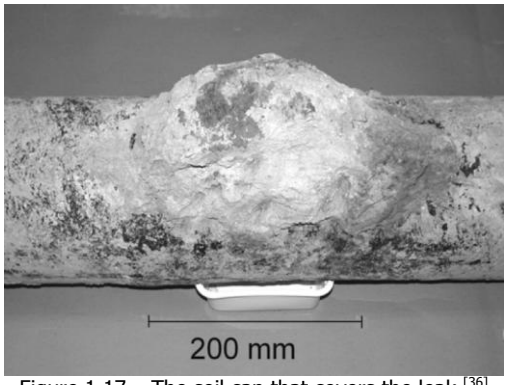

Figure 1.17 – The soil cap that covers the leak [36]

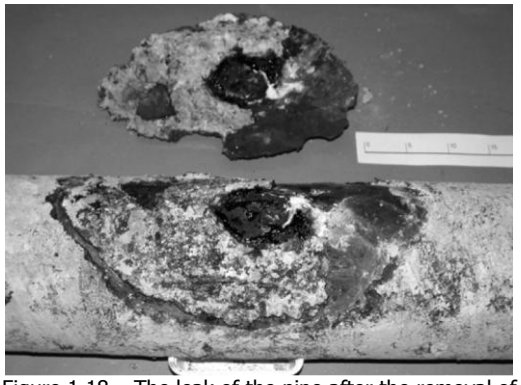
Figure 1.18 – The leak of the pipe after the removal of the soil cap [36]

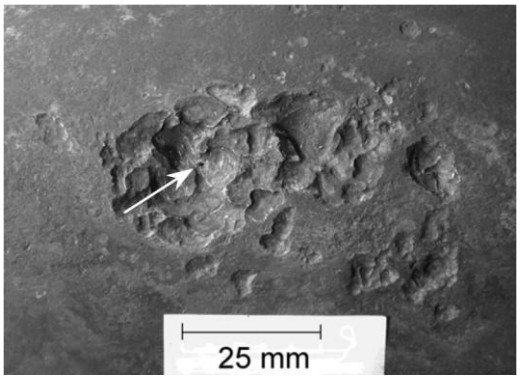

Figure 1.19 – The corroded area after cleaning. The arrow indicates the leak [36]

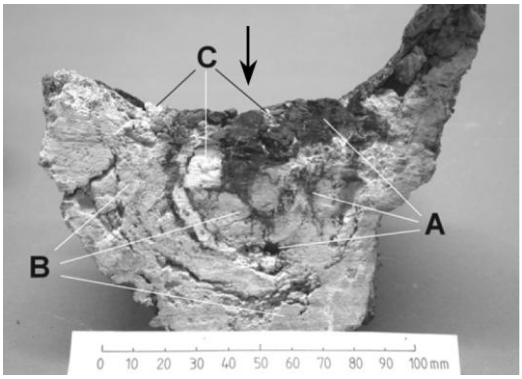

Figure 1.20 – Cross section of the soil cap. Letters indicate different materials [36]

1.6 AC CORROSION MECHANISM

Different theories have been proposed about the mechanism by which AC produces and enhances corrosion of carbon steel (even in CP condition), although no one is able to fully explain the phenomenon. Some AC corrosion mechanisms proposed in literature are now discussed. They refer to cathodically protected structures as well as to structures in the absence of CP (free corrosion condition).

The technical specification CEN/TS 15280:2006 [12] reports a simplified description of the AC corrosion mechanism described below. As reported by the technical specification, a corrosion reaction is associated with a current that leaves the metal surface (anodic behavior). In the presence of an AV induced on the pipeline in CP, an alternating current flows through the metal surface corresponding to the coating defects. The intensity of this current depends on the impedance of the system. During the positive half wave, the current leaves the metal surface if the AV is sufficiently large. This current causes the charge of the double layer capacitance and oxidation of the pipeline.
The technical specification reports that, since the current that leaves the metal surface is consumed by several non-corrosive processes, generally voltages between 4 V and 10 V are required to result in a significant corrosion attack of the metal. Nevertheless, as discussed before, various additional parameters influence this process, as leakage resistance of the defect, soil composition, CP level.
The electrochemical processes on the metal surface are schematically illustrated in Figure 1.21. During the positive half wave, the bare metal surface is oxidized resulting in the formation of a passive film, due to the current that leaves the metal surface. During the negative half wave (cathodic behavior), the passive film is reduced to iron hydroxide. In the following anodic cycle a new passive film grows. As a result of the further reduction of the passive film, the amount of iron hydroxide increases. Hence every AC cycle results in the oxidation of the metal. In the long term this can result in a significant metal loss.

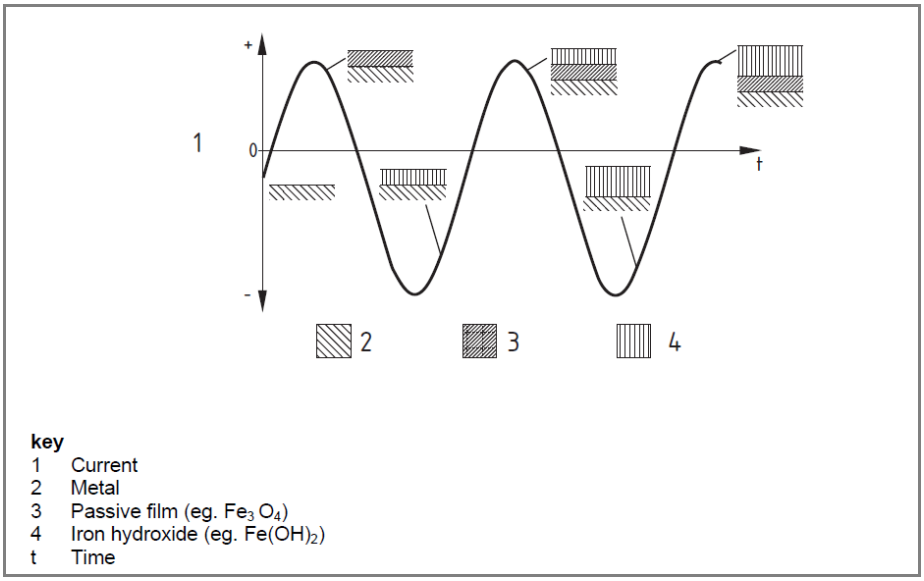

Figure 1.21 – Scheme of the AC corrosion mechanism with CP as reported by the technical specification [12]

Nevertheless, the description of the AC corrosion mechanism reported by the technical specification is not exhaustive, particularly as it applies to CP in soils. As a result, several proposals of AC corrosion mechanism could be found in literature. Some aspects need a further investigation, as the individuation of the more influencing parameters in the AC

corrosion process, the existence of a critical value of AC density (or AV), the assessment of CP criteria in the presence of AC, the influence of AC on the electrochemical behavior of the metal (thermodynamic and kinetic effects). Some proposals of AC corrosion mechanism are discussed in further detail in the following.

1.6.1 Electrical equivalent circuit analysis

Nielsen and Cohn [34] proposed an electrical equivalent circuit analysis helpful to understand the AC corrosion process and mechanism. An electrical equivalent diagram represents the impedances existing between pipe and remote earth and can model the AC corrosion process on the metal. Figure 1.22 shows the electrical circuit suggested by the authors [34]. AC and DC sources impose a DC and AC voltage between the pipeline and remote earth at a specific location or coating defect. In the case of AC interference on a pipeline in CP condition, the AC source is the HVTL, whereas the DC source represents the CP system. $E_0$1 and $E_0$2 represent the equilibrium potentials of the two reactions occurring at the metal interface (anodic and cathodic reactions). Other elements represent impedances related to the physical and chemical factors existing in the current path from remote earth to the coating defect.
Authors divided these elements in static and dynamic elements. *Static elements* are defined as elements which impedance is frequency-independent. Spread resistance and charge transfer resistance are examples of static elements. Conversely, *dynamic elements* are frequency-dependant. These include the double layer capacitance (interfacial capacitance) and diffusion elements. Each element is described below.
Soil resistance or spread resistance (R_S): the current flows through the soil from remote earth to the coating defect. The ohmic drop (IR) provided by the soil is controlled by factors related to the soil solution resistance, soil porosity and geometrical factors existing at the interface between the soil and the coating defect. Concerning geometrical factors, the majority of the IR drop takes place close to the pipe-to-soil interface, at the coating defect. Indeed, the current flux lines concentrate near the defect, causing a geometrical spread effect and an associated spread resistance (Figure 1.23).

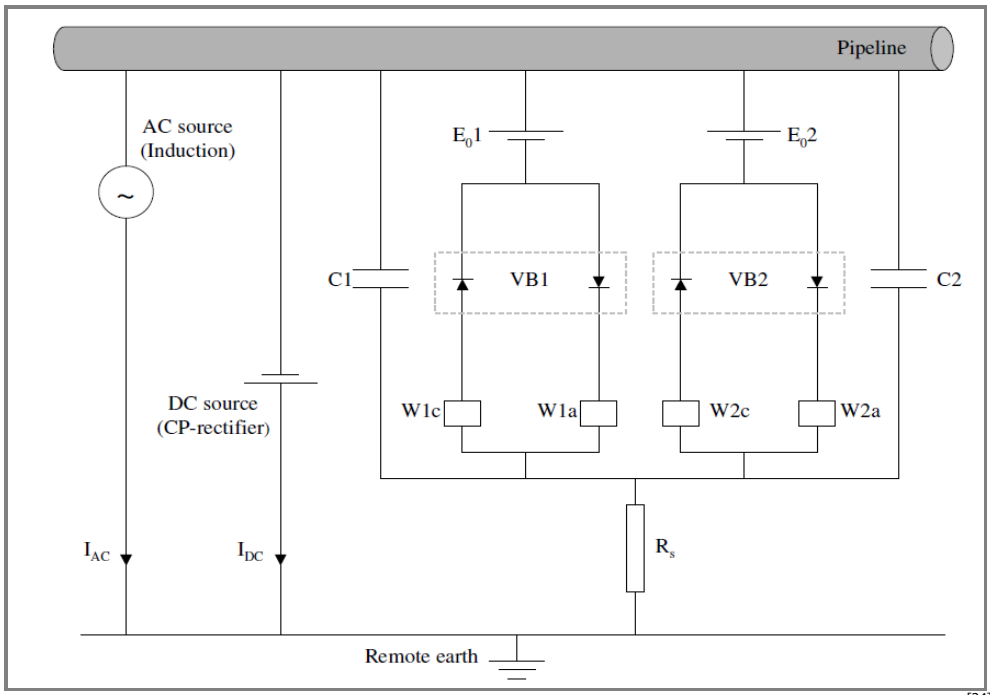

Figure 1.22 – A schematic illustration of the electrical equivalent circuit proposed by Nielsen and Cohn [34]

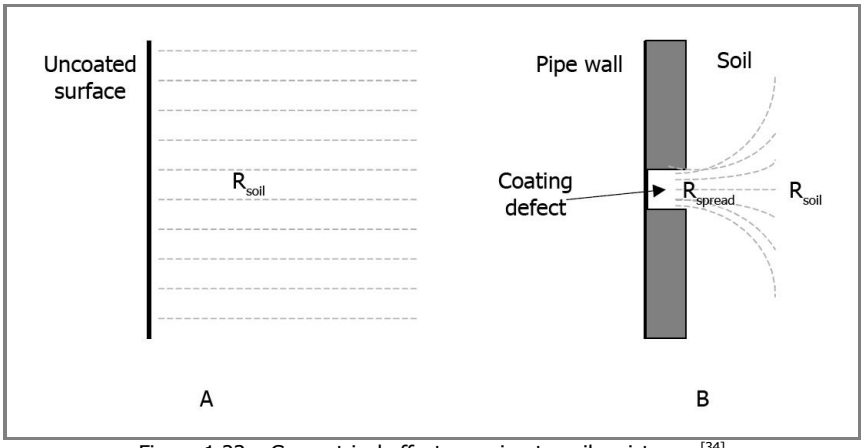

Figure 1.23 – Geometrical effects on pipe-to-soil resistance [34]

Authors studied the effect of electrode area on spread resistance using electrochemical impedance spectroscopy (EIS) measurements on steel electrodes with various areas exposed in artificial soil solution. Small defects have smaller spread resistances and are more susceptible to AC corrosion. Authors suggest the following relation to calculate R_s [$\Omega \cdot m^2$]:

(Eq. 1.10) $R_S = K \cdot d \cdot \rho_S$

where K is a constant depending on the geometry of the defect, d is a measure of the extension of the defect, and ρ_S is the soil specific resistivity.

Charge transfer diode analogy (VB-Elements): as discussed in Paragraph 1.1.1, a corrosion reaction consists of two semi-reactions: iron oxidation (Reaction 1) and the cathodic process of oxygen reduction and/or hydrogen evolution (Reaction 2):

Reaction 1
$Fe = Fe^{2+} + 2e^-$

Reaction 2
$2H_2O + O_2 + 4e^- = 4OH^-$
$2H^+ + 2e^- = H_2$
$2H_2O + 2e^- = H_2 + 2OH^-$

Authors indicate as $E_0$1 and $E_0$2 the equilibrium potentials of Reaction 1 and Reaction 2, respectively (Figure 1.22). For each reaction, two semi-reactions can be defined (*a*, anodic and *c*, cathodic), e.g. reaction *1a* refers to iron dissolution (oxidation) and reaction *1c* to iron re-deposition (reduction). In the circuit shown in Figure 1.22, charge transfer resistances for each single process are illustrated as diode elements. For each reaction, the relationship between potential (E) and current (I) at potentials different from the equilibrium potential (E_0) is described by the Butler-Volmer equation:

(Eq. 1.11) $$I_{F,a} = I_0 \left[\frac{C_{A,s}}{C_{A,b}} \exp\left(\frac{E - E_0}{\beta_a} \right) \right]$$

(Eq. 1.12) $$I_{F,c} = I_0 \left[-\frac{C_{B,s}}{C_{B,b}} \exp\left(\frac{E_0 - E}{\beta_c} \right) \right]$$

where I_F is the Faradaic current related to the anodic ($I_{F,a}$) or cathodic ($I_{F,c}$) process, I_0 the exchange current related to the process, $C_{i,s}$ the surface concentration of species i, $C_{i,b}$ the bulk concentration of species i and β indicates the Tafel slope related to the anodic (β_a) and cathodic (β_c) reactions. Anodic and cathodic Butler-Volmer equations can be described as exponential functions with a conducting voltage direction and an insulating voltage direction, analogous to diodes.
These directions oppose each other in the anode and the cathode branch. For this reason, each electrochemical equilibrium process is represented in the electrical circuit as two opposed diodes with the potential-current characteristics described by Eq. 1.11 and Eq. 1.12. Moreover, diffusion impedance (symbolized by W, Warburg impedance) is attached to each reaction. This impedance restricts the rate by which the reactions can occur as a result of diffusion processes of reactants. This impedance is frequency-dependent.

Diffusion (W-Elements): diffusion is defined as the movement of species in the presence of a concentration gradient. At the coating defect, species are consumed or produced and can diffuse in the direction of the concentration gradient. Cathodic reactions cause an increase of the pH of the electrolyte close to the metal (Eq. 1.5); since CP reactions take place at the steel surface, a pH gradient occurs with a consequent diffusion process. Diffusion process can be described by Fick's laws to determine the rate by which diffusion occurs. In the electrical circuit (Figure 1.22), the diffusion element is represented as a Warburg impedance element (W) which impedance Z_D is given by:

$$\text{(Eq. 1.13)} \quad Z_D = \frac{\sigma}{\sqrt{\pi f}} = \frac{RT}{z^2F^2A\sqrt{2}}\left(\frac{1}{C_{O,b}\sqrt{D_O}} + \frac{1}{C_{R,b}\sqrt{D_R}}\right)\cdot\frac{1}{\sqrt{\pi f}}$$

where σ is the Warburg coefficient, R the gas constant, T the temperature, z the number of electrons involved in the electrochemical process, F the Faraday's constant, A the area of the coating defect, $C_{O,b}$ the bulk concentration of oxidant, $C_{R,b}$ the bulk concentration of reductant and D_O and D_R are the related diffusion coefficients.

Interfacial Capacitance (C): the corrosion process implies that positively charged ions are dissolved in solution, whereas the excess electrons are accumulated in the steel-lattice. The accumulation of negative charge on the steel surface attracts positively charged ions from the electrolyte. The net result is the build-up of an electronegative front on the steel surface and of an electropositive front in the electrolyte (Figure 1.24). The interface acts as a capacitor, which capacitance is the so-called double layer capacitance. Generally, the impedance of a capacitor is defined by the expression:

$$\text{(Eq. 1.14)} \quad Z_C = \frac{1}{2\pi f C}$$

where f is the applied frequency and C is the capacitance. The impedance of the double layer capacitance depends on the applied frequency.

The key element of the corrosion process is the VB1 element (Figure 1.22) associated to metal dissolution. Corrosion occurs if the electrical charge during the anodic half-cycle exceeds the cathodic charge:

$$\text{(Eq. 1.15)} \quad I_a \cdot \delta t > I_c \cdot \delta t$$

If the opposite occurs, corrosion does not take place.

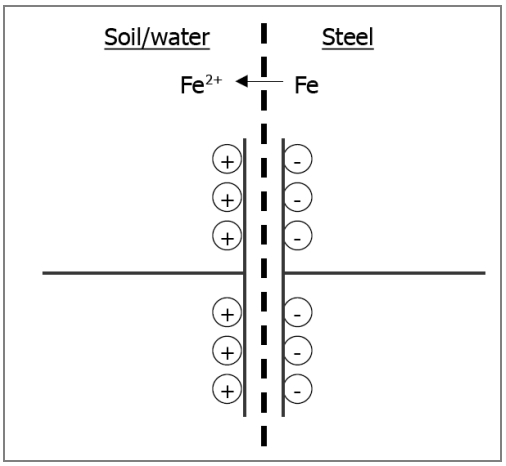

Figure 1.24 – Schematic illustration of the steel-water interface acting as a capacitor [34]

Authors discuss the effects of all the components of the electrical circuit. Because of the low impedance of the capacitance, the spread resistance (R_S) is the dominant (greatest) impedance element at a frequency of 50-60 Hz and plays the main role in controlling the AC corrosion magnitude. R_S determines the amount of AV lost across the soil resistance (magnitude of the IR drop related to AV): if R_S is high, a high degree of AV is lost across the soil resistance with a decrease of the amount of AV induced to the metal. Furthermore, this parameter is strong related to the electrical resistance of the soil close to the coating defect. This means that, depending on the modification of soil chemistry at the coating defect caused by AC and DC, soil resistance may increase, may be unaffected, or may decrease with time. Summarizing, by the proposed circuit, chemical composition at the steel-soil interface and spread resistance play the main role in the assessment of AC corrosion.
These parameters are the basis for the AC corrosion mechanism proposed by Voûte and Stalder [37] that takes into account the effect of soil chemical composition on spread resistance, considering the ratio between earth-alkaline and alkaline cations.

1.6.2 Earth-alkaline vs. alkaline cations

As mentioned before (Paragraph 1.6.1), Voûte and Stalder [37] proposed that the main role on the assessment of AC corrosion is played by the chemical composition of the environment at the steel-soil interface. Accordingly, the spread resistance at the coating defect represents the main parameter that affects AC corrosion.
The authors consider the concentration ratio in soil between earth-alkaline cations (as Ca^{2+} and Mg^{2+}) and alkaline cations (as Na^+, K^+, or Li^+). Earth-alkaline cations form hydroxides [$Ca(OH)_2$, $Mg(OH)_2$] due to the alkaline pH close to the metal surface in CP condition. The pH increase (due to the cathodic reactions occurring on the metal) shifts the carbonate-bicarbonate equilibrium towards the precipitation of carbonates ($CaCO_3$, $MgCO_3$), with the formation of a calcareous deposit, as discussed in Paragraph 1.4.4. Hydroxides and carbonates of earth alkaline cations produce solid precipitates with low solubility. Solid deposits with low solubility act to increase the spread resistance (R_S) associated with the coating holidays.
Conversely, hydroxides and carbonates formed with alkaline cations (NaOH, KOH, Na_2CO_3) are soluble. Authors suggest that earth-alkaline cations in soil lead to a higher spread resistance and a correspondingly lower magnitude of AC at the coating holiday (lower corrosion risk). In addition, earth-alkaline cations have a passivate effect on the metal, with an extension of the passivity region expected from Pourbaix diagram of iron [21], with a decrease of the anodic dissolution process.

1.6.3 A conventional electrochemical approach in the absence of CP

Yunovich and Thompson [32] proposed a conventional electrochemical approach to develop an AC corrosion model in the absence of CP (free corrosion condition). As discussed before (Paragraph 1.4.6), only a small amount of the 50-60 Hz AC charge passes through the resistive component of the circuit, with corrosion of the metal. The model is based on the conventional (DC-based) study of the corrosion process. In this analysis, it is assumed that metal loss reactions are non-reversible and the cathodic reaction is oxygen reduction. Likewise, it is assumed that metal loss is the only available oxidation reaction.
The model assumes that each electrochemical reaction has a specific time constant; this assumption implies that the time constant is sufficiently small that the reaction sequence is applicable at 60 Hz. An example of a corrosion process under the influence of AC signal is illustrated in Figure 1.25. The graph is based on realistic potential and current values: the assumed corrosion potential (E_{corr}) is -0.7 V CSE and the corrosion current (i_{corr}) is 4.7 mA (which corresponds to a corrosion rate of 0.08 mm/y for a 4,580 mm^2 specimen exposed surface). The imposition of an AC signal results in a shift in the anodic (positive) and cathodic (negative) direction of corrosion potential; the absolute value of the potential shift is 0.150 V. During the anodic period of the signal ($A \rightarrow B \rightarrow O$ in Figure 1.25), the anodic current density increases to the maximum value denoted $i_{AC\text{-}OX(B)}$; during the cathodic half wave ($O \rightarrow C \rightarrow A$ in Figure 1.25), the anodic current density decreases to the value denoted $i_{AC\text{-}OX(C)}$. As a result, the average anodic current for a single AC imposed signal is greater than the corrosion rate in free corrosion condition in the absence of AC, due to the semi-logarithmic relation between potential and the current. AC polarization of the metal produces a net anodic (oxidation) current greater than the free-corrosion current. For an active metal, the potential-current relationship is defined by the Tafel's law:

(Eq. 1.16) $$E = b + \beta_a \mathrm{Log}(i)$$

where β_a is the anodic Tafel slope of the metal in soil (assumed 0.150 V per decade of current). At the time t, the potential of the metal (E) is the sum of the corrosion potential (E_{corr}) and the alternating potential due to the presence of the AC signal (E_{AC}):

(Eq. 1.17) $$E = E_{corr} + E_{AC} = E_{corr} + E_A \sin(2\pi f t)$$

where E_A is the amplitude of the AC potential shift (0.150 V) and f is the frequency (60 Hz). Substituting Eq. 1.16 in Eq. 1.17, the relationship between current and potential becomes:

(Eq. 1.18) $$i = 10^{\frac{E_{corr}+E_{AC}-b}{\beta_a}} = 10^{\frac{E_{cor}+E_A \sin(2\pi f t)-b}{\beta_a}}$$

The potential sinusoidal shift doesn't correspond to a sinusoidal shift of the current, due to the non-linear relationship between potential and current. Figure 1.26 illustrates potential and current shifts for a single period of 60 Hz current (with 0.150 V of potential shift). During the anodic half wave, the current exhibits values greater than the free corrosion current. During the cathodic half wave, the oxidation current decreases compared to the free corrosion current, but not of the same magnitude of the increase during the anodic half wave. Therefore, the complete AC cycle results in a net positive increase of the oxidation current.

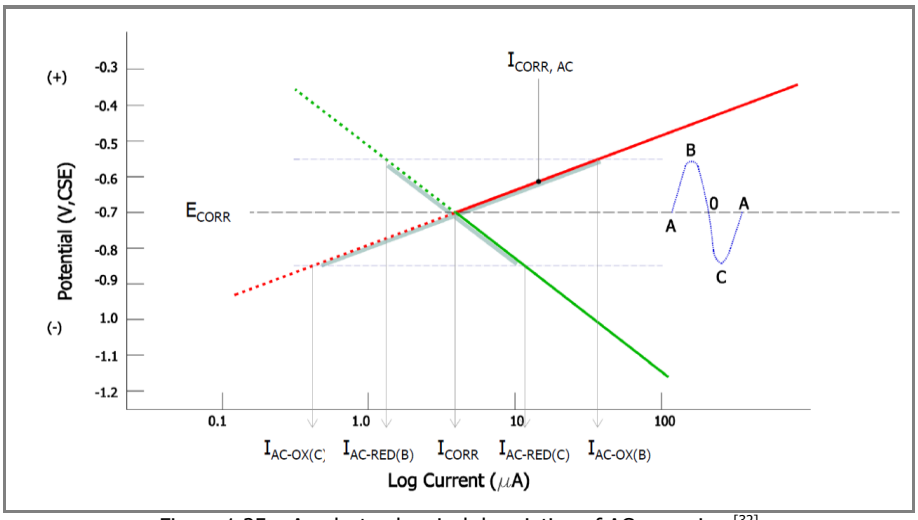

Figure 1.25 – An electrochemical description of AC corrosion [32]

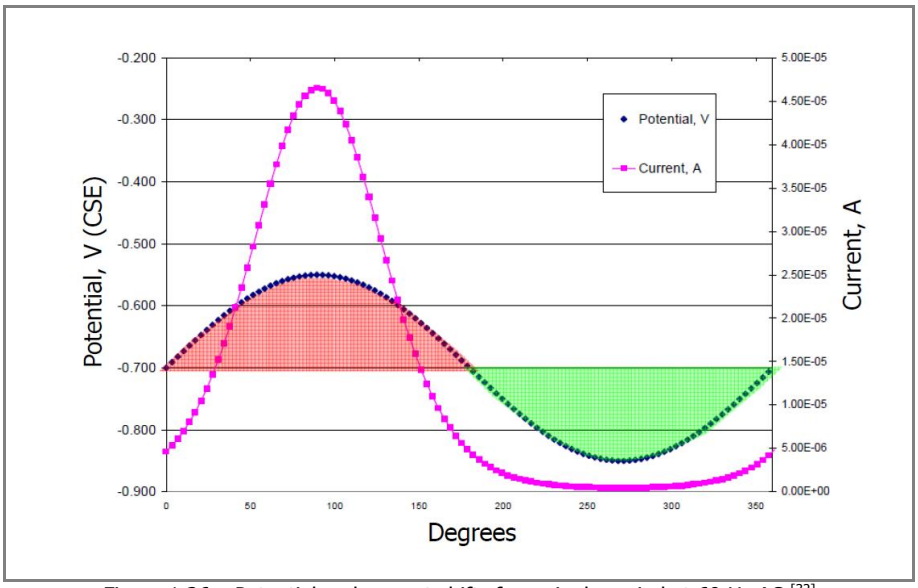

Figure 1.26 – Potential and current shifts for a single period at 60 Hz AC [32]

1.6.4 The alkalization mechanism

Nielsen et al. [38-40] proposed the so-called alkalization theory. Authors state that the combined action of high pH and potential oscillation caused by AC interference may induce corrosion attacks.

The alkalization mechanism is based on two effects associated with AC interference: (1) the alkalization of the environment close to the coating defect in the presence of high protection current density (Eq. 1.5) and (2) potential oscillations between the passive, the immunity and the high-pH corrosion region of steel potential-pH diagram in the presence of AC interference. Indeed, in CP condition, hydroxyl ions accumulate close to the surface of the coating defect (Figure 1.27), with a pH increase. The authors reports the existence of an "incubation period" defined as the time to reach a critical pH value in the electrolyte in contact with the metal. Then, potential oscillations could cause corrosion due to different time constants associated to iron dissolution (fast) and the formation of a passive film (slower). At very alkaline pH (close to 14), the formation of dissolved $HFeO_2^-$ ions may cause corrosion with high penetration rate.

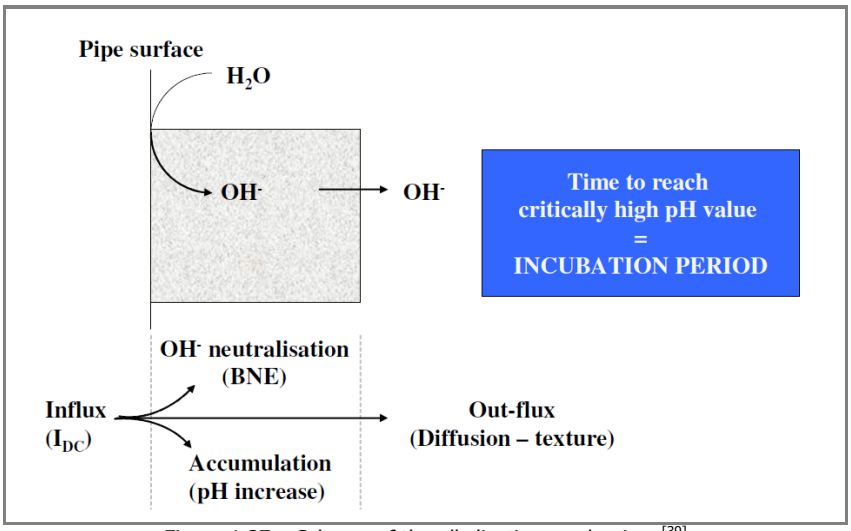

Figure 1.27 – Scheme of the alkalization mechanism [39]

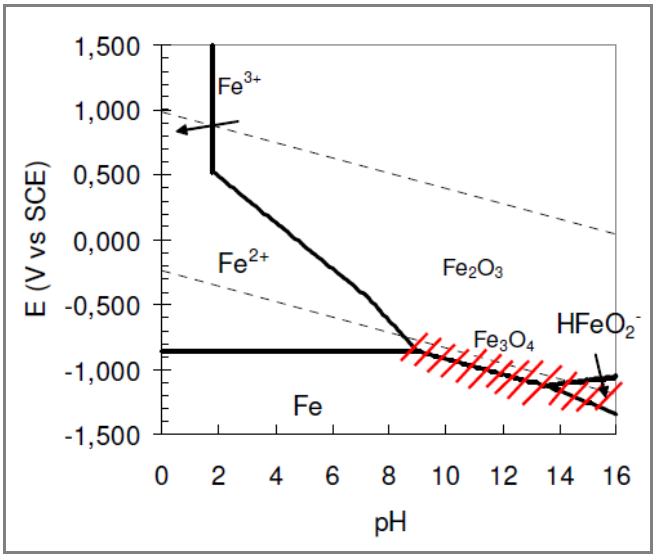

Figure 1.28 – Pourbaix diagram: the hatched area indicates the critical AC corrosion zone [39]

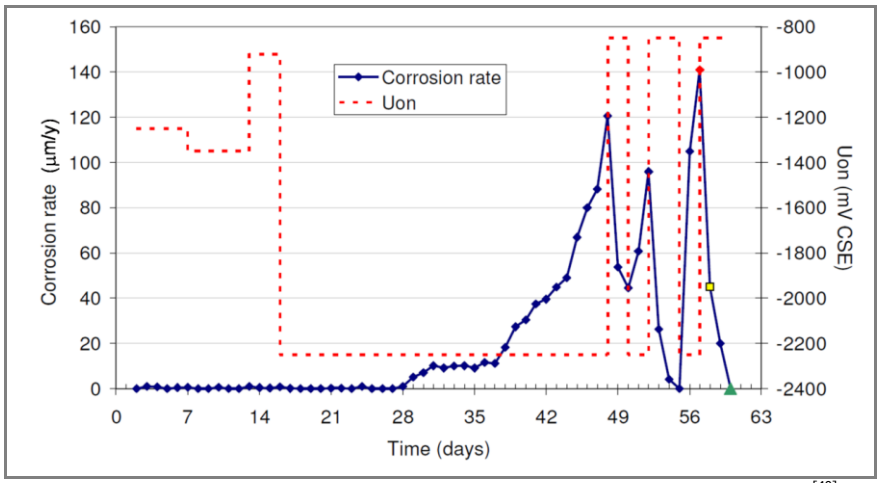

Figure 1.29 – DC on-potential (U_{on}) and corrosion rate measured with ER coupon [40]

Hydroxyl ions accumulation is low if the production rate of these ions is modest (small influx) and their diffusion transport away from the surface (out-flux) is not prevented. Additionally, a neutralizing effect could occur if soil chemical species react with the produced OH^- (base neutralizing effect, BNE). Nevertheless, high CP current can increase the pH locally at the coating defect and, in combination with potential oscillations, could lead to the periodic entry in the high-pH corrosion domain in the Pourbaix diagram (Figure 1.28). An aspect that should be investigated is if the electrochemical reactions are fast enough to occur within the time during which the potential crosses the corrosion area. As a consequence, AC corrosion is not avoided by adding a surplus of CP, as in the case of DC stray current corrosion. Authors state that in the presence of AC interference, high CP current density should be avoided.
In order to investigate the influence of the DC level on AC corrosion, a controlled soil box experiment was carried out in inert quartz sand with a dilute solution of sodium chloride [40]. AV on the coupon was fixed at 15 V. CP on-potential was change during the test to study the effect of different protection polarizations on corrosion behavior.
Experimental data show that AC density increases by increasing the DC density (if the AV is controlled at 15 V) and that the spread resistance (calculated as the ratio between AV and the measured AC) is inversely proportional to DC density. As a consequence, corrosion rate increases as a function not only of AC density but also of DC density (Figure 1.29). After an incubation period at very low on-potential, corrosion rate increases up to 120 μm/y.

1.6.5 Theoretical corrosion models

Some authors [17, 29, 41-45] pointed out that the ratio of the anodic and cathodic Tafel slopes (indicated as $r = \beta_a/\beta_c$) determines the sensitivity of the corroding system with regard to the AC caused polarization (DC potential shift). Indeed, if anodic and cathodic curves are asymmetric ($r = \beta_a/\beta_c \neq 1$), when an external sinusoidal voltage is applied, a shift of the corrosion potential can results. Lalvani and Lin [41] derived an analytical solution that described the relationship between corrosion rate and the AV amplitude for a corroding system under activation control. They extended their work in a revised model [42], in which they introduced the effect of the double layer capacity. Authors didn't consider in their models the resistance of the electrolyte (that, as discussed in Paragraph 1.6.1 and Paragraph 1.6.2, some authors consider as the main parameter controlling AC corrosion). Figure 1.30 (*a* and *b*) reports corrosion potential shift estimated using the analytical solution of the first version of the model [41], as a function of the peak AV (E_P) and of the ratio of anodic and cathodic Tafel slopes (r). For the two cases ($r < 1$ and $r > 1$), corrosion potential decreases and increases by increasing the peak alternating potential (E_P), respectively. The corrosion current increases rapidly with E_P for all values of r (Figure 1.31*a* and Figure 1.31*b*).
The results obtained in the revised model [42] for corrosion current as a function of the peak potential are the same reported in the first model, in which authors didn't consider the double layer capacitance. Potentiodynamic polarization curves (E_{DC} vs. i_{rms}) were obtained theoretically using the revised model in the following conditions: 60 Hz frequency; DC corrosion potential of -0.7 V SCE[2] and a double layer capacitance of 20 μF. Figure 1.32 shows DC potential as a function of the root-mean-square current for the case $r > 1$ (i.e. the anodic Tafel slope is greater than the cathodic Tafel slope). An increase in the peak potential (from 0.2 to 1.5 V) results in an increase of the root-mean-square current and in a shift towards more anodic direction of DC potential at which the root-mean-square current has a minimum. This DC potential is denoted as $E_{rms,min}$.

The $E_{rms,min}$ potential and the corresponding root-mean-square current ($i_{rms,min}$) are reported as a function of the ratio of the anodic to cathodic Tafel slopes in Figure 1.33 and Figure 1.34, respectively. If $r = 1$, corrosion potential doesn't change for all peak potentials. If $r < 1$, the

[2] SCE, saturated calomel electrode, +0.244 V SHE

potential becomes more cathodic with respect free corrosion potential in the absence of AC; the greater the peak potential, the more cathodic is the shift. Potential becomes more anodic if r > 1, and potential shift increases by increasing the peak potential. Moreover, the root-mean-square current ($i_{rms,min}$) increases with Tafel slope ratio (Figure 1.34). For great values of the peak potential, there is initially a rapid increase of the current with Tafel slope ratio, up to an asymptotic value. These models [41, 42] predict that corrosion current and corrosion potential are independent on the frequency of the applied signal. Nevertheless, this is in contrast with several experimental data (Paragraph 1.4.6).

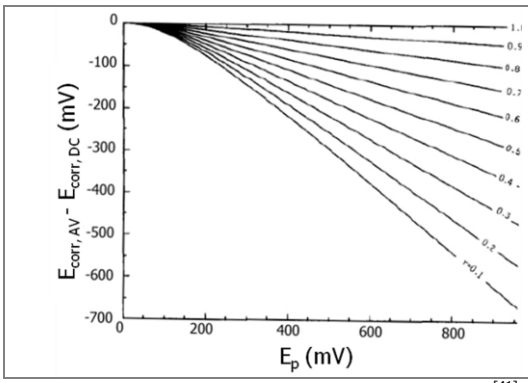

Figure 1.30*a* – Potential shift vs. E_P for r ≤ 1.0 [41]

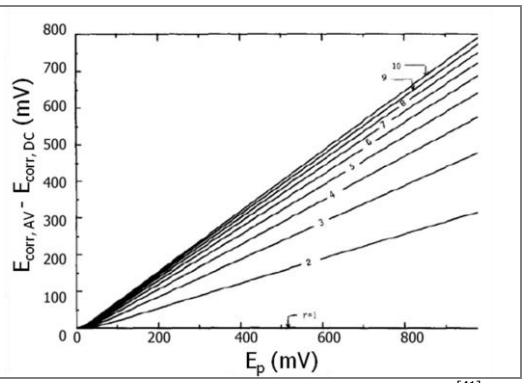

Figure 1.30*b* – Potential shift vs. E_P for r ≥ 1.0 [41]

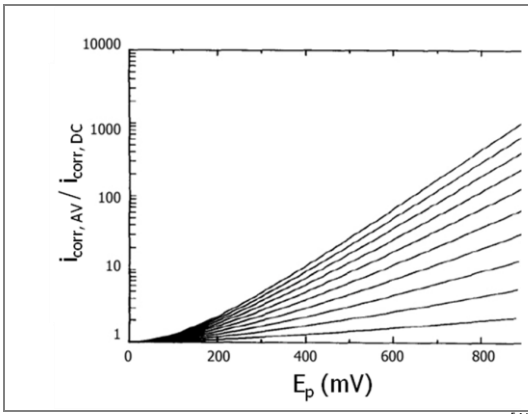

Figure 1.31*a* – Corrosion current vs. E_P for r ≤ 1.0 [41]

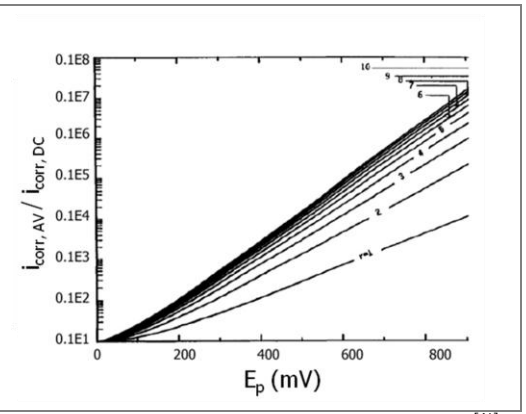

Figure 1.31*b* – Corrosion current vs. E_P for r ≥ 1.0 [41]

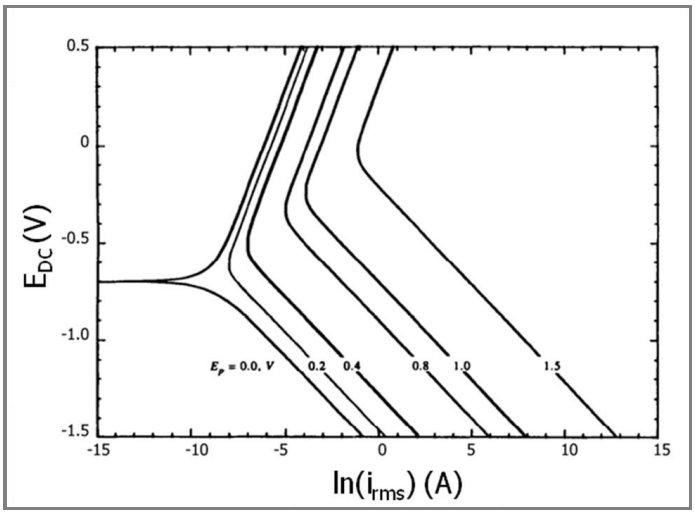

Figure 1.32 – DC potential vs. the root-mean-square current for the case r > 1 [42]

Recently, a linear model of AC induced corrosion was proposed by Xiao and Lalvani [43]: authors considered three elements involved in the corrosion process of a metal subjected to an induced AV: the polarization impedance (Z_P), the double layer capacitance (C_{dl}) and the solution resistance (R_S). Figure 1.35 shows the equivalent electric circuit of the model [43]. The model shows that an increase in the frequency of the applied signal lowers the corrosion current (Figure 1.36), in agreement with experimental data. The other observations are in agreement with models discussed previously. The model also shows that AC corrosion doesn't depend on DC corrosion potential (Figure 1.37) and this seems in contrast with the results obtained by other authors and discussed before (Paragraph 1.6.4).

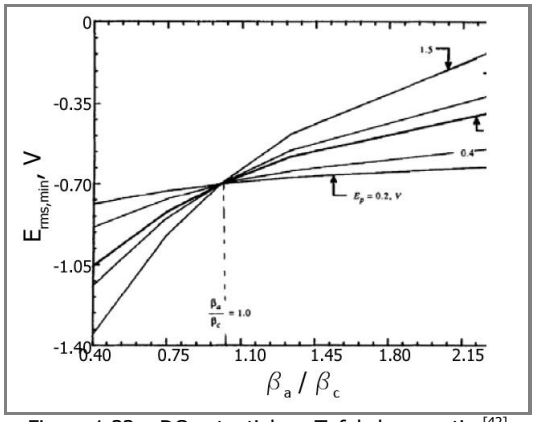

Figure 1.33 – DC potential vs. Tafel slopes ratio [42]

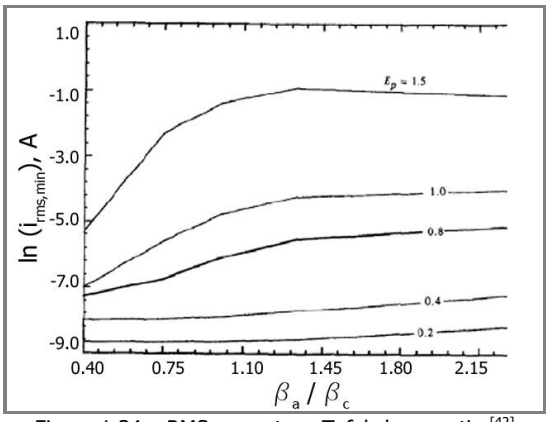

Figure 1.34 – RMS current vs. Tafel slopes ratio [42]

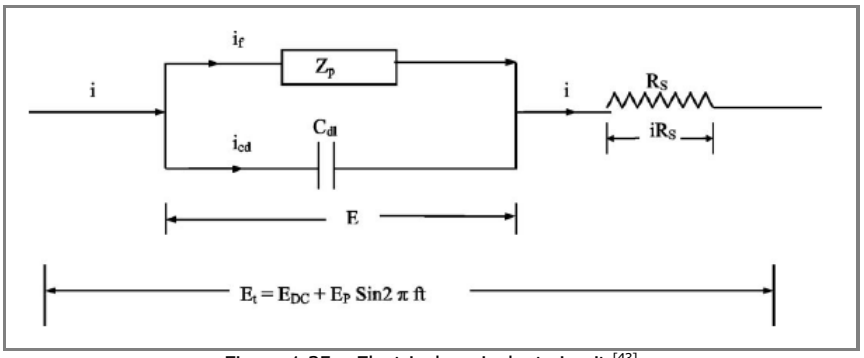

Figure 1.35 – Electrical equivalent circuit [43]

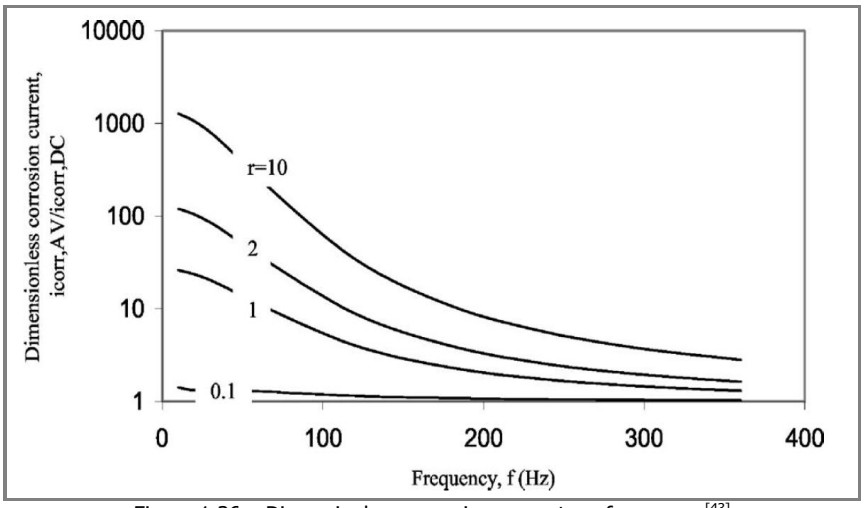

Figure 1.36 – Dimensionless corrosion current vs. frequency [43]

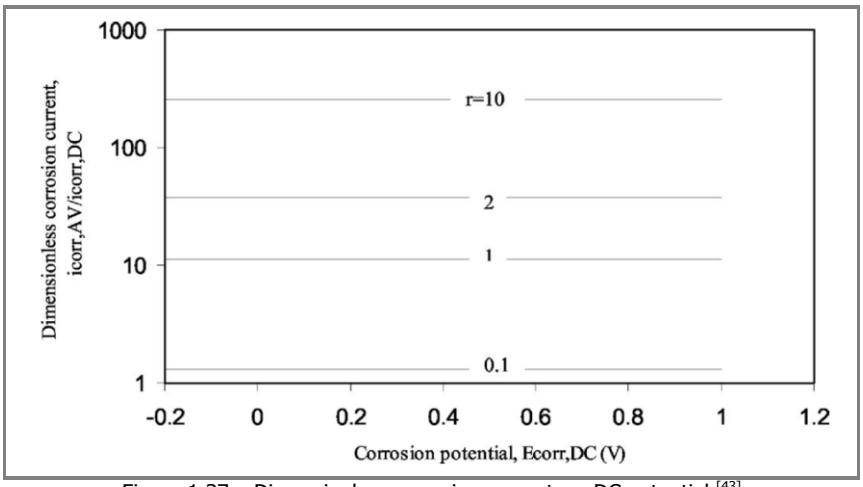

Figure 1.37 – Dimensionless corrosion current vs. DC potential [43]

1.6.6 AC effect on overpotentials

The corrosion rate increase in the presence of AC has been attributed by some authors to an effect on anodic and cathodic overpotentials. Goidanich et al. [46] reported that most probably several factors should be considered giving rise to a "mixed" mechanism. Authors studied the influence of AC on kinetic characteristics of carbon steel, galvanized steel, copper and zinc under several experimental conditions. Experimental results showed that AC has a strong influence on corrosion kinetic and on corrosion and equilibrium potential. The effect of AC on kinetic parameters such as Tafel slope and exchange current density depends on the system studied and on the supplied AC density. Authors report a general decrease of overpotentials and increase of exchange current density in the presence of AC and that, with the only exception of the tests in soil-simulating solution, corrosion and equilibrium potentials decrease. Tests in simulated soil solution (1.77 g/L Na_2SO_4 and 0.41 g/L $CaCl_2 \cdot 2H_2O$), showed that potential increases with AC density and the dependence of Tafel slopes with AC density is quite articulated. Figure 1.38 shows polarization curves of carbon steel in soil-simulating solution obtained by the authors [46].
Nielsen [39] reports DC polarization curves on a carbon steel coupon placed in a synthetic soil solution in the presence of different levels of AC density (from 10 to 300 A/m^2). DC current (and consequently the rate by which hydroxyl ions are produced in CP condition) increases by increasing AC density (Figure 1.39). Authors state that the effect of AC indirectly contributes to the alkalization process discussed before (Paragraph 1.6.4).

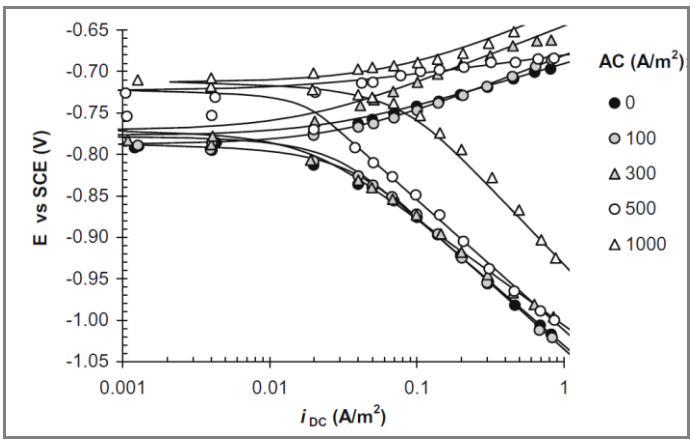

Figure 1.38 – Polarization curves of carbon steel in soil-simulating solution varying AC density [46]

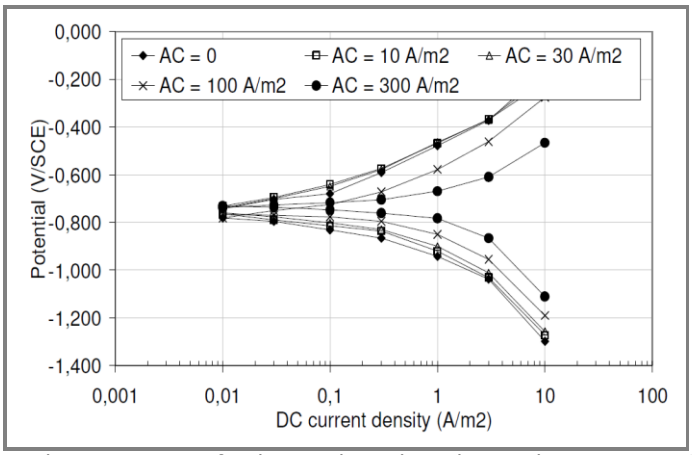

Figure 1.39 – Polarization curves of carbon steel in soil-simulating solution varying AC density [39]

1.7 CATHODIC PROTECTION CRITERIA

The technical specification CEN/TS 15280:2006 [12] states that "as AC corrosion phenomena are linked to the switching, according to the pH, between immunity, and passivity condition, the coupon-to-soil off potential should be more negative than, but as close as possible to, the limiting critical potential (which is –0.850 V CSE for iron or steel in aerobic or –0.950 V CSE in anaerobic soil containing sulphate reducing bacteria)". The standard reports that to fully evaluate AC corrosion likelihood on buried pipelines, other factors should be considered. Nowadays, the issue regarding what level of CP should be applied to mitigate AC corrosion is under investigation. As discussed in Paragraph 1.4, several authors refer critical values of AC density and AV below which the corrosion likelihood is low, but there is a scarcity of data about information regarding the CP potential to apply in the presence of AC interference.

Hosokawa et al. [47] proposed a CP criteria based on field and laboratory studies and literature research. The criterion is based on AC and DC densities and doesn't take into account the protection potential of the metal. Figure 1.40 reports the graphic illustration of the CP criteria for buried steel pipelines reported on this study. Authors propose a critical value not only of AC density, but also of DC density. In Figure 1.40, CP area is indicated in gray while the outside area indicates corrosion. Corrosion activity can be divided in three zones corresponding to the possible risks of DC corrosion, AC corrosion and overprotection. This study shows that AC corrosion could be mitigated to a negligible corrosion rate if AC density is below 70 A/m^2. AC corrosion remains probable if AC density is over this threshold value. Authors report that DC densities lower than 0.1 A/m^2 cause DC corrosion due to the lack of CP and DC densities greater than 20 A/m^2 should be avoided for the achievement of overprotection condition. The diagram shows that the lowest corrosion risk occurs in the presence of CP current densities between 1 and 20 A/m^2. This criterion seems to conflict with field test observations and failure case analysis according to which AC corrosion may be related to the presence of high CP current density. The paper [47] offers the following criteria for AC corrosion protection based on the values of CP current density (i_{DC}) and AC current density (i_{AC}):

- 0.1 A/m^2 ≤ i_{DC} ≤ 1.0 A/m^2 and $i_{AC} < 25\ i_{DC}$
- 1.0 A/m^2 ≤ i_{DC} ≤ 20 A/m^2 and i_{AC} < 70 A/m^2

Conversely, field tests results by Nielsen [39] showed that the CP level has a dramatic influence on the AC corrosion, as discussed in Paragraph 1.6.4. The author reports that in the presence of a CP current density of about 10 A/m^2 and off-potentials of approximately -1.1 V CSE, corrosion rate increases to 10 mm/y (measured by electrical resistance probes). Corrosion rate decreases by reducing the CP level, in the presence of a fixed AV (15 V).

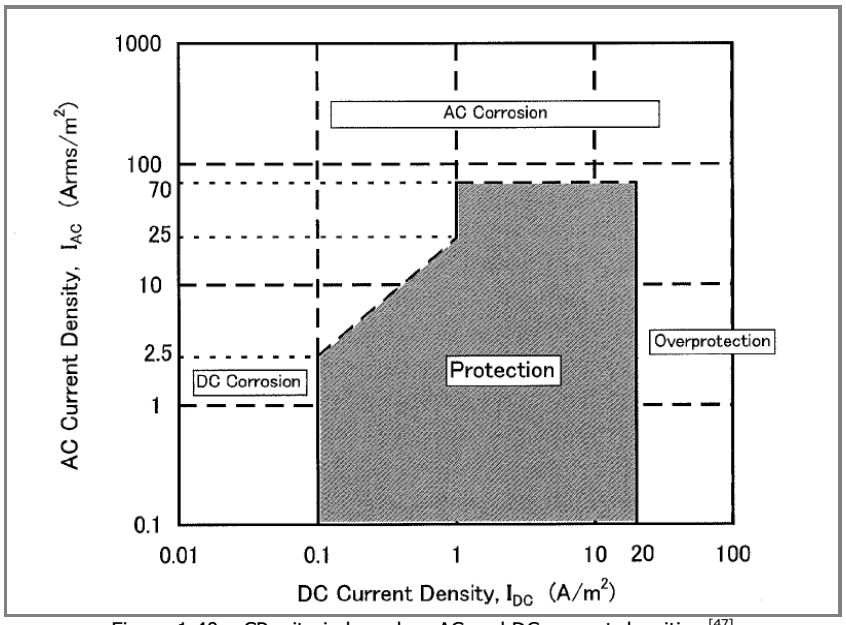

Figure 1.40 – CP criteria based on AC and DC current densities [47]

Carpentiers et al. [48] state that steel corrosion in CP condition can occur under the influence of AC interference in environments and in potential ranges that would be perfectly passivating if AC is absent. Furthermore, they state that steel protection in the presence of AC interference is achieved only when the potential is within the immunity region of the Pourbaix diagram (Figure 1.28). For the authors, the off-potential must remain always in the immunity domain, and the presence of very high pH must be considered to define the immunity potential. Protection criteria may thus be more severe in the presence than in the absence of AC, because AC can destroy passivation films that would be perfectly protective in the absence of AC. Authors state that IR-free potential measurements (off-potential) are essential in the presence of AC. Due to the local alkalization at the metal surface in CP condition, they recommended off-potentials below –1.150 V SCE at all times.

1.8 AC CORROSION MONITORING

The technical specification CEN/TS 15280:2006 [12] reports AV as the primary parameter for characterizing the AC corrosion likelihood on a metallic structure. However, this measurement (as described by the specification) includes the IR drop contribution that depends on several factors including soil resistance, the distance between the pipeline and the electrode, spread resistance, holiday size, holiday distribution. As widely discussed, although AV is an appropriate parameter for safety concerns (step-and-touch voltages), it is not the only parameter to take into account in order to assess AC corrosion likelihood. Other parameters, as the off-potential, the spread resistance and the pH at the steel/soil interface seem to be critical to define AC corrosion risk.

The technical specification CEN/TS 15280:2006 [12] reports that in areas where AC interference is known, the maintenance plans should include:

- periodic measurements of AV;
- potential, AC and DC measurements on corrosion coupons;
- current measurements on existing AC discharge devices through relevant groundings;
- voltage measurements at the installation site of AC discharge devices, after its disconnection, in respect of safety measures;
- periodic measurement of the electrical resistance of the groundings.

As a general rule, the efficiency of the equipment and components should be verified with an annual frequency. Once it is known or suspected that a pipeline is influenced by AC interference, a coating fault survey is recommended and excavations should be performed after a careful examination of all the parameters of interest to confirm the presence of AC corrosion. Due to the fact that many electrical and electrochemical parameters cannot be measured directly on the pipeline, the use of coupon test stations (CTS) is particularly recommended for evaluating AC corrosion likelihood.

1.8.1 Coupon test stations (CTS)

AC corrosion coupons consist of a steel plate having a known bare surface area, in order to simulate a coating defect. They are buried close to the pipeline and connected to it through a test post. These coupons can either be used for measuring and/or for verifying local protection conditions. The size of CTS can represent a key-factor in the assessment of AC corrosion likelihood. Gummow et al. [49] reported that the highest corrosion rates occur at holidays having a surface area in the range of 1-3 cm^2. Corrosion rate increases by decreasing holiday surface area reaching a maximum for a holiday surface area of 1 cm^2.
The technical specification CEN/TS 15280:2006 [12] reports that CTS can be used for measuring and/or verifying local protection conditions in the presence of AC interference. In order to verify protection conditions, three coupons may be installed at the same place (it is recommended to keep at least one meter between each coupon). CTS should be buried at the same time for statistical examination. After installation (e.g. after several months), CTS should be excavated and the following information should be collected:

- local soil resistivity;
- pH at the coupon-to-soil interface.

Weight loss and visual examination of corrosion coupons should be performed. If an excavated coupon is corroded by AC, further investigations on the pipeline may be necessary and consequent mitigation measures should be taken.
As an alternative to coupons, the standard describes other two techniques available to evaluate AC corrosion: the electric resistance technique and the coulometric technique.

1.8.2 Electric resistance technique

This technique consists of measuring the change of the electric resistance of a steel plate integrated in a coupon (ER coupon), due to the metal loss caused by AC corrosion. Indeed, the thickness variation of the steel coupon can be assessed by measuring its electric resistance (R_C), which for plate geometry is proportional to the dimensions of the coupon in accordance with the following equation:

$$R_c = \rho \frac{L_c}{\sigma_c w_c} \quad \text{(Eq. 1.19)}$$

where ρ is the specific resistivity of the coupon material [Ω·m], L_c is the length [m], w_c is the width [m] and σ_c is the thickness of the coupon [m].
For compensation of the resistivity-temperature dependence, a reference coupon (made of the identical material of the exposed coupon) should be positioned in the coupon assembly but isolated from the corrosive environment by a protective coating. The thickness of the exposed coupon at time t, $\sigma_c(t)$, can be assessed using the following equation:

$$\sigma_c(t) = \sigma_0 \cdot \frac{R_{c,0}}{R_{ref,0}} \cdot \frac{R_{ref,t}}{R_{c,t}} \quad \text{(Eq. 1.20)}$$

where the subscript 'ref' indicates the reference coupon and '0' the initial condition (t = 0). Corrosion rate (CR) of the coupon can be assessed as the thickness reduction per unit time:

(Eq. 1.21) $$CR = -\frac{\partial \sigma_c}{\partial t}$$

Nielsen et al. [38] reported the response of AC corrosion monitoring by means of ER coupons installed on a field station owned by DONG – the National Oil and Gas Company of Denmark. A probe resolution in the region of 0.1 μΩ was realized through an high-resolution instrumentation [50]. The active area of the simulating coating defect is 0.4 cm^2. Figure 1.41 shows electric resistance monitoring by means of the ER probe over a period of 10 hours and the conversion between electric resistance and metal thickness. Figure 1.42 shows corrosion rate and the measured AV on the pipe over a period of 3 weeks. On the basis of these data, authors report two empirical relations between corrosion rate and AV, referred to the initial and to the steady stage of corrosion [38].

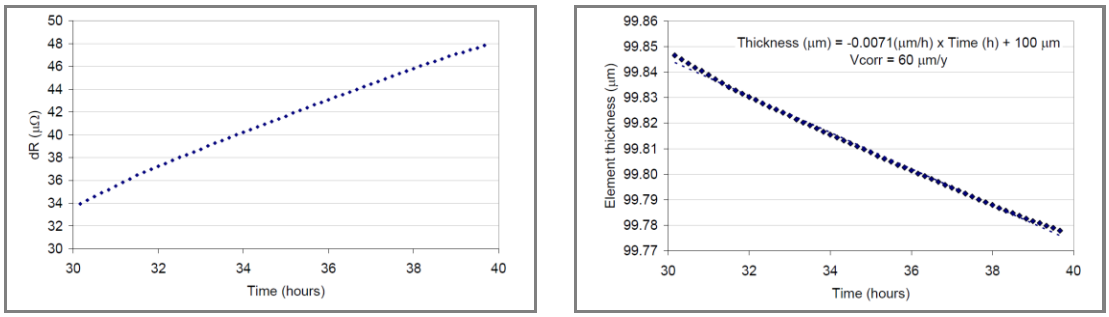

a) b)

Figure 1.41 – Response from ER probe: electric resistance (a) and metal thickness conversion (b) [38]

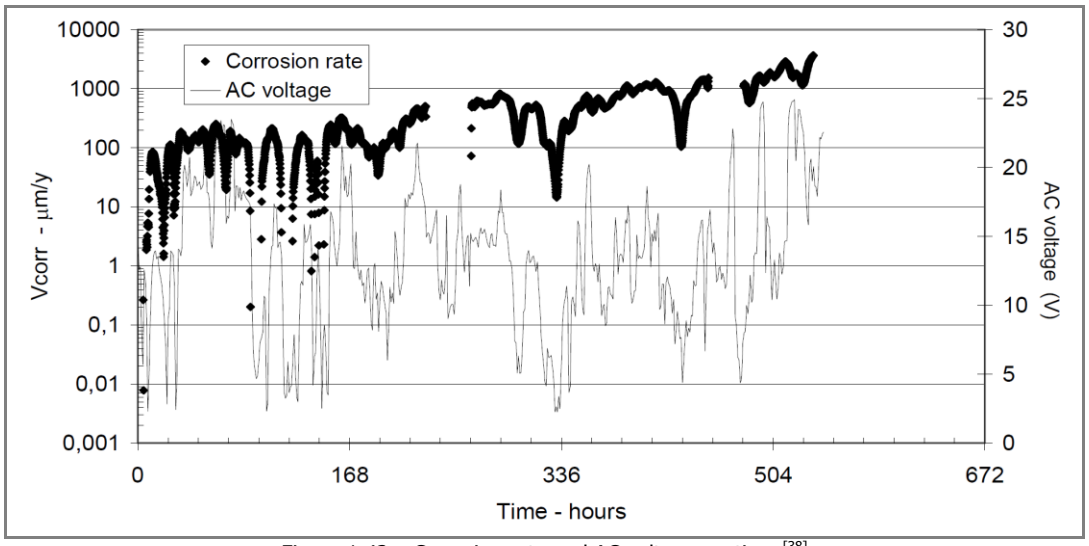

Figure 1.42 – Corrosion rate and AC voltage vs. time [38]

1.8.3 Coulometric oxidation of corrosion products

AC corrosion products are generally accumulated at the metal surface. The CP current prevents part of these corrosion products from further oxidation from Fe^{2+} to Fe^{3+}.
As discussed before (Paragraph 1.6), the technical specification CEN/TS 15280:2006 [12] reports that AC corrosion process primarily takes place in alkaline conditions in the pH-range

where passivation of steel is possible. In these conditions, it is possible to determine the amount of Fe^{2+} ions by coulometric oxidation to Fe^{3+}. By polarizing corrosion coupons with an anodic current, a passive film is formed on the steel surface. Additionally, the Fe^{2+} ions accumulated in the corrosion products in front of the steel surface are oxidized to Fe^{3+}. Complete passivation is possible after all Fe^{2+} ions are oxidized.
Experimentally, this point is reached when oxygen evolution is taking place on the surface of the coupon or the potential is more positive than +0.4 V CSE. To determine the potential of the steel surface during the measurements, the anodic current is interrupted at intervals of five seconds for one second and the off-potential of the coupon is measured. The off-potential is recorded as a function of the polarization time and the anodic current. The amount of charge required for the passivation of the coupon is an indicator for the amount of accumulated corrosion products (Table 1) [12]. Additionally, the pH-value at the coupon/soil interface can be estimated by the potential at which the oxygen evolution is taking place.

Table 1.1 – Corrosion level of the coupon related to the charge required for the passivation [12]

Charge (C/cm^2)	Corrosion level	Description
0	0	No corrosion
0 to 0.1	1	Slight corrosion
0.1 to 1	2	Medium corrosion
1 to 5	3	Strong corrosion
More than 5	4	Very strong corrosion

1.9 AC MITIGATION

AC mitigation in conjunction with CP is frequently used to minimize any effect of AC interference on corrosion. Although CP has a beneficial effect, AC corrosion can occur even if "conventional" protection criteria are met. Further, as discussed before, the increase of the protection current to control AC corrosion may result in the opposite effect, due to the pH increase and the reduction of the spread resistance at the coating defect surface. Historically, several methods, such as the installation of decoupling or grounding devices, were used to reduce AC interference. The typical way of AC mitigation is provide by ground earths at critical locations in order to transfer the AC discharge point from the pipeline to the grounding conductors. Nowadays, AC mitigation methods are based mainly on electric safety considerations with a secondary beneficial effect on the reduction of AC corrosion risk. Nevertheless, in some cases, the effectiveness of AC corrosion mitigation measures evaluated by safety considerations may not be sufficient for AC corrosion control.
The description of the AC mitigation available methods is not reported. The standard NACE SP0177-2007 [9] describes various protective devices used to mitigate AC effects on metallic structures subject to hazardous AC conditions, to minimize damage to the structures, and to reduce the electrical hazard to people coming in contact with these structures.

Chapter 2

Experimental

Laboratory tests were carried out on carbon steel specimens in cathodic protection (CP) condition in the presence of AC interference in order to simulate the corrosion behavior of coating defects of a cathodically protected buried pipeline interfered by AC. Furthermore, laboratory tests were carried out on passive metals (as carbon steel in alkaline environment and stainless steels in neutral solution) in free corrosion condition (in the absence of CP).
These tests aim to investigate some aspects related to the effect of AC on electrochemical passivity of metals. The details about such investigation on which the research focused will be provided in the following chapters. Most of the tests were conducted in the laboratories of the corrosion research group PoliLaPP ("Laboratorio di Corrosione dei Materiali Pietro Pedeferri") of Dipartimento di Chimica, Materiali e Ingegneria Chimica "Giulio Natta" of Politecnico di Milano. During an internship period of four months, tests were carried out in collaboration with the AC corrosion group of the Metallurgical and Materials Engineering Department of Colorado School of Mines (Golden, CO, USA).
Experimental tests are divided in two groups:

- AC corrosion initiation tests;
- AC corrosion propagation tests.

Before discussing the experimental tests, the electrical circuit used is described.

2.1 ELECTRICAL CIRCUIT

Laboratory tests were carried out by means of an electrical circuit designed during the first phase of the research project and described elsewhere [46]. The electrical circuit allows separating, controlling and measuring DC and AC, in order to assure reliable and unaffected measurements during CP tests in the presence of AC interference. The electrical circuit is represented in Figure 2.1 and Figure 2.2. The electrical circuit has two different meshes (Figure 2.1): the AC mesh on the left side and the DC mesh on the right side.

2.1.1 The AC mesh

The AC mesh can be described as follows (Figure 2.1):

- AC is supplied by an AC feeder (variac device, variable voltage transformer) and flows between the specimen (working electrode, W) and the counter electrode (CE_{AC});
- AC is measured by means of the shunt R_1 (10 Ω, 250 W);
- DC circulation in the AC mesh is forbidden by a capacitor (500 μF capacitance).

The capacitor prevents DC circulation in the AC mesh: it works as a high-pass filter, blocking the low frequencies (DC current included). The capacitive reactance (X_C, Ω) measures the capacitor opposition to the current flow and varies with the frequency of the electrical signal:

(Eq. 2.1) $$X_C = \frac{1}{2\pi fC}$$

where f is the frequency (Hz) and C is the capacitance (F), given by the ratio between the charge and the voltage applied between the plates of the capacitor. X_C tends to infinite in the presence of DC (zero-frequency current). X_C of the AC mesh is 6.4 Ω at 50 Hz frequency.

2.1.2 The DC mesh

The DC mesh can be described as follows (Figure 2.1):

- DC is supplied by a DC feeder (galvanostat) and flows between the specimen (working electrode, W) and the counter electrode (CE_{DC});
- DC is measured by means of the shunt R_2 (10 Ω, 250 W);
- AC circulation in the DC mesh is forbidden by an inductor (20 H inductance).

The inductor prevents AC circulation in the DC mesh: it works as a low-pass filter, blocking the high frequencies. The inductive reactance (X_L, Ω) varies with AC frequency:

(Eq. 2.2) $X_L = 2\pi fL$

where f is the frequency (Hz) and L is the inductance (H). The inductive reactance of the DC mesh is 6.3 kΩ at 50 Hz frequency.

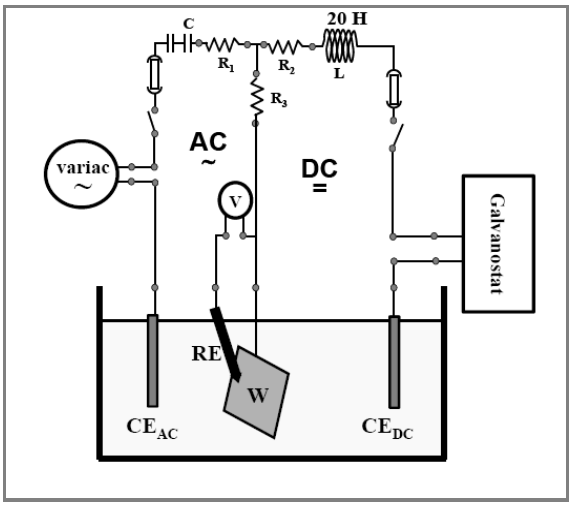

Figure 2.1 – Schematic view of the electrical circuit

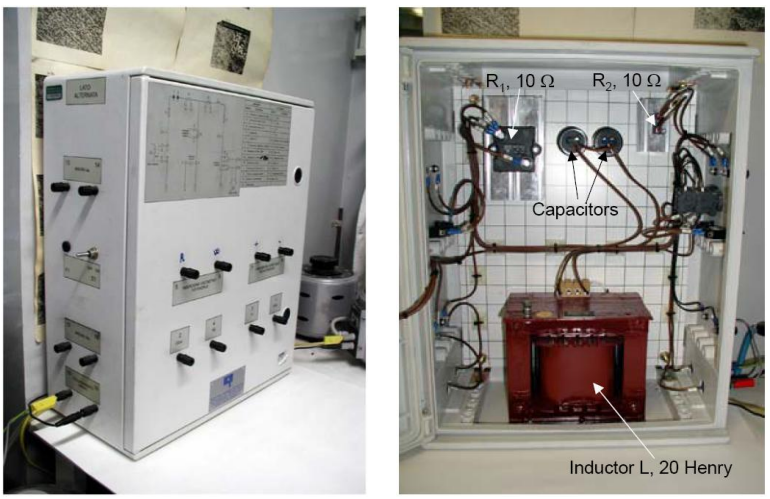

Figure 2.2 – Electrical circuit (case and internal view)

2.1.3 Efficiency of the circuit

AC and the DC meshes share a common branch (Figure 2.1), where AC and DC overlap and flow to the working electrode (W). The efficiency of the DC filter is 100%, i.e. no DC flows in the AC mesh. Conversely, despite of the 20 H inductance, a small part (less than 1% of the total AC) flows in the DC mesh. Such AC filter was considered sufficient for the planned tests.

2.2 AC CORROSION INITIATION TESTS

AC corrosion initiation tests aim to investigate AC corrosion initiation mechanism of carbon steel in CP condition. Furthermore, in order to investigate some aspects related to the effect of AC on electrochemical passivity, tests were carried out on some passive metals in free corrosion condition (in the absence of CP), as carbon steel in alkaline environment and stainless steels in neutral solution. Chapter 4 will provide a detailed description about such investigation on which the research focused. The following experimental tests were performed:

- galvanostatic test: AC effect on protection potential
- potentiostatic test: AC effect on protection current
- potentiodynamic test: AC effect on polarization curves
- linear polarization resistance measurement
- alternating voltage measurement
- tests on passive metals
  - AC effect on critical chlorides threshold
  - potentiodynamic test: AC effect on polarization curves
  - alternating voltage measurement
- pH measurement in CP condition

2.2.1 Galvanostatic test: AC effect on protection potential

As discussed in Paragraph 1.1.5, the general criterion used to verify the corrosion protection of a metallic structure is based on the protection potential measurement. The aim of this test is to investigate the effect of AC superimposition on the protection potential of carbon steel. Galvanostatic tests were carried out on carbon steel specimens, grade API 5L X52 [51] (Table 2.1), in the presence of AC interference. After preparation and cleaning operations according to ASTM G1-03 [52], carbon steel specimens were placed in a PTFE cylindrical sample holder (Figure 2.3) made of two watertight caps. A circular area of 1 cm^2 of the metal was exposed to the electrolyte. A metal rod was screwed in a hole on the top of the sample holder to provide the electrical contact with the specimen inside the cap. In order to prevent the contact between the metal rod and the surrounding environment, a glass tube was placed around the screw and was pressed against the sample holder interposing an o-ring joint between them (Figure 2.3). Samples were placed in a cylindrical cell (diameter 150 mm; height 200 mm) containing soil, composed by silica sand and a soil-simulating solution (200 mg/L chlorides and 500 mg/L sulphate ions). Electrical resistivity ($\rho \cong 5\ \Omega\cdot m$) was measured according to the two electrode soil box method [53]. Generally, soil aggressiveness is not influenced directly by its type or composition but instead is determined by the characteristics of the water it retains, such as resistivity, salt content, pH and oxygen availability. Empirical correlations consider the corrosiveness of a soil with resistivity between 5 and 10 $\Omega\cdot m$ as severe [2].

Table 2.1 – API 5L X52: chemical composition by weight [51]

Grade	% C max	% Mn max	% P max	% S max
API 5L X 52	0.31	1.35	0.030	0.030

Table 2.2 – Galvanostatic test: experimental conditions

CP current density (A/m^2)	AC density (A/m^2)*
0.1	10; 30; 50; 100; 200
0.3	10; 30; 50; 100; 200
0.5	10; 30; 50; 100; 200
1.0	10; 30; 50; 100; 200
2.0	10; 30; 50; 100; 200
10.0	10; 30; 50; 100; 200

*steps every 30 minutes

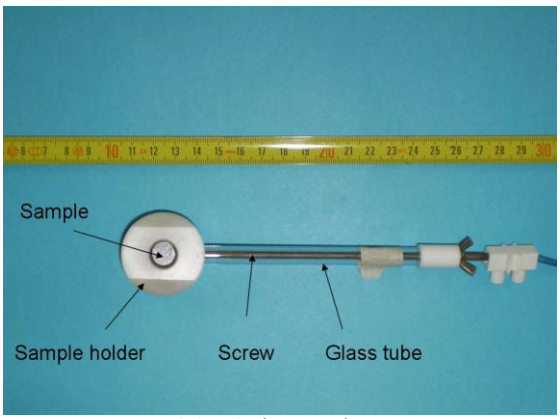

Figure 2.3 – Carbon steel specimen

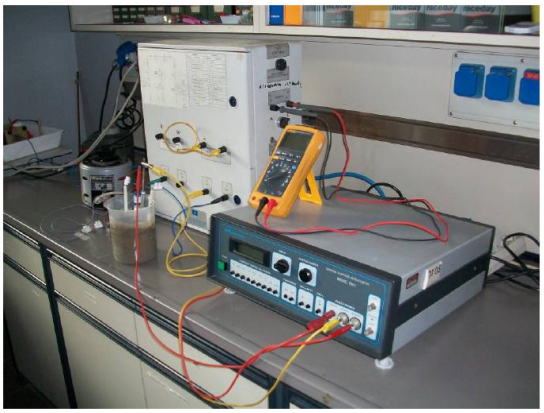
Figure 2.4 – Galvanostatic and potentiostatic tests: experimental arrangement

In a galvanostatic test, a constant polarization current is supplied to the metal and potential is measured. A fixed cathodic current density was provided to the sample (working electrode) by a DC feeder AMEL Model 2051 Potentiostat-Galvanostat through an activated titanium anode. AC was overlapped to the sample by means of the electrical circuit described in Paragraph 2.1 through a further activated titanium counter electrode. Figure 2.4 shows the experimental arrangement.
CP was applied for 24 hours, without AC interference. Six values of cathodic current density were applied in the range between 0.1 and 10 A/m^2. AC was overlapped to the sample by steps, increasing AC density every 30 minutes from 10 to 200 A/m^2. During the experiment, protection potential was measured by means of an external SSC[1] reference electrode and a high impedance voltmeter. A Luggin capillary filled with the test solution was used to hold the reference electrode in order to measure the IR-free potential in close proximity to the working electrode. For each step (30 minutes), protection potential was measured every 5 minutes. Table 2.2 summarizes experimental conditions.

2.2.2 Potentiostatic test: AC effect on protection current density

The aim of this test is to investigate the effect of AC on the protection current density that, as discussed in Paragraph 1.1.3, is the current that must be supplied to the structure to protect it from corrosion; this current depends mainly on the cathodic processes that take place on the metal surface. Potentiostatic tests were carried out on carbon steel specimens, grade API 5L X52 (Table 2.1), in the presence of AC interference. The experimental set-up is the same adopted for galvanostatic tests (Paragraph 2.2.1). After preparation and cleaning operations according to ASTM G1-03 [52], the specimen was placed in a sample holder (Figure 2.3) that allows exposing a net surface area of 1 cm^2 of the sample to the electrolyte. The specimen was placed in a cylindrical cell (diameter 100 mm; height 150 mm) containing soil, composed

[1] SSC, silver-silver chloride electrode, +0.197 V SHE (saturated)

by silica sand and the same soil-simulating solution used for galvanostatic tests (200 mg/L chlorides and 500 mg/L sulphate ions). Electrical resistivity is about 5 Ω·m.
In a potentiostatic test, the metal is polarized to a constant potential value and polarization current is measured. Carbon steel was cathodically polarized by a potentiostat AMEL Model 2051 Potentiostat-Galvanostat through an activated titanium anode. AC was overlapped to the sample by means of the electrical circuit described in Paragraph 2.1 through a further activated titanium counter electrode. CP was applied for 24 hours, without AC interference. Six tests were carried out varying protection potential in the range between -0.850 V CSE and -1.350 V CSE[2]. AC was overlapped to the sample by steps, increasing AC density every 30 minutes from 10 to 200 A/m^2. A Luggin capillary filled with the test solution was used to hold the reference electrode in order to measure IR-free potential in close proximity to the specimen. For each step (30 minutes), protection current was measured every 5 minutes. Table 2.3 summarizes experimental conditions.

Table 2.3 – Potentiostatic test: experimental conditions

CP potential (V CSE)	AC density (A/m^2)*
-0.850	10; 30; 50; 100; 200
-0.950	10; 30; 50; 100; 200
-1.050	10; 30; 50; 100; 200
-1.150	10; 30; 50; 100; 200
-1.250	10; 30; 50; 100; 200
-1.350	10; 30; 50; 100; 200

*steps every 30 minutes

2.2.3 Potentiodynamic test: AC effect on polarization curves

Potentiodynamic polarization tests were carried out in order to investigate the AC influence on the electrochemical kinetic of anodic and cathodic reactions (anodic and cathodic polarization curves) varying AC density. Tests were performed on carbon steel and on magnesium alloy specimens. Magnesium alloys are typically used as galvanic anodes in soil.
Potentiodynamic polarization test provides useful information regarding corrosion mechanism, corrosion rate and susceptibility of specific materials to corrosion in designated environments. The test involves the change of the working electrode potential and the measure of the current as a function of potential. The result is the so-called potential-current density curve. In the anodic polarization test, the potential is shifted in the anodic (or more positive) direction; in the cathodic polarization test, the working electrode is cathodically polarized.
If the working potential is displaced from the open-circuit value (free corrosion condition, E_{corr}), the current measured represents the difference between the anodic-reaction current and the cathodic-reaction current, or vice versa. If the potential displacement is sufficiently large, the net current is essentially equal to the anodic or cathodic-reaction current, depending on whether the potential is moved in the more positive or more negative direction with respect to the open-circuit potential, respectively. Figure 2.5 shows schematic anodic and cathodic polarization curves for an active metal in an electrochemical system where the cathodic reaction is the reduction of protons, as reported by the standard UNI EN ISO 17475:2008 [54].
In a potentiodynamic polarization test, the potential is displaced in a continuous mode at a controlled scan rate. Nevertheless, the kinetics of the electrochemical processes occurring on the surface can be time dependent, for example due to film formation, and hence the potential scan rate in potentiodynamic testing can be critical [54].

[2] CSE, copper-copper sulphate electrode, +0.318 V SHE

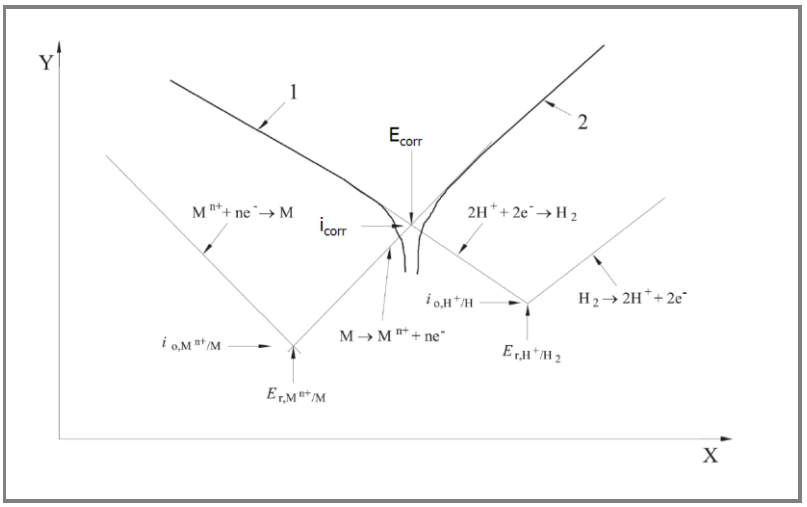

X	Potential
Y	Log (current density)
1	Cathodic curve
2	Anodic curve
E_{corr}	Corrosion potential
i_{corr}	Corrosion current density
E_r	Reversible electrode potential
i_0	Exchange current density

Figure 2.5 – Schematic anodic and cathodic polarization curves for metals in a system where the cathodic reaction is the reduction of protons [54]

2.2.3.1 Potentiodynamic test on carbon steel

Anodic and cathodic polarization curves were obtained on carbon steel specimens, grade API 5L X52 (Table 2.1), in the presence of AC interference. After preparation and cleaning operations according to ASTM G1-03 [52], the specimen was placed in a sample holder (Figure 2.3) that allows exposing a net surface area of 1 cm^2 of the sample to the electrolyte. The sample was placed in a cylindrical cell (diameter 100 mm; height 150 mm) containing soil, composed by silica sand and the same soil-simulating solution used for galvanostatic and potentiostatic tests (200 mg/L chlorides and 500 mg/L sulphate ions). Electrical resistivity is about 5 Ω·m. The test cell contains the working electrode, a SSC saturated reference electrode and two counter electrodes to supply the polarization (DC) and the interference (AC) currents by means of the electrical circuit described in Paragraph 2.1. Counter electrodes were positioned so that the current distribution around the specimen is symmetrical.
In order to minimize the potential drop between the reference electrode and the working electrode, a Luggin capillary was used.
Polarization curves were obtained in the presence of 100 and 240 A/m^2 AC density, the same values adopted in AC propagation test described in Paragraph 2.3.2. Polarization curves in the presence of AC were compared with the control curve obtained without AC in a continuous mode by means of a EG&G Model 273 potentiostat with a scan rate of 0.17 $mV \cdot s^{-1}$, according to the standard [54]. Nevertheless, for experimental limits in the presence of AC, potentiodynamic test wasn't carried out in a continuous mode (continuous displacement of potential) but by steps, varying the potential of 10 mV every 60 seconds so that the same scan rate of the control test was adopted. The general test procedure is outlined as follows:

- preparation and cleaning operations of the sample, according to ASTM G1-03 [52];
- positioning of the sample in the sample holder (Figure 2.3);
- assembly of the test cell with DC and AC counter electrodes and the reference electrode;
- recording of the open-circuit potential of the specimen with time for one hour. This period allows to attain a steady value of the open-circuit potential [54];
- AC superimposition for 24 hours;
- potential scan in the anodic or cathodic direction, starting from the corrosion potential and recording of the external current supplied.

In the anodic polarization test, carbon steel was polarized from the corrosion potential to 0.0 V CSE; in the cathodic polarization test, the sample was polarized to -1.4 V CSE, starting from the corrosion potential.

2.2.3.2 Potentiodynamic test on magnesium alloy anode

Anodic and cathodic polarization curves were obtained on AZ63D (UNS M11636 [55], Table 2.4) magnesium alloy specimens used as galvanic anode in the AC propagation tests (Paragraph 2.3.2). Cylindrical samples (20 mm diameter and 40 mm height) were obtained from a commercial bar and were electrically connected to a copper cable by a rivet on the upper surface. Electrical connection was isolated with epoxy resin. The net surface area exposed to the soil-simulating environment was 28.3 cm^2. After preparation and cleaning operations according to ASTM G1-03 [52], the specimen was placed in the same cell test described in Paragraph 2.2.3.1.

Table 2.4 – AZ63D (UNS M11636): chemical composition by weight [55]

Grade	UNS	% Al	% Zn	% Mn	% Si	% Cu	% Ni	% Fe	% Mg
AZ63D	M11636	5.0-7.0	2.0-4.0	0.15-0.7	0.30	0.10	0.003	0.003	balance

Polarization curves were obtained in the presence of 5 and 13 A/m^2 AC density, the same measured on magnesium alloy anodes used in AC propagation test (Paragraph 2.3.2). AC and DC were overlapped to the sample by means of the electrical circuit described in Paragraph 2.1 through two activated titanium counter electrodes. Polarization curves with AC stationary interference were compared with the reference curve obtained without AC by means of a EG&G Model 273 potentiostat with a scan rate of 0.17 $mV \cdot s^{-1}$, according to the standard [54]. As discussed before (Paragraph 2.2.3.1), potentiodynamic tests in the presence of AC were carried out by steps, varying the potential of 10 mV every 60 seconds so that the same scan rate of the test without AC was used. In the anodic polarization test, specimen was polarized to -0.6 V CSE, starting from the corrosion potential. In the cathodic polarization test, the sample was polarized to -2.0 V CSE, starting from corrosion potential.

2.2.4 Linear polarization resistance measurement

As discussed in Paragraph 1.7 regarding CP criteria assessment in the presence of AC, there are some evidences about the formation of protective passive film on iron in CP condition. For instance, Carpentiers et al. [48] state that high pH is favorable because of the formation of a "perfectly protective passive film".
Alkaline pH is achieved in the electrolyte close to the metal surface due to the cathodic reactions that occur on the metal in CP condition (Eq. 1.5). A widely discussion on this topic will be provided in Chapter 4.
During this research, linear polarization resistance (LPR) measurements were carried out on carbon steel specimens after a cathodic pre-polarization period. The aim of this test is to investigate the effect of a cathodic pre-polarization period on LPR, which is strongly affected by the presence of a protective and adherent oxide film on the metal surface able to reduce corrosion rate with respect to corrosion rate measured in active condition without a previous cathodic pre-polarization.
LPR measurement is an accurate and rapid way to measure the general corrosion rate of metals corresponding to the corrosion potential, E_{corr} [56]. A small potential scan, ΔE (t), defined with respect to the corrosion potential ($\Delta E = E - E_{corr}$), is applied to the metal and the current is recorded. The relation between potential (E) and the current density (i) is:

$$\text{(Eq. 2.3)} \qquad i = i_{corr}\left[\exp\left(\frac{2.303(E-E_{corr})}{\beta_a}\right) - \exp\left(\frac{-2.303(E-E_{corr})}{\beta_c}\right)\right]$$

where β_a and β_c are anodic and cathodic Tafel slopes, respectively. The current varies approximately linearly with potential within a few millivolts of polarization from corrosion

potential, E_{corr}. Eq. 2.3 can be mathematically linearized by taking its series expansion and by neglecting higher terms when $\Delta E/\beta < 0.1$. LPR is defined as the slope of the potential-current curve at i = 0:

(Eq. 2.4) $$LPR = \left(\frac{\partial \Delta E}{\partial i} \right)_{i=0;dE/dt \to 0}$$

Corrosion current density, i_{corr}, is related to LPR by the Stern-Geary coefficient, B:

(Eq. 2.5) $$i_{corr} = 10^3 \frac{B}{LPR}$$

LPR is expressed in $\Omega \cdot cm^2$, i_{corr} in mA/cm^2 and B in Volts. The Stern-Geary coefficient is given by the following equation:

(Eq. 2.6) $$B = \frac{\beta_a \beta_c}{2.303(\beta_a + \beta_c)}$$

Corrosion rate, CR (mm/year) can be determined from Eq. 2.7 in which EW is the equivalent weight (g/96,489 A·s) and ρ is the density of the metal (g/cm^3):

(Eq. 2.7) $$CR = 3.27 \times 10^{-3} \frac{i_{corr} EW}{\rho} = 3.27 \times \frac{B \cdot EW}{LPR \cdot \rho}$$

Eq. 2.5 shows that corrosion current density (related to corrosion rate by Eq. 2.7) increases by decreasing the polarization resistance.

LPR measurements were carried out on carbon steel specimens grade API 5L X52 (Table 2.1) cathodically pre-polarized to different values of the protection potential. After preparation and cleaning operations according to ASTM G1-03 [52], the specimen was placed in the sample holder shown in Figure 2.3, exposing a net surface area of 1 cm^2. The sample was placed in a cylindrical cell (diameter 100 mm; height 150 mm) containing soil, composed by silica sand and a soil-simulating solution (200 mg/L chlorides and 500 mg/L sulphate ions). Electrical resistivity is about 5 $\Omega \cdot m$. The test cell contains the working electrode, a SSC saturated reference electrode and a counter electrode to provide the DC polarization current. In order to minimize the potential drop between the reference electrode and the sample, a Luggin capillary was adopted.

After ten minutes in free corrosion condition, specimens were cathodically polarized in a potentiostatic mode for three days at different CP levels by means of an EG&G Model 273 potentiostat. Applied protection potentials were: -0.850 V, -0.950 V, -1.100 V and -1.200 V CSE. After the polarization time, specimens were maintained in free corrosion condition (without CP) until the open-circuit potential initially measured (before cathodic polarization) was attained. The time required to reach the initial potential (de-polarization time) increases by decreasing the protection potential applied previously. LPR measurements were carried out according to the standards [54, 56].

In this test, the assumption is that the surface condition of the metal doesn't change during the de-polarization time that runs between the end of the pre-polarization period and the LPR measurement in free corrosion condition. Although this assumption could be too restrictive, LPR measurement can be useful to investigate the effect of CP on the formation of a protective passive film. In all tests, the de-polarization time was in the range from ten to twenty minutes.

2.2.5 Alternating voltage measurement

As discussed in Paragraph 1.4.1, the technical specification CEN/TS 15280:2006 [12] reports alternating voltage (AV) of an interfered structure as the most important parameter to take into account in order to evaluate AC corrosion likelihood. AV can be directly measured on a pipeline (Figure 2.6) by means of a high input impedance AC voltmeter connected with one pole to a reference electrode, which is placed in contact with the soil above the pipeline, and with one pole connected to the pipeline at a test station [12]. The voltmeter indicates the instantaneous value of the induced AV on the pipeline. Nevertheless, this measurement includes the ohmic drop contribution that should be eliminated (or minimized) in order to evaluate the true AV induced on the structure. The ohmic contribution depends on the distance between the reference electrode and the metal, the environment resistivity and the circulating current (second Ohm's law).
This test aims to measure the IR-free AV and the corresponding AC density exchanged by a carbon steel sample cathodically protected and interfered by AC. Potentiostatic tests were carried out on carbon steel specimens, grade API 5L X52 (Table 2.1), in the presence of AC interference. After preparation and cleaning operations according to ASTM G1-03 [52], the specimen was placed in a sample holder (Figure 2.3), exposing a net surface area of 1 cm^2.
The test cell (Figure 2.7) consists of the working electrode, two activated titanium counter electrodes and a SSC saturated reference electrode in a Luggin capillary with salt-bridge connection. Test cell was filled with 1 L of a solution containing 500 mg/L of sulphate ions. Electrical resistivity is 8.2 Ω·m. The Luggin tube was filled with the test solution and the tip was positioned in close proximity to the working electrode in order to minimize the ohmic drop contribution. Carbon steel sample was cathodically polarized by a potentiostat AMEL Model 2051 Potentiostat through an activated titanium anode for three days, until a steady value of the protection current density was reached. Then, an AV was overlapped to the sample by means of the electrical circuit described in Paragraph 2.1 through a further activated titanium counter electrode (Figure 2.7). The AV between the sample and the reference electrode in the Luggin tube was increased by steps (about 10 mV every minute) and the corresponding AC was measured by means of a digital amperometer connected in series to the circuit. Three values of the protection potential were applied: -1.1 V, -1.2 V and -1.3 V CSE.

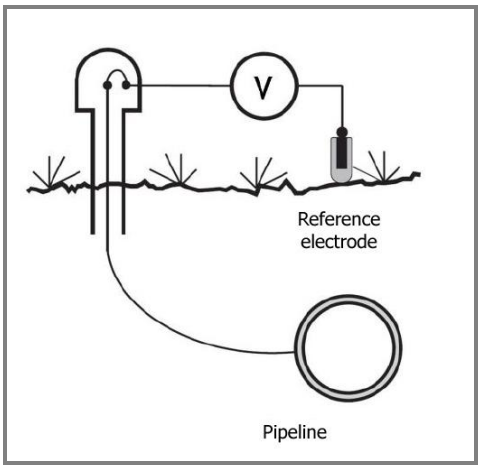

Figure 2.6 – AC voltage measurement on a pipeline

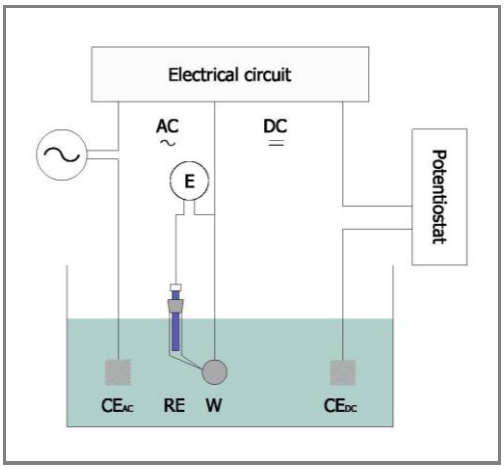

Figure 2.7 – AV measurement: test cell arrangement

2.2.6 Tests on passive metals

As mentioned, laboratory tests were carried out on passive metals, i.e. in the presence of a thin, adherent, protective layer formed on the metal surface.

These tests aim to study the effect of AC interference on passivity by means of:
- critical chlorides threshold measurement in the presence of AC;
- potentiodynamic test: AC effect on polarization curves;
- AV measurement.

Tests were performed on carbon steel in alkaline solution and on stainless steels in neutral solution.

2.2.6.1 Critical chlorides threshold measurement in the presence of AC

The test aims to study the AC effect on critical chloride threshold. Halogens, as chloride ions, are depassivating agents that, over certain content in the solution in contact with the metal (the so-called critical threshold), cause the local breakdown of the protective film on the surface. As a consequence, localized corrosion (as pitting corrosion) occurs.
Long-term exposition tests were carried out on austenitic stainless steel type EN 1.4401 X5 CrNiMo 17-12-2 (UNS S31600, Figure 2.8) in neutral solution. Stainless steel chemical composition is reported in Table 2.5 [57]. Specimens (15 x 15 x 2 mm) were obtained from commercial plane slabs; a net surface area of 2.25 cm^2 was exposed to the solution. The electrical connection was insulated with epoxy resin (Figure 2.9). Tests were carried out in neutral solution, initially chlorides-free. Samples were placed in cylindrical cells (diameter 150 mm; height 200 mm) and connected to an external AC feeder (variac device) to provide a voltage-adjustable source of AC electricity. Four values of AC density were applied for 90 days (stationary interference): 10, 20, 40 and 50 A/m^2. For each value of AC density, four specimens were prepared to ensure test repeatability. Chlorides were added in the solution by steps (250 mg/L each week). Critical chloride threshold was measured according to the appearance of corrosion products on the metal surface.

Critical chloride threshold measurement was also carried out on carbon steel specimens in alkaline solution. Indeed, in aerated alkaline environment with pH > 11.5 and in the absence of chlorides, carbon steel is protected from corrosion by a thin passive film. Carbon steel specimens (diameter 10 mm, length 20 mm) were obtained from commercial steel concrete reinforcements (type B 450 C, Figure 2.10). Chemical composition [58] is reported in Table 2.6. Specimens were electrically connected to a copper cable and insulated with epoxy resin, so that a net surface area of 78.5 mm^2 was exposed to the solution. Tests were carried out in synthetic concrete pore simulating solution (NaOH 0.01 M saturated with $Ca(OH)_2$, pH 12.6). During the first week, solution was chlorides free; then, chlorides were periodically added in solution by steps for 50 days. Five values of AC density were applied by means of an external AC feeder (variac device): 10, 20, 30, 40 and 50 A/m^2.
During the test, steel potential was measured by means of an external SSC saturated reference electrode and a high impedance voltmeter (Figure 2.11). Critical chloride threshold was measured according to the appearance of corrosion products on the metal surface and by potential monitoring, as will be discussed in Chapter 4. Control tests were also performed in the absence of AC interference. In all the tests, temperature was maintained at 20°C (± 2°C) by means of an external water circuit.

Table 2.5 – X5 CrNiMo 17-12-2 (UNS S31600): chemical composition by weight [57]

EN	UNS	% C max	% Cr	% Ni	% Mo	% Mn max	% Si max	% P max	% S max
1.4401	S31600	0.07	16.5-18.5	10.0-13.0	2.0-2.5	2.00	1.00	0.045	0.015

Table 2.6 – B 450 C: chemical composition by weight [58]

EN	% C max	% S max	% P max	% N max	% Cu max	% Carbon equivalent max
10080:2005	0.24	0.055	0.055	0.014	0.85	0.52

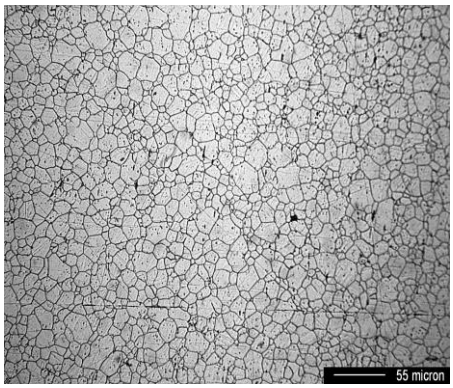

Figure 2.8 - X5 CrNiMo 17-12-2: microstructural analysis

Figure 2.9 - X5 CrNiMo 17-12-2: specimen

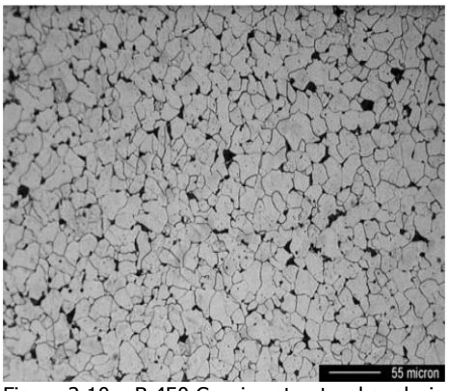

Figure 2.10 – B 450 C: microstructural analysis

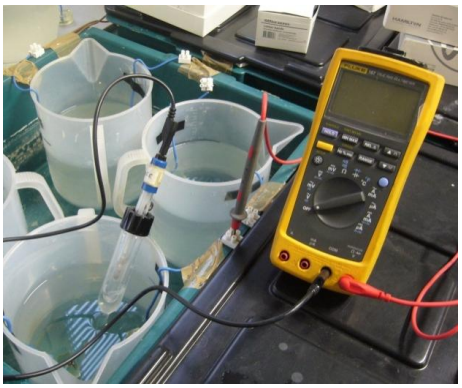

Figure 2.11 – Potential monitoring

Table 2.7 – X12 Cr 13 (UNS S41000): chemical composition by weight [57]

EN	UNS	% C max	% Cr	% Ni max	% Mn max	% Si max	% P max	% S max
1.4006	S41000	0.08-0.15	11.5-13.5	0.75	1.50	1.00	0.040	0.015

2.2.6.2 Potentiodynamic test on passive metals: AC effect on polarization curves

As discussed in Paragraph 2.2.3, potentiodynamic polarization test can provide useful information regarding corrosion mechanism, corrosion rate and susceptibility of specific materials to corrosion in designated environments.
Potentiodynamic tests were carried out during an internship period of four months in the AC corrosion group of the Metallurgical and Materials Engineering Department of Colorado School of Mines (Golden, CO, USA). Tests were performed on 13% chromium super martensitic stainless steel in artificial sea water in the presence of AC interference.
This research aims to provide a thought understanding of the AC corrosion mechanism of stainless steel pipelines in the subsea oil&gas production in the presence of direct electrical heating systems (DEH) [59]. Indeed, the formation in the pipeline of hydrates that starts around 25°C (depending on process conditions) can be prevented by using thermal insulation and DEH systems by forcing a large AC through the pipeline. Figure 2.12 shows a sketch of the DEH system [60]. In a DEH system, the pipe is an active conductor in a single-phase electric circuit in which AC is typically supplied from the platform main power. Sea water acts as an electric conductor in parallel with the pipe: the current supplied is divided between the pipe and sea water. Typically, 40% of the total current flows in sea water. Potentiodynamic polarization tests were carried out on super martensitic stainless steel type EN 1.4006 X12 Cr 13 (UNS S41000) in artificial sea water. Chemical composition is reported in Table 2.7 [57].

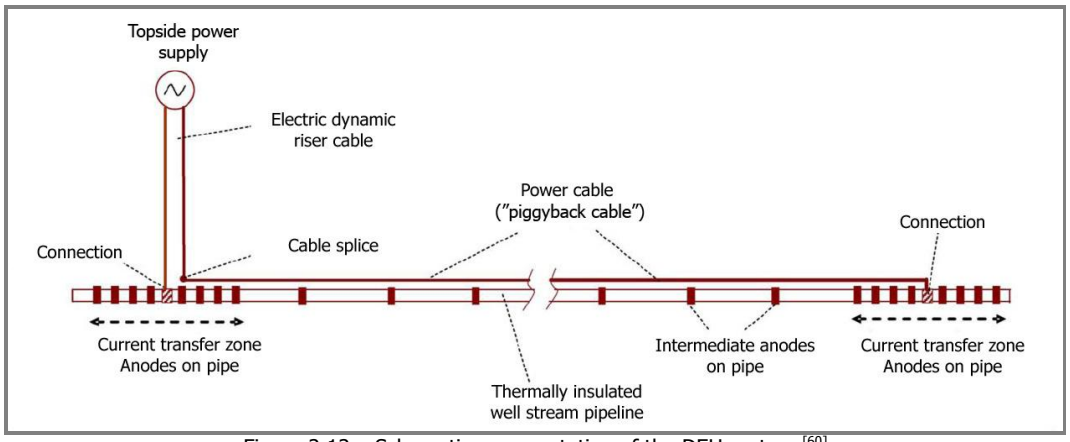

Figure 2.12 – Schematic representation of the DEH system [60]

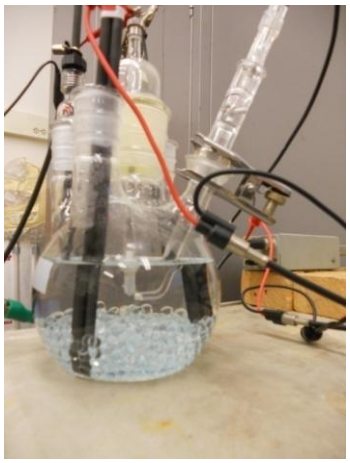

Figure 2.13 – Electrochemical cell for potentiodynamic tests

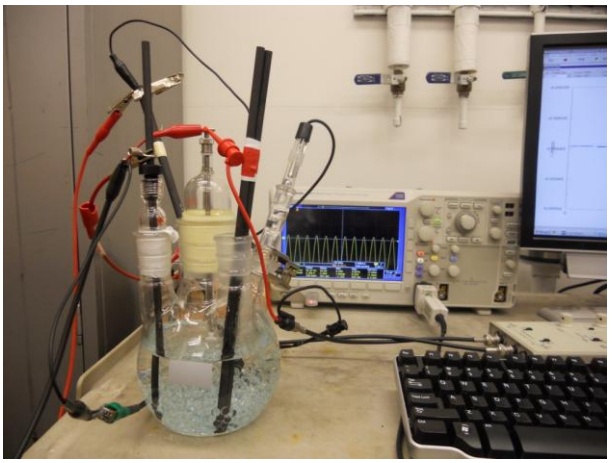

Figure 2.14 – Potentiodynamic tests: experimental arrangement

Anodic and cathodic polarization curves were obtained on stainless steel specimens in the presence of AC. After preparation and cleaning operations according to ASTM G1-03 [52], the specimen was placed in a suitable electrochemical cell (Figure 2.13) containing substitute ocean water, according to the standard designation ASTM D 1141–98 (Reapproved 2008) [61]. The pH of the solution was 8.225 ± 0.025 at 25°C.

The test cell contains the working electrode, a SCE[3] reference electrode and two graphite counter electrodes to supply the polarization (DC) and the interference (AC) currents by means of the electrical circuit similar to that described in Paragraph 2.1.

In order to minimize the potential drop between the reference electrode and the working electrode, a Luggin capillary was adopted. Anodic and cathodic polarization curves were performed in the presence of 40, 240 and 500 A/m^2 of AC densities [59]. Initially, samples were maintained in free corrosion condition for one hour to attain a steady value of the open-circuit potential [54]. Then, AC was applied for a calculated time, so that the electrical charge (current × time) transferred by the sample was kept constant. Corrosion potential was also monitored by means of a Tektronix DPO 3012 digital oscilloscope (Figure 2.14). DC potential was applied from -1.4 V to 0.2 V SCE by means of a EG&G Model 273 potentiostat with a scan rate of 0.17 mV·s^{-1} [54].

[3] SCE, saturated calomel electrode, +0.244 V SHE

2.2.6.3 Alternating voltage measurement

Alternating voltage (AV) measurements were carried out on two austenitic stainless steels with different PREN (Pitting Resistance Equivalent Number), accordingly to the procedure described in Paragraph 2.2.5:

- type EN 1.4301 X5 CrNi 18-10 (UNS S30400, PREN 18);
- type EN 1.4401 X5 CrNiMo 17-12-2 (UNS S31600, PREN 25).

Steels chemical composition is reported in Table 2.8 [57]. The test cell (Figure 2.15) consists of the working electrode, a SSC saturated reference electrode placed in a Luggin tube with salt-bridge connection and an activated titanium counter electrode to supply AC to the sample. The test cell was filled with 1 L of a solution containing 500 mg/L of sulphate ions. Electrical resistivity is 8.2 Ω·m. The AV between the sample and the reference electrode in the Luggin tube was increased by steps (about 10 mV every minute) and the corresponding AC was measured by means of a digital amperometer connected in series to the circuit. Three tests for each material were carried out.
Moreover, the effect of a chemical passivation treatment on austenitic stainless steel type EN 1.4401 X5 CrNiMo 17-12-2 (UNS S31600) was studied. The formation of the protective passive film on a stainless steel occurs spontaneously in air or other oxygen-containing environment. Nevertheless, chemical treatments may facilitate the more rapid formation of the passive film on a stainless steel surface free of oxide scale and foreign matter. Such treatments, also called passivation treatments in common usage, are designed as post-cleaning treatments that provide a stronger passivation on the metal surface [62]. Passivation treatment was carried out by immersion of the samples for 30 minutes in a solution containing 40% volume of nitric acid at 25°C, according to the standard [62].

Table 2.8 – X5 CrNi 18-10 (UNS S30400) and X5 CrNiMo 17-12-2 (S31600): chemical composition by weight [57]

EN	% C max	% Cr	% Ni	% Mo	% Mn max	% Si max	% P max	% S max	PREN
1.4301	0.07	17.0-19.5	8.0-10.5	-	2.00	1.00	0.045	0.015	18
1.4401	0.07	16.5-18.5	10.0-13.0	2.0-2.5	2.00	1.00	0.045	0.015	25

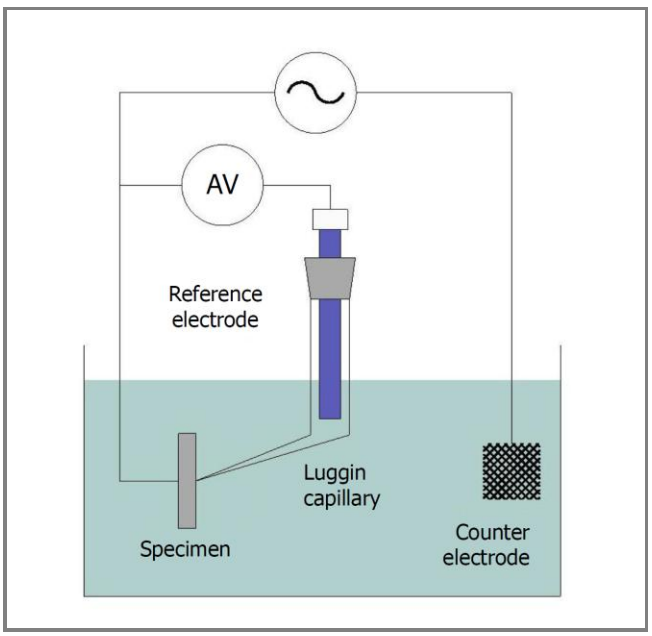

Figure 2.15 – AV measurement: schematic representation of test cell arrangement

2.2.7 pH measurement in cathodic protection condition

As widely discussed in Chapter 1 (Paragraph 1.6.4), the pH at the interface between the environment and the metal in CP condition could be an important factor in order to define corrosion condition in the presence of AC interference. It's well known that, in CP condition, the alkalization of the environment close to the metal occurs due to the cathodic reactions on the metal, according to Eq. 1.5.
This test aims to measure the pH profile at the interface between carbon steel in CP condition and the electrolyte varying the protection current density. A suitable cylindrical test cell (diameter 150 mm; height 200 mm) was designed in order to perform the pH measurement (Figure 2.16). After preparation and cleaning operations according to ASTM G1-03 [52], a circular carbon steel specimen, grade API 5L X52 (Table 2.1), was placed on the bottom of the cell so that only the top-surface (diameter 25 mm) was exposed to the solution in the cell. The sample simulates a circular defect of an insulator coating of a buried pipeline. A soil-simulating solution (100 mg/L chlorides and 200 mg/L sulphate ions) was used. The sample was electrically connected by means of a screw on the side of the cell. CP was applied through an activated titanium counter electrode and an AMEL 2051 Potentiostat-Galvanostat in a galvanostatic mode.

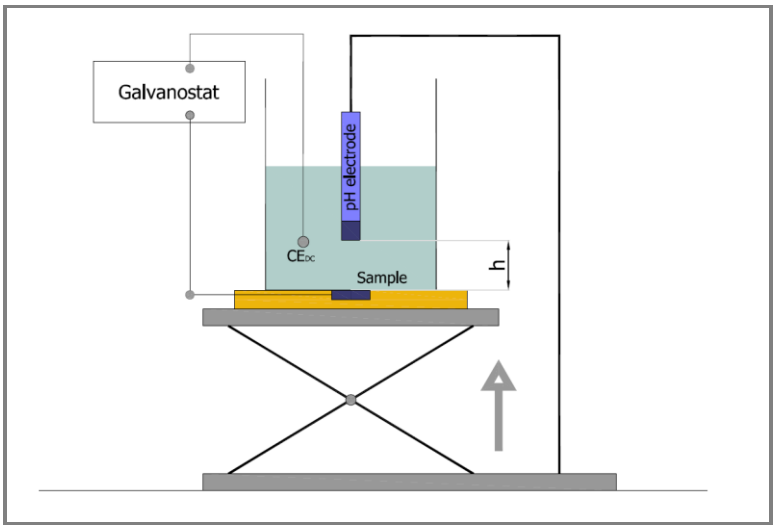

Figure 2.16 – pH measurement in CP condition: experimental arrangement


Figure 2.17 – Test cell for pH measurement


Figure 2.18 – Probe for pH measurement

A digital pH-meter (± 0.1 pH unit) was set above the sample and fixed on a vertical support (Figure 2.16 and Figure 2.17). The pH-meter has a flat probe on the bottom surface (Figure 2.18). The pH profile was measured varying the distance (h) between the pH probe and the metal surface by means of a pantograph system which vertical displacement was regulated by the rotation of a screw with an accuracy of 0.5 mm for each full rotation. Distance was measured by a digital caliber (accuracy = ±0.01 mm). The pH-meter was calibrated before each measurement. The sample was cathodically polarized for one hour to attain a steady value of the protection potential. Four CP current densities were applied: 0.5, 1, 5 and 7 A/m^2. Then, the distance (h) between the sample and the pH electrode was decreased by steps until the contact between the pH meter and the metal. Electric interference prevented to carry out the pH measurement in the presence of AC.

2.3 AC CORROSION PROPAGATION TESTS

AC corrosion propagation tests aim to measure corrosion rate of cathodically protected carbon steel specimens in the presence of AC interference, varying protection and interference conditions. Corrosion rate was measured by means of corrosion mass loss and penetration depth measurements. Nevertheless, some considerations should be stated beforehand. Since AC corrosion morphology is localized, penetration depth measurement represents the proper method to evaluate AC corrosion damage. Conversely, mass loss rate is not recommended to predict the service (or the remaining) life of a structure and can be misleading if corrosion is localized. Corrosion rate measurements by mass loss were carried out in order to estimate AC corrosion likelihood in different protection and interference conditions and results will be discussed in Chapter 4. A more accurate analysis of AC corrosion propagation was also carried out by means of penetration depth, number and size of corrosion attacks measurements and will be discussed in Chapter 5. Moreover, while corrosion rate calculated by mass loss measurements is the average corrosion rate in the period of AC interference, penetration depth measurements were carried out varying the exposition time to AC interference in order to provide information of penetration depth-time dependence.

2.3.1 Mass loss test

Long-term exposition tests were carried out on carbon steel specimens, grade API 5L X52 [51], in CP condition and in the presence of AC stationary interference. After preparation and cleaning operations according to ASTM G1-03 [52], carbon steel specimens were placed in a cylindrical sample holder (Figure 2.3), exposing a net surface area of 1 cm^2 to the electrolyte. Samples were placed in a cylindrical cell (diameter 150 mm; height 200 mm) containing soil, composed by silica sand and a soil-simulating solution (200 mg/L chlorides and 500 mg/L sulphate ions). Electrical resistivity is about 5 Ω·m.
CP was applied in either galvanostatic or potentiostatic way by means of an external DC feeder. Current was provided to the carbon steel specimen (working electrode) through an activated titanium insoluble anode (Ti-MMO). Protection current density and potential were applied in the range from 0.1 to 10 A/m^2 and from -0.850 V CSE to -1.500 V CSE, respectively. AC was overlapped to the sample by means of the electrical circuit described in Paragraph 2.1 through a further activated titanium counter electrode or by means of a second carbon steel specimen. AC was applied up to 800 A/m^2 in order to obtain different interference conditions. In order to check protection condition, protection potential was measured twice a week by means of an external SSC saturated reference electrode in a Luggin capillary tube and a high impedance voltmeter. A schematic view of the electrical system is reported in Figure 2.1. An external cooling water circuit was adopted to prevent the heating of the solution due to Joule effect (temperature = 20 ± 2 °C). After 120 days, specimens were extracted and mass loss was measured in order to calculate corrosion rate.

Average corrosion rate (CR) by mass loss measurement was calculated as follows, according to ASTM G1-03 [52]:

(Eq. 2.8) $$CR = \frac{8.76 \cdot 10^7 \cdot W}{A \cdot t \cdot \rho}$$

where W is the mass loss (g), A is the area of the specimen (cm^2), t is the time of exposure (hours) and ρ is the metal density (g/cm^3). Corrosion rate is assumed constant during the exposition time. Chemical and mechanical procedures were adopted to remove corrosion products from the surface. Mass loss was determined after every cleaning cycle by weighing the specimen, according to ASTM G1-03 [52]. Chemical cleaning was carried out by immersion of the specimen in a solution containing 500 mL hydrochloric acid, 3.5 g hexamethylene tetramine and reagent water to make 1000 mL for 10 minutes at 20 to 25°C [52]. Hexamethylene tetramine allows minimizing the dissolution of the metal base. Ultrasonic mechanical cleaning was used to remove heavily encrusted corrosion products in addition to chemical cleaning.

2.3.2 Penetration depth test

Since AC corrosion is localized, mass loss measurement is not ordinarily recommended to assess corrosion propagation because it doesn't provide information about corrosion penetration depth. In addition to mass loss measurements described in Paragraph 2.3.1, AC corrosion was evaluated by means of:

- penetration depth measurement;
- attacks number measurement;
- attacks size measurement.

Furthermore, the effect on AC of magnesium anode consumption was investigated.

2.3.2.1 Materials

Test was carried out on carbon steel specimens, grade API 5L X52, cathodically protected by means of a galvanic magnesium alloy, grade AZ63D (UNS M11636). Chemical composition of carbon steel and magnesium alloy is reported in Table 2.1 and Table 2.4, respectively.
After preparation and cleaning operations according to ASTM G1-03 [52], an insulated copper cable was welded to a circular carbon steel sample (diameter 14 mm). Electrical connection was insulated with epoxy resin, so that only a net surface area of 150 mm^2 was exposed to the surrounding environment. The specimen simulates a defect of a polymeric coating of a pipeline in CP condition (Figure 2.19). Galvanic anodes were obtained from a commercial cylindrical rod (diameter 20 mm, Figure 2.20). Galvanic anodes were sized according to the procedure described in Paragraph 2.3.2.2.

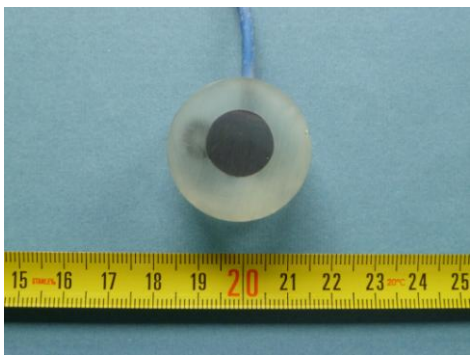

Figure 2.19 – Carbon steel specimen

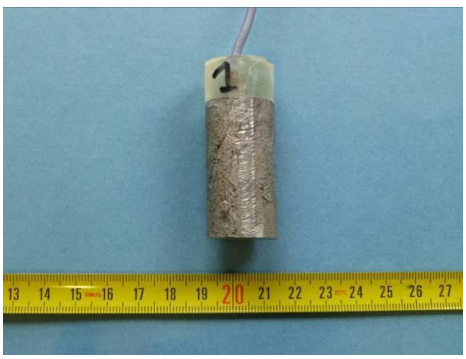

Figure 2.20 – Magnesium anode

2.3.2.2 Galvanic anode sizing

Two parameters, working potential and capacity, determine the protection performance of an anode [2]. Working potential determines the driving voltage and anode current output; the capacity, that is the charge per unit mass, defines the anode's consumption and therefore the mass necessary to ensure the duration of protection. Electrochemical properties of magnesium alloy AZ63D (UNS M11636) are reported in Table 2.9. When the anode works, it is consumed according to the anodic reaction that takes place on its surface. The metal mass loss is proportional to the charge it supplies to the cathode and is given by Faraday's law. Hence, for an anode, a theoretical consumption is defined as the mass that dissolves for each unit of charge produced. It is the inverse of capacity.

Table 2.9 – AZ63D (UNS M11636): electrochemical properties

Grade	UNS	Potential V CSE	Theoretical Capacity (A·h/kg)	Theoretical Consumption C_{th} (kg/A·y)	Efficiency (ε)
AZ63D	M11636	-1.55	2,200	3.98	50 %

The current supplied by the anode is given by Ohm's law:

(Eq. 2.9) $$I = \frac{\Delta E}{R}$$

where ΔE is the driving voltage given by the difference between cathode and anode potential and R is the total resistance, expressed as:

(Eq. 2.10) $$R = R_i + R_{cable}$$

where R_i is the electrolyte's ohmic resistance and R_{cable} is the metallic circuit resistance. Electrolyte resistance (R_i) is the sum of the cathodic and anodic local resistance, calculated from empirical equations.

The general galvanic anode sizing procedure is outlined as follows:

1) Calculation of the total protection current (I_{CP}), given by:

(Eq. 2.11) $$I_{CP} = i_{CP} \cdot S_{cath}$$

where i_{CP} is the protection current density and S_{cath} is the cathodic surface to protect (150 mm^2). To attain a protection current density of about 1 A/m^2, the galvanic anode must supply a current of 0.15 mA.

2) Calculation of the anode's total mass (W_{Mg}), given by:

(Eq. 2.12) $$W_{Mg} = I_{CP} \cdot C_{Mg} \cdot t$$

where t is time and C_{Mg} is the practical consumption of magnesium anode, given by:

(Eq. 2.13) $$C_{Mg} = \frac{C_{th}}{\varepsilon}$$

where C_{th} is the theoretical consumption and ε is the efficiency (Table 2.9). The practical consumption (C_{Mg}) is 7.96 kg/A·y. Nevertheless, in the presence of AC stationary interference, an over-consumption should be considered. Goidanich [63]

reported by experimental tests carried out in the first phase of this research project that steel-coupled magnesium anode corrosion increases in the presence of AC interference. Magnesium steel-coupled consumption increases of about one order of magnitude in the presence of 240 A/m^2 AC density, by extrapolation of corrosion rate data of Figure 2.21 [63]. Practical consumption was assumed one order of magnitude greater (79.6 kg/A·y) than the one in the absence of AC interference. With this assumption, the anodic mass required for one year is 12 g (by Eq. 2.12) that corresponds to a volume of 6.9 cm^3 (magnesium mass density = 1.74 g/cm^3). Considering a cylindrical anode (diameter 20 mm), the minimum length is 22 mm; the adopted one is 40 mm that corresponds to a surface area of 28.3 cm^2.

3) Calculation of the anodic resistance (R_a) with the empirical Mac Coy formula:

$$R_a = \frac{0.315\rho}{\sqrt{A}} \qquad \text{(Eq. 2.14)}$$

where ρ is soil resistivity (assumed 200 Ω·m in dry period) and A is the anodic surface area ($28.3 \cdot 10^{-4}$ m^2). Anodic resistance results 1,185 Ω.

4) Calculation of the total resistance of the CP system (Eq. 2.10). Generally, the electrolyte's ohmic resistance (R_i) may be considered the sum of two contributions:

$$R_i = R_a + R_c \qquad \text{(Eq. 2.15)}$$

where R_a is the anodic resistance and R_c is the resistance (assumed negligible) close to the cathode. The metallic circuit resistance (R_{cable} in Eq. 2.10) is 200 Ω due to the presence of shunts for voltage measurements. Total resistance (Eq. 2.10) is 1,385 Ω.

5) Calculation of the current supplied by the magnesium anode by the ratio between the driving voltage and the total resistance. The driving voltage of steel structures protected with magnesium anodes typically assumes a value of 0.8 V. The calculated protection current supplied by the anode is 0.58 mA, greater than the one required (Point 1, 0.15 mA).

Summarizing, cylindrical magnesium anodes (diameter 20 mm; length 40 mm) were used.

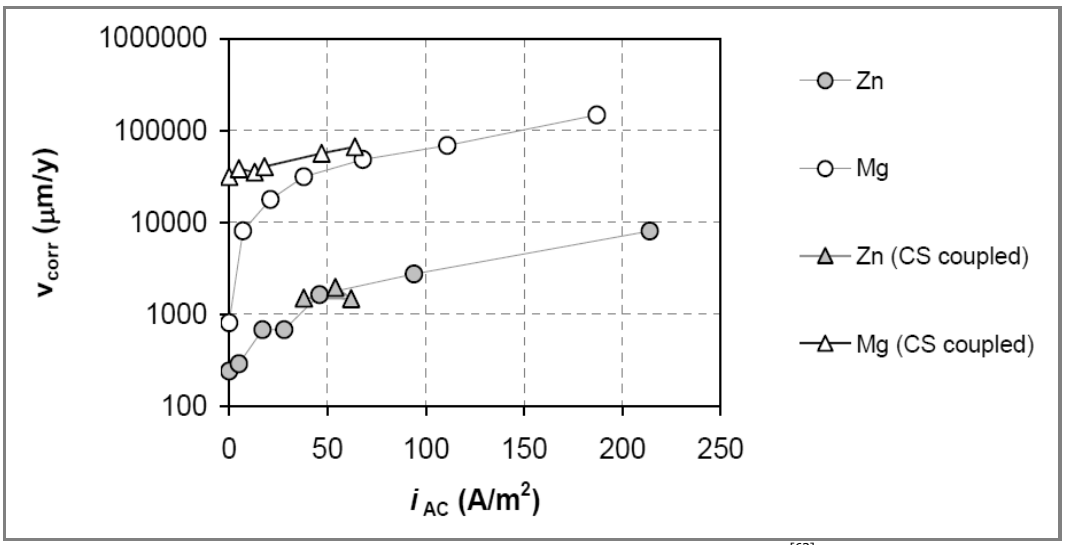

Figure 2.21 – Effect of AC density on corrosion rate from [63]

2.3.2.3 Cell test

The steel sample and the galvanic anode were placed in a corrosion cell (height 80 mm, diameter 85 mm, Figure 2.22) containing soil, composed by silica sand and a soil-simulating solution (200 mg/L chlorides and 500 mg/L sulphate ions). Electrical resistivity is 5 Ω·m.
Four batches (A-D) were prepared (Figure 2.23), each consisting of eight corrosion cells. 240 A/m^2 AC was applied in seven cells; the remaining one is the control cell in which AC interference wasn't applied. Samples and anodes of each batch were extracted every month from one to four months, in order to evaluate AC corrosion penetration depth with time (Table 2.10).

2.3.2.4 Electrical circuit

Cells were connected in series in order to apply the same AC to the samples (Figure 2.24). A capacitor (C = 10 μF; V_{max} = 630 V) allows AC circulation between the cells but prevents DC interference among the meshes of the circuit. In each cell, the galvanic anode provides the protection current (DC) and the interference current (AC) through a suitable electrical circuit shown in Figure 2.24. 240 A/m^2 stationary AC density was applied to the working electrode; this value corresponds to 13 A/m^2 to the galvanic anode, due to the greater anodic surface area. CP current was calculated by means of the voltage drop measurement through the shunt R_{CP} that connects the working to the anode. AC was provided by an AC feeder (variac device) and was checked by means of the shunt R_{AC}. A suitable ratio between R_{CP} and R_{AC} was adopted to force the AC flowing in the cell. In the external branch in parallel to the cell, AC was less than 1% of the total current.

Figure 2.22 – Test cell


Figure 2.23 – Experimental arrangement

Table 2.10 – AC propagation test: batches and cells test

Batch	# cells PC + AC	AC density (A/m^2)	# cells only PC	# total cells	Test time (months)
A	8	240	1	9	1
B	7	240	1	8	2
C	7	240	1	8	3
D	7	240	1	8	4

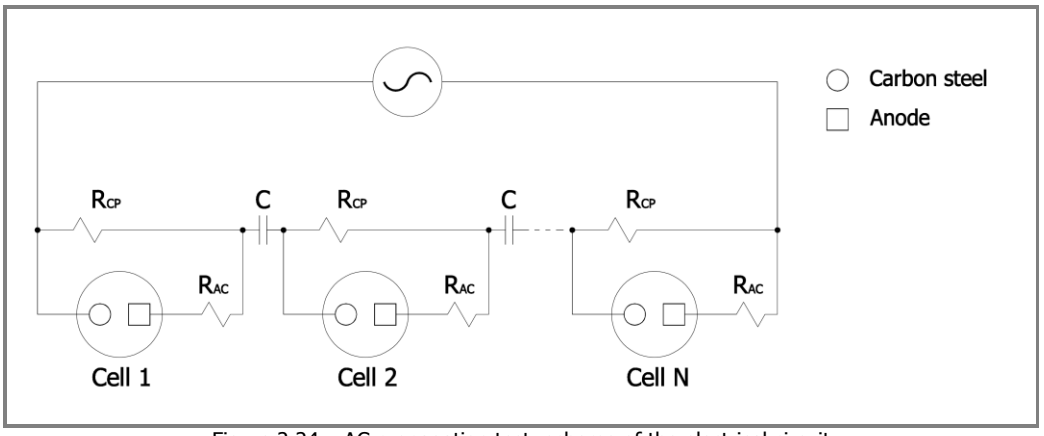

Figure 2.24 – AC propagation test: scheme of the electrical circuit

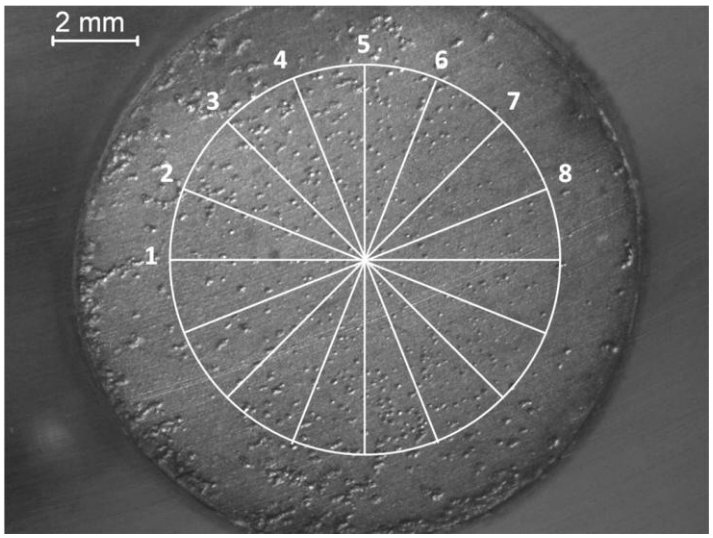

Figure 2.25 – Scanning of the metal surface for penetration depth measurements by laser profilometer

2.3.2.5 Monitoring

CP protection was applied for one week, by means of the connection between carbon steel and magnesium anode. CP monitoring was carried out by means of protection potential and protection current measurements. Protection potential was measured by means of an external CSE reference electrode and a high impedance voltmeter. AC was supplied in a stationary way, keeping constant the AV drop through R_{AC} shunt (Figure 2.24) by adjusting the AC power supply.

2.3.2.6 Corrosion penetration depth measurement

As discussed previously, AC corrosion attacks are localized on the metal surface, hence the most proper method to evaluate AC corrosion damage is penetration depth measurement.
After drawing, corrosion products were removed from the samples by chemical and mechanical procedures. Chemical cleaning was carried out by immersion of the specimen in a solution containing 500 mL hydrochloric acid, 3.5 g hexamethylene tetramine and reagent water to make 1000 mL for 10 minutes at 20 to 25°C [52]. Hexamethylene tetramine allows minimizing the dissolution of the metal base. An ultrasonic mechanical cleaning was used to remove heavily encrusted corrosion products in addition to the chemical cleaning.

Penetration depth measurement was carried out by means of an optical laser profilometer UBM Microfocus, by scanning eight diameters (9 mm long) of a circular area of 64 mm^2 (Figure 2.25). Due to experimental limitations it wasn't possible to scan the entire surface area of the sample. Lateral and vertical resolution is 0.01 μm.
X-ray diffraction technique was carried out to analyze corrosion products and scale formed on the metal surface during the exposition time.

2.3.2.7 Number and size of corrosion attacks

The number of corrosion attacks was determined by means of a photo editing technique applied on surface images obtained with a digital camera Leica DFC 290 of a stereoscope model Wild 6X-50X (6X magnification). Each image was divided in four squares (1024 x 768 pixels) using the software Microsoft Office Picture Manager. Corrosion attacks were counted by using the software GIMP 2.6 (GNU Image Manipulation Program). The software allows setting the diameter of a circular pointer, refereed to the length of the marker in the image obtained at the stereoscope. Three values of the pointer diameter were chosen: 100 μm, 200 μm and 400 μm: if the border line of the corrosion attack was completely inscribed in the pointer, then its maximum size (d) is lower than the diameter of the pointer itself. Corrosion attacks were divided in three dimensional classes, depending on the diameter of the attack (attacks with diameter smaller than 100 μm weren't considered):

- 100 μm < d < 200 μm
- 200 μm < d < 400 μm
- d > 400 μm

Corrosion attacks were also divided in central (bulk) or board attacks. In board attacks, the border line of the corrosion attack is partially enclosed in the metal, due to the presence of the epoxy resin at the edge. In central attacks, instead, the border line is completely included on metal surface.

2.3.2.8 Anodic consumption in the presence of AC

Magnesium alloy consumption was evaluated by means of mass loss measurement. As discussed in Paragraph 2.3.2.2, magnesium anodes were over-sized to take into account the increase in the anodic consumption in the presence of AC interference, taken from previous tests carried out in the research project [63]. After drawing, sand and corrosion products were removed from the metal surface, according to the standard [52]. In addition, ultrasonic mechanical cleaning was used to remove heavily encrusted corrosion products in addition to the chemical cleaning. Mass loss measurement was carried out by means of a digital balance (accuracy = ±0.1 mg).

Chapter 3

Results

Part 1 – AC effect on protection potential and current

As discussed in Paragraph 1.1.5, cathodic protection (CP) criteria are generally based on the value of the structure-to-electrolyte potential. The potential measurement of a metallic structure as a buried pipeline is therefore necessary in order to assess CP effectiveness [3, 4]. Nevertheless, the potential measurement could be affected by errors, e.g. caused by the IR drop contribution due to the protection current or any other current in the environment between the structure and the reference electrode. The potential measured without IR drop is called IR-free potential (Paragraph 1.1.5). According to the standard [3], carbon steel structures in soil with IR free potentials below -0.850 V CSE (or -0.950 V CSE in the presence of sulphate reducing bacteria) operate in protection condition, i.e. corrosion rate is negligible or acceptable (lower than 0.01 mm/y [3]) so that corrosion damage cannot occur during the designed lifetime of the structure. Experimental tests were carried out in order to investigate the effect of AC on IR-free protection potential and protection current.

3.1 AC EFFECT ON PROTECTION POTENTIAL

As widely discussed in Chapter 1, in the presence of AC interference corrosion can occur on carbon steel structures in CP condition even if the potential matches the -0.850 V CSE criterion. Galvanostatic tests (Paragraph 2.2.1) were carried out on carbon steel specimens, grade API 5L X52 (Table 2.1) in the presence of stationary AC interference in order to study the AC effect on protection potential. In a galvanostatic test, a constant current (DC) is applied and the potential is measured. Protection current density was applied in the range between 0.1 and 10 A/m^2 by means of an external DC feeder. AC was overlapped to the sample by steps, increasing AC density every 30 minutes from 10 up to 200 A/m^2. Experimental conditions are summarized in Table 2.2. During each step (30 minutes long), protection potential was measured every five minutes by means of an external reference electrode placed in a Luggin tube in close proximity to the metal surface, in order to minimize the ohmic drop contribution in the potential measurement (IR-free potential). Figures 3.1 to 3.6 show IR-free protection potentials recorded at the end of each period in the presence of AC interference.

Protection potential is shifted in the more negative direction by increasing the protection current, as expected. Protection potential matches the protection criterion in every test condition, i.e. the potential is lower than -0.850 V CSE. Potential moves in the more positive (anodic) direction when AC is on, holding a fixed value of the protection current density supplied by the galvanostat.

Figure 3.1 reports potential monitoring of a carbon steel specimen cathodically protected by means of 0.1 A/m^2 CP current density in the presence of AC. If AC is absent, protection potential is -1.086 V CSE. Then, the potential increases due to AC overlap. In the presence of 200 A/m^2 AC density (the worst interference condition considered), the potential is -0.885 V CSE, with an anodic shift of 0.201 V with respect to the no-interference condition.

Protection potential is -1.173 V CSE applying 0.3 A/m^2 CP current density (Figure 3.2). Even in this case, AC moves the potential to higher values: the anodic shift is 0.034 V in the presence of 10 A/m^2 AC and grows proportionally to the magnitude of the AC overlapped. DC potential is -0.994 V CSE with 200 A/m^2, with a net polarization of 0.179 V.
Figure 3.3 refers to the galvanostatic test carried out at 0.5 A/m^2 DC. Protection potential is -1.223 V CSE. As discussed previously, AC acts by polarizing the metal in the anodic direction: the potential moves to more positive values up to -1.013 V CSE at the end of the test when 200 A/m^2 AC density is applied. The potential shift is 0.210 V.

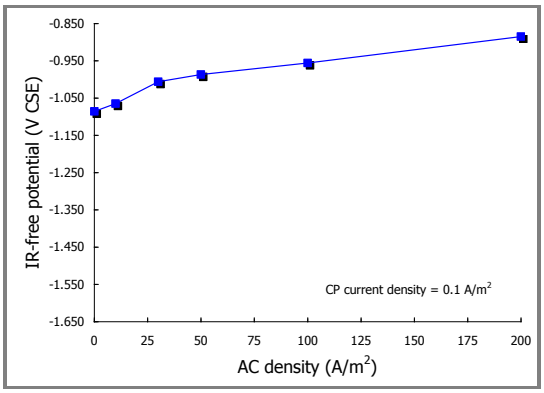

Figure 3.1 – DC potential vs. AC density (DC = 0.1 A/m^2)

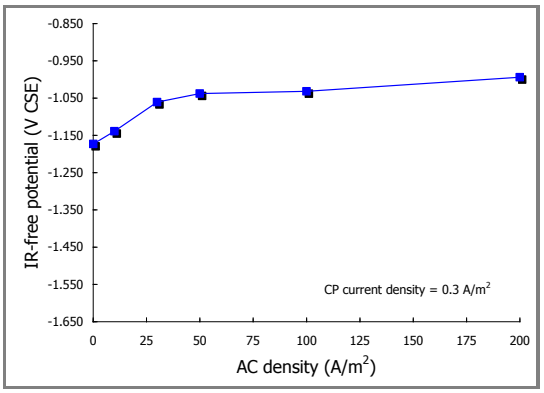

Figure 3.2 – DC potential vs. AC density (DC = 0.3 A/m^2)

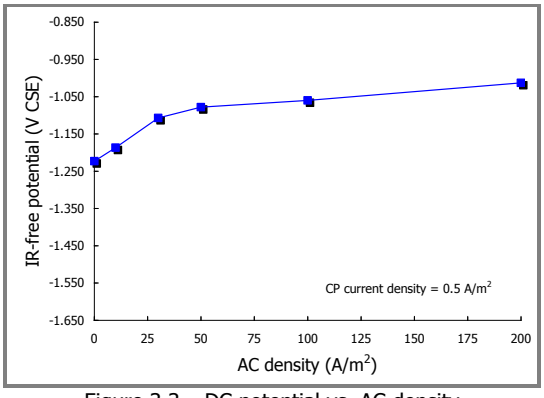

Figure 3.3 – DC potential vs. AC density (DC = 0.5 A/m^2)

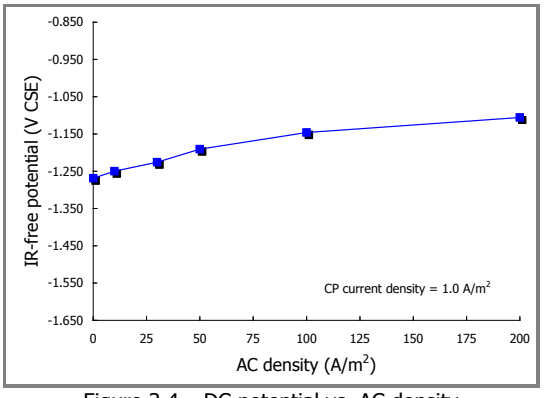

Figure 3.4 – DC potential vs. AC density (DC = 1.0 A/m^2)

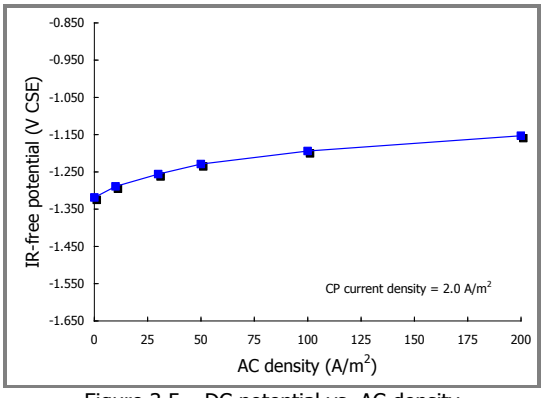

Figure 3.5 – DC potential vs. AC density (DC = 2.0 A/m^2)

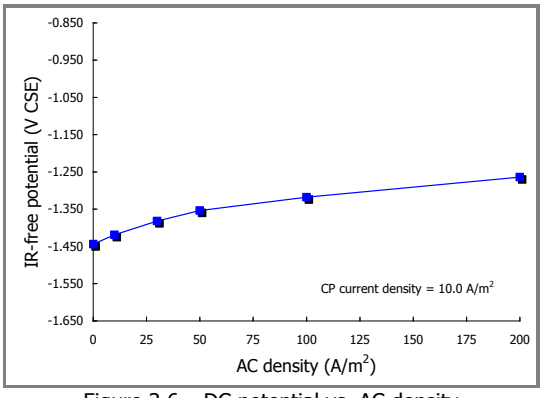

Figure 3.6 – DC potential vs. AC density (DC = 10.0 A/m^2)

In the presence of 1 A/m^2 cathodic current density (Figure 3.4), the potential is to -1.269 V CSE, if AC is absent. Potential increases up to -1.106 V CSE in the presence of 200 A/m^2 AC density, with a shift of 0.163 V. The same considerations can be extended to the last two cases shown in Figure 3.5 and Figure 3.6 which report potential monitoring of carbon steel specimens cathodically protected by 2 and 10 A/m^2 cathodic current density, respectively. Before AC is applied, potential is -1.319 V CSE in the presence of 2 A/m^2 and -1.444 V CSE with 10 A/m^2 AC density. When AC is turned on, the potential becomes more anodic. In the presence of 200 A/m^2 AC density, the positive shift is 0.166 V and 0.180 V with respect to the no-interference condition, respectively.
Figure 3.7 and Figure 3.8 summarize the effect of AC density on protection potential. Figure 3.7 reports IR-free protection potentials of carbon steel varying AC density and cathodic current. Figure 3.8 reports protection potential shift, calculated as the difference between the potential in the presence of AC and the potential before applying AC interference. Potential shifts and experimental conditions are reported in Table 3.1.

Carbon steel protection potential was also monitored during long-term tests carried out to study AC corrosion propagation (Paragraph 2.3). Specimens were cathodically protected by means of a magnesium alloy anode in soil-simulating environment. Two AC densities were applied: 100 and 240 A/m^2.

Table 3.1 – Protection potential in the presence of AC interference

AC density (A/m^2)	DC density (A/m^2)	IR-free potential (V CSE)	Potential shift (V)
0	0.1	-1.086	0
	0.3	-1.173	0
	0.5	-1.223	0
	1.0	-1.269	0
	2.0	-1.319	0
	10.0	-1.444	0
10	0.1	-1.065	0.021
	0.3	-1.139	0.034
	0.5	-1.187	0.036
	1.0	-1.250	0.019
	2.0	-1.289	0.030
	10.0	-1.419	0.025
30	0.1	-1.006	0.080
	0.3	-1.061	0.112
	0.5	-1.107	0.116
	1.0	-1.226	0.043
	2.0	-1.256	0.063
	10.0	-1.382	0.062
50	0.1	-0.987	0.099
	0.3	-1.038	0.135
	0.5	-1.078	0.145
	1.0	-1.191	0.078
	2.0	-1.229	0.090
	10.0	-1.354	0.090
100	0.1	-0.956	0.130
	0.3	-1.032	0.141
	0.5	-1.060	0.163
	1.0	-1.146	0.123
	2.0	-1.194	0.125
	10.0	-1.318	0.126
200	0.1	-0.885	0.201
	0.3	-0.994	0.179
	0.5	-1.013	0.210
	1.0	-1.106	0.163
	2.0	-1.153	0.166
	10.0	-1.264	0.180

Figure 3.9 shows potential monitoring of carbon steel specimens cathodically protected during long-term tests by means of a magnesium galvanic anode in soil-simulating environment in the presence of 100 and 240 A/m^2 AC density. Corrosion potential (open circuit potential, OCP) is the range between -0.700 V and -0.750 V CSE. OCP in soil depends mainly on oxygen limiting current density, i.e. the potential decreases by decreasing the oxygen limiting current density. During the test, soil was maintained in wet condition by the soil-pores saturation with the test solution. In such condition, oxygen permeability in soil is low as well as OCP.
CP was maintained for a week in the absence of AC interference: potential is lowered in the range from -1.257 V to -1.308 V CSE due to the cathodic current (between 0.970 and 1.290 A/m^2) supplied by the magnesium anode connected to the sample.
When AC is turned on, the potential moves to more noble value and the magnitude of the anodic shift increases by increasing AC density from 100 to 240 A/m^2.
100 A/m^2 AC density shifts the potential in the range between -1.130 V and -1.166 V CSE, with a mean anodic shift of 0.125 V. At 240 A/m^2 AC density, the potential increases in the range from -1.002 V to -1.095 V CSE, with a shift of 0.219 V compared to the no-interference condition.

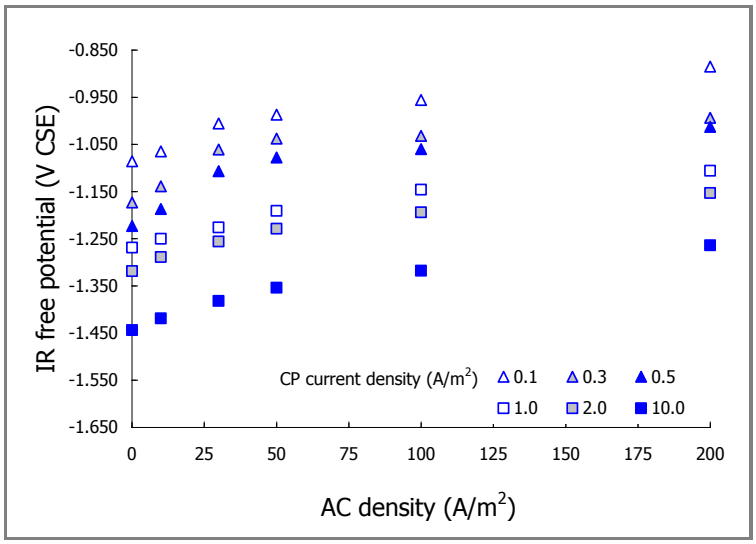

Figure 3.7 – DC potential vs. AC density varying protection current density

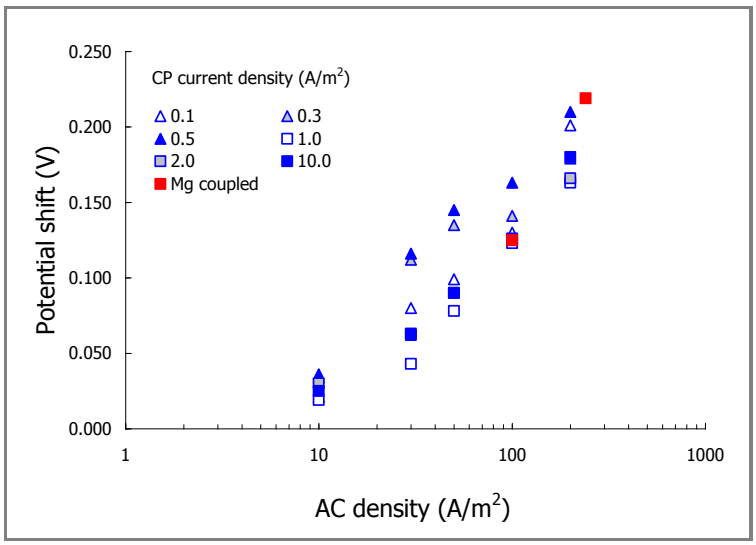

Figure 3.8 – Protection potential shift vs. AC density varying protection current density

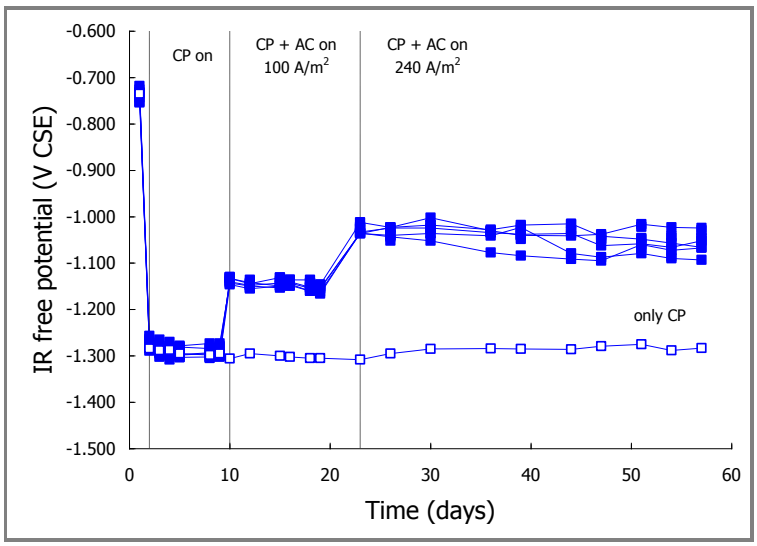

Figure 3.9 – Magnesium-coupled steel potential vs. time in the presence of 100 and 240 A/m^2 AC density

Moreover, an AC effect on protection current density was measured and will be discussed in Paragraph 3.2. Indeed, unlike a galvanostatic test in which the protection current is fixed by an external DC feeder, when a metal is protected by a galvanic protection system both current and potential change because the values they assume are regulated by the electrochemical galvanic coupling between the metals.
Potential shifts in the presence of AC interference are represented in Figure 3.8 by red markers. Data are in good agreement with those obtained by galvanostatic tests. The potential shift is lower than 0.040 V in the presence of 10 A/m^2 AC density, regardless the cathodic current applied. Potential variation becomes considerable corresponding to AC densities higher than 30 A/m^2. Furthermore, strong data dispersion is observed, i.e. potential shift varies from 0.043 V up to 0.116 V at 30 A/m^2 AC density. Potential shift increases up to 0.210 V if AC density is 100 A/m^2. A fitting curve of potential shift data was obtained by means of the least squares method. Figure 3.10 reports the linear regression line in a logarithmic scale current. Fitting was carried out considering all experimental data, regardless protection conditions. Fitting curve indicates a protection potential variation of 0.120 V per decade of current (slope of the curve). The linear regression coefficient (with current in a logarithmic scale) is 0.88.

In the first phase of the research project of corrosion group PoliLaPP ("Laboratorio di Corrosione dei Materiali Pietro Pedeferri") of Politecnico di Milano, the effect of AC interference on free corrosion potential and on protection potential of carbon steel was studied. Bolzoni et al. [64] carried out laboratory tests of AC interference on carbon steel in different conditions: free corrosion condition, anodic and cathodic polarization. Tests were performed in sulphate and chloride aqueous solutions, aerated or de-aerate. Figure 3.11 shows potential shifts varying AC density measured on carbon steel specimens in the presence of CP current densities from 1 to 10 A/m^2. In both sulphate (Figure 3.11*a*) and chloride (Figure 3.11*b*) containing solutions, protection potential increases by increasing AC density, with a positive (anodic) shift in the range from 20 to 150 mV in the presence of AC densities from 30 to 100 A/m^2.

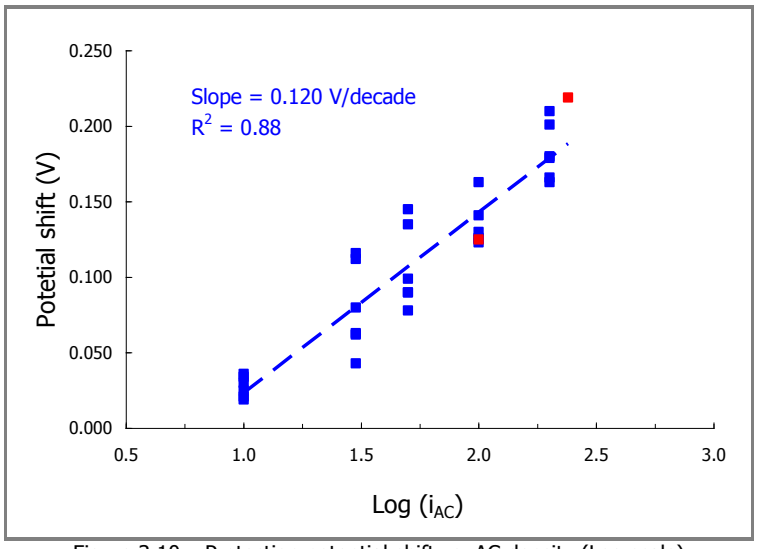

Figure 3.10 – Protection potential shift vs. AC density (Log scale)

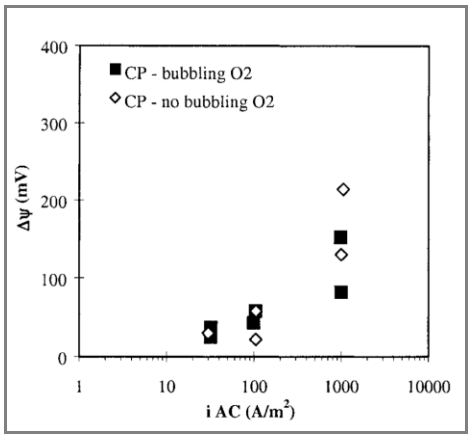

(a) Sulphate solutions

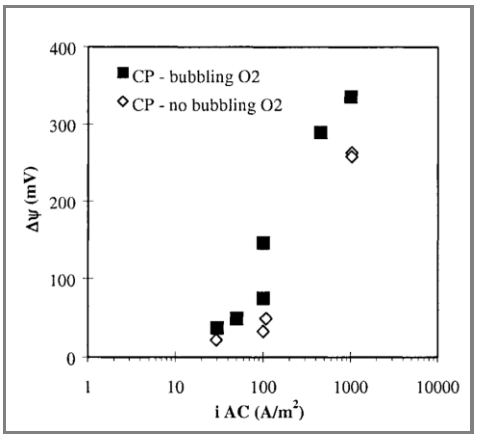

(b) Chloride solutions

Figure 3.11 (*a-b*) – Protection potential shift vs. AC density (from [64]). CP current density is in the range 1-10 A/m^2

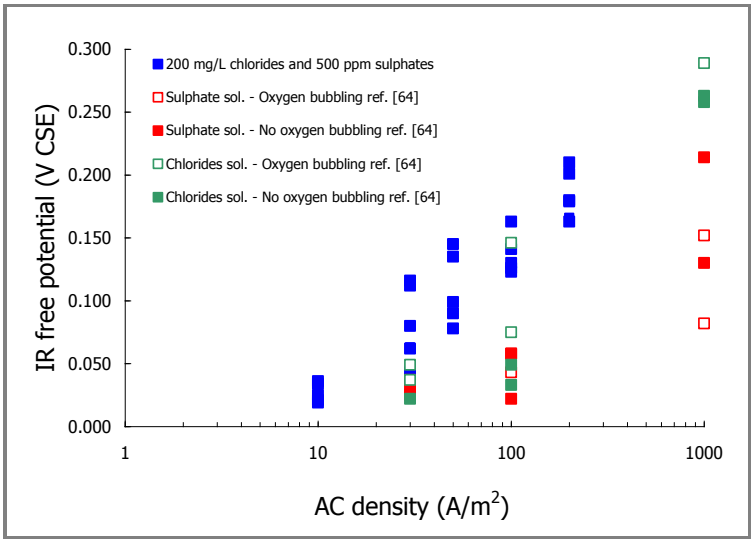

Figure 3.12 – Protection potential shift vs. AC density (comparison with data from [64])

Authors related the potential variation after the application of AC to a reduction of the cathodic overpotential [64]. A description of the AC effect on overpotentials is provided by the authors in recent works [15, 46]. Data reported in Figure 3.11(*a-b*) are compared in Figure 3.12 with those obtained during this work.
The potential shift magnitude depends on the surrounding environment in which CP is applied. In any case, protection potential shift is negligible if AC density is lower than 30 A/m^2, regardless the electrolyte characteristics.
The observed effect of AC on protection potential was studied by means of potentiodynamic tests carried out on carbon steel in soil-simulating environment in the presence of interference. These tests will be discussed in Paragraph 3.3.

3.2 AC EFFECT ON PROTECTION CURRENT

Experimental tests were performed in order to investigate the effect of AC on the protection current density, i.e. the current that flow into a metallic structure from the electrolytic environment in order to protect the structure [4].
Potentiostatic tests (Paragraph 2.2.2) were carried out on carbon steel specimens, grade API 5L X52 (Table 2.1) in the presence of stationary AC interference. In a potentiostatic test, a constant potential is applied and the polarization current (DC) is measured. Protection potential was applied in the range between -0.850 V and -1.350 V CSE. AC was overlapped to the sample by steps, increasing AC density every 30 minutes from 10 up to 200 A/m^2. Experimental conditions are summarized in Table 2.3. During each step (30 minutes long), cathodic polarization current was measured every five minutes.
Figures 3.13 to 3.18 show protection current density monitoring. CP current density increases by decreasing the protection potential of the metal, as expected. Polarization current increases when AC is on, regardless the applied level of CP, i.e. more current is required to polarize the metal if AC is overlapped.
Figure 3.13 reports protection current monitoring of a carbon steel specimen cathodically protected at -0.850 V CSE. If AC is absent, protection current is 0.010 A/m^2. Then, the current density increases due to AC overlap. In the presence of 100 and 200 A/m^2 AC density (the worst interference conditions considered), CP current density is 0.044 and 0.097 A/m^2, respectively.
Figure 3.14 reports protection current measurements corresponding to a CP potential of -0.950 V CSE. CP current density is 0.020 A/m^2 without AC and increases to 0.079 A/m^2 in the presence of 100 A/m^2 AC density. The current is about one order of magnitude greater if 200 A/m^2 AC density is overlapped to the sample (0.174 A/m^2). Figure 3.15 refers to the potentiostatic test performed at -1.050 V CSE. In no-interference condition, CP current density is 0.078 A/m^2. In the presence of 200 A/m^2, the measured current is 0.912 A/m^2, one order of magnitude greater than the current measured without AC.
Figure 3.16 reports protection current measurements of carbon steel cathodically protected at -1.150 V CSE and interfered by AC. CP current density is 0.347 A/m^2 and moves to higher values by increasing AC density: 0.955 A/m^2 at 100 A/m^2 and 1.905 A/m^2 at 200 A/m^2 AC density. The same considerations can be extended to the last two cases, reported in Figure 3.17 and Figure 3.18, in which carbon steel specimens are cathodically protected at -1.250 V and -1.350 V CSE and interfered by AC. If AC is absent, protection current density is 0.850 and 1.660 A/m^2, respectively. At -1.250 V CSE, the current increases up to 2.399 A/m^2 in the presence of 100 A/m^2 AC density and reaches 5.248 A/m^2 at the end of the test with 200 A/m^2. At -1.350 V CSE, the current is 4.169 A/m^2 in the presence of 100 A/m^2 AC density and 6.310 A/m^2 at the end of the test with 200 A/m^2.

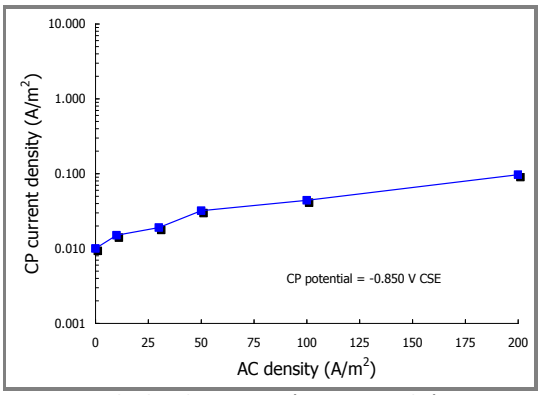

Figure 3.13 – CP current density vs. AC density (CP potential = -0.850 V CSE)

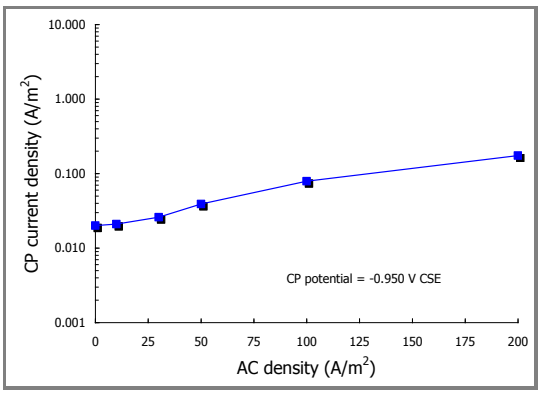

Figure 3.14 – CP current density vs. AC density (CP potential = -0.950 V CSE)

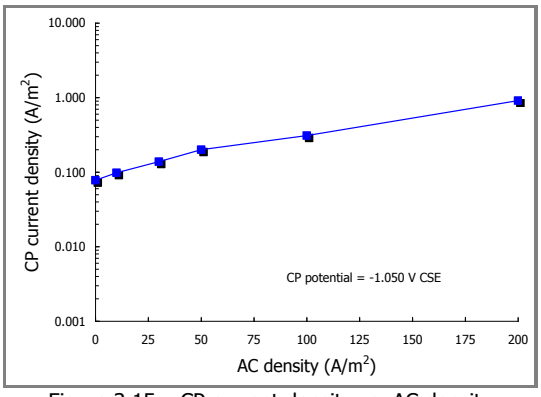

Figure 3.15 – CP current density vs. AC density (CP potential = -1.050 V CSE)

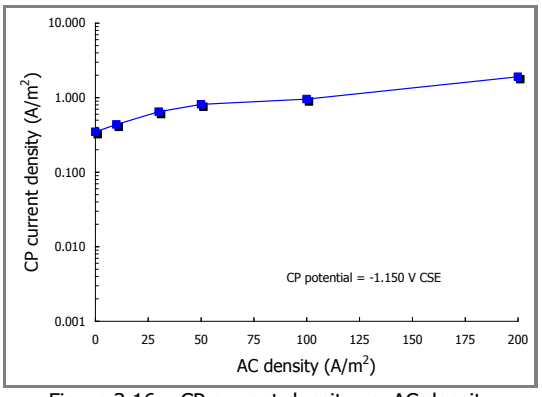

Figure 3.16 – CP current density vs. AC density (CP potential = -1.150 V CSE)

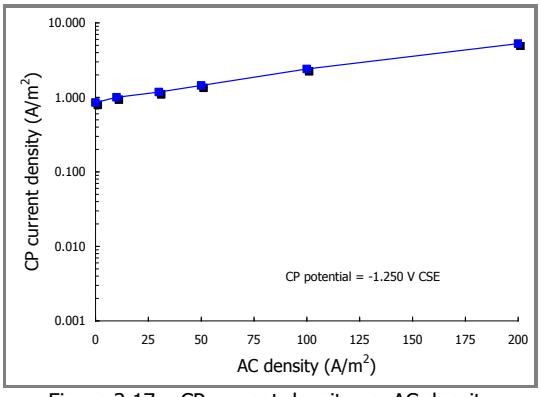

Figure 3.17 – CP current density vs. AC density (CP potential = -1.250 V CSE)

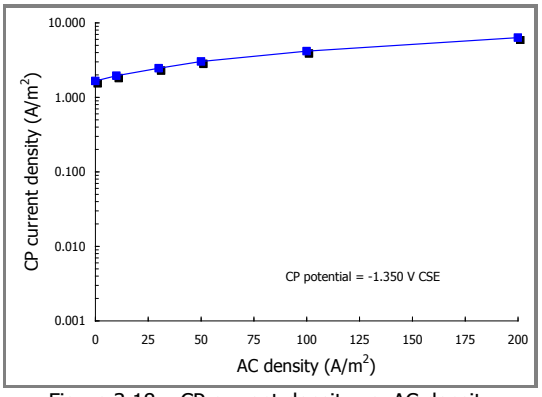

Figure 3.18 – CP current density vs. AC density (CP potential = -1.350 V CSE)

Figure 3.19 and Figure 3.20 summarize the effect of AC on protection current density. Figure 3.19 reports CP current density measured on carbon steel varying AC density for each protection condition considered. Figure 3.20 reports protection current shift, calculated as the difference between the current density in the presence of AC and the current density before applying AC. Current shifts are also reported in Table 3.2. CP current density in the presence of AC was also monitored during long-term tests (Paragraph 2.3.2) carried out on carbon steel specimens cathodically protected by means of a magnesium galvanic anode in soil-simulating environment. Figure 3.21 shows CP current density monitoring in the presence of 100 and 240 A/m^2 AC density. CP was applied for a week: CP current density for all the samples is in the range between 0.970 and 1.290 A/m^2. As shown previously, the presence of

AC provokes an increase of the protection current. With 100 A/m^2 AC density, CP current density is in the range between 1.840 and 2.300 A/m^2, almost twice the cathodic current densities measured in the no-interference condition. After 20 days protection, AC density was increased up to 240 A/m^2; simultaneously, cathodic current density increases up to values in the range from 2.180 to 3.030 A/m^2.

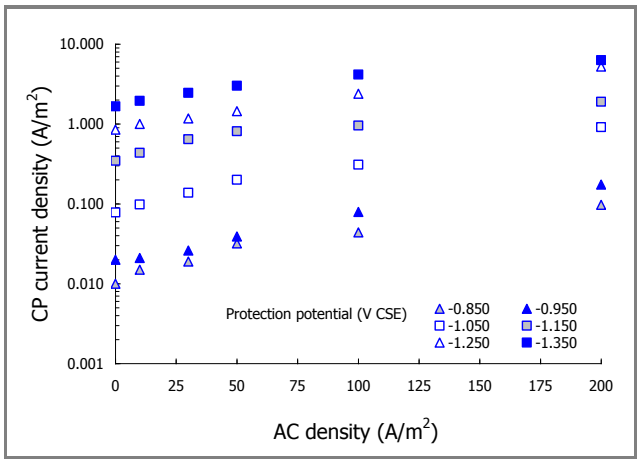

Figure 3.19 – DC density vs. AC density varying protection potential

Table 3.2 – CP current density in the presence of AC interference

AC density (A/m^2)	Protection potential (V CSE)	CP current density (A/m^2)	Current shift (A/m^2)
0	-0.850	0.010	0
	-0.950	0.020	0
	-1.050	0.078	0
	-1.150	0.347	0
	-1.250	0.851	0
	-1.350	1.660	0
10	-0.850	0.015	0.005
	-0.950	0.021	0.001
	-1.050	0.098	0.020
	-1.150	0.437	0.090
	-1.250	1.000	0.149
	-1.350	1.950	0.290
30	-0.850	0.019	0.009
	-0.950	0.026	0.006
	-1.050	0.138	0.060
	-1.150	0.646	0.299
	-1.250	1.175	0.324
	-1.350	2.455	0.795
50	-0.850	0.032	0.022
	-0.950	0.039	0.019
	-1.050	0.200	0.122
	-1.150	0.813	0.466
	-1.250	1.445	0.594
	-1.350	3.020	1.360
100	-0.850	0.044	0.034
	-0.950	0.079	0.059
	-1.050	0.309	0.231
	-1.150	0.955	0.608
	-1.250	2.399	1.548
	-1.350	4.169	2.509
200	-0.850	0.097	0.087
	-0.950	0.174	0.154
	-1.050	0.912	0.834
	-1.150	1.905	1.558
	-1.250	5.248	4.397
	-1.350	6.310	4.650

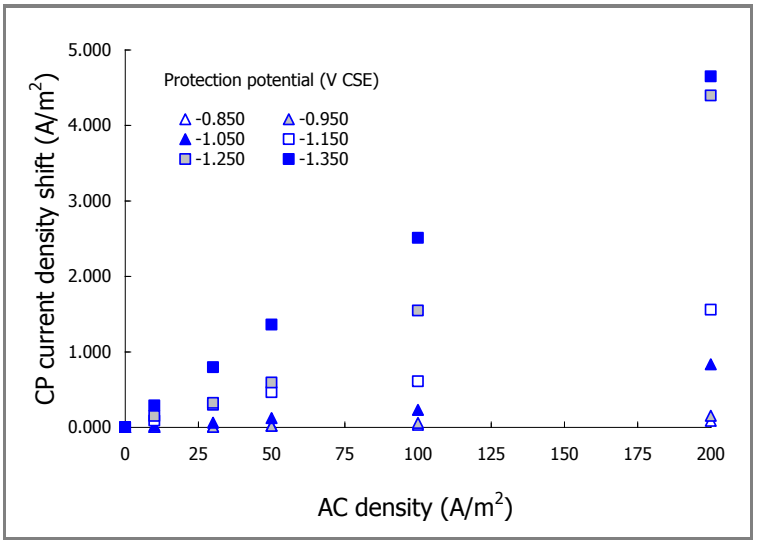

Figure 3.20 – Protection current density shift vs. AC density varying protection potential

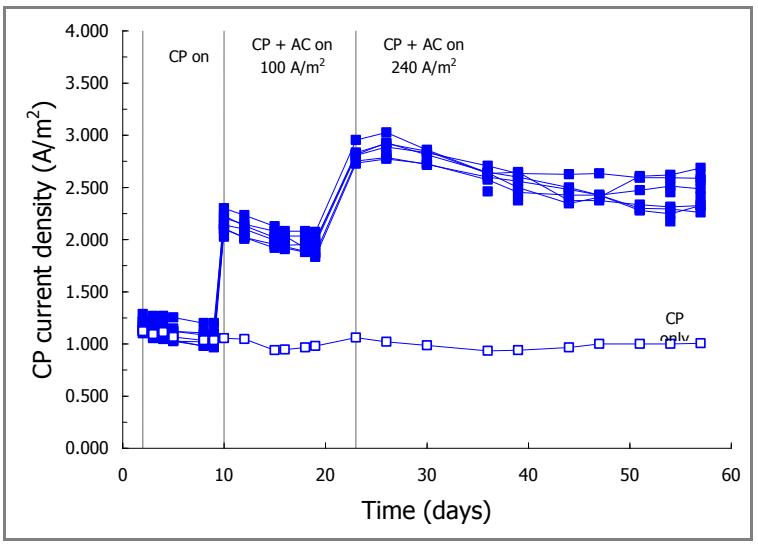

Figure 3.21 – CP current density of magnesium-coupled steel in the presence of 100 and 240 A/m^2 AC density

3.3 POTENTIODYNAMIC TESTS

The main conclusions of galvanostatic (Paragraph 3.1) and potentiostatic (Paragraph 3.2) tests can be summarized as follows:

- protection potential increases in the presence of AC interference;
- protection current increases in the presence of AC interference;
- AC effect on protection potential and current depends on the magnitude of AC density and on environmental characteristics.

In order to investigate the effect of AC on protection potential and current density, potentiodynamic tests were carried out on carbon steel in the presence of AC interference. Experimental conditions are described in Paragraph 2.2.3. Potentiodynamic tests provide useful information regarding the electrochemical kinetics of anodic and cathodic reactions (anodic and cathodic polarization curves). The test involves changing of the metal potential and monitoring of the polarization current as a function of potential. The result is the so-called potential-current density curve.

Potentiodynamic tests were carried out carbon steel specimens, grade API 5L X52 (Table 2.1) in soil, composed by silica sand and the same soil-simulating solution used for galvanostatic and potentiostatic tests (200 mg/L chlorides and 500 mg/L sulphate ions). Polarization curves were obtained in the presence of 100 and 240 A/m^2 AC densities and were compared with the reference curve in the absence of interference.
Figure 3.22 shows potentiodynamic curves (E-log(i)) of carbon steel in the presence of zero, 100 and 240 A/m^2 AC densities. As discussed in Paragraph 2.2.3, if the potential is displaced from the open-circuit potential (OCP), the current measured represents the difference between the anodic-reaction current and the cathodic-reaction current, or vice versa. If the potential displacement is sufficiently large, the net current will be essentially equal to the anodic or cathodic-reaction current, depending on whether the potential is made respectively more positive or more negative with respect to OCP.

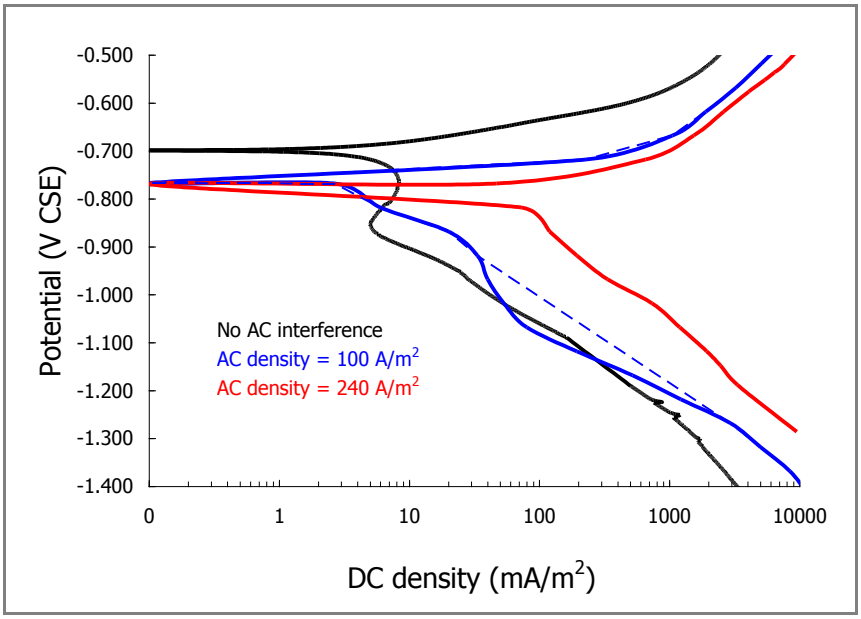

Figure 3.22 – Polarization curves on API 5L X52 carbon steel in the presence of AC

The polarization current is zero corresponding to the open circuit potential (OCP), i.e. no current is exchanged by the metal. In the absence of AC interference (black curve in Figure 3.22), corrosion potential is -0.700 V CSE. The presence of AC interference moves OCP (the "zero-current potential") towards more negative values. OCP is shifted to -0.767 V CSE and to -0.770 V CSE in the presence of 100 and 240 A/m^2 AC density, respectively.
The main effect of AC is related to the curves shift towards high polarization currents, changing anodic and cathodic overpotentials. However, in this work the effect of AC on anodic and cathodic overpotentials (anodic and cathodic Tafel slopes, corrosion potential and corrosion current density) is not widely discussed. Indeed, the study of the AC effect on such parameters was already carried out during the first phase of the research project and was described elsewhere [15, 46]. In brief, authors tested different metal/solution systems and stated that AC has a strong influence on corrosion kinetic parameters and on corrosion or equilibrium potential, in terms of a general decrease in overpotentials and an increase in corrosion or exchange current density for the different conditions tested. Authors measured a decrease of corrosion or equilibrium potential in the presence of AC, with the only exception of carbon steel in soil-simulating solution (containing 1200 mg/L sulphate ions and 200 mg/L chloride ions), in disagreement with the behavior described above and shown in Figure 3.22. Moreover, authors compared their results with mathematical models based on the asymmetry of anodic and cathodic processes (Paragraph 1.6.5). These models [41, 43] provide a

mathematical approach to study the effect of AC on corrosion potential and corrosion current density as functions of the peak alternating voltage and of anodic (β_a) and cathodic (β_c) Tafel slopes ratio ($r = \beta a/\beta c$). According to these mathematical models, for the conditions $r < 1$ and $r > 1$ the increase in the peak alternating voltage results respectively in the decrease and in the increase of OCP but doesn't affect Tafel slopes (Figure 1.30, Figure 1.32 and Figure 1.33). This is in contrast to the previous results obtained in this research project [46] which showed that AC has an effect also on Tafel slopes.
The experimental results obtained in this work confirm that AC has a strong influence on anodic and cathodic polarization curves and on corrosion potential. Nevertheless, these aspects weren't pursued further during this work.

In order to study the effect on protection potential and current, the following discussion will concern mainly on the cathodic behavior of the metal, related to the cathodic processes that occur when the metal is in CP condition.
In the absence of AC interference, the cathodic processes that take place on the metal are oxygen reduction and hydrogen evolution at low potentials.
Generally, oxygen reduction overpotential consists of two contributions [21, 65]: the activation and the concentration polarization. The first is associated to the activation energy that is required by the cathodic reaction to occur. Activation polarization increases with current density in accordance with Tafel equation and is therefore represented by a linear trend in the E-log (i) plot. By increasing the cathodic current, a deviation from linearity occurs due to oxygen diffusion process. Indeed, oxygen is consumed on the metal surface due to the cathodic reduction and is replaced by diffusion process from the bulk solution where its concentration is approximately constant. The formation of a diffusion layer at the interface between the electrolyte and the metal occurs if the diffusion rate is not fast enough to carry all the electrons supplied on the metal surface. Concentration overpotential increases by increasing the cathodic current until a limiting value is reached, called *oxygen limiting diffusion current*. This value depends on oxygen bulk concentration, diffusion coefficient and on the thickness of the diffusion layer [21, 65]. Oxygen limiting diffusion current in soil varies from about 1 mA/m^2 in water saturated soils (as clayey soils) where oxygen is almost absent, to 150 mA/m^2 in well-aerated soils, as sandy soils [2]. Potentiodynamic curves were obtained in silica sand saturated with the test soil-simulating solution; such environment could be considered analogous to a clayey soil in stagnant condition, in which oxygen limiting diffusion current (i_L, mA/m^2) can be approximated as follows:

(Eq. 3.1) $\quad i_L \cong K \cdot [O_2]$

where K is a constant ranging from 8 at 10°C to 10 at 30°C [2, 21] and $[O_2]$ is oxygen concentration in mg/L. Oxygen limiting diffusion current is well-defined in the cathodic curve obtained in no-interference condition (Figure 3.22). The oxygen limiting current density is in the range between 5 and 8 mA/m^2 and corresponds to an oxygen concentration around 1 mg/L. A further potential decrease lead to the hydrogen evolution that adds to oxygen reduction reaction.
In the presence of AC interference, the oxygen limiting diffusion current is not well defined (at 100 A/m^2) or disappears (at 240 A/m^2) and cathodic process is described only by the hydrogen evolution in the potential range studied. Hydrogen evolution curve moves to high polarization current and this could be due to an effect of AC of exchange current density of hydrogen evolution reaction, i.e. AC may act as a catalyst of hydrogen evolution on the metal surface. Nevertheless, no changes of the hydrogen evolution Tafel slope are measured (about 0.140 V/decade of current).
As it can be seen from the curve obtained in the presence of 100 A/m^2 AC density, oxygen limiting current density may bow down the cathodic polarization curve a low current density (in the range 3-8 mA/m^2) after while hydrogen reaction with 0.140 V/decade is more

dominant. An odd variation of cathodic discharge curve is also observed corresponding to current densities higher than 30 mA/m^2. This could be correlated with an ohmic drop contribution due to hydrogen bubbling on the metal surface during the cathodic polarization which fakes the potential measurement. The dotted line in Figure 3.22 represents the experimental cathodic curve corrected by the ohmic drop contribution.
Polarization curves confirm an AC effect on overpotentials, i.e. on cathodic and anodic reactions kinetics, which study is still ongoing.

3.3.1 Effect on protection potential

Figure 3.23 reports experimental polarization curves (Figure 3.22) compared with galvanostatic tests data (square markers) in the presence of zero, 100 and 200 A/m^2 AC density (Table 3.1). Good agreement is observed. As discussed previously, the cathodic polarization curve is shifted towards high polarization current by increasing AC density. Only in the case of 100 A/m^2 AC density, potential data obtained by galvanostatic tests deviate slightly toward more noble values from the polarization curve.
The effect of AC on protection potential could be explained by means of potentiodynamic curves. Galvanostatic test showed that protection potential increases in the presence of AC interference. As discussed in Paragraph 3.1, in a galvanostatic test a constant current (DC) is applied and potential is measured. This condition can be represented in Figure 3.24 and Figure 3.25 by fixing a protection current density value and measuring the potential given by the intersection with the experimental cathodic curve. Polarization curves at zero and 240 A/m^2 AC density are considered.
For instance, 100 mA/m^2 of cathodic current density (Figure 3.24) results in a protection potential of -1.060 V CSE according to the control curve (no interference) and of -0.840 V CSE considering the intersection with the cathodic curve obtained in the presence of 240 A/m^2.
Galvanostatic test performed with the same cathodic current density (100 mA/m^2) provides protection potentials of -1.086 V CSE and -0.885 V CSE in the presence of zero and 200 A/m^2 AC density, respectively (Table 3.1). Once more, 2,000 mA/m^2 of cathodic current density (Figure 3.25) results in a protection potential of -1.320 V CSE according to the control curve (no interference) and of -1.120 V CSE considering the intersection with the cathodic curve obtained in the presence of 240 A/m^2 AC density. Galvanostatic test performed with the same cathodic current density (2,000 mA/m^2) provides protection potentials of -1.319 V CSE and -1.153 V CSE in the presence of zero and 200 A/m^2 AC density, respectively (Table 3.1).

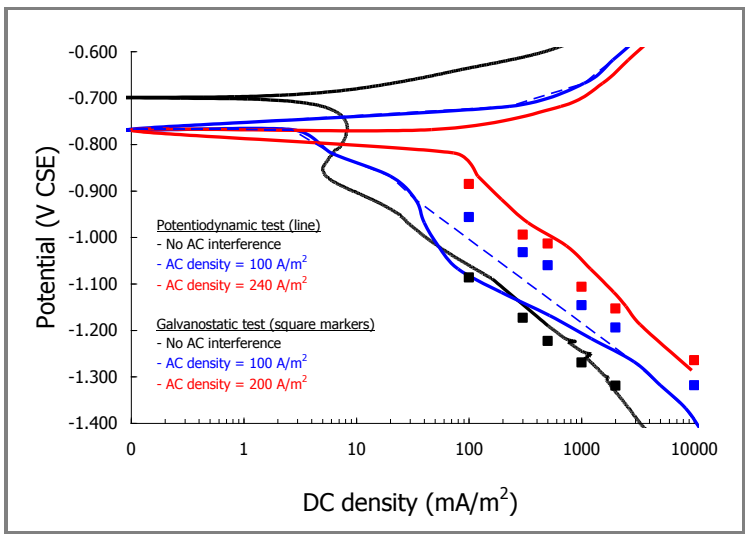

Figure 3.23 –Polarization curves on carbon steel in the presence of AC compared with galvanostatic test results

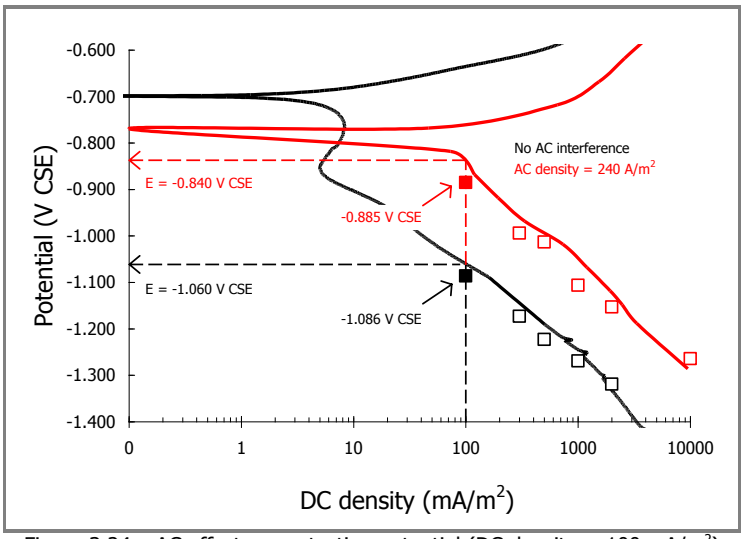

Figure 3.24 – AC effect on protection potential (DC density = 100 mA/m^2)

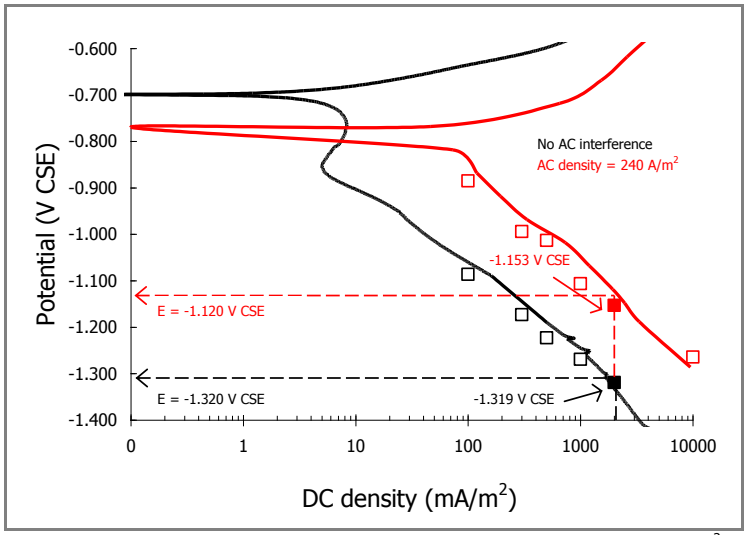

Figure 3.25 - AC effect on protection potential (DC density = 2,000 mA/m^2)

The good agreement observed between galvanostatic test data and polarization curves allows to state that AC causes the increase of protection potential in the experimental condition considered, as a consequence of the effect of AC on cathodic polarization curves. Furthermore, the potential shift (anodic shift) depends on the superimposed AC density magnitude, i.e. it increases by increasing AC density. Nevertheless, it should be pointed out that the magnitude of the potential shift depends on the metal/electrolyte system and on the cathodic processes occurring on the metal surface, as discussed in Paragraph 3.1 and shown in Figure 3.12.

3.3.2 Effect on protection current

Figure 3.26 reports experimental polarization curves (Figure 3.22) compared with potentiostatic tests data (square markers) in the presence of zero, 100 and 200 A/m^2 AC density (Table 3.2). As in the case discussed in Paragraph 3.3.1, a good agreement between polarization curves and potentiostatic test data is observed, as expected.

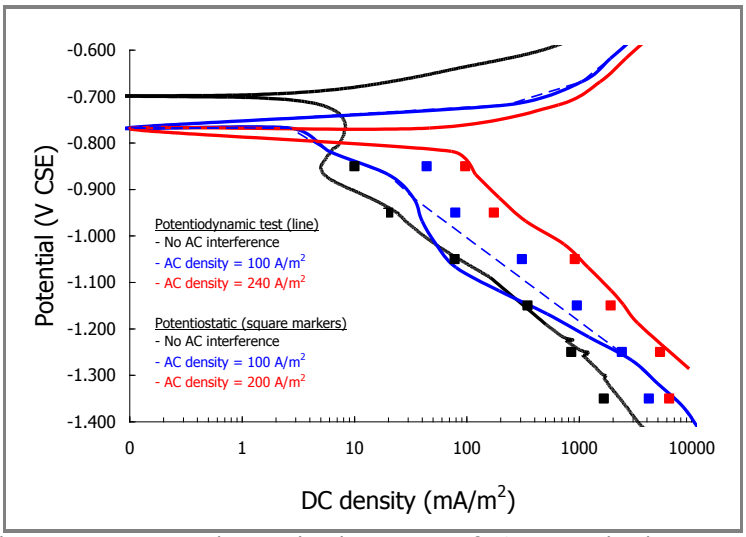

Figure 3.26 – Polarization curves on carbon steel in the presence of AC compared with potentiostatic test results

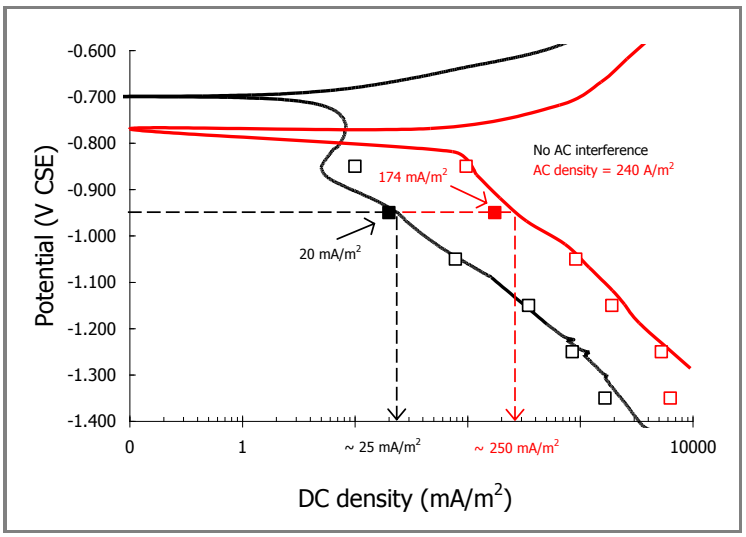

Figure 3.27 – AC effect on protection current density (DC potential = -0.950 V CSE)

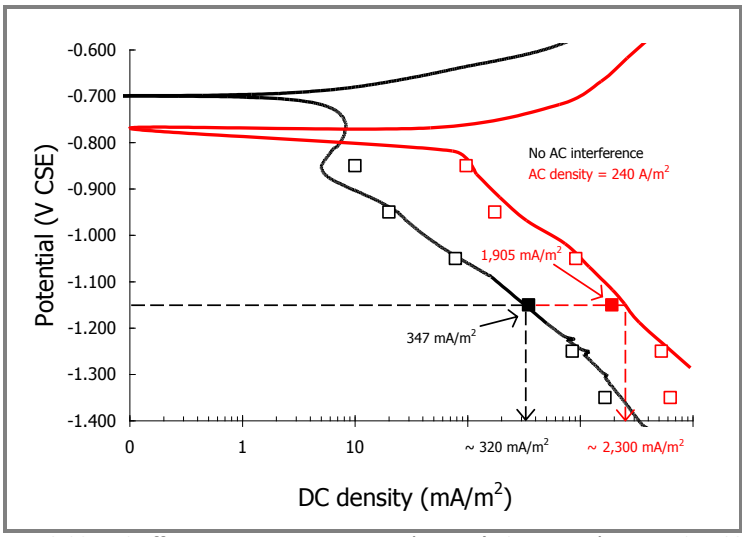

Figure 3.28 –AC effect on protection current density (DC potential = -1.150 V CSE)

Potentiostatic test showed that protection current increases in the presence of AC interference. The effect of AC on protection current could be explained by means of potentiodynamic curves. As discussed in Paragraph 3.2, in a potentiostatic test a fix potential is applied and DC is measured. This condition can be represented in Figure 3.27 and Figure 3.28 by considering a protection potential value and measuring the cathodic current density given by the intersection with the experimental cathodic curve. Polarization curves at zero and 240 A/m^2 AC density are considered, as in the cases discussed in Paragraph 3.3.1.
For instance, a protection potential of -0.950 V CSE (Figure 3.27) results in a protection current density of about 25 mA/m^2 according to the control curve (no interference) and of 250 mA/m^2 considering the intersection with the cathodic curve in the presence of 240 A/m^2.
Potentiostatic test performed at the same cathodic potential (-0.950 V CSE) provides protection current densities of 20 mA/m^2 and 174 mA/m^2 in the presence of zero and 200 A/m^2 AC density, respectively (Table 3.2). Once more, a protection potential of -1.150 V CSE (Figure 3.28) results in a protection current density of 320 mA/m^2 according to the control curve (no interference) and of 2,300 mA/m^2 considering the intersection with the cathodic curve in the presence of 240 A/m^2. Potentiostatic test performed at the same cathodic potential (-1.150 V CSE) provides protection current densities of 347 mA/m^2 and 1,905 mA/m^2 in the presence of zero and 200 A/m^2 AC density, respectively (Table 3.2).
The good agreement observed between potentiostatic test data and polarization curves allows to state that AC causes the increase of the protection current density in the experimental condition considered, as a consequence of the effect of AC on cathodic polarization curves. Furthermore, the current shift depends on the superimposed AC density, i.e. it increases by increasing AC density.

3.3.3 Galvanic anode system

As discussed in Paragraph 3.1 and Paragraph 3.2, carbon steel protection potential and current were also monitored during long-term tests carried out to study AC corrosion propagation (Paragraph 2.3.2). Specimens were cathodically protected by means of a magnesium anode, grade AZ63D, in soil-simulating environment. Two AC densities were applied on carbon steel: 100 and 240 A/m^2. These values correspond to about 5 and 13 A/m^2 on magnesium anode due to the higher surface area (28 cm^2) with respect carbon steel specimens (1.5 cm^2). Figure 3.9 and Figure 3.21 show the increase of protection potential and current density in the presence of AC interference. Furthermore, potential and current variations become larger according to the increase of AC density magnitude.
As widely discussed in Chapter 1 (Paragraph 1.1), CP by sacrificial anodes is achieved through the galvanic coupling of the structure to protect with a less noble metal, as magnesium for carbon steel in soil. The galvanic current lowers the potential of the metal structure and reduces (or halts) its corrosion rate. The current supplied by the anode is given by the ratio between the driving voltage (defined by cathode and anode potential difference) and the total resistance of the system.
Unlike the impressed current system that makes use of a DC feeder (i.e. current or potential are set by an external device), in a galvanic system the protection condition (protection potential and current) are defined by the coupling between the metals, i.e. galvanic coupling is a self-regulated system. The simultaneous increase of the protection potential and current due to the presence of AC seems to disagree with the cathodic behavior of the metal, i.e. the increase of the cathodic current should produce the decrease of potential, rather than an increase (Figure 3.9 and Figure 3.21). Even in this case, the AC effect on protection potential and current of magnesium-coupled carbon steel could be explained by means of potentiodynamic curves of both the metals. Potentiodynamic tests (Figure 3.29 and Figure 3.30) were carried out on carbon steel in the presence of zero, 100 and 240 A/m^2 AC density (previously described, Figure 3.22) and on magnesium alloy anode in the presence of zero, 5 and 13 A/m^2 AC densities, the same measured during AC propagation test (Paragraph 2.3.2).

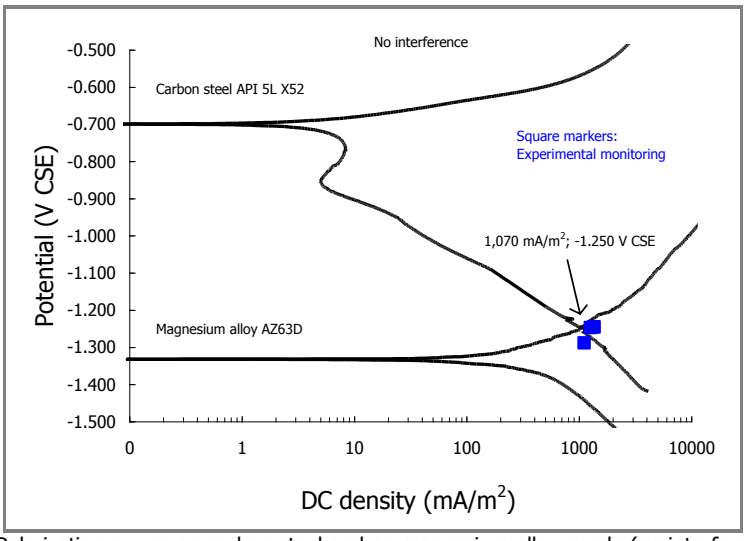

Figure 3.29 – Polarization curves on carbon steel and on magnesium alloy anode (no interference condition)

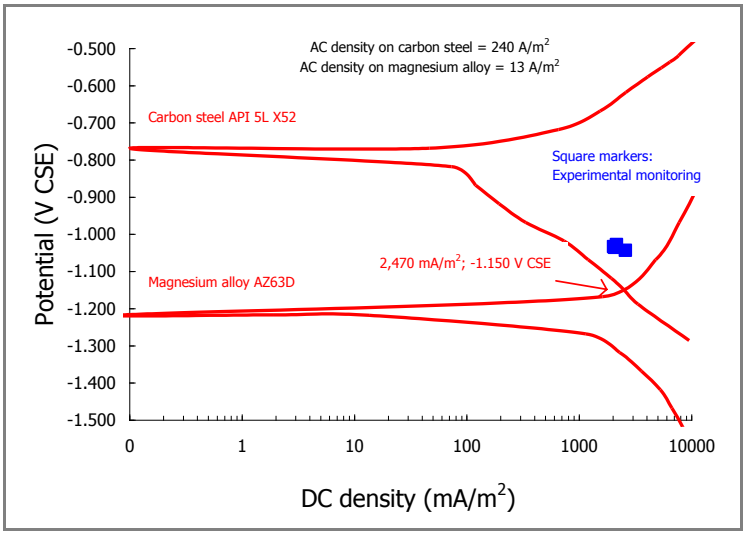

Figure 3.30 – Polarization curves on carbon steel and on magnesium alloy anode (AC density = 240 A/m^2)

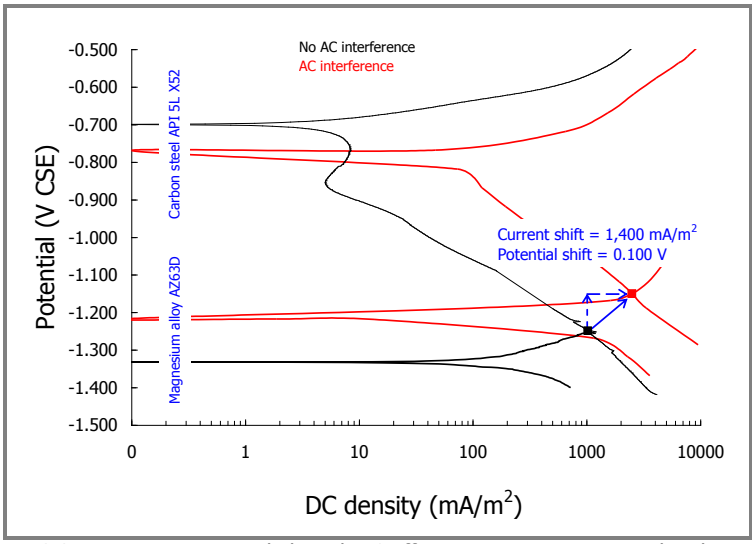

Figure 3.31 – Magnesium-coupled steel: AC effect on protection potential and current

Since electrical charge cannot accumulate (Kirkhoff's law), the current supplied to the structure by the anode must be the same used by the cathodic process. Accordingly, due to the different surface area between carbon steel and magnesium alloy specimens, polarization curves were normalized by multiplying the current density on magnesium anode for the anode and cathode specimens surface area ratio (S_{cath}/S_{anode} = 18.7).
Blue square markers refer to protection potential and current monitored during AC propagation tests. Each indicator represents the mean value of DC potential and current of carbon steel samples cathodically protected by galvanic magnesium anodes and exposed to one to four months to AC interference. The details about such investigation are provided in Paragraph 2.3.2.
Conversely to what observed on carbon steel (Figure 3.22), polarization curves on magnesium alloy show that AC interference moves OCP (the "zero-current potential") towards more positive values. OCP is shifted from -1.330 V CSE (no-interference condition) to -1.220 V CSE in the presence of 13 A/m^2 AC density, with an anodic shift of 0.110 V.
Magnesium anode operates electrochemically in pitting conditions, at a potential more noble by about 1 V than its standard potential (-2.363 V SHE, Standard Hydrogen Electrode) [2]. The simultaneous effect on corrosion potential of carbon steel (a decrease) and on magnesium alloy (an increase) results in the reduction of the driving voltage from 0.630 V in no-interference condition to 0.450 V in the presence of 240 A/m^2 AC density.
Due to the galvanic coupling between carbon steel and magnesium, the electrical working point (potential and current) of the galvanic system is given by the intersection between the cathodic curve of carbon steel (the cathode) and the anodic curve of the magnesium, that works as anode. Due to the low resistivity of the adopted soil-simulating solution (5 Ω·m), the ohmic drop contribution is neglected. Good agreement is observed between potentiodynamic curves and the experimental corrosion and current monitoring (blue markers, Figure 3.29). Protection potential and current given by the intersection point of electrochemical characteristics are -1.250 V CSE and 1,070 mA/m^2, respectively.
AC shifts potentiodynamic curves towards high polarization currents. Accordingly, the working potential of the galvanic coupling is shifted in the presence of AC. In the presence of 240 A/m^2 on carbon steel specimen (i.e. 13 A/m^2 on magnesium anode), protection potential and current are -1.150 V CSE and 2,470 mA/m^2, respectively (Figure 3.30).

While good agreement is observed between the protection current density provided by potentiodynamic tests and the values measured during long-term exposition tests (blue markers, Figure 3.30), more noble potentials (of about 0.100 V) were measured during exposition tests with respect to potentials obtained by polarization curves. Nevertheless, polarization curves show that the simultaneous protection potential and current increase of magnesium-coupled carbon steel specimens in the presence of AC interference could be explained by means of the AC effect on anodic and cathodic characteristics (Figure 3.31).

3.4 SUMMARY

Galvanostatic and potentiostatic tests were carried out to investigate the effect of AC interference on protection potential and protection current. The main conclusions can be summarized as follows:

- AC shifts the protection potential of carbon steel in soil-simulating environment towards more positive values (anodic shift);
- AC causes the increase of protection current density;
- AC effects depend on the magnitude of AC density and on environmental characteristics (solution chemical composition);
- the effect on potential and current could be due to the variation of the characteristics curves (E- log(i)) of carbon steel in the presence of AC.

Chapter 4

Results

Part 2 – AC corrosion mechanism

As discussed in Chapter 1 (Paragraph 1.6) the technical specification CEN/TS 15280:2006 "Evaluation of a.c. corrosion likelihood of buried pipelines – Application to cathodically protected pipelines" provides a simplified description of the AC corrosion mechanism of cathodically protected carbon steel structures [12]. The technical specification has been prepared by the Technical Committee CEN/TC 219 "Cathodic protection", and is currently under review. Furthermore, it states that, in the presence of AC interference, cathodic protection (CP) criteria given by the European Standard EN 12954:2002 "Cathodic protection of buried or immersed metallic structures – General principles and application for pipelines" [3] are not sufficient to demonstrate that steel is protected against corrosion. As reported by the technical specification, alternating voltages between 4 V and 10 V result in a significant corrosion attack on the pipeline and various additional parameters, as defect spread resistance, soil composition, and CP level may influence the corrosion process. Nevertheless, the AC corrosion mechanism description provided by the technical specification is considered not exhaustive; as a result, several proposals have been proposed and can be found in literature. Some of these models are widely discussed in Paragraph 1.6. They refer to cathodically protected structures as well as to structures in the absence of CP (free corrosion condition) and are based both on theoretical considerations and on experimental tests (laboratory results, field tests or corrosion cases study). Theoretical models focuses mainly on electrical equivalent circuit analysis (Paragraph 1.6.1 and Paragraph 1.6.5) or electrochemical approaches (Paragraph 1.6.3). However, none of these models fully explains the phenomenon, especially regarding the AC corrosion mechanism of carbon steel in CP condition, the individuation of the more influencing parameters and the definition of protection criteria to adopt in the presence of AC interference.

This work is a part of a project of the research group PoliLaPP ("Laboratorio di Corrosione dei Materiali Pietro Pedeferri") of Politecnico di Milano, on the effect of AC interference on steel corrosion, even on CP condition. The first phase of the research started in 2002 and was focused mainly on the set-up of a proper instrumentation to measure and apply separately DC and AC signal, on the individuation of critical parameters for AC corrosion and on CP criteria assessment in the presence of AC. These results have been published earlier [15, 46, 63, 64, 66-68].
The second phase of the research is currently ongoing and aims to propose a corrosion mechanism of carbon steel in CP condition in the presence of AC.
Laboratory tests were carried out varying protection and interference conditions. Moreover, in order to investigate some aspects related to the effect of AC on electrochemical passivity, tests were performed on passive metals in free corrosion condition (in the absence of CP), as carbon steel in alkaline environment and stainless steel in neutral solution. The details about such investigation on which the research focused will be provided in the following paragraphs. Most of the tests were conducted in the laboratories of the research group PoliLaPP of Politecnico di Milano. Furthermore, during an internship period of four months tests were

carried out in collaboration with the AC corrosion group of the Metallurgical and Materials Engineering Department of Colorado School of Mines (Golden, CO, USA).

4.1 AC CORROSION RISK DIAGRAM

As widely discussed in Paragraph 1.4, several factors may influence AC corrosion phenomenon, including AC density on the exposed metal and protection condition, defined by protection potential and protection current density. In addition, the aforementioned technical specification CEN/TS 15280:2006 reports that several other factors may influence AC corrosion likelihood of buried pipelines, as the induced AC voltage and the characteristics of the environment surrounding the metal (as soil resistivity and chemical composition).

However, doubts are revealed about the use of induced AC voltage and soil characteristics as critical parameters for the assessment of AC corrosion likelihood of a buried pipeline. Concerning AC voltage, the technical specification reports that AC voltage measurements should be performed on pipelines or sections of them where unacceptable AC interference is suspected or may be expected. In a first instance, instantaneous measurements should be performed on all test points; at a later stage, measurements may be restricted to a few particular positions, chosen along the most influenced areas.
The measurement is carried out by connecting a high input impedance AC voltmeter with one pole to a reference electrode which is placed on the soil above the pipeline and the other at the test station. In order to reduce AC corrosion likelihood on a buried pipeline, AC voltage should not exceed at any time 10 V and 4 V where local soil resistivity is greater or lower than 25 Ω·m, as reported by the technical specification (Paragraph 1.4.1). These values are based on long term practical experience of European operators.
While no uncertainties are expressed regarding the role of induced AC voltage on corrosion phenomenon, doubts remain about its meaning by the procedure described. Indeed, AC voltage represents the driving force of the current exchange at a coating fault between the pipeline and the environment. As a consequence, AC voltage reduction below critical values provides the primary way to mitigate AC flow and corrosion. Nevertheless, the induced AC voltage measured by means of the procedure reported by the technical specification inevitably contains an ohmic drop contribution not related to the AC corrosion phenomenon. This contribution fakes the measurement and lead to a misleading interpretation. Ohmic drop contribution depends on several factors, as soil resistivity (mainly determined by retained water and salt content) and current distribution. Such parameters could change due to the presence of not homogeneous area and should be considered to evaluate the IR-free AC voltage induced on a structure.
On the other hand, as discussed in Paragraph 1.4.4 and Paragraph 1.6.2, some authors considers the characteristics of the environment surrounding the metal (as soil resistivity, soil chemical composition, alkali and earth-alkali ions ratio) the main AC corrosion-related parameters, due to their effect on spread resistance associated to a coating defect. Even in this case, doubts are expressed about the assessment of AC corrosion likelihood by means of soil characteristics. Even if the knowledge of these parameters could be useful to recognize critical area or section where unacceptable AC interference is expected and AC corrosion is most likely to happen, these parameters don't provide a description of the AC corrosion mechanism. Furthermore, soil characteristics as soil composition at the metal-to-electrolyte interface could be strongly affected by the cathodic current supplied to the protected metal, i.e. CP electric field and diffusion process modify the electrolyte chemical composition which results to be significantly different from that of the surrounding environment. For the aforementioned reasons, uncertainties remain about AC corrosion assessment by means of AC voltage and soil-related parameters.

These considerations lead to take AC density and DC polarization as the main parameters related to AC-induced corrosion. In the following, an experimental AC corrosion risk diagram is discussed, varying AC interference level (in terms of AC density) and protection condition (expressed by protection potential and protection current density).

Long-term exposition tests were carried out on carbon steel, type API 5L X52 (Table 2.1), in order to study the effect of AC density and DC polarization on corrosion rate, calculated by means of mass loss measurement. CP was applied by means of an external DC feeder in both galvanostatic and potentiostatic way in soil-simulation environment: protection potential and current density were applied in the range from -0.850 V to -1.500 V CSE and from 0.2 to 10 A/m^2, respectively. AC density (from 1 to 800 A/m^2) was overlapped to the specimens by means of the electrical circuit described in Paragraph 2.1. At the end of the test (120 days), mass loss was measured and corrosion rate was calculated by means of Eq. 2.8, according to the standard [52]. It should be point out that corrosion rate calculated from mass loss test can be misleading if corrosion is localized, as AC corrosion. The calculated value provides the average corrosion rate assumed constant during the exposition time. This value is not recommended as a measure of the service life of a structure; nevertheless, it provides information about AC corrosion likelihood in different CP and AC conditions. A more accurate analysis of AC corrosion propagation was carried out by means of penetration depth, number and size of AC corrosion attacks measurements and will be discussed in Chapter 5.
Corrosion rates are reported in Table 4.1 varying protection condition (protection potential and current density) and AC interference level (expressed by means of AC density and by the ratio between AC and DC densities), regardless soil-simulating solution chemical composition, i.e. sulphate ions were added in solution in the range 170-1200 mg/L and chloride ions in the range 0-200 mg/L. Table 4.1 includes also previous experimental results obtained in the first phase of the research project.
Figure 4.1 shows corrosion rate data varying AC density; data are gathered on the basis of the CP current density (lower than 0.5 A/m^2, between 0.5 and 1 A/m^2, higher than 1 A/m^2) supplied to the metal with both galvanic anode and impressed current system. In the absence of AC interference the residual corrosion rate is negligible, and steel operates in protection condition, as expected. In protection condition corrosion rate is lower than 10 μm/y and is sufficient low so that corrosion damage cannot occur during the designed lifetime of the structure, as reported by the standard [3]. This critical corrosion rate threshold is shown by a dotted line in Figure 4.1. Experimental results show that in the presence of AC interference, corrosion rate increases by increasing AC density even if a cathodic current is supplied to the metal. The technical specification CEN/TS 15280:2006 [12] reports that AC corrosion likelihood is absent or low if AC density is lower than 30 A/m^2 and high for AC density higher than 100 A/m^2 (Paragraph 1.4.2). Experimental results show that maximum corrosion rates are measured corresponding to AC densities higher than 30 A/m^2 (Figure 4.1). In the worse conditions, regardless the presence of CP, corrosion rates as high as 200 μm/y are measured. Corrosion rate increases of about one order of magnitude with respect to the critical threshold (10 μm/y) corresponding to AC densities in the order of 100 A/m^2. Nevertheless, in the presence of CP current density higher than 1 A/m^2 (red markers), corrosion is not negligible even at 10 A/m^2 AC density.
Figure 4.1 shows that the highest corrosion rates are measured in the presence of high CP current densities (higher than 1 A/m^2), i.e. the critical AC density threshold decreases. For instance, in the presence of 10 A/m^2 AC density, corrosion rate as high as 40 μm/y are measured if DC densities is higher than 1 A/m^2. Otherwise, no corrosion is observed in the presence of DC densities lower than 1 A/m^2, at the same interference level. Summarizing, even if the -0.850 V CSE criterion is matched in all the considered conditions (Table 4.1), corrosion is possible and corrosion rate, as discussed previously, is higher in the presence of high CP current densities.

Table 4.1 – Corrosion rate data

IR-free potential V CSE	AC density A/m²	DC density A/m²	i_{AC} / i_{CP} Adimensional	Corrosion rate μm/y
-0.850	544	0.5	1088	207
-0.850	329	0.5	658	83
-0.850	657	1.0	657	34
-0.856	823	1.0	823	48
-0.850	581	0.4	1660	41
-0.870	301	0.2	1254	35
-0.900	297	1.0	297	33
-0.900	100	0.2	500	39
-0.900	475	0.5	950	60
-0.930	207	0.5	414	1
-0.930	650	0.9	691	129
-0.950	290	0.8	345	56
-0.960	175	1.0	175	30
-0.960	424	0.8	537	106
-0.990	63	0.5	126	1
-0.990	101	0.5	202	1
-1.000	1	0.5	2	1
-1.000	100	0.5	200	10
-1.000	50	0.2	250	49
-1.010	34	1.0	34	10
-1.050	15	0.5	30	5
-1.080	29	0.5	58	1
-1.080	99	1.0	99	29
-1.100	430	10.0	43	240
-1.110	88	1.0	88	72
-1.110	188	1.0	188	66
-1.218	500	2.0	250	45
-1.131	0	1.5	0	1
-1.260	1	1.0	1	1
-1.260	11	1.0	11	1
-1.260	87	1.0	87	33
-1.260	295	1.0	295	52
-1.270	479	10.0	48	212
-1.300	1	10.0	0	8
-1.300	10	10.0	1	13
-1.318	100	2.0	50	63
-1.350	100	10.0	10	48
-1.370	385	10.0	39	177
-1.470	102	10.0	10	140

Figure 4.2 shows corrosion rate data as a function of the i_{AC} (AC density) and i_{DC} (DC density) ratio (i_{AC}/i_{DC}). Data are gathered in two sets, depending on the protection potential assumed by the metal (higher or lower than -1.1 V CSE).
In the following, *overprotection condition* will be referred to carbon steel IR-free potentials lower than -1.1 V CSE. This value is reported by cathodic protection guidelines [3] as the limiting critical potential below which detrimental effects on coatings could occur, as blistering or gradual cathodic disbonding at faults in thick as well as in thin protective coating.
The i_{AC}/i_{DC} ratio doesn't depend on the area of the metal exposed to the electrolyte and provides a supplementary indication to define AC corrosion risk. Technical specification CEN/TS 15280:2006 [12] reports a low AC corrosion likelihood if i_{AC}/i_{DC} ratio is lower than 5 and a high corrosion likelihood if i_{AC}/i_{DC} ratio is greater than 10. Figure 4.2 shows that overprotection is the most dangerous condition. Even in the presence of i_{AC}/i_{DC} ratio lower than 10, corrosion rate is not negligible (> 10 μm/y) if the protection potential is more negative than -1.1 V CSE. The aforementioned current densities ratio criterion seems to be applicable only if overprotection conditions are not matched. As discussed in Paragraph 1.4.3, it should be pointed out that the only use of the i_{AC}/i_{DC} ratio is not recommended to define the AC corrosion risk, because of the misleading meaning that could be associated to it.

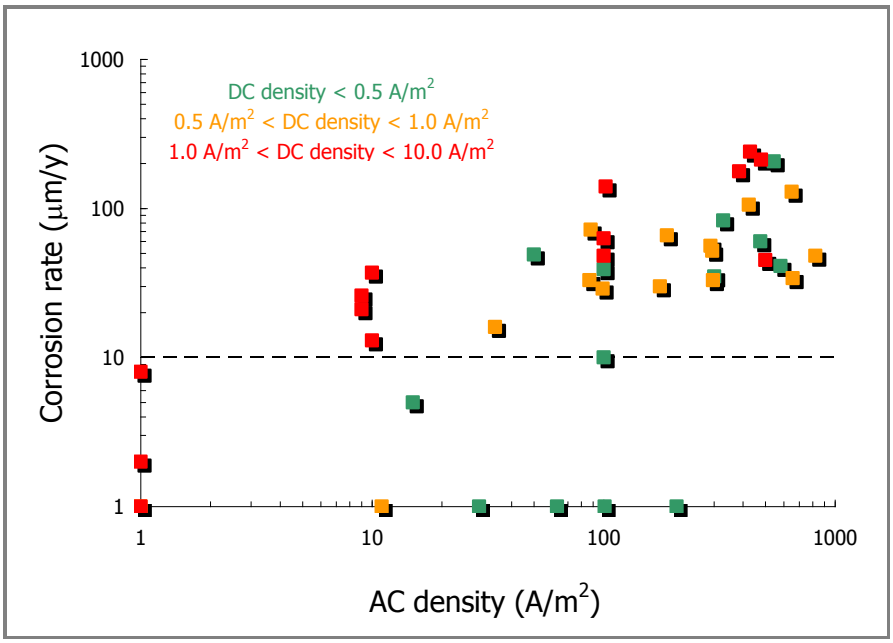

Figure 4.1 – Corrosion rate vs. AC density varying DC density

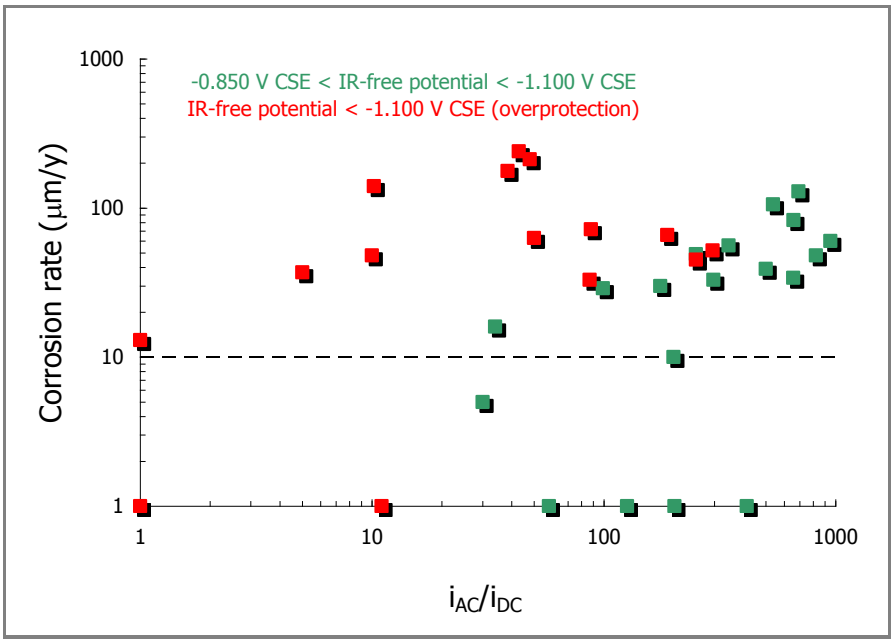

Figure 4.2 – Corrosion rate vs. AC-DC densities ratio varying protection potential

For instance, an i_{AC}/i_{DC} ratio equal to 10 can result by different protection and interference levels, e.g. 30 A/m^2 AC in the presence of 3 A/m^2 DC or 3 A/m^2 AC in the presence of 0.3 A/m^2 DC. Even if the i_{AC}/i_{DC} ratio is the same, the interference condition (and corrosion risk) is different, i.e. 3 A/m^2 AC density is not recognized as a critical value, differently from 30 A/m^2 (Paragraph 1.4.2).

Laboratory test results show that AC corrosion likelihood is influenced by AC interference level, as expected, but also by protection condition, expressed by protection potential and protection current density. Since CP criteria are generally based on protection potential measurement (Paragraph 1.1.5), it's more practical to relate AC corrosion risk to protection potential than to protection current density.

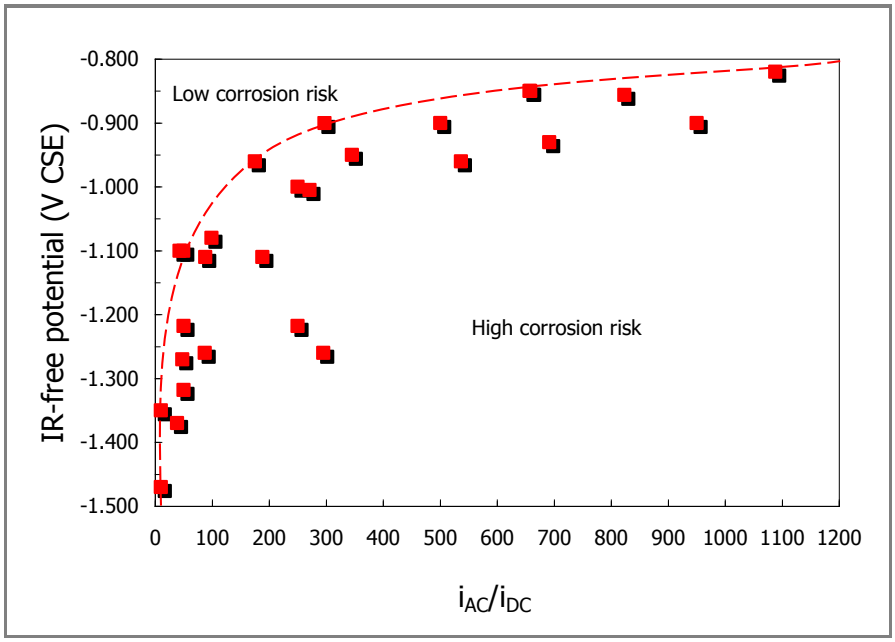

Figure 4.3 – AC corrosion risk diagram

Figure 4.3 reports the so-called *AC corrosion risk diagram* that correlates protection potential to the adimensional AC and DC densities ratio. This empirical diagram allows assessing CP effectiveness in the presence of AC interference by means of IR-free potential and current densities measurements, e.g. carried out by means of corrosion probes or corrosion coupons (Paragraph 1.8.1). Two corrosion risk levels are identified, low and high. High corrosion risk corresponds to corrosion rates greater than the maximum acceptable level, fixed by CP guidelines [3] at 10 μm/y. The markers in the diagram refer to high risk corrosion conditions (i.e. corrosion rate > 10 μm/y), tested in the experiments.

Corrosion risk increases by increasing the i_{AC}/i_{DC} ratio, according to Figure 4.2. Corrosion protection is achieved up to a critical value of the i_{AC}/i_{DC} ratio, above which corrosion rate is not negligible. Nevertheless, the critical current densities ratio depends on the protection potential of the metal, i.e. it decreases by decreasing the protection potential. Overprotection (potential lower than -1.1 V CSE) is the most dangerous condition as regard AC corrosion risk and must be avoided. In the absence of AC interference, corrosion doesn't occur: the metal is protected by the cathodic current. In overprotection condition, corrosion occurs even in the presence of AC densities lower than 30 A/m^2, the level proposed by the technical specification (Paragraph 1.4.2). Indeed, just a few A/m^2 of AC density can cause corrosion of overprotected carbon steel.

In agreement to the showed experimental results, the influence of the CP level on AC corrosion was observed also by Nielsen et al. [38-40] that proposed the so-called alkalinization mechanism, described in Paragraph 1.6.4. Authors state that AC corrosion is not avoided by adding a surplus of CP, as in the case of DC stray current corrosion. In the presence of AC interference, the CP level has a dramatic influence on the AC corrosion process, i.e. excessive CP increases AC corrosion rate and should therefore be avoided.

The main conclusions may be summarized as follows:

- corrosion rate increases by increasing AC density, even if CP is applied;
- AC density cannot be considered as the only parameter to estimate AC corrosion likelihood;
- IR-free protection potential and i_{AC}/i_{DC} ratio must be taken into account in order to evaluate AC corrosion risk;

- the -0.850 V CSE criterion is not always safe in the presence of AC interference;
- overprotection (potential lower than -1.1 V CSE) is the most dangerous condition and must be avoided.

In the presence of AC interference, the criteria given by the standard EN 12954:2002 "Cathodic protection of buried or immersed metallic structures – General principles and application for pipelines" [3] are not sufficient to demonstrate that steel is protected against corrosion. The definition of CP criteria in the presence of AC is still ongoing, in order to provides limits, measurements procedures and mitigation measures.
As discussed, CP criteria should consider not only the interference condition, by means of the AC voltage and AC density magnitude, but also the IR-free potential (also called true potential) that define the CP level of a metal structure.
The experimental results obtained during the research project carried out by the research group PoliLaPP of Politecnico di Milano led to a proposal of CP criteria in the presence of AC interference (described elsewhere [68]). Nevertheless, the definition and the discussion of CP criteria in the presence of AC interference are beyond the scope of this work, which main topic is AC corrosion mechanism.

4.2 A TWO-STEPS MECHANISM

Several AC corrosion mechanisms have been proposed and are widely discussed in Paragraph 1.6. AC corrosion models are based both on theoretical considerations (e.g. electrical equivalent circuit analysis and electrochemical approaches) and on experimental tests (laboratory results, field tests or corrosion cases study). However, none of these models provides a full description of the process.

In this work, a two-steps AC corrosion mechanism of carbon steel in CP condition is proposed:
- **Step 1**: AC causes the breakdown of the passive film formed on carbon steel surface in CP condition due to electro-mechanical stresses in the film;
- **Step 2**: after passive film breakdown, corrosion occurs if the pH of the environment at the metal-to-electrolyte interface is close to 14.

Before describing the proposed mechanism, some thermodynamic considerations are discussed.

4.3 THERMODYNAMIC CONSIDERATIONS

The potential-pH diagram of the iron-water system could be helpful to a better understanding of CP effectiveness. Potential-pH diagrams (also called Pourbaix diagrams) have been adopted universally since their introduction in late 1940s. A potential-pH diagram represents the stability of the metal as a function of potential and pH. Similarly to chemical phase equilibrium diagrams, a stable phase can be determined corresponding to a combination of pH and potential. These diagrams are determined from calculations based on Nernst equation and solubility data for metal and its species. The major uses of such diagrams are (1) predicting whether or not corrosion can occur; (2) estimating the composition of corrosion products formed and (3) predicting environmental changes that will prevent or reduce corrosion attacks. Nevertheless, Pourbaix diagrams are purely based on thermodynamic data and do not provide any information on reaction kinetics.
Generally, in a potential-pH diagram three possible regions (or domains) can be identified:
- *Immunity domain*: corresponding to the state of a metal in which corrosion is thermodynamically impossible;
- *Corrosion domain*: corresponding to the state of a metal in which corrosion is possible and the metal reacts with the surrounding environment;
- *Passivation domain*: corresponding to the state of a metal that leads to more or less perfect passivity condition. Passivity refers to the state of the metal in which corrosion

is prevented by modifications of its surface, for instance, by the formation of a thin protective layer of oxide.

Figure 4.4 shows the equilibrium potential-pH diagram of the system iron-water at 25°C, assuming passivation from the formation of a film of Fe_2O_3 and Fe_3O_4, as reported by Pourbaix in the *Atlas of Electrochemical Equilibria in Aqueous Solutions* [69, 70]. Lines (a) and (b) refer to hydrogen evolution and oxygen reduction reactions, respectively. Equilibrium lines in the diagrams correspond to a solubility of metal and its oxide equal to 10^{-6} mol/L.
Four domains can be identified: the immunity region, two corrosion regions and the passivation region. The region of stability of iron is entirely below the region of stability of water (delimited by lines (a) and (b)) at 1 atm pressure. This means that iron tends, if not passivated, to corrode with reduction of water and hydrogen evolution. Corrosion is possible in two domains with the formation at low pH of green ferrous ions Fe^{2+} and yellow ferric ions Fe^{3+} (at low and high potential, respectively) and green dihypoferrite ions FeO_2H^- at high pH. The diagram shows also the existence of a passivation region in which iron is protected by insoluble products (Fe_2O_3 and Fe_3O_4) which are sufficiently adherent that corrosion of the underlying metal is essentially prevented and the metal is in the so-called "passive condition". In passive condition, the protection will be perfect or imperfect depending on whether or not the film perfectly shields the metal from the contact with the solution.

As discussed in Paragraph 1.1.2, CP effectiveness depends on two distinct effects of the potential lowering: a thermodynamic effect which reduces (or brings to zero) the driving voltage of the corrosion process, and a kinetic effect that depends on the increase of the reaction resistance.
From a thermodynamic point of view, CP could be generally defined as the establishment of a state of immunity by a cathodic polarization, i.e. by making the potential of the metal more negative. CP thermodynamic effect can be schematically represented in Figure 4.5 using iron Pourbaix diagram. The potential assumed by a buried steel structure in a neutral soil (pH 7) can be represented approximately by the point (1) in Figure 4.5. Steel is in free corrosion condition. Generally, corrosion potential depends on several factors that affect anodic and cathodic reactions occurring on the metal surface, as soil water content, salt content, pH and oxygen availability. In order to reduce or halts the driving voltage of the corrosion process, the potential can be lowered (cathodic polarization) by means of an external DC feeder or by the coupling with a less noble metal (galvanic anode). If the metal potential is below the equilibrium potential (defined by Nernst's equation, Paragraph 1.1.1), the anodic process cannot take place, i.e. thermodynamic immunity is established (point (2) in Figure 4.5). When potential lowering is not sufficient to set to zero the driving voltage, quasi-immunity condition is established and the potential is brought to values close enough to the equilibrium potential to make corrosion rate acceptable. This value is -0.850 V CSE (or -0.950 V CSE in the presence of sulphate reducing bacteria) for steel in soil, as reported by CP guidelines [3]. This value corresponds about to -0.530 V SHE (Standard Hydrogen Electrode) which Pourbaix diagram refers.
Over time, however, the pH will increase as a result of the cathodic reactions that occur on the metal cathodically polarized. As mentioned, the cathodic reactions which generally occur on carbon steel in CP are oxygen reduction and, at lower potential, hydrogen evolution (Chapter 1, Eq. 1.5). In both cases, hydroxyl ions formation brings to the increase of the pH of the electrolyte in contact with the metal. Since hydroxyl ions production is regulated by the cathodic current supplied to the metal, the local pH increase will be greater corresponding to high CP levels, i.e. high cathodic current or more negative potentials.

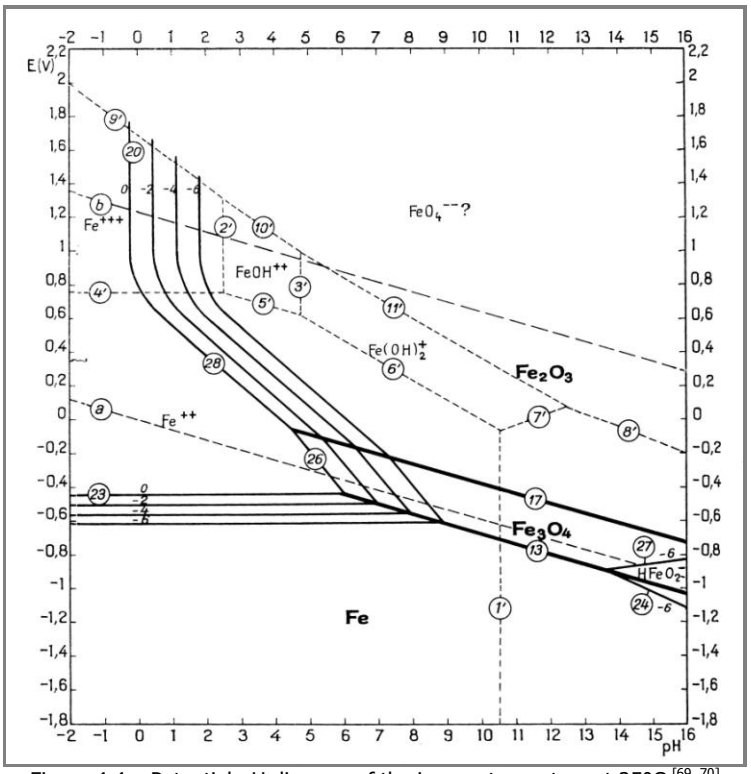

Figure 4.4 – Potential-pH diagram of the iron-water system at 25°C [69, 70]

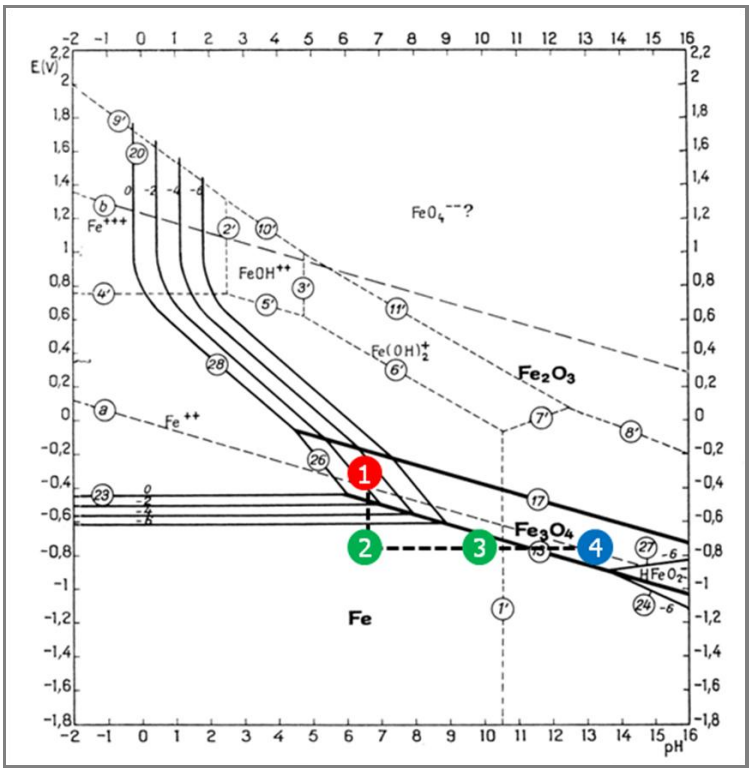

Figure 4.5 – CP thermodynamic effectiveness using potential-pH diagram of the iron-water system

The pH increase identifies a new thermodynamic condition that is represented by a point on the horizontal line 2-3-4 in Figure 4.5. Depending on the pH of the electrolyte in contact with the metal, the thermodynamic condition will be given by a point on this line, keeping constant the protection potential. For instance, as a result of the alkalization process, the metal will be in the immunity region, point (3), or in the passivation region, point (4), depending on potential and pH value.
The effects of electrolyte alkalinization are well-known in sea-water CP application. Indeed, as discussed in Paragraph 1.1.4, the alkalization due to the cathodic current causes the growth on steel surface of a calcium carbonate and magnesium hydroxide scale, commonly known as calcareous deposit, particularly beneficial because reduces the protection current by acting as a barrier that limits oxygen diffusion and maintains alkalinity at the metal surface.
There is a lack of data about electrochemical protection mechanism provided by CP on steel in soil, mainly due to the complexity of the electrochemical system. Even the aforementioned standard [3] defines CP as an electrochemical protection achieved by decreasing the potential of the metal to a level whereby corrosion rate is significantly reduced but doesn't provide a description of the protection mechanism.
Pourbaix [70] studied the influence of pH and electrode potential on the electrochemical behavior of iron. Anodic polarization experiments were carried out in the presence of oxygen-free solutions of pH between 1.5 and 14.5. For each experiment, passivation potential and passivation current densities were noted. These conditions are illustrated in Figure 4.6. Experimental data are in good agreement with theoretical predictions. Passivation potential and passivation current density decrease by increasing the pH of the electrolyte, i.e. the thermodynamic stability of the passivation condition on iron increase by increasing the metal-to-electrolyte pH.

Freinman et al. [71], taking into account Kolotyrkin works, outlined the concept of *"cathodic passivation".* Authors criticized some common views in literature on CP mechanism of metallic structures that don't take into account the effect of pH on the metallic electrochemical behavior. A brief summary of their investigation is reported below.
In soil the transport of chemical species occurs much slower than in aqueous solutions due to soil nature that is a (almost) convection-free, highly viscous medium. Furthermore, the transport kinetic laws in soil depend on its mean moisture content (W) and compactness. Hydroxyl ions can diffuse in soil only through liquid-filled channels, whereas the diffusivity of oxygen in the gaseous phase is three orders of magnitude higher than in the aqueous one. This means that in soils the pH close to the metal surface (indicated as pH_S) increase with cathodic current density, reaching a considerably higher level (11–12, and higher) than in bulk aqueous solutions [72] (Figure 4.7). In such conditions, the metal potential (E) can become higher (less negative) than the passivation potential (E_{pas}) due to their dependence on pH. As a result, the cathodic polarization can induce a passivation condition on the metal. Authors state that this induced passivation isn't associated with the formation of thick layers of deposits and oxides, frequently observed on steel upon long term cathodic polarization in soils or waters.
Authors refer to this protection mechanism as *"cathodically induced anodic passivation"*. Furthermore, they compared the calculated dependence of pH_S on potential (E) with the empirically known effects of pH on E_{PAS} of iron. The straight line 1 in Figure 4.8 represents the E_{pas}-pH dependence and the straight line 2 the E-pH_S dependence in sand (with W = 10%). Corresponding to -0.950 V CSE (E*), the straight lines 1 and 2 intersect: the passive region ($|E| < |E_{pas}|$) is located to the left of the vertical line containing E*, whereas the active region ($|E| > |E_{pas}|$) is on the right of it. Thermodynamic conditions are so strictly connected to the potential-pH condition.

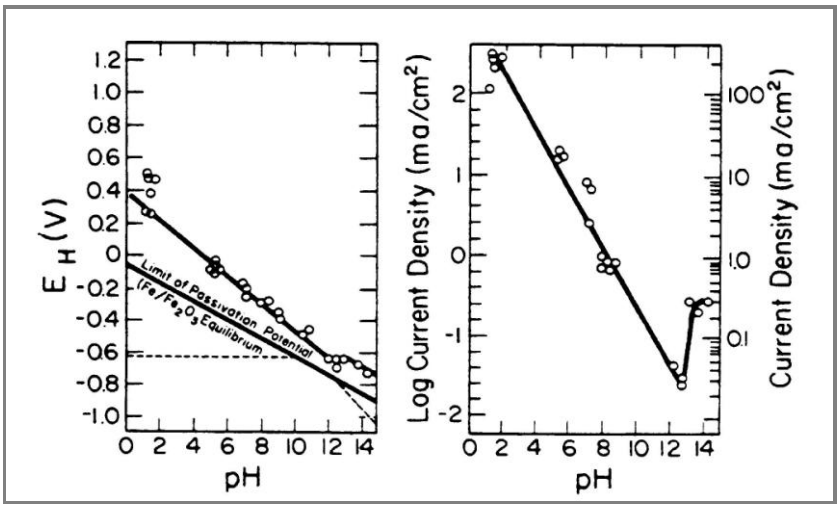

Figure 4.6 – Influence of pH on passivation potential (left) and on passivation current density (right) of iron [70]

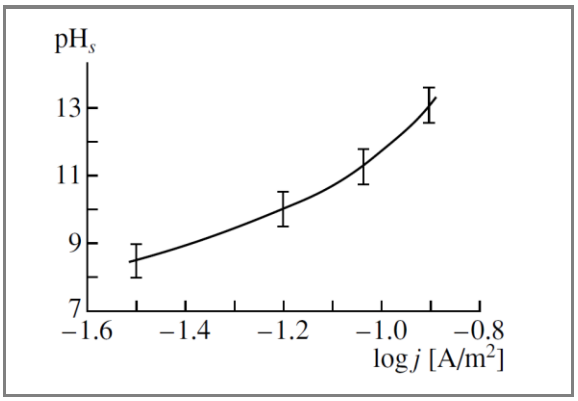

Figure 4.7 – Dependence of pH_S on cathodic current density in sand moistened with tap water [72]

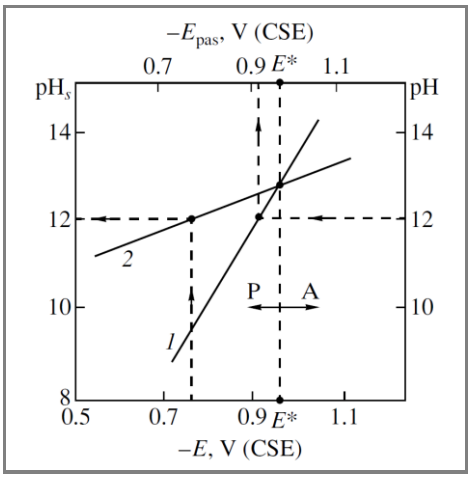

Figure 4.8 – Empirical dependence of iron passivation potential (E_{pas}) on pH (straight line 1) and the calculated dependence of pH_S on steel potential (E, straight line 2) [71]

Figure 4.9 shows anodic polarization curves plotted before (curve 1) and after (curve 2) cathodic polarization of mild steel in sand (W = 10%). Curves 1 and 2 are typical of an active and a passive metal, respectively; curve 3 was obtained without preliminary cathodic polarization but in sand moistened with an alkaline solution, in which the steel is capable of self-passivation.

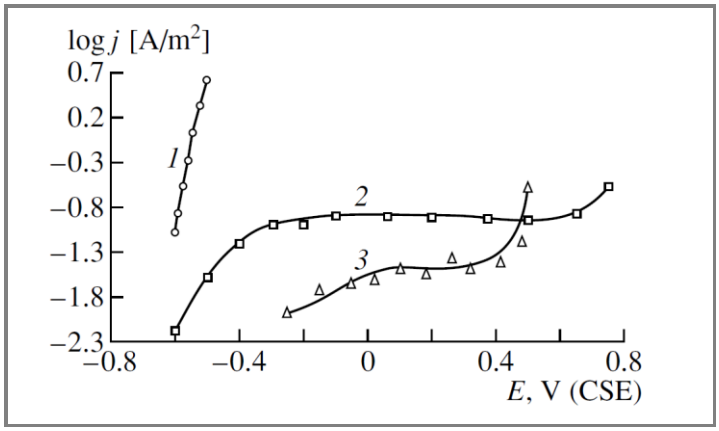

Figure 4.9 – Anodic curves on iron in sand: (1) from E_{corr} moistening with 0.03 M NaCl; (2) after 24-hours cathodic polarization at -0.9 V CSE moistening with tap water; (3) from E_{corr} moistening with 0.1 M NaOH [71]

Leeds and Cottis [73, 74] investigated cathodically-formed surface films on steel specimens in 3.5% sodium chloride solution, artificial seawater and in alkaline solution (pH 10) of composition similar to that found between a disbonded coating and a pipeline [74]. Although doubts are expressed about some results discussed in these works (particularly the reported corrosion rates of steel on CP condition) some considerations are now reported. Authors state that films can form on the metal surface as a direct consequence of the applied CP.

Protective films are progressively formed over a three day period as a direct result of the cathodic polarization and longer times are needed to form coherent films. In pure 3.5% sodium chloride [73], more coherent films are formed corresponding to very negative potentials (-1.3 V SSC) and are composed mostly of magnetite. Furthermore, authors state that the presence of surface films has a strong influence on the current required to maintain CP. The created protective film may act as an insulator reducing the conductive properties of the metal surface and the total area of the metal exposed to the environment, with a consequent decrease with time of the CP current density needed to polarize the metal. On specimens exposed to the alkaline pipe solution, a coherent film is also observed. However, conversely to that reported by the authors, it should be point out that passivation condition (thermodynamically defined by the potential-pH diagram) should be distinguished by the calcareous deposit formation occurring on the metal surface as a result of the alkalization process.

In order to study AC corrosion and protection criteria, Carpentiers et al. [48] conducted a large number of tests varying the metal potential and the pH of the electrolyte. Authors state that local alkalization via CP at the metal surface is very important and there is a clear difference between the cases where AC is absent or present. In the absence of AC, high pH is favorable because of the formation of a "perfectly protective passive film". At high pH, potentials more negative than -0.850 V CSE correspond to a protection by "perfect passivation", where no general or localized corrosion can occur.

Summarizing, although there is a lack of data about the real protection mechanism (by immunity or by passivation) offered by CP to carbon steel, there are some experimental evidences that a protective passive film may form on the cathodically protected metal, especially if exposed in soil.

It should be pointed out that a metal in CP condition represents a complex electrochemical system and further analyses are mandatory. The simultaneous action of potential lowering and pH increase creates electrochemical condition at the metal-electrolyte interface that could be completely different to the bulk condition. Furthermore, as discussed also by Pourbaix in his Atlas [69], potential-pH diagrams are purely based on thermodynamic data and refer to the

specified conditions of ions activity and temperature. For instance, as regard the position of the domains boundaries, diagrams showed in Figure 4.4 and Figure 4.5 refer to certain hypothetical conditions in the absence of substances capable of forming soluble complexes or insoluble salts with iron. For instance, the presence of earth-alkaline ions (as Ca^{2+} and Mg^{2+}) or insoluble salts (phosphates, sulfides) extends the passivation region expected from Pourbaix diagram [21, 70].
While several information are available on the nature of passive film formed on anodically polarized iron, there is a scarcity of data regarding the composition and the structure of films formed in the considered condition. Regarding the composition of the passive film anodically formed on iron, the consensus view is that Fe_2O_3 is responsible for passivity while Fe_3O_4 provides the basis for formation of the higher oxidation state but doesn't contribute directly to lower the anodic dissolution [75]. At this stage of the research, experimental tests are mandatory in order to investigate the presence and the physical-chemical nature of the passive layer formed in CP.

The two-steps mechanism proposed (Paragraph 4.2) is based on the effect of AC on the breakdown of the passive film formed on steel in CP condition. Namely, the model assumed the presence of a protective film on the metal surface in CP condition. Surface characterization of iron in CP condition has not yet been done during this phase of the research. The study of the protection mechanism of carbon steel in CP condition could represent an interesting and mandatory aspect to investigate in the future and further analyses are scheduled.
Although these aspects need a more accurate investigation, a preliminary study by means of linear polarization resistance measurements on cathodically pre-polarized carbon steel was carried out. Details about such investigation are provided in the following paragraph.

4.3.1 Linear polarization resistance measurement

As discussed in Paragraph 2.2.4, linear polarization resistance (LPR) measurement is an accurate and rapid way to measure general corrosion rate of metals by means of a small potential scan defined with respect to the corrosion potential. LPR is defined as the slope of the potential-current curve at zero current, i.e. corresponding to the free corrosion potential (Eq. 2.4). Corrosion current density (related to corrosion rate) is inversely proportional to LPR through the Stern-Geary coefficient (Eq. 2.5) that depends on anodic (β_a) and cathodic (β_c) Tafel slopes (Eq. 2.6).
LPR measurements were carried out on carbon steel specimens grade API 5L X52 (Table 2.1) cathodically pre-polarized. The aim of the test is to investigate the effect of a cathodic pre-polarization on linear polarization resistance of carbon steel.
LPR measurement was carried out according to ASTM G59 "Standard test method for conducting potentiodynamic polarization resistance measurements" [56] on carbon steel specimens after three days cathodic polarization. Four CP levels were applied in a potentiostatic mode: -0.850 V, -0.950 V, -1.100 V and -1.200 V CSE. After three days protection, CP was turned off and specimens were maintained in free corrosion condition until the open-circuit potential measured before CP was attained. The time required to reach the initial potential (de-polarization time) varies depending on the CP potential applied previously, i.e. it increases by decreasing the protection potential. In any case, the de-polarization time was in the range from ten to twenty minutes. After free corrosion condition attainment, LPR measurement was carried out according to the standard [56].
Some considerations should be clear up. The measurement carried out according to the procedure described above doesn't provide the LPR value (and the related corrosion rate) of carbon steel in CP condition. As discussed before, LPR is associated to free corrosion potential, by definition. As a consequence, the calculated corrosion rate from LPR measurement doesn't refer to the metal in CP but to free corrosion condition.

Nevertheless, it is assumed that the surface condition formed on the metal in CP (e.g. the formation of a passive film) doesn't change during the de-polarization time that runs between the end of the pre-polarization period and the LPR measurement in free corrosion condition.
Even if these assumptions could be too restrictive, LPR measurement can be useful to investigate the effect of CP on the formation of a protective passive film. Indeed, LPR is strongly related to the presence of a protective and adherent oxide film on the metal surface which reduces corrosion rate of the metal with respect to the corrosion rate measured in active condition without a cathodic pre-polarization. For comparative purpose, corrosion rate was calculated assuming a Stern-Geary coefficient of 0.026 V [21].
Figures 4.10 to Figure 4.14 show potential-current curves carried out to measure LPR as the slope of the curve corresponding to the free corrosion potential ("zero-current potential"), varying the CP level in the pre-polarization period. Figure 4.10 shows the potentiodynamic curve in the reference condition (no cathodic pre-polarization before LPR measurement). As discussed in Paragraph 2.2.4, potential-current relation is linear within a few millivolts of polarization from corrosion potential, in agreement with LPR definition. LPR calculation was carried out by a curve fitting and data are reported in Table 4.2.
LPR values after 72 hours of cathodic pre-polarization are about one order of magnitude greater than the value measured without a preliminary polarization. In the absence of pre-polarization, corrosion potential is -0.629 V CSE and LPR is 0.4 $\Omega \cdot m^2$. Assuming a Stern-Geary coefficient of 0.026 V, corrosion current is 74.2 mA/m^2 which corresponds to a corrosion rate of 87 $\mu m/y$, i.e. the metal is in active condition and corrosion is not negligible.
After a cathodic polarization at -0.850 V CSE for three days, LPR is 3.3 $\Omega \cdot m^2$, one order of magnitude greater than the value measured without pre-polarization. Corrosion current is 7.9 mA/m^2 and corrosion rate is 9 $\mu m/y$. Corrosion rate diminution could be explained by the presence of a thin oxide film formed on CP condition that doesn't disappear instantly, i.e. in free corrosion, active condition (no passive film) is achieved after the transition time. After a cathodic polarization at -0.950 V CSE, LPR is 6.3 $\Omega \cdot m^2$. Corrosion current is 4.2 mA/m^2 and corrosion rate is 5 $\mu m/y$, more than one order of magnitude lower than corrosion rate in the absence of pre-polarization. After a cathodic polarization at -1.100 and -1.200 V CSE for 72 hours, LPR is 4.0 and 3.9 $\Omega \cdot m^2$, respectively. Even in these cases, corrosion rate are lower than the safe value 10 $\mu m/y$ [3].
As discussed in Paragraph 4.3, there is a lack of data about the electrochemical condition of the metal in CP. LPR measurement doesn't provide direct information about the presence of a protective film created by CP condition on the metal surface. Such information could be obtained by more accurate electrochemical analysis or by in-situ methods of surface characterization on CP. However, an effect of CP on LPR measurement was measured and could be associated to the presence of a passive film formed on the metal during the cathodic pre-polarization. Further investigations on the better understanding of protection mechanism of carbon steel cathodically protected (i.e. by immunity or passivity protection) are mandatory and are still ongoing.

Table 4.2 – LPR measurement

Pre-polarization potential	**LPR**	**Corrosion current(*)**	**Corrosion rate**
V CSE	**$\Omega \cdot m^2$**	**mA/m^2**	**$\mu m/y$**
No pre-polarization	0.4	74.2	87
-0.850	3.3	7.9	9
-0.950	6.3	4.2	5
-1.100	4.0	6.5	8
-1.200	3.9	6.6	8

*calculated by means of Eq. 2.5, assuming B = 0.026 V

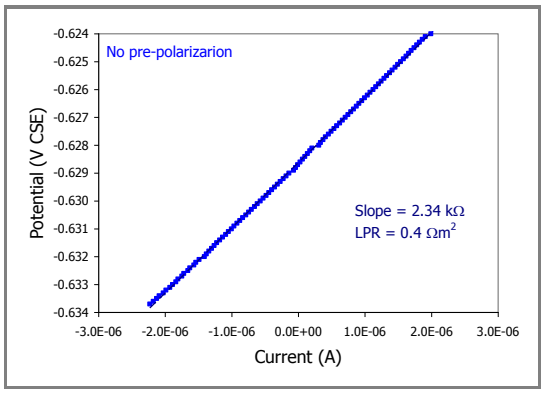

Figure 4.10 – LPR measurement on carbon steel without a cathodic pre-polarization

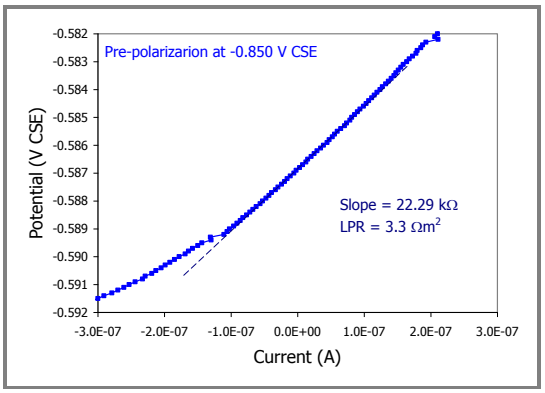

Figure 4.11 – LPR measurement on carbon steel with a cathodic pre-polarization at -0.850 V CSE

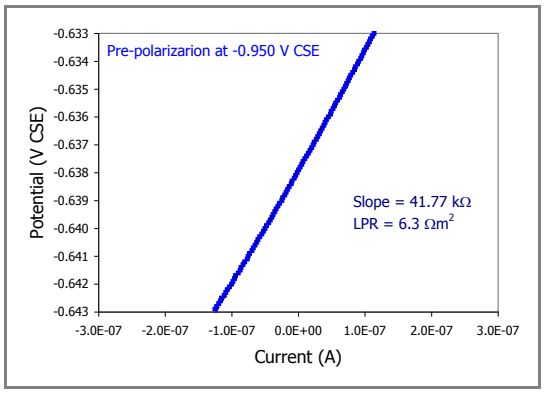

Figure 4.12 – LPR measurement on carbon steel with a cathodic pre-polarization at -0.950 V CSE

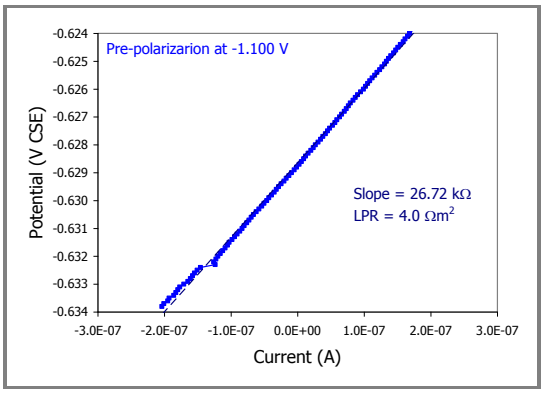

Figure 4.13 – LPR measurement on carbon steel with a cathodic pre-polarization at -1.100 V CSE

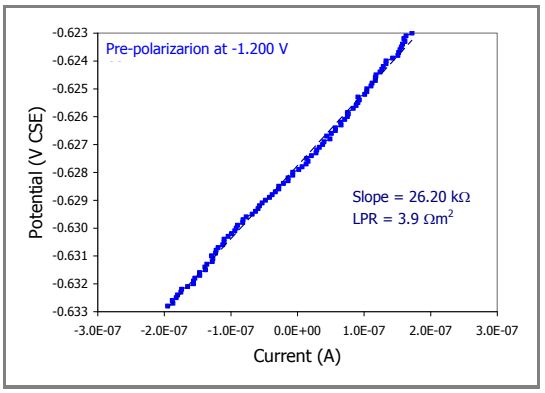

Figure 4.14 – LPR measurement on carbon steel with a cathodic pre-polarization at -1.200 V CSE

4.4 STEP 1: THE FILM BREAKDOWN MECHANISM

As discussed in Paragraph 4.2, a two-steps AC corrosion mechanism of carbon steel in CP condition is proposed. In the first step (Step 1), AC causes the breakdown of the passive layer that CP condition forms of the metal surface (Paragraph 4.3). After passivity breakdown, high-pH corrosion occurs (Step 2). In this section, the film breakdown mechanism is discussed.

In Step 1, the electro-mechanical breakdown of the passive film due to the presence of high alternating electric field within the oxide layer is proposed. This represents an absolute novelty regarding the description and the investigation of AC corrosion initiation mechanism.

Although some AC corrosion models deal possible harmful effects of AC on passivation condition, no one provides a description of the mechanism by which AC corrodes passive metals. Indeed, some models (widely discussed in Paragraph 1.6) report a kind of "imperfect passivity" resulting from potential oscillation induced by the presence of the alternating signal overlapped to the metal. For instance, Nielsen et al. [38-40] in the alkalization model (Paragraph 1.6.4) state that AC-induced potential oscillations between the passive, the immunity and the high-pH corrosion domains of the Pourbaix diagram can cause corrosion. Accordingly, Carpentiers et al. [48] state that non protective films can form when the potential oscillates between the passivation domain and the immunity domain and that superimposed AC can destroy passivation films that would be perfectly protective in the absence of AC. Even the technical specification CEN/TS 15280:2006 [12] reports that during the anodic AC-induced potential oscillation the metal surface is oxidized with the formation of a passive film, while during the cathodic oscillation the passive film is reduced to iron hydroxide. As a result, every AC cycle results in a net metal corrosion. Summarizing, these models emphasize the harmful AC effect on the formation of a steady passive condition on the metal surface but don't provide information about the mechanism by which AC affects the passive condition.
Even though more than one theory in literature may be considered, in the following a possible corrosion initiation model applied for the first time to AC corrosion is described. It should be truly pointed out that the proposed "electro-mechanical film breakdown mechanism" is a novelty considering the application on AC corrosion but is well-known in the field of localized corrosion, as in the description of pitting phenomena.
Indeed, several models have been proposed to describe localized corrosion of passive metals based either on breakdown processes of the passive film or on the presence of structural defects/heterogeneities of the underlying metal as dislocations, grain boundaries, second phase precipitates, or nonmetallic inclusions. Certainly a strict differentiation of the two approaches is not always possible, since film breakdown and structural parameters of the underlying metal may be correlated [76].
Theoretical models that describe the initiation process of passive film breakdown may be grouped into three classes [76, 77]:

1) adsorption-induced mechanism, where the adsorption of aggressive ions as chlorides is of major importance;
2) ion migration and penetration models;
3) mechanical film breakdown theories.

The adsorption mechanism (Figure 4.15), discussed first by Kolotyrkin [78], starts with adsorption of aggressive anions at the oxide surface, which enhances catalytically the transfer of metal cations from the oxide to the electrolyte. This effect leads to thinning of the passive layer with possible final total removal and the initiation of intense localized dissolution.
The penetration mechanism (Figure 4.16), first discussed by Hoar et al. [79], involves the transfer of anions through the oxide film towards the metal surface where they accumulate causing stresses in the film, until its breakdown.
The film breaking mechanism (Figure 4.17), proposed by Vetter and Strehblow [80] and Sato et al. [81], requires the film breakdown due to a sudden change of the electrode potential; the resulting mechanical film cracking gives direct assess of the anions to the unprotected metal.
Nevertheless, as discussed by Strehblow [77], a strict separation of these mechanisms might not always be appropriate. The discussion will be now focused on the film breaking mechanism taking into account the description provided by Sato [81]. Stresses in oxide films can arise for several reasons: interfacial tension in the film, electrostriction pressure resulting from the presence of a high electric field in the film, internal stresses caused by the volume ratio of the film and the metal, internal stresses due to partial hydration or dehydration of the film and local stresses caused by impurities. As a result, the existence of stresses in anodic films depends on several factors as metal surface condition, impurities, and film formation and growth mechanism.

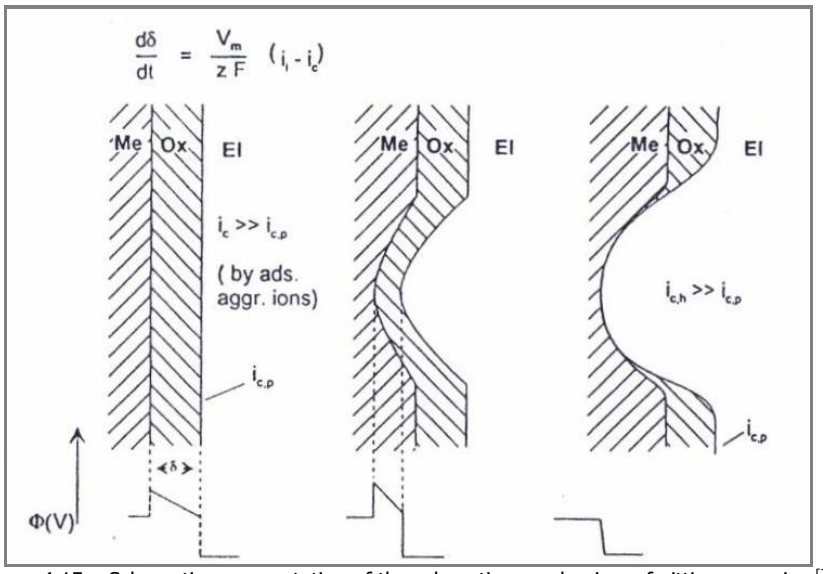

Figure 4.15 – Schematic representation of the adsorption mechanism of pitting corrosion [77]

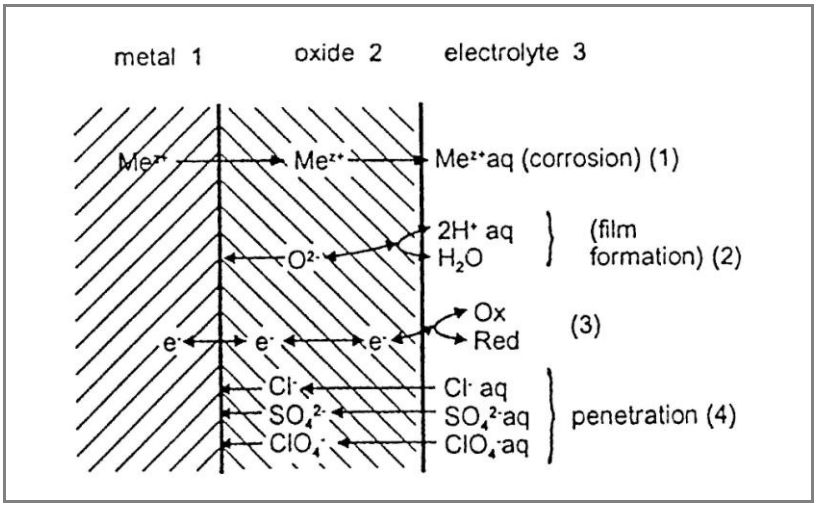

Figure 4.16 – Schematic representation of the penetration mechanism of pitting corrosion [77]

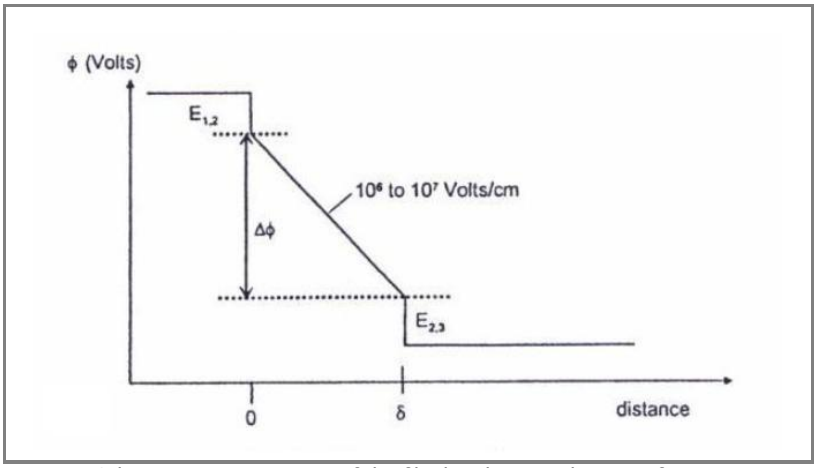

Figure 4.17 – Schematic representation of the film breaking mechanism of pitting corrosion [77]

Using a thermodynamic framework, Sato [81] suggested that mechanical failure of the film can result from brittle cracking or plastic deformation driven by high electromechanical stresses generated by the presence of electric fields across the film. The author derived thermodynamically the stress in passive films produced by interfacial tension (not negligible due to the thin thickness of the passive film) and by electrostriction pressure. Generally, electrostriction is defined as the deformation of a dielectric body as the result of an applied electric field that polarizes the randomly-aligned electrical domains within the material. Due to the presence of an electric field within the film, the opposite sides of the domains become differently charged and attract each other, reducing material thickness in the direction of the applied field.
The author considers the simplest polarization model of a dielectric oxide layer in the presence of a constant electric field. The system under study consists of a dielectric film of thickness L in contact with the metal on one side and with the electrolyte on the other side. The film is mechanically free to deform on the electrolyte side but is constrained on the metal surface. The film pressure (σ) acts vertically to the film and is determined by the atmospheric pressure (σ_0), the *electrostriction pressure* (σ_E) that arises due to the presence of an electric field (E) across the film, and the interfacial tension (σ_γ) [81]:

(Eq. 4.1) $$\sigma - \sigma_0 = \sigma^* = \frac{\varepsilon(\varepsilon - 1)E^2}{8\pi} - \frac{\gamma}{L} = \sigma_E - \sigma_\gamma$$

where ε is the dielectric constant of the film related to the dipole moment per unit volume of the film (P) as follows:

(Eq. 4.2) $$P = \chi E = \frac{(\varepsilon - 1)E}{4\pi}$$

where χ is the electric susceptibility of the film. It can be shown that a mechanical stress can arise in metal oxide or hydroxide due to the presence of an electric field in the film. The electrostriction pressure (σ_E) depends on the electric properties of the passive film (by means of the dielectric constant of the oxide) and on the square of the electric field across the film. The interfacial effect is high at low film thickness and decreases by increasing film thickness, i.e. film pressure (σ) tends to the electrostriction pressure increasing the thickness of the film. Accordingly, if the electrostriction pressure is higher than the critical breakdown stress of the film, there is a critical film thickness beyond which mechanical breakdown occurs that decreases by increasing the electric field strength in the film.
The film cracking occurs when stress reaches the film mechanical breakdown stress (σ_{BD}), corresponding to the critical electric field (E_{BD}):

(Eq. 4.3) $$E_{BD} = \sqrt{\frac{\left(\sigma_{BD} + \frac{\gamma}{L}\right) \cdot 8\pi}{\varepsilon(\varepsilon - 1)}}$$

The critical electric field of breakdown decreases by increasing the dielectric constant of the oxide, i.e. high dielectric constant results in higher electrostriction pressure, due to the larger polarization of the domains of the passive film. As expected, the critical electric field of breakdown increases by increasing the mechanical properties of the oxide, expressed by σ_{BD}. As discussed previously, the interfacial tension effect increases by decreasing the film thickness, so that critical electric field of breakdown (E_{BD}) is higher at low film thickness, keeping constant mechanical and electrical properties of the film.

As reported by Sato [81] and Strehblow [77], metal oxides or hydroxide in the presence of electric field in the order of 10^6-10^7 V/cm could deform or break mechanically because of the high electrostriction pressure. Electric field in the oxide can arise in several processes, e.g. during the oxidation process of metals carried out in order to improve corrosion and wear resistance by thickening the natural oxide, or due to formation of galvanic couples that lead to electric potential differences that consume the oxide layers.
The model shows that mechanical failure of the film can result from the high levels of electro-mechanical stress generated by electric fields. After Sato's thermodynamic model, more accurate models were proposed in order to investigate the electromechanical behavior of passive and/or anodic oxide film that protect metals from corrosion.
Tang et al. in a recent work [82] state that Sato's model is limited by the assumption of a homogeneous isotropic film pressure and provide a continuum mechanics model that analyzes the electromechanical coupling between the environment and the passive film. Analytical solutions, obtained for a finite-thick film in a uniform electric field, illustrate the existence of a critical combination of electric field strength, initial film thickness and shape, beyond which the passivating oxide can become thin enough to undergo dielectric breakdown. Similarly, Vanhumbeeck et al. [83] proposed a model introducing a second stress contribution in addition to the compressive stress described above. This contribution arises from the effect of dipole alignment in the material along the direction of the applied field, with the resulting modification of the material dielectric constant (dielectrostriction effect).
The aforementioned Sato's model refers to a simplified approach on electrostriction that takes into account the response of a dielectric oxide on a metal surface subjected to electric fields, accordingly to the simple parallel plate capacitor model. Indeed, the oxide film behaves as a capacitor which dielectric is polarized by external electric fields until a critical value of the electric field between the metallic plates is reached. Over this critical value (the so-called *breakdown voltage*) the dielectric breaks due to polarization effect in the molecular structure.
It should be pointed out that, although the model proposed by Sato is indicated by many authors as one of the most accredited passivity breakdown mechanism, it provides only a simplified description of the electric response of the oxide films formed on metals. As known, passive films are semiconductors and electric field-induced effects should be dealt with the semi-conductive properties of passive films. In particular, as discussed by several authors, the electrochemical behavior of passive metals can be interpreted in terms of the semi-conductive properties of the film by means of electronic measurements using the Mott-Schottky model. Electrochemical investigations of the passive film on iron have suggested, as for instance reported by Cheng [84], that passivation on iron occurs due to the presence of an n-type semi-conductive film that covers the metallic substrate.
However, all the mentioned models, even though differ in some assumptions, establish a correlation between the occurring of breakdown phenomena of passive film to mechanical stresses induced by the presence of electric field across the film.

In this work, the electro-mechanical breakdown due to alternating electric fields in the passive film is proposed. The application of this breaking mechanism represents a novelty in the field of AC corrosion. Nevertheless, the eventuality that a corrosion phenomenon can be described not only by means of electrochemical laws isn't a singularity; just think for instance on stress corrosion cracking or corrosion fatigue in which corrosion is strictly correlated to mechanical behavior of the corroding metal. Obviously, this work represents only the first phase and several tests are necessary to validate the proposal.
Experimental tests were carried out primarily to investigate some possible harmful AC effects on passive condition by means of tests on stainless steels in neutral solution and on carbon steel in alkaline environment. Furthermore, AC voltage measurements were performed in order to ascertain if the corrosion AC voltages experimentally measured could be correlated to the breakdown voltages reported in literature. Indeed, as discussed previously, the mechanical breakdown occurs corresponding to electric fields in the order of 10^6-10^7 V/cm.

The phenomenon was studied mainly by means of corrosion tests, even though some investigations of the physical, electronic and mechanical behavior of passive films are recognized to be necessary for a full analysis of the phenomenon.

4.4.1 AC effect on passive condition

In order to study the effect of AC on passive condition, laboratory tests were carried out on passive metals. Tests were performed on carbon steel in alkaline environment and stainless steels in neutral solution in free corrosion condition, i.e. in the absence of CP, reducing the electric signal applied to the metal to the only AC field. AC effect on passive condition was investigated by means of critical chlorides threshold measurement and potentiodynamic polarization test in the presence of AC interference.

4.4.1.1 AC effect on critical chlorides threshold

Halogens, as chloride ions, are depassivating agents that, over certain content in contact with the metal (the so-called critical chlorides threshold), cause the local breakdown of the protective film on the surface. As a consequence, pitting corrosion can occur. Long-term exposition tests were carried out on austenitic stainless steel type EN 1.4401 X5 CrNiMo 17-12-2 (UNS S31600, Table 2.5) in neutral solution containing chlorides. The test aims to study the effect of AC on the critical chlorides threshold that causes the local breakdown of the passive film on the metal surface. The solution was initially chlorides-free. Then, chloride ions were added in the solution by steps (250 mg/L each week). Four values of AC density were applied for 90 days (stationary interference): 10, 20, 40 and 50 A/m^2. Figure 4.18 shows critical chloride threshold as a function of AC density.
If AC is absent, corrosion starts in the presence of 2000 mg/L of chloride ions. The presence of 2500 mg/L chlorides causes corrosion of all the samples. Stainless steel corrosion behavior doesn't change if 10 A/m^2 AC density is overlapped to the sample. Corrosion starts corresponding to critical chloride content comparable to that measured in the control condition. In the presence of 20 A/m^2 localized corrosion occurs corresponding to lower chloride ions content in solution. Corrosion starts at 700 mg/L for one specimen and in the presence of 2000 mg/L for the remaining. Large data dispersion is observed in the presence of 40 A/m^2: critical chlorides threshold varies in the range from 700 to 2000 mg/L. It should be pointed out that pitting corrosion (and generally localized corrosion) shows a stochastic aspect in its occurrence.

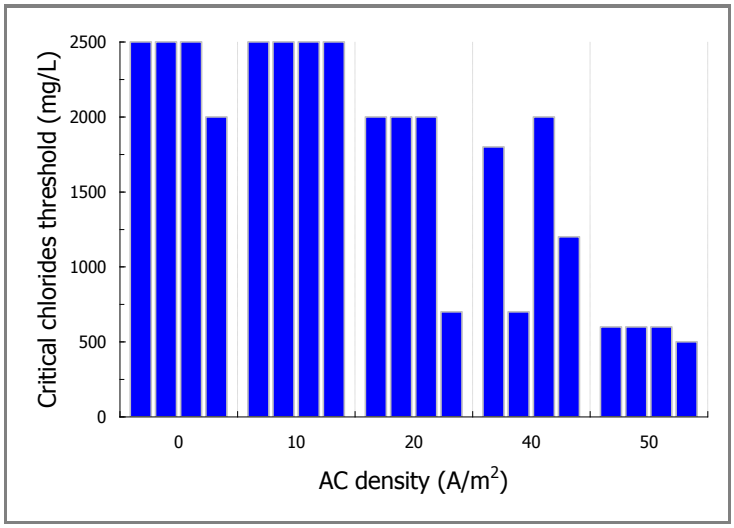

Figure 4.18 – EN 1.4401 X5 CrNiMo 17-12-2 stainless steel: critical chlorides threshold vs. AC density

This may be associated to non-uniformities in the metal (e.g. presence of inclusions in the metallic structure, defects or different thickness of the passive film, local different chemical composition of the metal), in the environment (e.g. difference in oxygen concentration, pH or ions concentration) or in the assembly (e.g. gaps and contact areas between parts, gaskets or seals, cracks or scratch, spaces filled with deposits). The largest data dispersion was measured with 40 A/m^2 AC density, above which a strong localized corrosion resistance drop is measured. In the presence of 50 A/m^2 AC interference, corrosion starts with 500 mg/L chloride ions, i.e. the critical chlorides threshold is four times lower than the value measured if AC isn't applied. Experimental data show that AC provokes a weakening of the passive film of stainless steel in neutral solution resulting in the decrease of critical chlorides threshold. Nevertheless, such decrease occurs only over a critical AC density value, comprised in the range between 20 and 40 A/m^2.

Critical chlorides threshold measurement was also carried out on carbon steel specimens, type B 450 C (Table 2.6), in a synthetic concrete pore simulating solution (pH 12.6). Indeed, in aerated alkaline solutions with pH > 11.5 and in the absence of chlorides, carbon steel is protected from corrosion by a thin oxide film [69, 85]. During the first week, solution was chlorides free; then, chlorides were periodically added in the solution by steps for 50 days. Five values of AC density were applied to the samples: 10, 20, 30, 40 and 50 A/m^2. Free corrosion potential was also monitored by means of an external SCE reference electrode.
Figure 4.19 to Figure 4.23 report corrosion potential monitoring of carbon steel specimens exposed to the test solution in the presence of AC interference. In the absence of AC interference, corrosion potential is in the range between -0.080 V and -0.220 V SCE and the metal is in passive condition. Then, chlorides were gradually added to the solution. After 45 days, corrosion potential decreases to -0.540 V and -0.445 V SCE for the two samples, with a net shift to more negative values of 0.373 V and 0.364 V, respectively.
Chloride ions cause [21, 85] the lowering of pitting potential of passive metals and, above a critical content dissolved in the solution, the local breakdown of the passive film. If corrosion occurs, corrosion potential decreases due to local active areas formation on the metal surface. In the presence of 10 A/m^2 AC density (Figure 4.19) corrosion starts after 31 days corresponding to the corrosion potential shift in the more negative direction. Two samples remain in passive condition until 34 days of testing. After corrosion initiation, the metal operates at corrosion potential lower than -0.450 V SCE.
In the presence of AC densities higher than 10 A/m^2 (Figure 4.20 to Figure 4.23), corrosion potential increases. Before AC is applied, corrosion potential is in the range between -0.122 V and 0.195 V SCE. Then, potential moves to more noble values with a mean shift of 0.158 V, 0.178 V, 0.104 V and 0.128 V in the presence of 20, 30, 40 and 50 A/m^2 AC density, respectively.
As discussed previously, corresponding to the achievement of the critical chlorides content in solution, corrosion occurs and corrosion potential decreases of about 0.500 V. Critical chlorides threshold was noted for each specimen corresponding to the strong corrosion potential drop and according to the appearance of corrosion products on the metal surface.

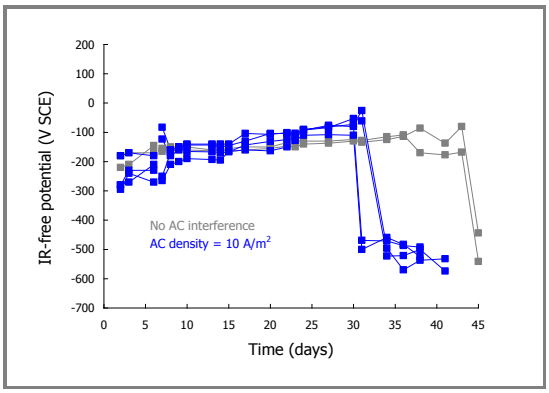

Figure 4.19 – DC potential vs. time in the presence of 10 A/m^2 AC density

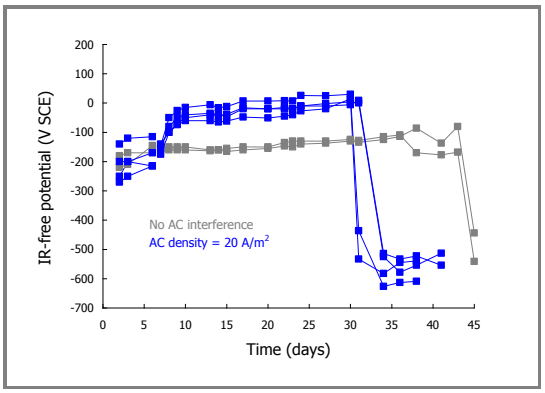

Figure 4.20 – DC potential vs. time in the presence of 20 A/m^2 AC density

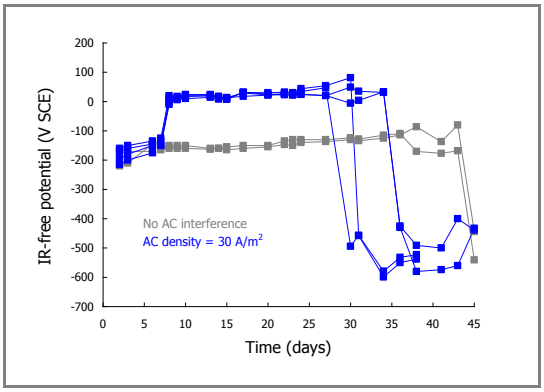

Figure 4.21 – DC potential vs. time in the presence of 30 A/m^2 AC density

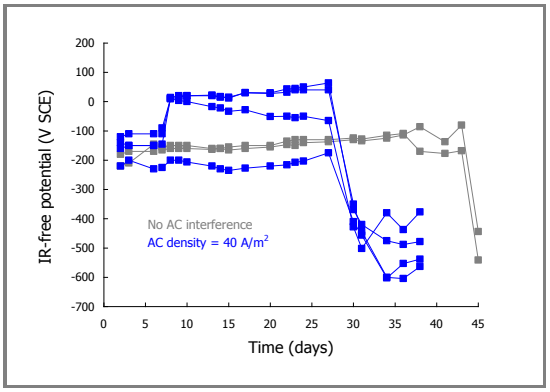

Figure 4.22 – DC potential vs. time in the presence of 40 A/m^2 AC density

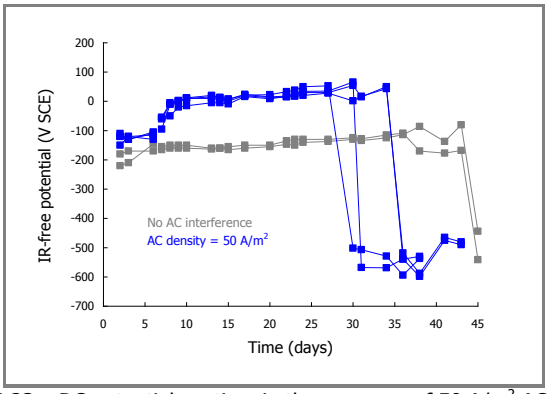

Figure 4.23 – DC potential vs. time in the presence of 50 A/m^2 AC density

Figure 4.24 reports the $[Cl^-]/[OH^-]$ critical threshold ratio for carbon steel in alkaline solution as a function of AC density. The data obtained during this research are reported in addition to those obtained in the previous phase of the research. The $[Cl^-]/[OH^-]$ ratio is considered the most accurate parameter to take into account to probe chloride-induced corrosion initiation in reinforced concrete [85, 86]. Although several authors found a variability of the dependence of corrosion initiation on the $[Cl^-]/[OH^-]$ ratio as a consequence of the stochastic nature of pitting initiation [85], a ratio of 0.6 in concrete-simulating solution is considered critical [85, 86]. At pH 12.6, this value corresponds to a molar chlorides content of 0.024 mol/L. AC interference causes the decrease of the critical chlorides threshold, expressed by the $[Cl^-]/[OH^-]$ ratio. In the presence of 30 A/m^2 AC density, critical chlorides threshold is in the range between 0.012 and 0.018 mol/L that corresponds to a $[Cl^-]/[OH^-]$ ratio in the range between 0.31 and 0.46.

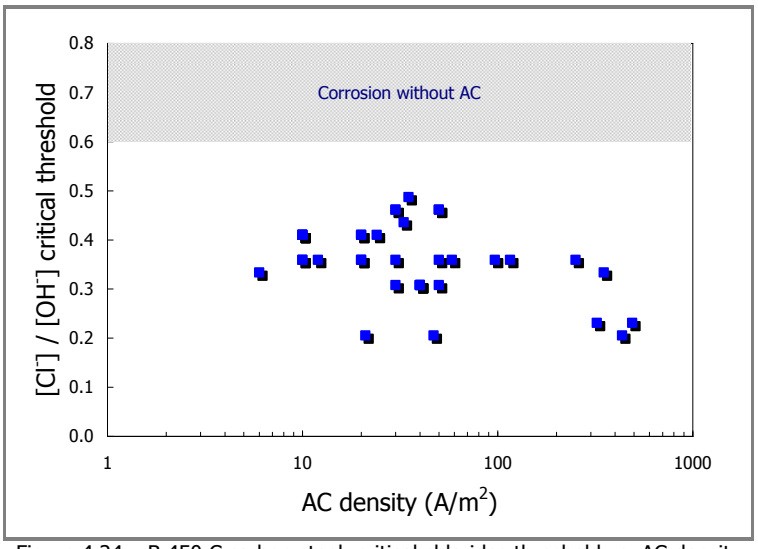

Figure 4.24 – B 450 C carbon steel: critical chlorides threshold vs. AC density

4.4.1.2 AC effect on anodic and cathodic polarization curves

During an internship period of four months in the AC corrosion group of the Metallurgical and Materials Engineering Department of Colorado School of Mines (Golden, CO, USA), potentiodynamic tests were carried out on 13% chromium super martensitic stainless steel in artificial sea water in the presence of AC interference. As discussed in Paragraph 2.2.6.2, this research aims to study AC corrosion mechanism of stainless steel pipelines in the subsea oil&gas production in the presence of direct electrical heating (DEH) systems [59, 60]. The DEH system, in combination with thermal insulation, can be adopted to prevent hydrates formation inside a pipeline which starts around 25°C (depending on process conditions). In this heating system (Figure 2.12), an external feeder provides AC to the pipeline, heated by Joule's effect over the critical temperature.
Anodic and cathodic polarization curves were carried out by means of potentiodynamic tests on super martensitic stainless steel type EN 1.4006 X12 Cr 13 (UNS S41000, Table 2.7) in artificial sea water in the presence of 40, 240 and 500 A/m^2 AC densities [59]. As discussed in Paragraph 2.2.6.2, before starting potentiodynamic test, samples were maintained one hour in free corrosion condition to attain a steady value of the open-circuit potential. AC was then applied so that the electrical charge (current $\times$ time) supplied to the sample was kept constant. Potential was monitored by means of a Tektronix DPO 3012 digital oscilloscope that records the potential oscillation in the AC signal period (frequency 60 Hz).
Figures 4.25 to 4.27 show potential monitoring spectrum recorded by oscilloscope in the presence of 40, 240 and 500 A/m^2 AC densities, respectively.
In the presence of AC interference, the potential of the metal can be written as the sum of a DC potential, E_{DC}, and the alternating voltage signal, $E_P \sin\omega t$, where E_P and ω are the peak voltage and the frequency of the signal, respectively:

(Eq. 4.4) $$E = E_{DC} + E_{AC} = E_{DC} + E_P \sin\omega t$$

In the presence of AC interference, the potential (E) oscillates around the mean value (corrosion potential) with the same frequency (60 Hz) of the applied signal, accordingly to models reported in literature [34, 41-44]. Maximum, minimum and peak-to-peak values (the last one called amplitude in Figures 4.25 to 4.27) of potential oscillation are reported in Table 4.3.

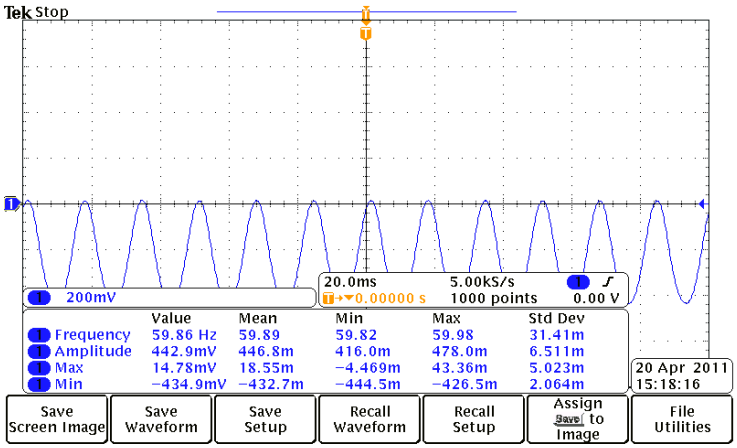

Figure 4.25 – Potential monitoring spectrum recorded by oscilloscope in the presence of 40 A/m^2 AC density

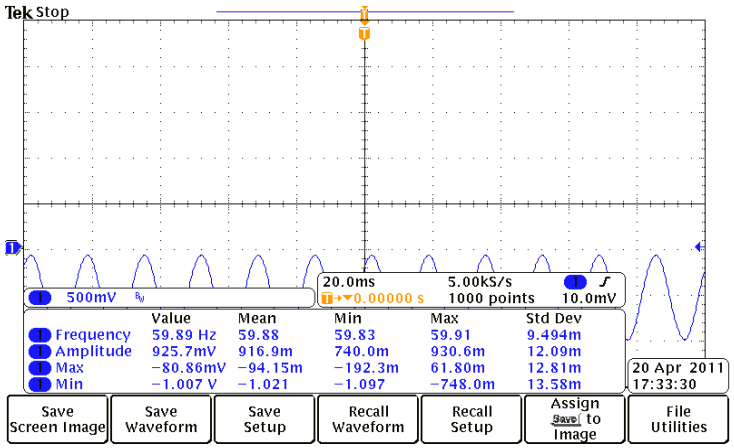

Figure 4.26 – Potential monitoring spectrum recorded by oscilloscope in the presence of 240 A/m^2 AC density

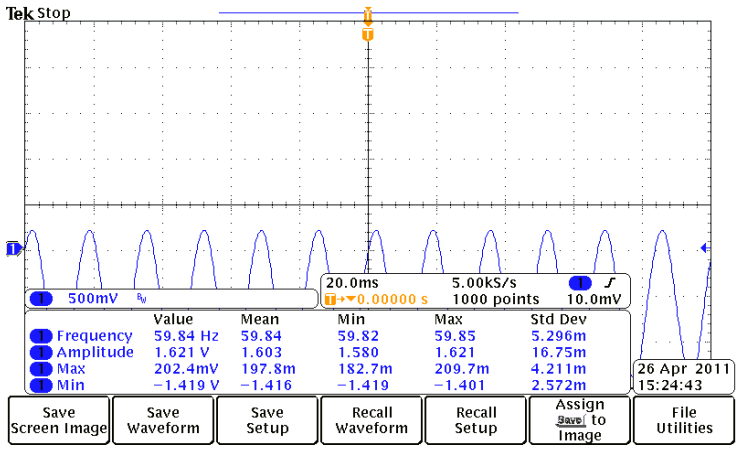

Figure 4.27 – Potential monitoring spectrum recorded by oscilloscope in the presence of 500 A/m^2 AC density

Table 4.3 – Potential oscillation data in the presence of AC interference (frequency 60 Hz)

AC density A/m^2	Minimum V SCE	Maximum V SCE	Amplitude V	Peak-to-peak V	Mean V SCE
40	-0.435	0.015	0.222	0.443	-0.213
240	-1.007	-0.081	0.463	0.926	-0.544
500	-1.419	0.202	0.813	1.626	-0.609

In the absence of AC interference, corrosion potential is -0.505 V SCE. 40 A/m^2 AC density moves the corrosion potential to -0.213 V SCE, with a shift in the anodic direction in agreement to that reported in Paragraph 4.4.1.2 for carbon steel in alkaline solution. Nevertheless, a potential decrease was observed by increasing AC to 240 and 500 A/m^2: corrosion potential is -0.544 V and -0.609 V SCE, respectively.
The amplitude of potential oscillation increases by increasing the AC interference from 0.222 V at 40 A/m^2 to 0.813 V at 500 A/m^2 AC density. Potential oscillates with the same frequency of the applied sinusoidal signal and doesn't show any particular distortion.
After corrosion potential monitoring, potentiodynamic tests were carried out. As discussed in Paragraph 2.2.3, if the working potential is displaced from the open-circuit value (free corrosion condition), the current measured represents the difference between the anodic-reaction current and the cathodic-reaction current, or vice versa. If the potential displacement is sufficiently large, the net current will be essentially equal to the anodic or cathodic-reaction current, depending on whether the potential is made respectively more positive or more negative with respect to the open-circuit value. Figure 4.28 shows schematic anodic polarization curves for a passive metal with active-passive transition (Figure 4.28*a*) and without active-passive transition (Figure 4.28*b*), as reported in the standard [54].
In the presence of an active-passive transition, moving the potential in the anodic direction from corrosion potential, the potential initially increases linearly with the logarithm of the current (Tafel region). If the potential is increased further the current decreases significantly by several orders of magnitude due to the formation of the passive layer. The potential at which this process occurs is called passivation potential (E_{pp} in Figure 4.28) and the current decreases to a value called passivation current, i_p. By increasing the potential to higher values, the thickness of the film increases but the current in the passive range remains essentially constant. A significant current increase occurs above a critical potential (the breakdown potential, E_b) associated with local instabilities and breakdown of the passive film.

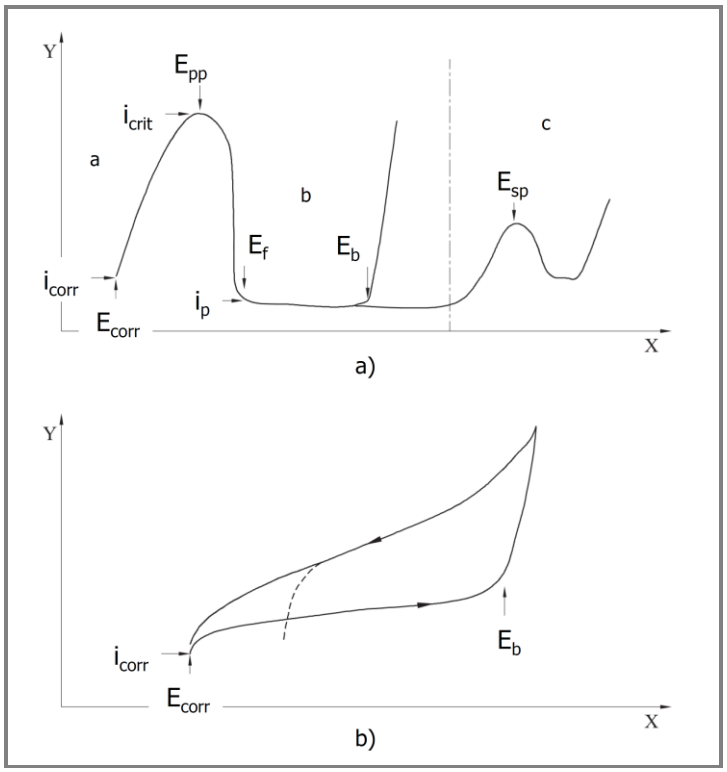

X	Potential
Y	Log (current density)
E_{corr}	Corrosion potential
i_{corr}	Corrosion current density
E_{pp}	passivation potential
i_{crit}	critical current density for passivation
i_p	passive current density
E_f	flade potential
E_b	breakdown potential
E_{sp}	secondary passivation potential
a	active
b	passive
c	transpassive

Figure 4.28 – Schematic anodic and cathodic polarization curves for a passive metal a) with active-passive transition and b) without active-passive transition [54]

Figure 4.29 shows anodic and cathodic polarization curves in the experimental condition tested. The passive region (i.e. the potential region between the flade potential and the breakdown potential, Figure 4.28) is well defined in the control curve obtained with zero AC density. The metal is in passive condition and corrosion current is equal to the passive current density. Faraday's law provides corrosion rate (CR, mm/y) using corrosion current density:

$$\text{(Eq. 4.5)} \qquad CR = K \cdot \frac{i_{corr}}{\rho} \cdot EW$$

where K is a constant ($3.27 \cdot 10^{-3}$ mm·g/μA·cm·y), i_{corr} is the corrosion current in μA/cm^2, ρ is the density (7.75 g/cm^3) and EW is the adimensional equivalent weight (25.94). In the absence of AC, passive current density is 1.5 μA/cm^2 and corresponds to a corrosion rate of 0.015 mm/y, i.e. corrosion is negligible.
The main effect of AC is the shift of polarization curves towards high polarization current. Furthermore, a well-defined passive region disappears in the presence of 40 and 240 A/m^2. As discussed before, a potentiodynamic test records the external current supplied by the DC feeder. In the anodic region, this current is given by the difference between anodic and cathodic current. If the potential displacement is sufficiently large, the net current will be essentially equal to the anodic current, i.e. the passive current density (i_p) if the metal is in passive condition. Nevertheless, in the presence of 40 and 240 A/m^2 corrosion potential falls in close proximity to the breakdown potential above which the current increase due to the simultaneous effect on corrosion and breakdown potentials (discussed in the following).
In these conditions the passive region above corrosion potential is very narrow and not observable by the test. Conversely, the passive region is well defined in the presence of 500 A/m^2 AC density and the passive current density is about 80 μA/cm^2. By Eq. 4.5, the corresponding corrosion rate is 0.880 mm/y, about two orders of magnitude greater than the corrosion rate calculated if the absence of AC.

Anodic curves are also reported in Figure 4.30 with current in linear scale. Breakdown potential (E_b) decreases by increasing AC density. The breakdown potential was measured corresponding to a polarization current of 100 μA/cm^2: E_b is +0.053 V, -0.256 V and -0.293 V SCE in the presence of 40, 240 and 500 A/m^2, respectively.
In the reference condition, the breakdown potential is +0.026 V SCE. Figure 4.31 compares the maximum potential assumed by the metal during oscillation (Table 4.3) with breakdown potential obtained by potentiodynamic curves. A sketch of the anodic and cathodic half waves is also overlapped to experimental point. Breakdown potential is higher than the maximum potential only in the presence of 40 A/m^2. During oscillation, potential crosses breakdown potential in the presence of 240 and 500 A/m^2. This means that potential enters periodically in the transpassive domain associated with local instabilities and breakdown of the passive film. An aspect that should be investigated is if the electrochemical reactions are fast enough to occur within the time during which the potential crosses the corrosion area.
Figure 4.32 reports corrosion rate data calculated by means of weight loss tests carried out exposing the metal at 40, 150, 240 and 500 A/m^2 AC density. Localized corrosion was observed in the presence of 150 A/m^2 or higher AC densities. In previous tests [59], Reyes et al. observed only small pits at 40 A/m^2 AC density. The low corrosion at 40 A/m^2 could be due to the potential permanence within the passive region during the anodic potential oscillation at 40 A/m^2 (Figure 4.31).

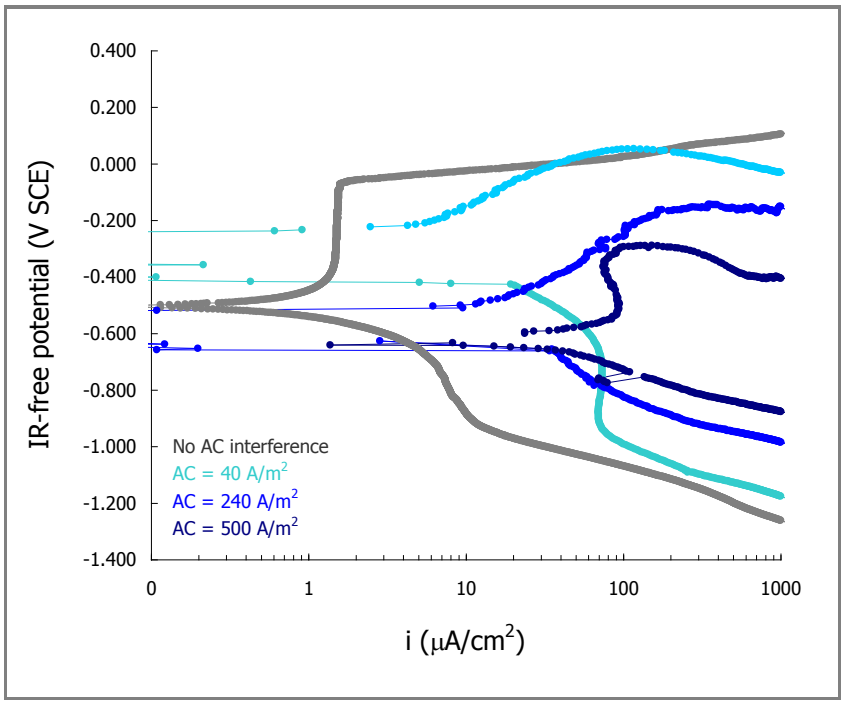

Figure 4.29 – Polarization curves on EN 1.4006 X12 Cr 13 stainless steel in the presence of AC (logarithmic scale)

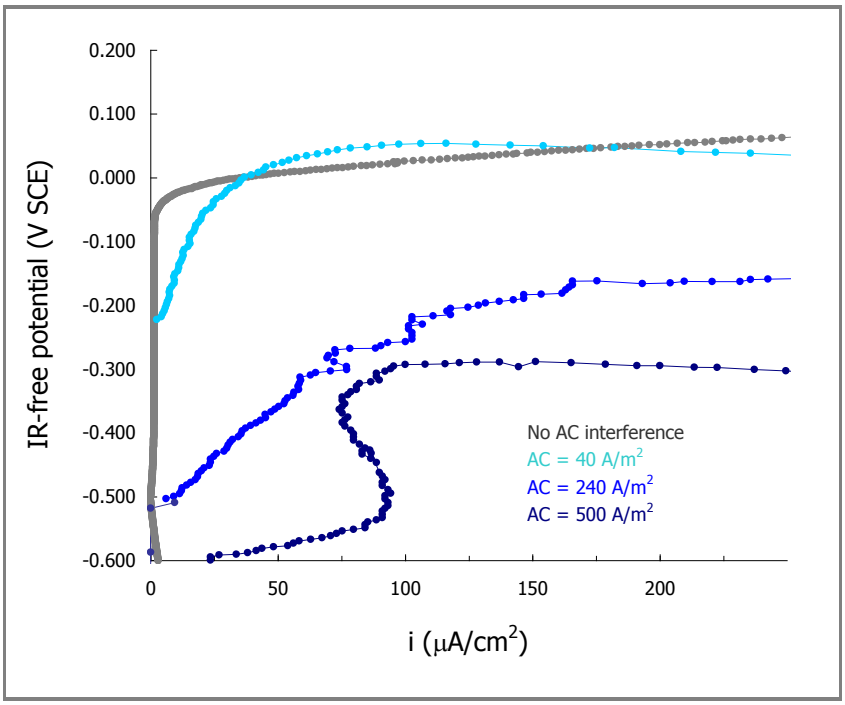

Figure 4.30 – Polarization curves on EN 1.4006 X12 Cr 13 stainless steel in the presence of AC (linear scale)

Figure 4.29 shows also an effect of AC on overpotential of cathodic reactions that occur on the metal. In the absence of AC interference, the cathodic processes that take place on the metal are oxygen reduction and hydrogen evolution at lower potential. Oxygen reduction overpotential consists of two contributions [21, 65]: activation and concentration polarization. The first is associated to the activation energy that the cathodic reaction required to proceed. Activation polarization increases with current density in accordance with Tafel equation and is

therefore represented by a linear trend in the E-log(i) plot. By increasing the polarization current, a deviation from linearity occurs due to oxygen diffusion process. Indeed, oxygen is consumed on the metal surface due to the cathodic reduction and is replaced by diffusion process from the bulk, where its concentration is approximately constant.

If the diffusion rate is not fast enough to carry all the electrons supplied on the metal surface, a diffusion layer may form at the metal-to-electrolyte interface. Polarization overpotential increases by increasing the cathodic current, until a limiting value (the so-called oxygen limiting current) is reached. Oxygen limiting current depends on oxygen bulk concentration, diffusion coefficient and on the thickness of the diffusion layer [21, 65]. A further potential decrease lead to hydrogen evolution that adds to oxygen reduction reaction. Oxygen limiting current is well-defined in the curves with zero and 40 A/m^2.
In the absence of AC, oxygen limiting current varies between 5 and 9 μA/cm^2 in stagnant condition. The presence of 40 A/m^2 lead to the increase of the limiting current density to 70 μA/cm^2, about one order of magnitude greater. Considering the highest values of the AC density applied (240 and 500 A/m^2), limiting current density disappears and cathodic process is described only by the hydrogen evolution in the potential range studied. Hydrogen evolution cathodic curve shifts to more noble value (Figure 4.29). This could be due to an effect of AC on equilibrium potential or exchange current density of hydrogen evolution reaction. As mentioned in Paragraph 3.3, the effect of AC on anodic and cathodic overpotentials (anodic and cathodic Tafel slopes, corrosion potential and corrosion current density) was already investigated during the first phase of the research project and is described elsewhere [15, 46]. Experimental tests showed that AC has a strong influence on corrosion kinetic parameters and on corrosion or equilibrium potential, in terms of a general decrease in overpotentials and an increase in corrosion or exchange current density for the different conditions tested. The effect of AC on cathodic and anodic reactions kinetics is still ongoing and a deep study will be considered in the future. Hydrogen evolution Tafel slope (β_c) was calculated from experimental curves; data are reported in Table 4.4. β_c is 190 mV/decade if AC is absent and decreases by increasing AC density: in the presence of 500 A/m^2, cathodic Tafel slope drops to 147 mV/decade of current.

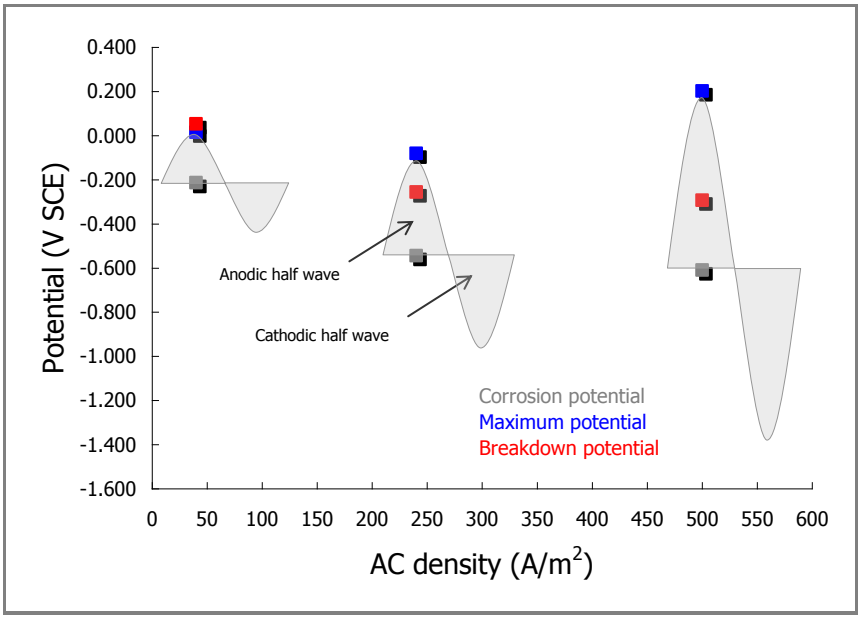

Figure 4.31 – EN 1.4006 X12 Cr 13 stainless steel: potential oscillation and breakdown potential in the presence of AC

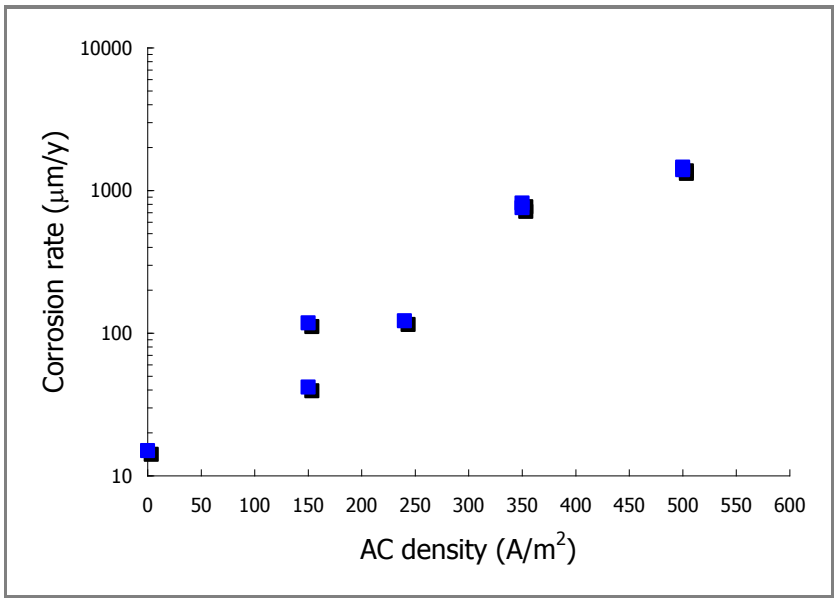

Figure 4.32 – EN 1.4006 X12 Cr 13 stainless steel: corrosion rate in the presence of AC

Table 4.4 – Cathodic Tafel slope on X12 Cr 13 (UNS S41000) stainless steel in the presence of AC interference

AC density A/m^2	Cathodic Tafel slope mV/decade
0	190
40	181
240	159
500	147

4.4.2 Alternating breakdown voltage measurement

As discussed in Paragraph 4.4, the proposed AC corrosion initiation model considers the electro-mechanical breakdown of the passive film formed on carbon steel in CP condition.
Experimental tests described in Paragraph 4.4.1 showed that AC has a harmful effect on passive condition, causing depassivation, local breakdown of the passive film and corrosion of the underlying metal. Alternating voltage (AV) measurements were performed in order to ascertain the presence of a critical breakdown voltage above which passive metal corrosion occurs.
The aim of the test is to correlate such measurement with the film breakdown electric field value reported in literature. As discussed previously, the mechanical breakdown of the passive film occurs corresponding to electric fields across the film in the order of 10^6-10^7 V/cm. It should be pointed out that this test represents only a first approach to the model and more accurate tests are mandatory to investigate the physical, electronic and mechanical behavior of passive films in the presence of alternating fields.
The AV experimentally measured hasn't the same meaning described by the technical specification CEN/TS 15280:2006 [12], carried out by means of a remote reference electrode in contact with the soil. Indeed, the measurement indicated by the specification includes the ohmic drop contribution that should be eliminated to evaluate correctly the true AV induced on the metal.
AV was measured with a SSC reference electrode placed in a Luggin tube which tip was positioned in close proximity to the metal surface (Figure 4.33*a*). AV was increased by steps and the corresponding AC density was measured by means of an amperometer connected in series to the electrical circuit. The Luggin tube allows reducing the ohmic drop contribution to few millivolts in the solution between the sample and the reference electrode. The response

of the test is the AV-AC curve. Generally, the measured AV is the sum of several contributions (Figure 4.33*a* and Figure 4.33*b*):

(Eq. 4.6) $$AV = AV_{solution} + AV_{oxide} + AV_{metal}$$

where $AV_{solution}$ is the voltage drop in the solution between the reference electrode and the specimen, AV_{oxide} is the voltage contribution across the passive protective film on the metal and AV_{metal} is the voltage drop in the metallic phase (specimen, electric cables). AV_{sol} is generally the sum of the ohmic drop (second Ohm's law) and of all the voltage drops which can occur at the interface between the metal and the solution, e.g. due to capacitive and resistive electrochemical components in the electrochemical double layer.
While the voltage drop in the metallic phase (AV_{metal}) can be reasonably neglected, it may be too restrictive to extend this assumption to the voltage drop in the electrolyte between the sample and the tip of the Luggin tube ($AV_{solution}$). Indeed, although the ohmic drop is reduced to few millivolts by the use of the Luggin tube, interfacial AV drops due to the presence of the electrical double layer may represent a substantial contribution.
Nevertheless, a first set of experimental tests were carried out in order to investigate the phenomenon with the assumption that also the solution voltage contribution can be neglected. Accordingly, the measurement provides only an estimation of the alternating field within the passive film. The alternating electric field (E_F) is given by the ratio between the alternating voltage between the opposite sides of the oxide and the thickness (L) of the passive film:

(Eq. 4.7) $$E_F = \frac{AV_{oxide}}{L} \cong \frac{AV}{L}$$

As discussed previously, according to the electro-mechanical film breakdown mechanism, the breakdown of the passive film occurs if the E_F within the film reaches the reported critical value of 10^6-10^7 V/cm. Summarizing, AV measurement described in this section aims to investigate the presence of a critical AV over which passive film breakdown occurs and to provide an estimation of the alternating electric field that causes corrosion in order to compare this value with the theoretical one. AV measurements were carried out on stainless steels and on carbon steel in CP condition.

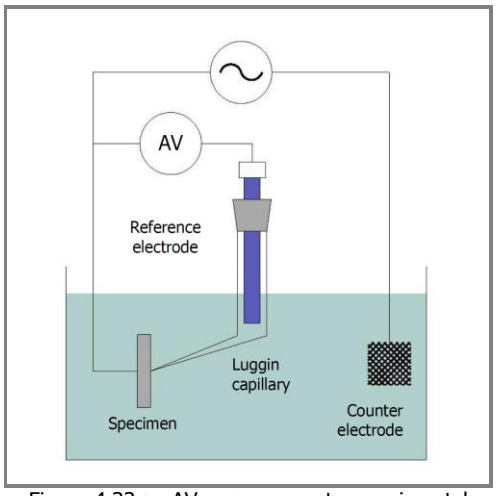

Figure 4.33*a* – AV measurement: experimental arrangement

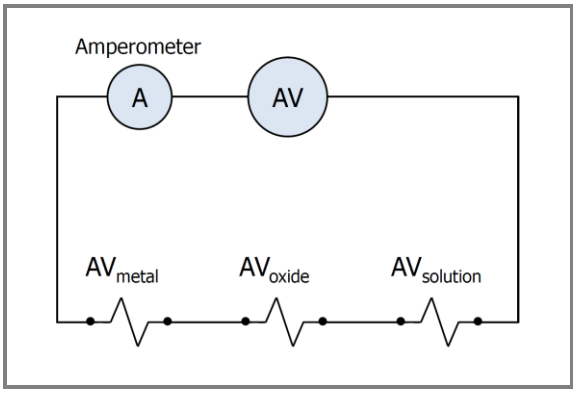

Figure 4.33*b* – Electrical representation of the AV measurement through the reference electrode in the Luggin tube (Figure 4.33*a*)

4.4.2.1 Tests on stainless steels

AV measurements were carried out in neutral solution on two austenitic stainless steel grades:

- EN 1.4301 X5 CrNi 18-10 (UNS S30400), PREN 18;
- EN 1.4401 X5 CrNiMo 17-12-2 (UNS S31600), PREN 25.

Furthermore, the effect of a chemical passivation treatment on austenitic stainless steel type EN 1.4401 X5 CrNiMo 17-12-2 (UNS S31600) was investigated. The passivation treatment facilitates the more rapid formation of the passive film on stainless steel surface.

AC was overlapped to the sample in free corrosion condition by increasing AV between the sample and the reference electrode, placed in the Luggin capillary Figure 4.33*a*. Three tests for each material were performed. DC corrosion potential was also monitored by switching the voltmeter in DC mode.

Figure 4.34 (*a-c*) shows AC density and DC potential as a function of the applied AV on EN 1.4301 X5 CrNi 18-10 stainless steel specimens. AC density increases by increasing AC voltage, as expected. Experimental curve can be divided in two sections due to a strong change of the curve slope. Corresponding to a critical value of AC voltage (AV_C), the slope of the curve increases, i.e. more current is exchanged by the metal corresponding to an AV step. A linear regression by means of least square method was carried out in order to calculate the slopes of the two parts of the curve (m_1 and m_2). An example is reported in Figure 4.34*d*.

The presence of AC interference shifts the DC potential to more positive (more noble) values, e.g. from -0.015 V SSC up to 0.063 V SSC in the case reported in Figure 4.34*a*. Then, corrosion potential remains stable until AV_C is reached. Corresponding to the slope-variation of the AC-AV curve, a strong drop of corrosion potential is observed.

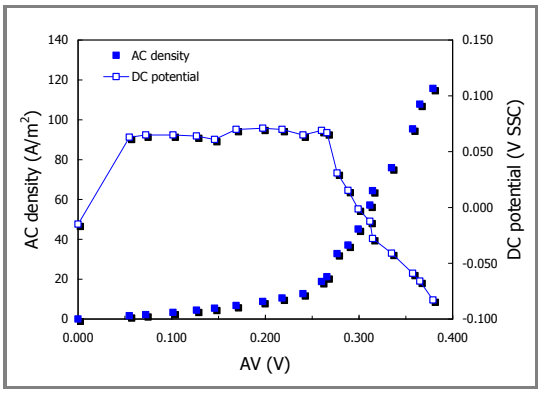

Figure 4.34*a* – EN 1.4301 X5 CrNi 18-10: AC-AV curve and DC potential monitoring (sample #1)

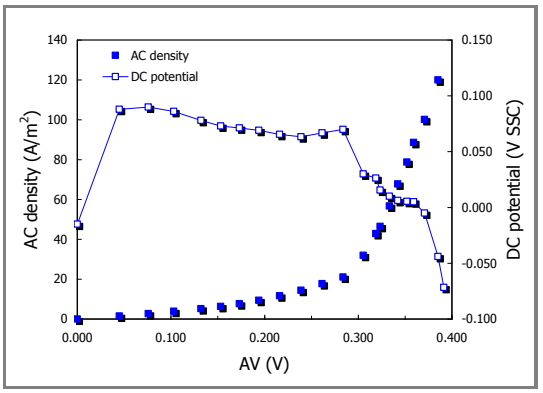

Figure 4.34*b* – EN 1.4301 X5 CrNi 18-10: AC-AV curve and DC potential monitoring (sample #2)

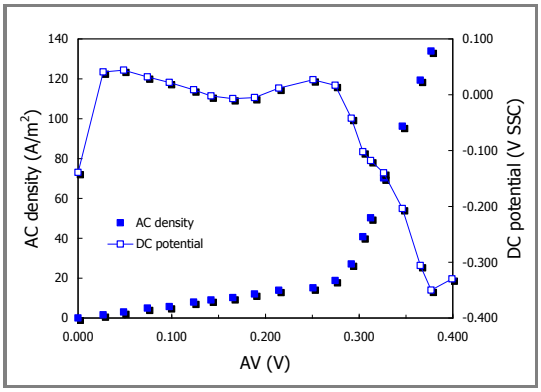

Figure 4.34*c* – EN 1.4301 X5 CrNi 18-10: AC-AV curve and DC potential monitoring (sample #3)

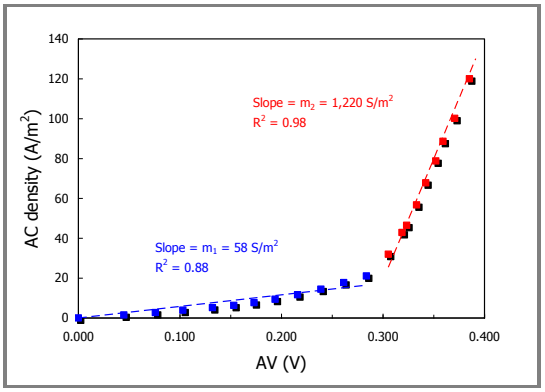

Figure 4.34*d* – Linear regression by means of least square method for AC-AV curve slope calculation

The mean value of AV_C and the corresponding AC density is 0.275 V and 20 A/m^2, respectively (Table 4.5). Data repeatability is good.
A further increase of AV causes the decrease of DC potential. Figure 4.35 (*a-c*) shows AC density and DC potential as a function of the AV applied by steps on EN 1.4401 X5 CrNiMo 17-12-2 stainless steel specimens. The same considerations discussed before could be extended: AC density increases by increasing the induced AV, until a critical value (AV_C) is reached. Corresponding to the slope-variation of the AC-AV curve, DC potential decreases. Table 4.6 reports the mean value of AV_C and of the corresponding AC density.

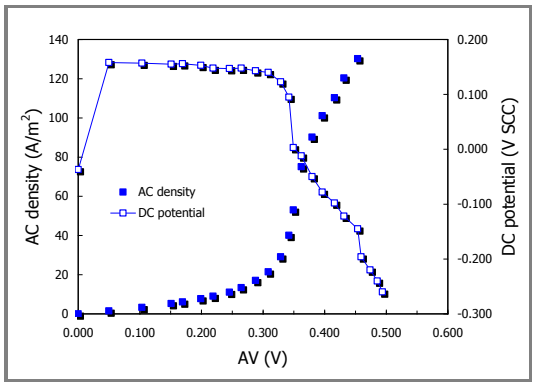

Figure 4.35*a* – EN 1.4401 X5 CrNiMo 17-12-2: AC-AV curve and DC potential monitoring (sample #1)

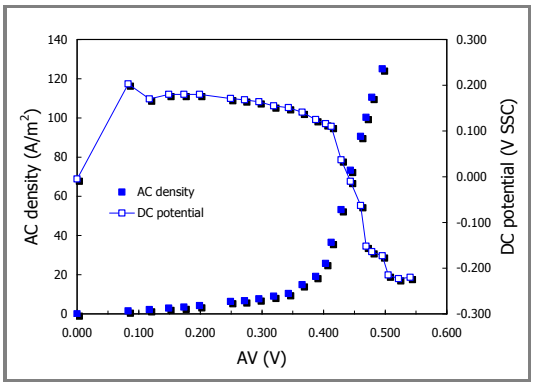

Figure 4.36*a* – EN 1.4401 X5 CrNiMo 17-12-2 with pre-passivation treatment: AC-AV curve and DC potential monitoring (sample #1)

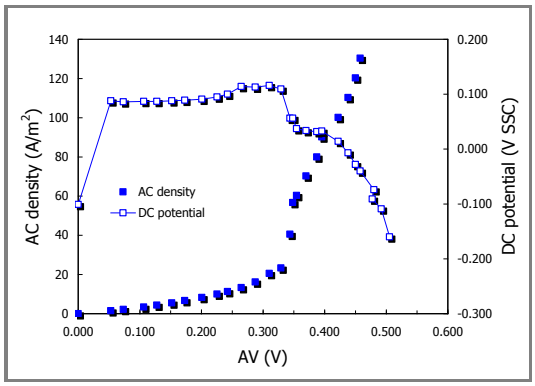

Figure 4.35*b* – EN 1.4401 X5 CrNiMo 17-12-2: AC-AV curve and DC potential monitoring (sample #2)

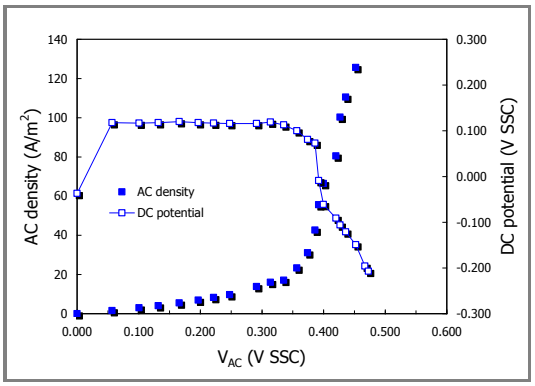

Figure 4.36*b* – EN 1.4401 X5 CrNiMo 17-12-2 with pre-passivation treatment: AC-AV curve and DC potential monitoring (sample #2)

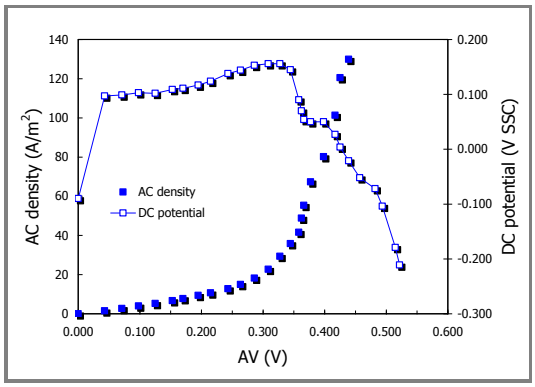

Figure 4.35*c* – EN 1.4401 X5 CrNiMo 17-12-2: AC-AV curve and DC potential monitoring (sample #3)

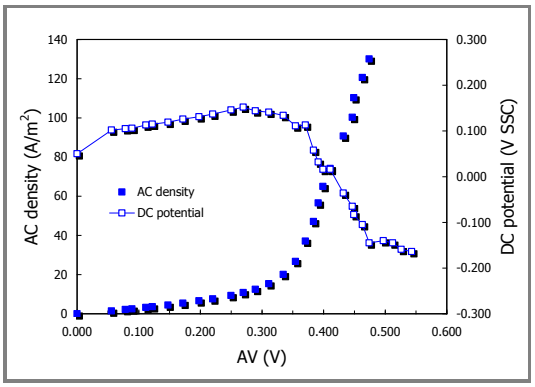

Figure 4.36*c* – EN 1.4401 X5 CrNiMo 17-12-2 with pre-passivation treatment: AC-AV curve and DC potential monitoring (sample #3)

Table 4.5 – Alternating voltage measurement on stainless steel, type EN 1.4301 X5 CrNi 18-10 (UNS S30400)

X5 CrNi 18-10 Specimen	m_1 ($\cdot 10^3$ S/m^2)	m_2 ($\cdot 10^3$ S/m^2)	Critical voltage (AV_C) V	Critical AC density A/m^2
1	0.056	0.850	0.266	21
2	0.058	1.220	0.284	20
3	0.064	1.280	0.274	19
Mean	**0.059**	**1.120**	**0.275**	**20**

Table 4.6 – Alternating voltage measurement on stainless steel, type EN 1.4401 X5 CrNiMo 17-12-2 (UNS S31600)

X5 CrNiMo 17-12-2 Specimen	m_1 ($\cdot 10^3$ S/m^2)	m_2 ($\cdot 10^3$ S/m^2)	Critical voltage (AV_C) V	Critical AC density A/m^2
1	0.051	0.870	0.308	22
2	0.054	0.810	0.329	23
3	0.057	0.840	0.308	23
Mean	**0.054**	**0.840**	**0.315**	**23**

Table 4.7 – Alternating voltage measurement on stainless steel, type EN 1.4401 X5 CrNiMo 17-12-2 (UNS S31600) with pre-passivation treatment

X5 CrNiMo 17-12-2 Specimen	m_1 ($\cdot 10^3$ S/m^2)	m_2 ($\cdot 10^3$ S/m^2)	Critical voltage (AV_C) V	Critical AC density A/m^2
1	0.032	1.200	0.387	19
2	0.048	1.250	0.357	23
3	0.043	0.850	0.335	20
Mean	**0.041**	**1.100**	**0.360**	**21**

Table 4.8 – Alternating electric field of breakdown calculated by Eq. 4.7

Material	PREN	Pre-passivation treatment	Breakdown electric field ($\cdot 10^6$ V/cm)	
			1 nm	5 nm
X5 CrNi 18-10	18	No	2.75	0.55
X5 CrNiMo 17-12-2	25	No	3.15	0.63
X5 CrNiMo 17-12-2	25	ASTM A967	3.60	0.72

A linear regression by means of least square method was carried out to calculate the slopes of each curve. The mean value of the slope of the first side of the curve is $0.054 \cdot 10^3$ S/m^2, similar to that measured in the case of stainless steel X5 CrNi 18-10 stainless steel discussed previously ($0.059 \cdot 10^3$ S/m^2, Table 4.5). Then, the slope increases of more than one order of magnitude to $0.84 \cdot 10^3$ S/m^2, corresponding to the decrease of the DC potential of about 0.100 V. The mean value of AV_C is 0.315 V and the corresponding AC density is about 23 A/m^2, both greater than the values measured for stainless steel X5 CrNi 18-10 (Table 4.5).
Figure 4.36 (*a-c*) shows AC density and DC potential as a function of the AV applied on EN 1.4401 X5 CrNiMo 17-12-2 subjected previously to a chemical passivation chemical treatment, as described in Paragraph 2.2.6.3. The same electrical behaviour described above is observed. Table 4.7 reports AV_C and the corresponding AC density measured for the three specimens. The slope of the AC-AV curve changes from $0.041 \cdot 10^3$ S/m^2 (lower than the value measured in the absence of the chemical passivation pre-treatment) to $1.10 \cdot 10^3$ S/m^2, corresponding to the DC potential drop. The mean value of AV_C is 0.360 V and the corresponding AC density is 21 A/m^2. AV_C is 85 mV and 45 mV greater than the mean values measured for stainless steels X5 CrNi 18-10 and X5 CrNiMo 17-12-2 without a chemical passivation treatment, respectively. No remarkable difference is measured for AC density.

As shown, corresponding to the slope variation of the AC-AV curve, corrosion potential decreases. The same electrochemical behaviour was observed in the tests described on Paragraph 4.4.1.1 on carbon steel in alkaline solution. A potential decrease was measured

corresponding to corrosion initiation, due to the formation of active area (pits) surrounded by a passive surface. Similarly, the drop of stainless steel DC potential corresponding to the slope variation of AC-AV curve could be related to the existence of a critical AV which causes the local breakdown of the passive film with the subsequent corrosion of the substrate and increase of the AC exchanged by the metal in the unprotected area.
According to the film breakdown mechanism described in Paragraph 4.4, this critical value (indicated as AV_C in Table 4.5 to 4.7) could be related to the so-called *breakdown voltage* which causes the electro-mechanical breakdown of the passive film due to the achievement of a critical alternating electric field in the oxide.
According to the assumptions discussed in Paragraph 4.4.2, the alternating electric field corresponding to the breakdown voltage was calculated by Eq. 4.7, assuming a passive film thickness of 1 and 5 nm, according to MacDougall and Graham that describe passivity as the state characterized by the presence of a thin oxide film 1-4 nm thick that isolates the metal surface from the corrosive aqueous environment [75].
Alternating electric field calculations are reported in Table 4.8. Electric field is in the order of 10^6 V/cm, in good agreement with theoretical prediction provided by literature [77, 81]. Experimental tests confirm the existence of a critical AV over which localized breakdown occurs; the critical AV is associated to the achievement of an alternating electric field threshold that could cause corrosion by electromechanical stresses.
Furthermore, critical alternating field (E_F) increases by increasing the protective properties of the passive film against corrosion. Considering a uniform film thickness of 1 nm, E_F increases from 2.75 to 3.15 MV/cm increasing PREN index from 18 to 25. As known, pitting corrosion resistance generally increases by increasing PREN (Pitting Resistance Equivalent Number), which depends on chemical composition. Moreover, a pre-passivation treatment allows increasing the alternating electric field of breakdown from 3.15 to 3.60 MV/cm.

4.4.2.2 Tests on carbon steel in CP condition

AV measurements were carried out on carbon steel specimens in CP condition, accordingly to the procedure described in Paragraph 2.2.5. Carbon steel specimens were cathodically polarized in a potentiostatic way for three days, until a steady value of the protection current density was reached. Then, AC was overlapped to the sample. Three values of the protection potential were applied: -1.1 V, -1.2 V and -1.3 V CSE.
As shown by AC corrosion risk diagram (Figure 4.3), potentials lower than -1.1 V CSE (overprotection condition) are considered the most dangerous regarding AC corrosion likelihood. Figure 4.37 (*a-c*) shows the measured AC density as a function of the applied AV. The same considerations made for stainless steel measurement could be extended. AC density increases linearly by increasing AV.
A change of the slope of the curve is observed corresponding to a critical value of AV (the *breakdown voltage,* AV_C). The slope of the curve increases after the achievement of the breakdown voltage. Linear regression by means of least square method was carried out in order to calculate the slopes of the two parts of the curve (Table 4.9). CP current density was also reported in Table 4.9. The slope of both sides of the curve (m_1 and m_2) decreases by decreasing the protection potential. These values are higher than slopes calculated for stainless steels (Table 4.5 to 4.7), indicating less conductive properties of stainless steels respect to cathodically protected carbon steel. AV_C changes significantly varying the protection potential applied to the metal, from 0.054 V at -1.1 V CSE to 0.184 V at -1.3 V CSE (Figure 4.38 and Table 4.9). These values are lower than breakdown voltages measured for the stainless steels discussed before. No remarkable difference of critical AC density is measured.
As discussed in Paragraph 4.4.2.1 for stainless steels, the slope variation of AC-AV curve could be related to the existence of a critical AV which causes the local breakdown of the passive film with the subsequent corrosion of the substrate and increase of the AC exchanged

by the metal. Similarly to the case discussed previously, the alternating electric field corresponding to the breakdown voltage (AV_C) was calculated by Eq. 4.7, assuming a passive film thickness of 1 and 5 nm. Alternating electric field calculations are reported in Table 4.10. Electric field is in the order of 10^5-10^6 V/cm, in good agreement with theoretical prediction provided by literature. Experimental tests confirm the existence of a critical AV over which localized breakdown occurs on carbon steel in CP condition. The critical breakdown alternating field increases by decreasing the CP potential, indicating that the passive film on the metal surface could have different electric properties (or thickness) depending on protection potential and formation condition.

Table 4.9 – Alternating voltage measurement on carbon steel in CP condition

CP potential V CSE	CP current density A/m²	m_1 ·10³ S/m²	m_2 ·10³ S/m²	Critical voltage (AV_C) V	Critical AC density A/m²
-1.100	0.220	0.570	7.650	0.054	30.6
-1.200	0.580	0.270	1.970	0.136	37.3
-1.300	1.250	0.130	1.580	0.184	24.1

Table 4.10 – Alternating electric field of breakdown on carbon steel in CP condition calculated by Eq. 4.7

CP potential	CP current density	i_{AC}/i_{DC}	Breakdown electric field (·10⁶ V/cm)	
V CSE	A/m²	-	1 nm	5 nm
-1.100	0.220	139	0.54	0.11
-1.200	0.580	64	1.36	0.27
-1.300	1.250	19	1.84	0.37

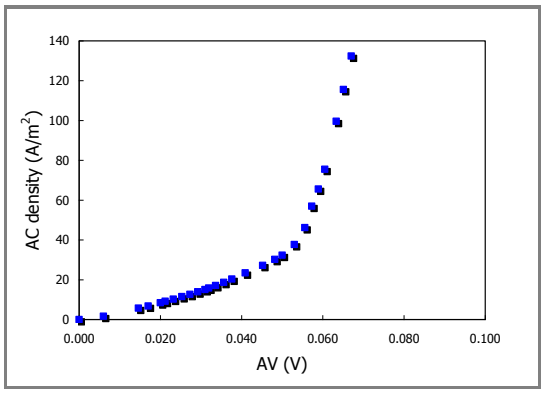

Figure 4.37*a* – AC-AV curve on carbon steel cathodically polarized at -1.1 V CSE

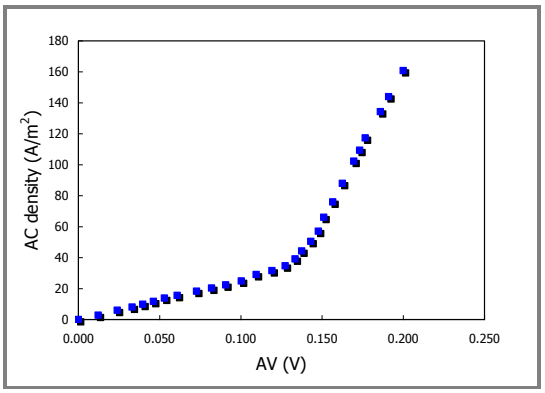

Figure 4.37*b* – AC-AV curve on carbon steel cathodically polarized at -1.2 V CSE

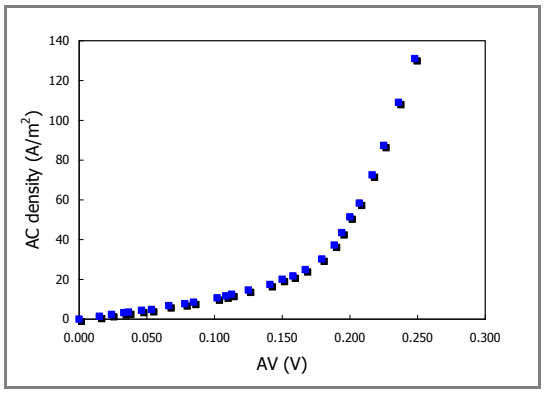

Figure 4.37*c* – AC-AV curve on carbon steel cathodically polarized at -1.3 V CSE

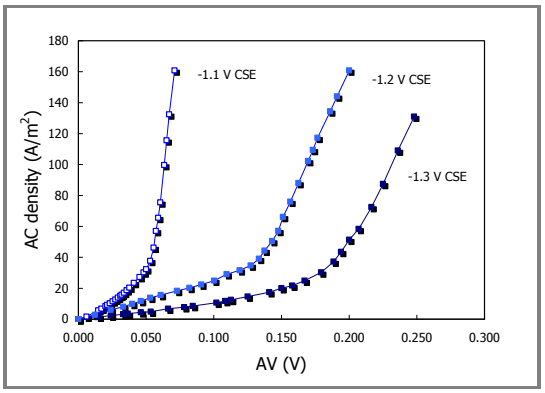

Figure 4.38 – AC-AV curve on carbon steel varying protection potential

At a first analysis, experimental tests show that AC corrosion is related to the existence of a critical AV below which corrosion doesn't occur. The superimposed AV to the metal provokes potential oscillation (Figure 4.25 to Figure 4.27) that results in electromechanical stresses inside the passive film that covers the metal. Electro-mechanical stresses depend on the electric properties of the film and on the magnitude of the electric field across the oxide.
AV measurements should be correlated to the AC corrosion risk diagram which defines corrosion risk on the basis of corrosion rates experimentally measured. Corrosion risk diagram (Figure 4.3 and Figure 4.39) shows that overprotection (potential lower than -1.1 V CSE) is the most dangerous condition and that the critical ratio between AC and DC density decreases by decreasing protection potential (Paragraph 4.1).
As discussed previously, corrosion occurs corresponding to a critical value of AV and AC density. While considerable differences of the breakdown voltage were measured, no remarkable differences of AC density were observed varying CP potential (Table 4.9).
The breakdown condition can be identified on the corrosion risk diagram by a combination of potential and i_{AC}/i_{DC} ratio. Blue markers in Figure 4.39 refer to the breakdown condition measured by AV measurement tests (Table 4.10), while red markers indicate high corrosion risk conditions on the basis of corrosion rate data. It should be pointed out that blue indicators refer only to the initiation step of AC corrosion but doesn't take into account corrosion propagation. Data are in good agreement. AV measurements confirm that the critical current densities ratio depends on the protection potential of the metal, i.e. it decreases by decreasing the protection potential.

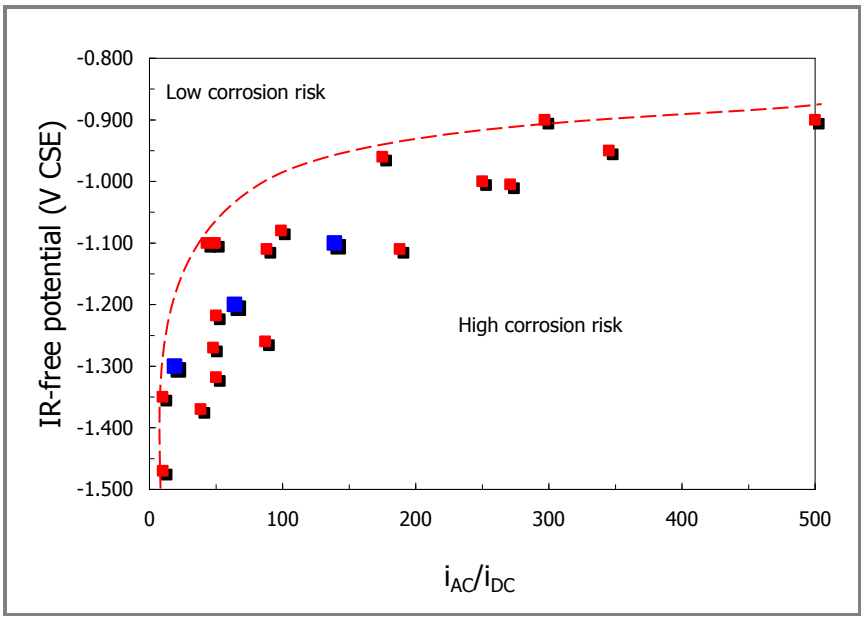

Figure 4.39 – AC corrosion risk diagram: corrosion rate data (red markers) and critical breakdown conditions by AC-AV measurement (blue markers)

4.4.3 Some considerations

Experimental tests showed that AC has a harmful effect on passive condition, causing the local breakdown of the passive film over a critical alternating voltage. A possible breakdown mechanism based on AC-induced electro-mechanical stresses in the film was proposed. Stresses could be generated in the film by electrostriction pressure due to high alternating field (in the order of MV/cm). This model represents an absolute novelty regarding the description and the investigation of AC corrosion initiation mechanism.

Further tests are mandatory to confirm the proposed model. Nevertheless, some considerations about the breakdown mechanism can be pointed out.

A "mechanical analogy". As widely discussed, AC corrosion of carbon steel in CP condition occurs corresponding to the achievement of a critical threshold of AV (or AC density), as indicated also by several authors. The presence of critical levels of interference could find an explanation considering the proposed mechanism: passivity breakdown occurs only over a critical electric field within the film, i.e. when the AC-induced mechanical stresses become equal to the breakdown stress of the metal. This behavior suggests a parallelism between the model and the laws of fracture mechanic of brittle materials (*mechanical analogy*).
Generally, in brittle materials, fracture occurs corresponding to the achievement of a critical value of the stress intensity factor at which a crack in the material begins to grow. Stress intensity factor is a property of material. As a result, the fracture of the material occurs corresponding to the achievement of a critical value of the applied stress or corresponding to a critical dimension of defects or cracks inside the material. Similarly, in the AC corrosion model, passive film breakdown occurs corresponding to the achievement of a critical alternating electric field across the film, in terms of a critical voltage threshold or a critical film thickness. Moreover, the adopted film breakdown mechanism generally considers a direct electric field across the film and doesn't take into account the electrostriction behavior in the presence of alternating fields. This could represent an interesting aspect to investigate in the future phases of the research. The possibility that a corrosion phenomenon can be described not only by means of electrochemical laws isn't a singularity; just think for instance on stress corrosion cracking or corrosion fatigue in which corrosion is strictly correlated to mechanical behavior of the corroding metal.
In particular, the mechanical breakdown due to the presence of alternating fields in the film may suggest an "*electro-mechanical fatigue*" mechanism, defined as the film mechanical cracking due to cyclic electrostriction stresses lower than the breakdown stress measured in the presence of a static load. Accordingly, the effect of frequency on AC corrosion (Paragraph 1.4.6) could undergo a new explanation and interpretation of corrosion phenomenon. Indeed, AC corrosion increases by decreasing the frequency of the interference signal, similarly to what happens in corrosion fatigue phenomena [21], i.e. initiation and crack propagation of corrosion fatigue decrease by increasing the frequency of the mechanical load. For instance, corrosion fatigue rate of carbon steel in sea water is about four times greater than corrosion rate in atmosphere at 0.1 Hz frequency but tends to this last value by increasing load frequency [21].

Corrosion morphology. AC corrosion is localized (Paragraph 1.5 and Chapter 5), i.e. corrosion starts corresponding to small area surrounded by not-corroded area. Generally, corrosion morphology could be useful for a better understanding of corrosion mechanism. The localized nature of AC corrosion suggests that the breakdown critical conditions are reached locally and not on the entire metal surface. This in agreement with the proposed model that suppose the cracking initiation corresponding to "weak points" in the passive film (as defects, presence of impurities, points with lower thickness) or disuniformities in AC distribution on the metal surface.

AC corrosion monitoring. In Paragraph 4.1, doubts were expressed about the use of induced AC voltage as critical parameter for the assessment of AC corrosion likelihood of a buried pipeline, preferring a description of AC corrosion in terms of protection potential and AC and DC current densities ratio.
Of course, no uncertainties are expressed regarding the role of induced AC voltage on corrosion, being the driving force of the corrosion phenomenon. However, doubts remain on the procedure described by the technical specification. As discussed, the measurement is carried out by connecting a high input impedance AC voltmeter with one pole to a reference

electrode placed on the soil above the pipeline and with one pole at the test station. This measurement inevitably contains an ohmic drop contribution not related to the AC corrosion phenomenon that fakes the measurement and doesn't provide information about the alternating voltage across the film, which measurement could be critical in field. Furthermore, it doesn't contain information about protection conditions which must take into account in order to evaluate corrosion risk.
Accordingly, from a practical point of view protection potential, AC and DC densities are the most indicative parameters to define corrosion risk.

Not only electrostriction. Electrostriction stresses could be a possible explanation of the film breakdown mechanism. Nevertheless, in the presence of high alternating electric field other breakdown mechanisms, as *avalanche breakdown*, can act. Generally, avalanche breakdown is a phenomenon that occurs in both insulators and semiconductors when current carriers are accelerated by the electric field to energies sufficient to free electron-hole pairs via collisions with bound electrons. In the presence of a voltage gradient in the semiconductor (as passive film) electrons will move towards the positive voltage while holes will "move" towards the negative. The presence of high voltages may move the free electrons fast enough to knock other electrons, creating more free-electron-hole pairs (i.e. more charge carriers), increasing the current. Due to avalanche effect, the whole crystal begins to conduct. Some kinds of diodes (avalanche diodes) are designed to breakdown by an avalanche mechanism.

4.5 STEP 2: HIGH pH CORROSION

After the breakdown of the passive film formed on steel in CP condition, corrosion of the underlying metal can occur only if thermodynamically possible. As discussed in Paragraph 4.3, thermodynamic conditions are defined by the potential-pH diagram of the iron-water system. The diagram shows two domains of possible corrosion. Iron corrodes in neutral and acidic solutions with formation of ferrous and ferric ions at low and high potential, respectively. Conversely, alkaline solutions have a beneficial effect on the formation of a protective passive film, if pH remains below the critical value of the high-pH corrosion domain. Figure 4.40 and Figure 4.41 show two versions of the potential-pH diagram of the iron-water system at 25°C, as reported by Pourbaix in his *Atlas* [69], depending on the stability of Fe_3O_4 and Fe_2O_3 or $Fe(OH)_2$ and $Fe(OH)_3$, respectively.

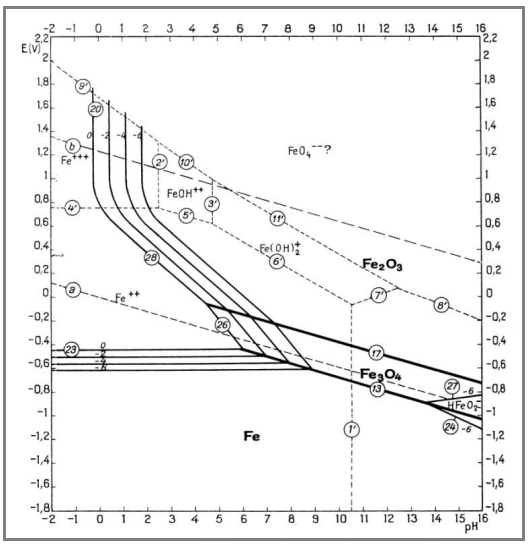

Figure 4.40 – Pourbaix diagram for the system iron-water at 25 °C considering as solid substances Fe, Fe_2O_3 and Fe_3O_4 [69]

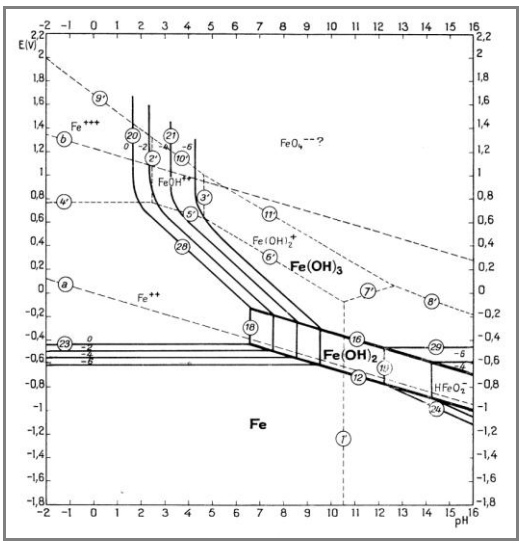

Figure 4.41 – Pourbaix diagram for the system iron-water at 25 °C considering as solid substances Fe, $Fe(OH)_2$ and $Fe(OH)_3$ [69]

As reported by CP guidelines [3], CP is established by lowering the potential in order to make corrosion rate acceptable. In the absence of sulphate reducing bacteria, protection potential of carbon steel in soil is -0.850 V CSE, that corresponds to -0.530 V SHE (Standard Hydrogen Electrode, which Pourbaix diagram refers). In the absence of AC interference, steel is protected if its potential is lower than this critical threshold and corrosion doesn't occur. Nevertheless, Figure 4.40 and Figure 4.41 show a corrosion domain corresponding to very high pH (close to 14) at potentials considered safe against corrosion. The two diagrams differ because of the "shape" of the high-pH corrosion domain. Considering as solid substance Fe_3O_4 and Fe_2O_3 (Figure 4.40), corrosion is possible in a triangular domain, i.e. the electrochemical equilibrium reactions (represented by the boundary lines 24 and 27) depend simultaneously on pH and potential:

(Eq. 4.8) $Fe + 2H_2O = HFeO_2^- + 3H^+ + 2e^-$ Reaction 24 (Figure 4.40)

(Eq. 4.9) $Fe_3O_4 + 2H_2O + 2e^- = 3HFeO_2^- + H^+$ Reaction 27 (Figure 4.40)

Conversely, the high-pH corrosion domain in the diagram showed in Figure 4.41 (that considers as solid substances $Fe(OH)_2$ and $Fe(OH)_3$) is delimited by a vertical equilibrium line. In a potential-pH diagram, this means that the reaction is potential-independent and occurs (obviously in a limited potential range) over a critical value of pH:

(Eq. 4.10) $FeO + H_2O = HFeO_2^- + H^+$ Reaction 19 (Figure 4.41)

In equilibrium condition (solubility of metal and its oxide equal to 10^{-6} mol/L, temperature 25°C) this pH is close to 14. High pH corrosion occurs with the formation of green dihypoferrite ions FeO_2H^-.
Summarizing, regardless the shape of the high-pH corrosion domain, Pourbaix diagrams show that corrosion is thermodynamically possible at potentials typically considered safe against steel corrosion. Nevertheless, in ordinary operative conditions and in the absence of stray currents, corrosion of cathodically protected steel doesn't occur because the critical pH corresponding to the corrosion domain is too high to be reached.
According to the proposed model (Paragraph 4.2), after the mechanical breakdown of the passive film formed on steel in CP condition, corrosion can occur only if the potential-pH condition of the interfered metal crosses the high-pH corrosion domain.

4.5.1 pH measurement in cathodic protection condition

Galvanostatic tests were carried out in order to measure the pH profile in the test solution in contact with a carbon steel specimen in CP condition. Carbon steel specimens, grade API 5L X52 (Table 2.1), were cathodically polarized by applying a constant CP current density for one hour to attain a steady value of the protection potential. Then, pH profile was measured by means of the experimental apparatus described in Paragraph 2.2.7.
Figure 4.42 to Figure 4.45 show pH profile in the presence of a CP current density of 0.5, 1, 5 and 7 A/m^2, respectively. The pH at the interface between the environment and the metal in CP condition is higher than the bulk solution pH (equal to 6.3). The alkalization of the environment close to the metal is due to the cathodic reactions on the metal that consume the electrons provided by the anodic process. The presence of a pH profile in the solution in contact with the metal is related to two effects: the diffusion process and the electrophoretic migration of charged particles. As mentioned, cathodic reaction produce hydroxyl ions (Eq. 1.5) that move from the metal surface where are produced to the bulk solution due to the presence of a concentration (or chemical activity) gradient. Moreover, a charge transfer must be considered in the spatial region between the metal (cathode) and the anode because of

the presence of an electric field that moves anions (as hydroxyl ions) from the cathode to the anode and cations in the opposite way. An equilibrium condition is so attained.
As expected by Faraday's law, the pH of the solution in close proximity to the metal increases by increasing CP current density. In the presence of 0.5, 1, 5 and 7 A/m^2 cathodic current density, the pH at about 0.3 mm distance from the surface is 11.6, 12.3, 13.1 and 13.3, respectively (Table 4.11).
Figure 4.46 shows pH value close to the metal surface (distance 0.3 mm) as a function of CP current density. A logarithmic trend is observed. The pH increases by increasing the CP current density. In the presence of high cathodic current (5 and 7 A/m^2), the pH is between 13 and 14.

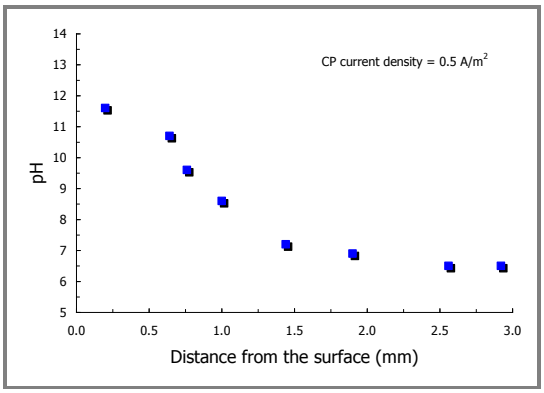

Figure 4.42 – pH measurement on carbon steel in CP (Protection current density = 0.5 A/m^2)

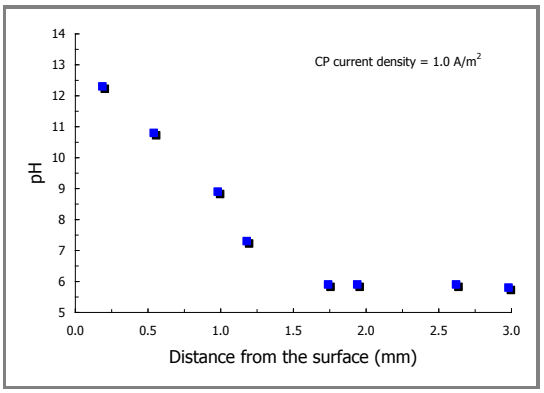

Figure 4.43 – pH measurement on carbon steel in CP (Protection current density = 1.0 A/m^2)

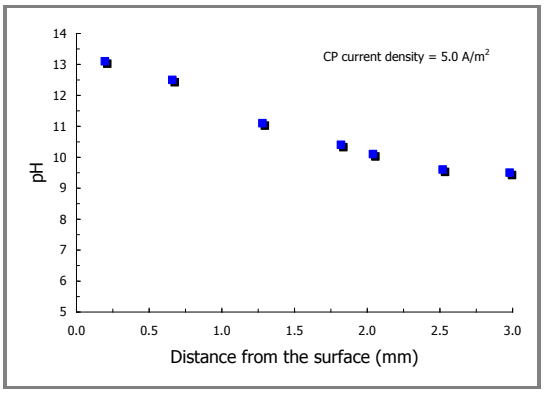

Figure 4.44 – pH measurement on carbon steel in CP (Protection current density = 5.0 A/m^2)

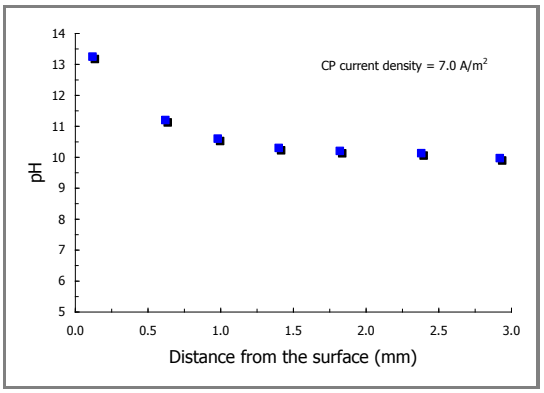

Figure 4.45 – pH measurement on carbon steel in CP (Protection current density = 7.0 A/m^2)

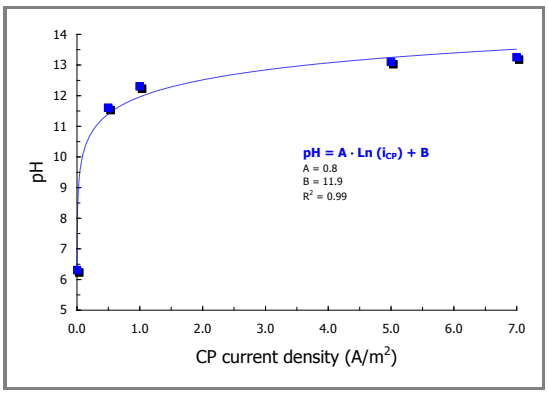

Figure 4.46 – pH at the metal-to-electrolyte interface (distance from the sample = 0.3 ± 0.1 mm)

Table 4.11 – pH measurement on carbon steel in CP condition

CP current density A/m^2	CP potential V CSE	pH Distance = 0.3 mm
0.0	-	6.3
0.5	-1.180	11.6
1.0	-1.250	12.3
5.0	-1.330	13.1
7.0	-1.370	13.3

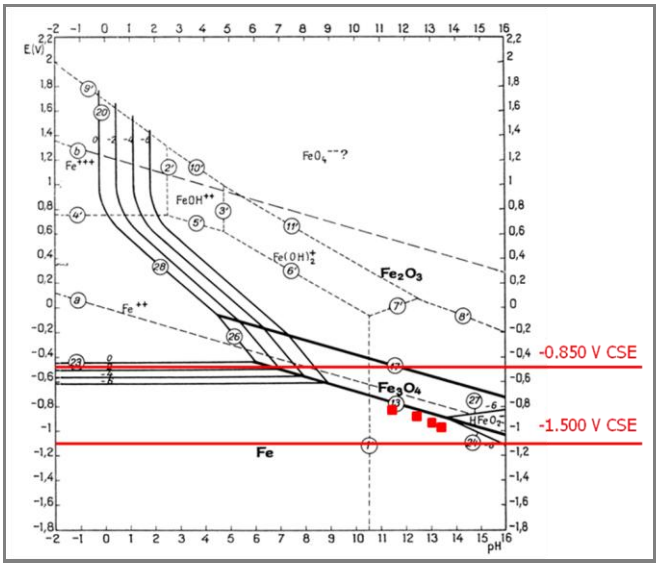

Figure 4.47 – Experimental thermodynamic conditions in the Pourbaix diagram of the system iron-water at 25 °C

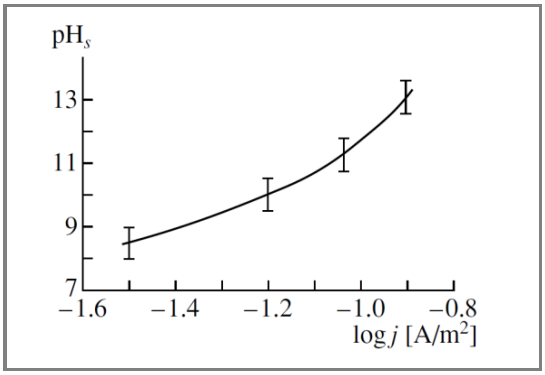

Figure 4.48 – Dependence of pH_S on cathodic current density in sand moistened with tap water [72]

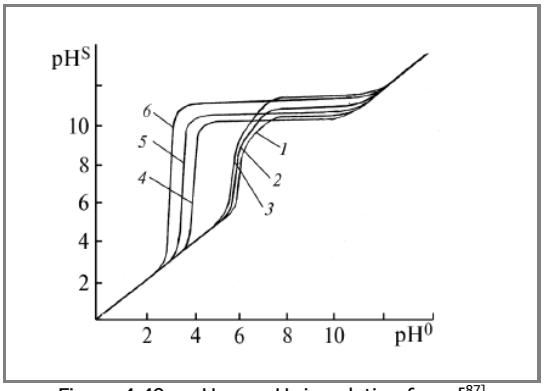

Figure 4.49 – pH_S vs. pH_0 in solution from [87]

Experimental potential-pH conditions are shown in the Pourbaix diagram in Figure 4.47. Red markers fall in the immunity region of iron stability, very close to the boundary condition of the passivation domain. In the presence of the highest CP current densities (5 and 7 A/m^2) the thermodynamic condition is close also to the high-corrosion region but it never cross it.

Freinman et al. [71] discussed the pH increase in CP condition due to the cathodic current supplied to the metal. Authors state that in soils the pH close to the metal surface (indicated as pH_S) increase with cathodic current density, reaching a considerably higher level (11–12, and higher) [72] (Figure 4.48).

Tkalenko et al. [87] developed a mathematical model in order to calculate the pH near the metal surface in aqueous solutions when the cathodic reaction is oxygen reduction. Authors correlate the pH of the bulk solution (pH_0) to the pH near the electrode (pH_S) and

demonstrate the substantial increase of alkalinity of the electrolyte close to the metal due to the accumulation of hydroxyl ions. Figure 4.49 shows pH_S as a function of pH_0 on a solution without (1-3) and with (4-6) the addition of 10 moles/L of KCl. In (1, 2, 4, 5) the current density is 0.6 A/m^2; in (3, 6) the current density is 6 A/m^2; in (1, 3, 4, 6) the thickness of the diffusion layer is 0.2 mm; in (2, 5) the thickness of the diffusion layer is 0.6 mm.

4.5.2 AC effect on high-pH corrosion

As discussed previously, a strong alkalization occurs in the electrolyte in close proximity to the metal in CP condition. Nevertheless, alkalization is not so high to corrode the metal. Indeed, in ordinary operative conditions and in the absence of stray currents, corrosion of cathodically protected steel doesn't occur. As reported by CP guidelines [3], overprotection condition (potentials lower that -1.1 V CSE) could be critical with respect to detrimental effects on coatings, as blistering or gradual cathodic disbonding, but effect on corrosion are not known.
According to the proposed corrosion model (Paragraph 4.3), after the breakdown of the passive film formed on steel in CP condition, corrosion of the underlying metal can occur in the absence of oxygen consumed by the cathodic process, only if locally the pH increases to values that correspond to corrosion (close to 14). This means that, in addition to the electro-mechanical breakdown of the passive film, a further effect of AC can be hypothesized.
Passive film breakdown by electro-mechanical stresses allows exposing the underlying metal to the solution that enters in the crack.
It should be pointed out that, as in pitting corrosion, the local environment in contact with the metal becomes more important than the bulk environment and should be considered in order to investigate the "true" corrosion condition.
For instance, it's well known the autocatalytic nature of pitting corrosion due to the self-stimulating and self-propagating corrosion reaction within the pit. Macro cell current exchanged between the pit and the surrounding area provokes chloride ions migration within the pit; furthermore, corrosion reactions cause the acidification with a strong decrease of pH. Considering pitting corrosion, as reported by Pourbaix [70], a cathodic treatment of steel leads to the potential decrease and to the pH increase of the solution inside cracks or pits, which become progressively neutral and then alkaline. This explains why both cracks and pits become inactive when CP is active.
Figure 4.50 shows schematically the influence of a cathodic polarization on pH condition inside a pit or crevice of carbon steel in contact with an aerated solution of 0.001 M NaCl and 0.001 M NaOH (bulk pH = 10.0). Dotted lines marked 0 refer to non-polarized steel; dotted lines marked 1 to 9 refer to increasing cathodic currents. For instance, dotted line 3 shows that when the protection potential is reached (-0.400 V SHE) the pH inside the pit, initially between 2.7 and 4.7, increases to about 7; a further cathodic polarization increases the pH up to 11. Again, Chen et al. [88] studied the effect of CP on corrosion of pipeline steel in the crevice area under disbonded coating through local potential, solution pH and dissolved oxygen concentration measurements. Results demonstrated that the main role of CP in corrosion mitigation is to enhance the local solution alkalinity.
Likewise, after the passive film breakdown due to AC interference, the local condition inside the crack may become more aggressive with respect to the bulk electrolyte. As widely discussed in Chapter 3, AC causes the increase of protection current density due to an effect on cathodic polarization curve (Paragraph 3.2 and Paragraph 3.3). As a consequence, the superimposition of a stationary AC interference could have the indirect effect of increasing the pH of the electrolyte in contact with the metal. For instance, in Paragraph 3.2 the effect of 100 and 240 A/m^2 AC density on CP current density of the galvanic system steel-magnesium was studied. Mean CP current density is about 1.1, 2.1 and 2.6 A/m^2 in the presence of zero, 100 and 240 A/m^2 AC density, respectively. According to the interpolation curve of Figure 4.46, the pH of the electrolyte near the metal surface will be 11.9, 12.5 and 12.7, respectively.

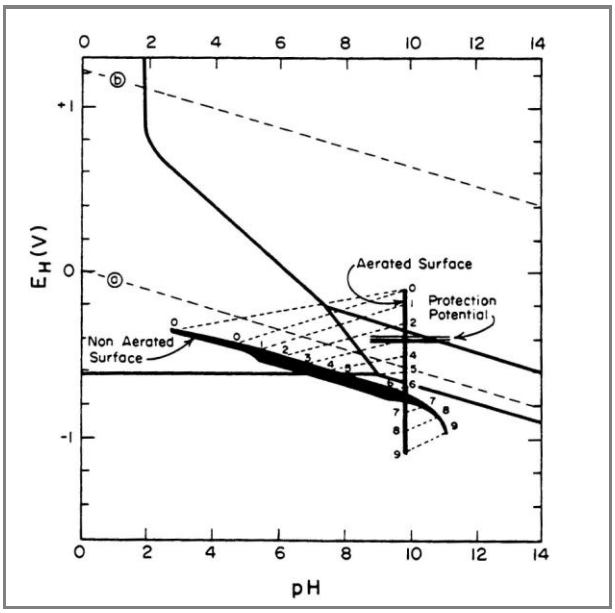

Figure 4.50 – Influence of a cathodic polarization on potential and pH conditions inside a pit (ordinary carbon steel with an aerated solution of 0.001 M NaOH and 0.001 M NaCl [70]

It should be pointed out that, generally, the local pH depends on several factors, as chemical composition, presence of electric fields, diffusion processes due to a concentration gradient, corrosion reactions and electrolyte convective properties. For instance, corrosion reactions reported by Eq. 4.8 to Eq. 4.10 show that corrosion reactions lead to protons production. At the same time, hydroxyl ions are produced by the cathodic process. The pH of the electrolyte will depend on the kinetics of the two processes and by diffusion and migration processes in the electrolyte due to concentration gradient and electric field.

Summarizing, corrosion can occurs only if particular potential-pH conditions are established on the metal surface, due to the simultaneous presence of CP and AC interference. Moreover, potential oscillations due to AC interference may be critical not only regarding the film breakdown mechanism but also with respect to high-pH corrosion likelihood. For instance, Nielsen et al. [38-40] in their alkalization mechanism reported that potential oscillation due to the superimposed alternating voltage could cause high pH corrosion if the potential crosses the corrosion region during its oscillation.
These considerations are in good agreement with the corrosion risk diagram. As discussed in Paragraph 4.1, corrosion rate measurements showed that overprotection condition is the most dangerous condition. Overprotection conditions are obtained by means of large cathodic current in order to obtain a strong cathodic polarization. High cathodic current produces a strong alkalization of the electrolyte close to the metal. As a consequence, just a few A/m^2 AC densities can be harmful because of the effect on CP current density and pH.

4.5.2.1 Chemical corrosion

The study of high-pH corrosion reaction mechanism is still ongoing. Nevertheless, some considerations should be advanced. As discussed previously, iron Pourbaix diagrams (Figure 4.40 and Figure 4.41) show a corrosion domain corresponding to pH close to 14 at potentials considered safe against corrosion. The two diagrams differ because of the "shape" of this domain. In particular, in the equilibrium diagram shown in Figure 4.41 (which considers as solid substances $Fe(OH)_2$ and $Fe(OH)_3$) the high-pH corrosion domain is delimited by a vertical

equilibrium line. This means that corrosion occurs (obviously in a limited potential range) over a critical pH value and is potential-independent.
Since electrons are not involved in the corrosion reaction (Eq. 4.10) the corrosion process is controlled by a chemical equilibrium between species, instead of electrochemical. The so-called *chemical corrosion* refers to this condition.
Chemical corrosion is well known for several metals, as aluminium. Figure 4.51 shows the potential-pH equilibrium diagram of the system aluminium-water at 25°C, as Pourbaix reported in his *Atlas* [69]. In non-complexing solutions of pH roughly between 4 and 9, aluminium tends to become covered with a thin film of oxide; the nature of the film is generally complex. The whole immunity domain lies below the line of water.
Conversely, aluminium corrosion is thermodynamically possible at low and high pH (amphoteric behaviour of aluminium) with formation of Al^{3+} and aluminate AlO_2^- ions, respectively. Corrosion domains are delimited by vertical lines, i.e. the dissolution process of aluminium oxide is potential-independent and occurs below (at low pH) and over (at high pH) critical pH thresholds.
Even if aluminium oxide is thermodynamically stable in the pH range from 4 to 9, pitting corrosion can occur in the presence of chlorides (for instance in sea water).
As widely discussed, pitting of passivable metals (as aluminium) may be avoided by a cathodic treatment which brings the metal into a state of perfect passivation. CP of aluminium by bringing the metal into a state of immunity (without protective oxide) is practically impossible, because it would require the achievement of potentials too negative, about -2.0 V SHE (Figure 4.51), with strong hydrogen evolution. This condition (high cathodic current density) could be prohibitive because of the alkaline corrosion of aluminium that occurs due to the pH increase of the solution in contact with the metal. As a result, aluminium can corrode even if a cathodic current on the metal is applied due to the main role played by pH on chemical corrosion reaction. As a consequence, CP of pitted aluminium is generally achieved by a potential lowering to potential between the repassivation potential and the immunity potential.
Similarly, chemical corrosion of carbon steel in CP condition in the presence of AC interference could be hypothesized. If chemical corrosion occurs, corrosion will be potential-independent and a further cathodic current supply to the metal could be harmful, due to the pH increase.

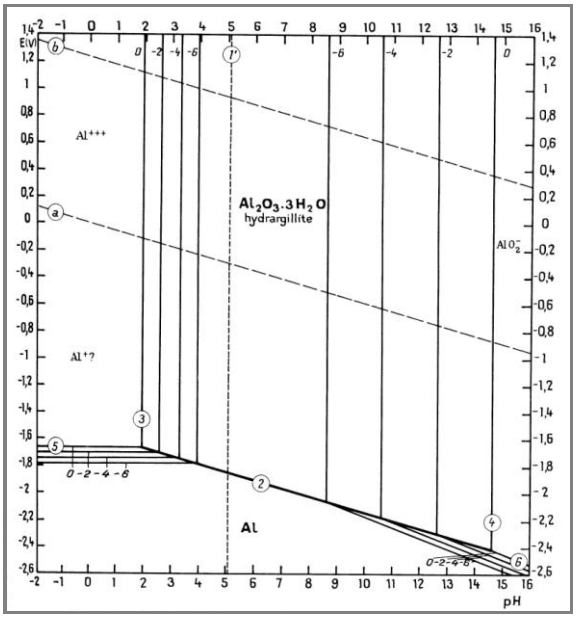

Figure 4.51 – Pourbaix diagram for the system aluminum-water at 25 °C [69]

4.6 SUMMARY

Experimental tests showed that in the presence of AC interference corrosion can occur, even if the -0.850 V CSE criterion is matched. Overprotection (potential lower than -1.1 V CSE) seems to be the most dangerous condition with respect to AC corrosion risk.
A two-steps AC corrosion mechanism of carbon steel in CP condition is proposed. In the first step AC causes the breakdown of the passive film that CP conditions form on carbon steel surface. The influence of AC on passive conditions was studied: AC has a harmful effect on the passive condition, reducing the critical chlorides threshold and causing a depassivation of the metal (by the increase of the passive current density and the decrease of pitting potential). An electro-mechanical breakdown mechanism is proposed. The presence of high alternating electric field (in the order of MV/cm) within the passive film could cause the film local breakdown. Electrostriction stresses could be a possible explanation.
After film breakdown, corrosion occurs only if the pH at the metal-to-electrolyte interface is close to 14. Such pH could be reached inside the corroded area in overprotection condition, due to the high CP current density supplied to the metal. Chemical corrosion (potential-independent corrosion) can be hypothesized.

This model represents an absolute novelty in the field of AC corrosion phenomenon description. Nevertheless, further tests are mandatory to confirm the proposed model obtained in this phase of the research.

Chapter 5

Results

Part 3 – AC corrosion propagation

In this section, AC corrosion propagation and corrosion morphology are discussed. As described in Paragraph 2.3.2, experimental tests were carried out on carbon steel specimens cathodically protected by means of a galvanic magnesium anode in the presence of 240 A/m^2 AC stationary interference. The carbon steel specimen (1.5 cm^2 exposed area) simulates a holiday of a pipeline coating. Four batches (A, B, C, D) were prepared, each consisting of eight cells with a steel specimen cathodically protected in soil-simulating environment by a magnesium anode sized according to the procedure described in Paragraph 2.3.2.2. AC was overlapped to both the sample and the anode by means of an external AC feeder. A control test cell was also prepared out without AC superimposition. Samples and anodes were extracted every month from one to four months of AC interference (Table 2.10).
Since AC corrosion is localized (Paragraph 1.5), mass loss measurement is not ordinarily recommended to assess corrosion propagation because it doesn't provide information about corrosion penetration depth. Therefore, corrosion was evaluated by means of:

- corrosion penetration depth measurement;
- corrosion attacks number measurement;
- corrosion attacks size measurement.

Moreover, the effect of AC on magnesium anode consumption was investigated. During the test, CP conditions were checked by means of protection potential and protection current measurements. AC effect on such parameters was already discussed in Chapter 3.
A preliminary description of AC corrosion morphology is provided.

5.1 AC CORROSION MORPHOLOGY

Figure 5.1 to Figure 5.4 show, as an example, digital camera images of carbon steel specimens before pickling extracted after one, two, three and four months at 240 A/m^2 AC stationary interference.
Carbon steel specimens are covered by corrosion products which form a non-adherent and non-protective layer on the metal surface. The presence of corrosion products is extended to the entire metal surface so that corrosion appears as uniform. A deposit of encrusted sand was often found on the metal surface.
Furthermore, the growth of a hemispherical agglomerate of sand and corrosion products was observed on some specimens, especially after the longest test time (four months). The presence of such agglomerate, as discussed in Paragraph 1.5, was also observed in several AC corrosion cases. For instance, Nielsen and Cohn [34] define a "distinct tubercle of stone hard soil frequently observed to grow from the coating defect in connection with AC corrosion incidents" (Figure 1.16, Chapter 1). Even Linhardt and Ball [36] in the corrosion case study reported in Paragraph 1.5.1 report a "hard cap of soil adhering to the pipe and covering the leak". In literature a univocal definition of this agglomerate which frequently grows from the metal corroded by AC isn't provided. Authors refer to it as a "stone hard soil", "hard cap of soil", "hard tubercle", "solid stony corrosion product" or "hemispherical shell of hard soil" [23,

[34, 36, 89]. Such agglomerate was removed from the surface and then X-ray diffraction (XRD) analysis was performed. XRD spectrum (Figure 5.5) indicates the presence of silica sand (quartz) used in addition with the soil-simulating solution (200 mg/L chlorides and 500 mg/L sulphate ions introduced as sodium and calcium salts). XRD spectrum indicates also the presence sodium and calcium compounds: albite, a white feldspar mineral of formula $Na(AlSi_3O_8)$ and anorthite, a calcium feldspar of formula $Ca(Al_2Si_2O_8)$. The presence of sodium and calcium is due to the introduction of sodium chloride and calcium sulphate in the test-solution. These ions in solution form solid compounds with aluminium and magnesium ions originated from the anodic dissolution of galvanic anode. Indeed, the galvanic anode is a magnesium-based alloy (AZ63D alloy, Table 2.4) containing aluminium in the range between 5 and 7%. After anodic dissolution, cations tend to migrate from the anode to the cathode (the steel specimen) due to the electric field between them. The formation of solid precipitates and mixed compounds could be due to local chemical modifications of the electrolyte in close proximity to the metal. Indeed, the solution alkalization due to cathodic reactions may shift chemical equilibriums leading to precipitates formation. The analysis of the aqueous extract of the agglomerate gave a weakly alkaline pH of 9.5. XRD spectrum indicates also the presence of clinochlore, i.e. a compound of the chlorite group with general formula $(Mg, Fe)_6(Si, Al)_4O_{10}(OH)_8$.
As suggested by some authors [36], the hemispherical shape of this agglomerate with soil and minor amounts of alkali (Na) and earth alkali (Ca, Mg) ions could be related to diffusion phenomena associated with high cathodic activity close to the metal. Hydrogen bubbles formation could create a "rounded shape" of the solid agglomerate during its formation.

Figure 5.1 – Carbon steel specimen before pickling after 1 month AC interference (batch A)

Figure 5.2 - Carbon steel specimen before pickling after 2 months AC interference (batch B)

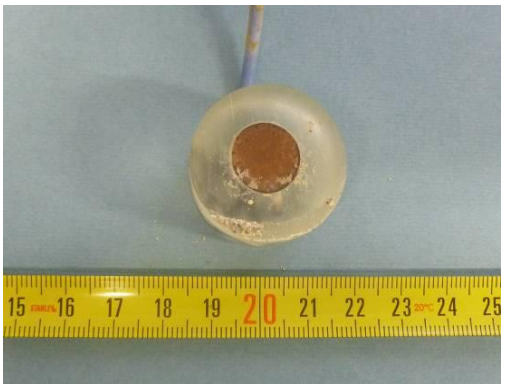

Figure 5.3 - Carbon steel specimen before pickling after 3 months AC interference (batch C)

Figure 5.4 - Carbon steel specimen before pickling after 4 months AC interference (batch D)

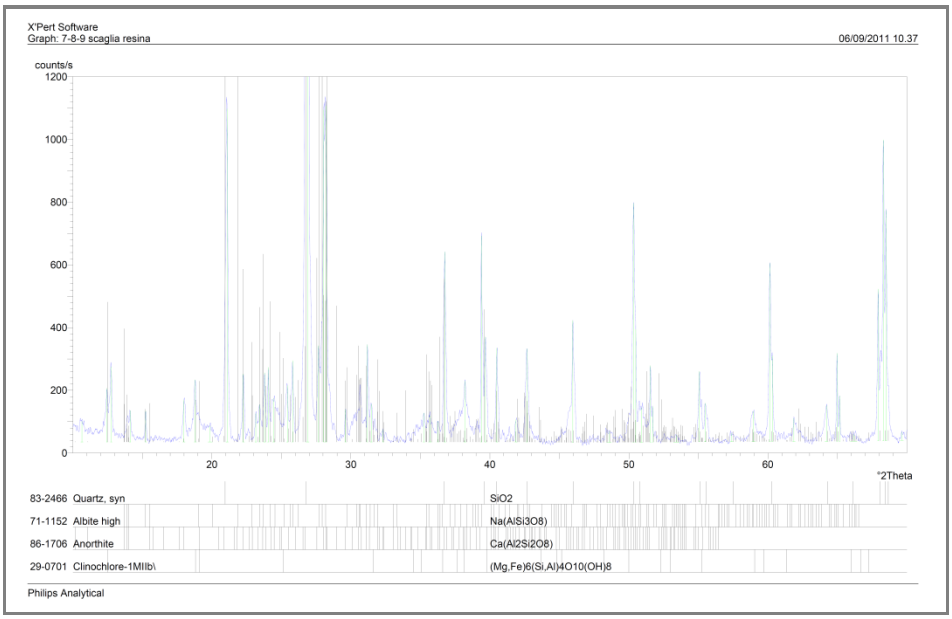

Figure 5.5 – XRD spectrum of the hemispherical soil agglomerate (Figure 5.4)

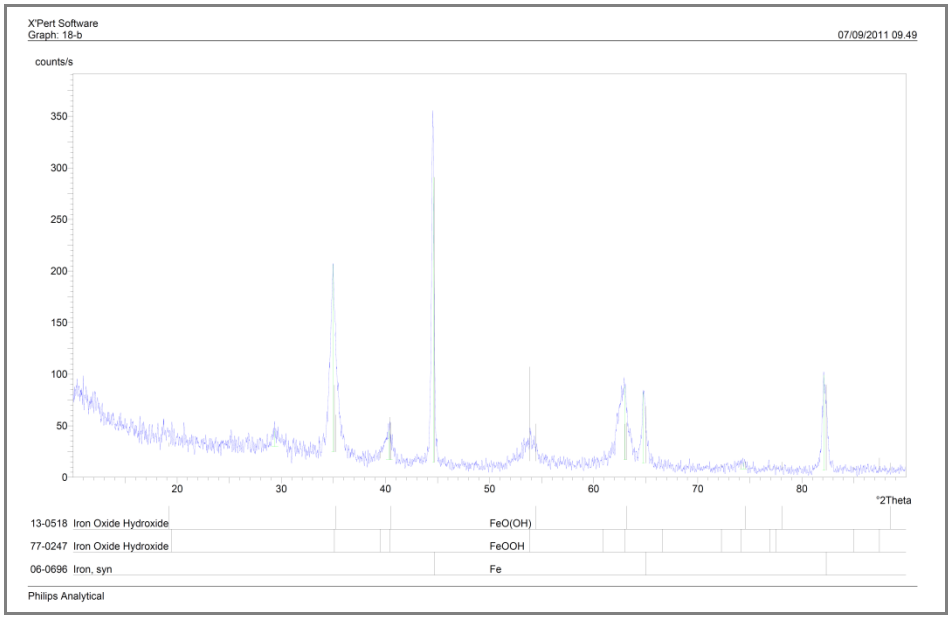

Figure 5.6 – XRD spectrum of steel corrosion products

Before picking, corrosion products were manually removed and analyzed by XRD technique; XRD spectrum (Figure 5.6) indicates the presence of iron hydroxide of formula FeO(OH). Corrosion products were then totally removed by chemical pickling and ultrasonic treatment. Figure 5.7 to Figure 5.10 show carbon steel images obtained after pickling with a digital camera Leica DFC 290 of a stereoscope model Wild 6X-50X (6X magnification), varying exposure time (one to four months). Before the removal of corrosion products, corrosion morphology appeared as uniform, due to the presence of distributed corrosion products on the entire surface. Conversely, localized corrosion is observed. After one month of AC interference, corrosion is not well-distributed on the metal surface and occurs mostly in proximity of the boundary between the specimen and the epoxy resin (Figure 5.7).

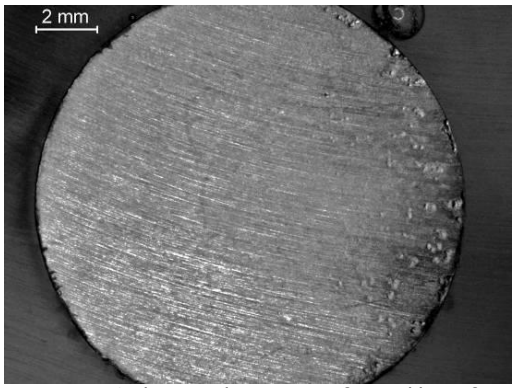

Figure 5.7 - Carbon steel specimen after pickling after 1 month AC interference (batch A)

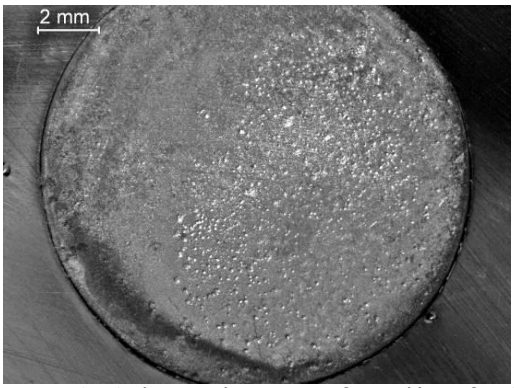

Figure 5.8 - Carbon steel specimen after pickling after 2 months AC interference (batch B)

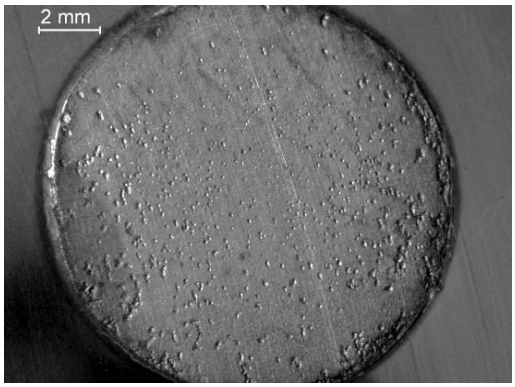

Figure 5.9 - Carbon steel specimen after pickling after 3 months AC interference (batch C)

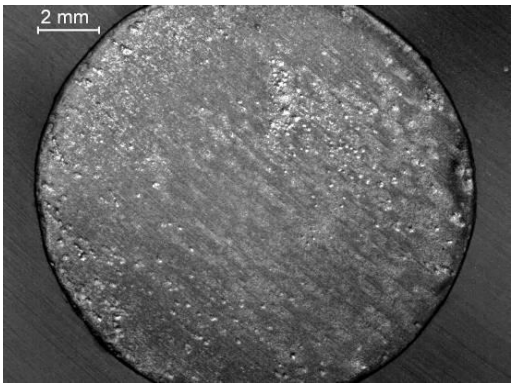

Figure 5.10 - Carbon steel specimen after pickling after 4 months AC interference (batch D)

The corroded area grows by increasing the exposition time to AC interference, as expected. After two months (Figure 5.8) corrosion is extended also in the central zone of the sample. After three and four months (Figure 5.9 and Figure 5.10), corrosion attacks are well-distributed on the surface of the metal exposed to interference. Corrosion morphology is characterized by the presence of small and large round point-shaped attacks.

In the first part of this research project, SEM-EDS analysis were performed on carbon steel specimens after 15 days of immersion in soil-simulating solution at different DC and AC interference conditions [15]. Analysis revealed that AC leads to the growth of thick but non-adherent films of corrosion products on the metal surface. Moreover, the nature, thickness and adhesion of the film change with AC density, type of metal and solution composition [15].

5.2 CORROSION PENETRATION DEPTH

As discussed previously, since AC corrosion morphology is localized, penetration depth measurement represents the most proper method to evaluate AC corrosion damage.
Penetration depth measurements were carried out on steel specimens cathodically protected by a magnesium alloy anode after one to four months AC interference, in order to evaluate AC corrosion propagation in terms of corrosion penetration. Corrosion penetration depths were measured by scanning eight diameters (9 mm long) on the metal surface by means of an optical laser profilometer (lateral and vertical resolution = 0.010 μm), as described in Paragraph 2.3.2.6. Due to experimental limitations it wasn't possible to scan the entire surface area.
As an example, Figure 5.11 reports the spectrum of a laser profilometry along a diametrical direction on the metal surface. Obviously, penetration depth measurements were obtained by

subtracting the mean value of the surface roughness (provided by the scan) to the peak depth. Table 5.1 to 5.4 report corrosion penetration depth measurements for each batch.

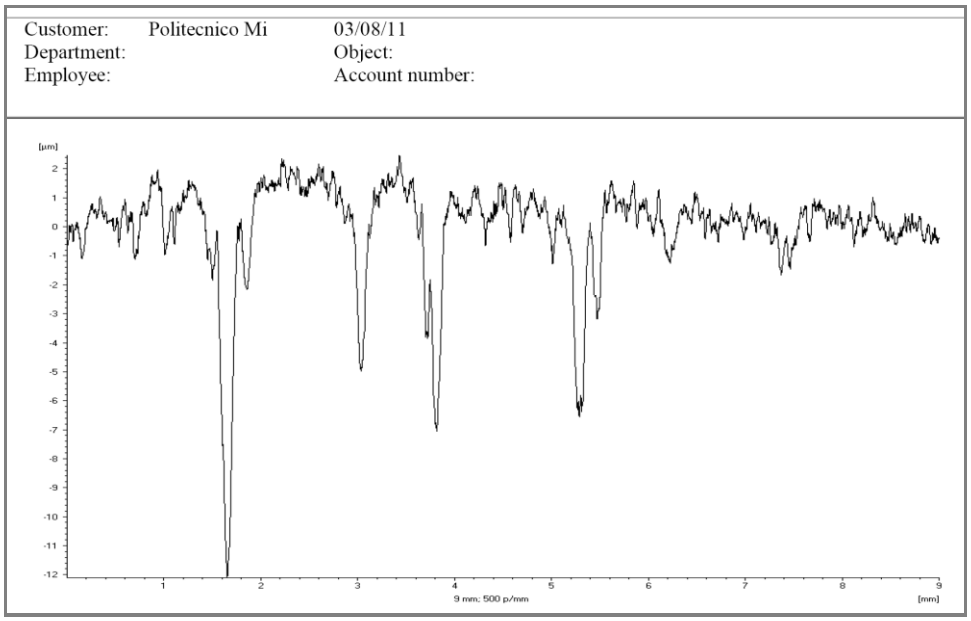

Figure 5.11 – Example of laser profilometry on a steel sample

Table 5.1 – Penetration depth measurements on specimens of batch A (1 month AC interference)

Sample	# attacks	Penetration depth (µm)														
A1	1	3.7														
A2	27	1.8	1.9	1.9	1.9	1.9	2.2	2.2	2.2	2.3	2.6	2.6	2.7	2.8	2.8	2.9
		2.9	3.1	3.1	3.8	4.0	4.4	4.6	4.6	4.6	4.6	5.7	6.2			
A3	8	2.1	2.5	2.7	2.9	3.0	3.2	3.4	3.7							
A4	4	3.2	3.6	4.2	4.4											
A5	14	3.3	3.3	3.4	3.4	3.6	3.6	3.6	3.7	3.9	3.9	4.1	4.6	4.8	4.8	
A6	11	2.4	2.5	2.6	2.8	2.9	3.0	3.0	3.2	3.4	3.7	3.9				
A7	5	3.6	3.8	3.8	4.0	6.7										
A8	23	3.2	3.5	3.6	3.6	3.6	3.6	3.7	3.7	3.8	3.8	3.8	3.8	3.9	4.0	4.0
		4.1	4.1	4.1	4.4	4.5	4.5	4.7	4.8							

Table 5.2 - Penetration depth measurements on specimens of batch B (2 months AC interference)

Sample	# attacks	Penetration depth (µm)														
B1	2	4.4	5.5													
B2	29	3.5	3.6	3.7	3.9	3.9	4.0	4.1	4.2	4.6	4.6	5.4	5.7	5.7	5.8	5.9
		6.0	6.0	6.5	6.6	6.7	6.7	6.8	7.1	7.3	8.6	9.1	9.6	14.3	16.0	
B3	46	1.8	2.0	2.0	2.0	2.1	2.2	2.3	2.5	2.6	2.6	2.6	2.7	2.8	2.8	2.9
		2.9	2.9	3.1	3.1	3.2	3.2	3.3	3.4	3.5	3.5	3.5	3.5	3.5	3.8	3.9
		4.8	4.9	5.0	5.2	5.3	5.3	5.6	5.7	5.7	6.0	6.0	6.6	6.6	7.6	8.7
		9.0														
B4	13	2.4	2.6	2.6	2.7	2.8	3.0	3.2	3.3	3.6	3.7	4.0	5.5	6.5		
B5	19	2.4	2.8	2.8	2.9	3.0	3.1	3.2	3.5	3.5	3.5	3.7	3.7	4.4	4.8	4.8
		5.0	5.1	5.4	8.4											
B6	13	3.8	3.8	4.0	4.1	4.1	4.5	5.1	5.1	5.3	5.6	6.3	6.6	7.5		
B7	28	2.7	2.8	2.8	2.8	3.0	3.1	3.3	3.3	3.4	3.5	3.7	4.0	4.5	4.5	5.4
		5.6	5.9	6.8	7.0	7.3	7.4	7.7	9.0	11.0	11.0	12.0	12.0	12.4		

Table 5.3 - Penetration depth measurements on specimens of batch C (3 months AC interference)

Sample	# attacks	Penetration depth (μm)														
C1	25	1.8	1.9	2.2	2.2	2.3	2.5	2.6	2.6	3.1	3.4	3.4	3.5	3.6	3.8	4.0
		5.0	5.2	5.5	5.6	5.7	6.0	6.3	6.9	7.8	8.6					
C2	45	2.6	3.7	3.9	4.1	4.1	4.1	4.1	4.3	4.4	4.9	5.2	5.3	5.4	5.4	5.4
		5.4	5.4	5.5	5.5	5.6	5.8	6.2	6.5	6.6	6.8	7.3	7.5	7.5	7.8	7.8
		7.9	7.9	7.9	8.0	8.3	8.3	8.6	8.9	9.1	9.7	10.8	11.0	11.2	11.4	12.2
C3	39	2.6	2.6	2.7	2.7	3.0	3.0	3.2	3.3	3.5	3.5	3.6	3.7	3.7	3.7	3.8
		3.9	3.9	4.0	4.0	4.0	4.1	4.1	4.3	4.4	4.4	4.4	4.4	4.8	4.8	5.1
		5.6	6.4	6.5	7.1	7.2	7.3	7.5	8.5	9.7						
C4	41	1.8	1.8	1.8	2.0	2.1	2.7	2.8	2.9	3.0	3.3	3.3	3.4	3.6	3.8	4.0
		4.2	4.5	4.5	4.6	4.6	4.7	4.8	4.9	5.2	5.5	5.7	5.9	6.1	6.2	6.8
		7.0	7.1	7.3	7.5	7.6	7.7	7.9	8.5	8.5	9.8	12.3				
C5	49	1.9	2.2	2.2	2.3	2.5	2.6	2.6	2.6	2.8	2.9	3.0	3.1	3.3	3.4	3.6
		3.7	4.2	4.2	4.2	4.5	4.6	4.6	4.6	4.7	5.0	5.2	5.3	5.4	5.5	5.8
		5.8	6.0	6.0	6.2	6.3	6.4	6.4	6.7	6.9	7.1	7.2	7.6	7.7	7.9	8.0
		8.4	8.4	9.6	17.2											
C6		Excluded from analysis														
C7	56	2.6	2.7	2.9	2.9	3.0	3.0	3.1	3.2	3.3	3.4	3.4	3.5	3.5	3.6	4.0
		4.0	4.1	4.2	4.4	4.5	4.6	4.6	4.6	4.6	4.8	4.8	4.9	5.1	5.1	5.2
		5.5	5.8	6.0	6.0	6.0	6.2	6.2	6.3	6.4	6.7	6.9	6.9	7.0	7.0	7.3
		7.4	7.6	7.9	8.0	8.1	8.2	8.7	8.7	8.9	10.1	15.8				

Table 5.4 - Penetration depth measurements on specimens of batch D (4 months AC interference)

Sample	# attacks	Penetration depth (μm)														
D1	52	2.7	2.8	2.9	3.0	3.0	3.2	3.2	3.6	3.6	3.6	3.7	3.8	3.8	3.8	3.9
		3.9	4.0	4.0	4.1	4.2	4.3	4.6	4.8	4.8	4.8	5.0	5.1	5.2	5.3	5.4
		5.5	5.8	6.1	6.3	6.5	6.6	6.7	6.8	7.0	7.2	7.5	7.6	7.7	7.8	9.2
		9.8	9.9	10.0	10.4	11.8	14.5	14.6								
D2	35	2.8	2.9	3.0	3.0	3.0	3.0	3.0	3.0	3.2	3.2	3.2	3.3	3.3	3.3	3.3
		3.5	3.5	3.5	3.6	3.6	3.6	3.6	3.7	3.7	3.8	3.9	4.0	4.0	4.0	4.1
		4.1	4.6	4.8	5.2	6.8										
D3	32	2.7	2.8	2.8	2.8	2.8	3.0	3.0	3.0	3.1	3.2	3.2	3.3	3.4	3.4	3.4
		3.6	3.7	3.7	3.7	3.9	4.0	4.0	4.2	4.2	4.7	4.9	5.1	5.4	6.2	9.1
		9.5	10.8													
D4	23	2.8	2.8	2.8	2.8	2.8	2.9	2.9	2.9	3.0	3.0	3.2	3.2	3.4	3.4	4.3
		4.4	5.0	5.2	5.4	7.0	8.1	9.4	11.8							
D5	38	2.6	2.6	2.7	2.7	2.8	2.8	2.8	2.8	2.8	3.0	3.0	3.0	3.0	3.1	3.2
		3.2	3.2	3.4	3.4	3.5	3.6	3.6	3.7	3.8	4.0	4.0	4.2	4.4	4.5	4.7
		4.7	4.8	5.3	7.7	8.7	9.5	10.7	10.8							
D6	38	2.5	2.6	2.6	2.7	2.7	2.8	2.9	2.9	3.0	3.0	3.1	3.1	3.2	3.3	3.3
		3.6	3.6	3.6	3.7	3.9	4.0	4.1	4.3	4.3	4.4	4.7	4.9	4.9	4.9	5.0
		5.3	5.4	5.4	6.2	6.4	6.9	7.6	8.1							
D7	54	2.8	3.0	3.0	3.1	3.1	3.2	3.3	3.4	3.4	3.4	3.5	3.5	3.7	3.8	3.8
		3.9	4.0	4.0	4.2	4.4	4.4	4.4	4.5	4.8	4.9	5.2	5.5	5.5	5.5	5.6
		5.7	5.8	6.1	6.1	6.2	6.4	6.7	6.9	7.4	7.9	7.9	7.9	8.0	8.7	8.7
		8.9	9.0	9.0	9.1	9.3	9.4	9.6	10.0	13.2						

Because of the large data variability, a statistical analysis of penetration depth measurements was carried out. Generally, several factors act to produce measured values that deviate from the expected one; in particular, it's well known that localized corrosion shows a stochastic aspect in its occurrence, generally associated to non-uniformities in the metal, in the environment or in the assembly which play a decisive role in controlling corrosion rate. Figure 5.12 to Figure 5.15 report probability distribution of penetration depth data obtained by plotting frequency versus measured values. Probability distribution is constructed by dividing

the range of penetration depth values into equal intervals (0.5 or 1 μm wide) on abscissa axis and then placing an histogram over each interval of height equal to the number of data points within that interval, according to the procedure reported by the standard guide ASTM G16 [90]. Probability distributions are not symmetrical and bell-shaped, especially for batches B, C and D. Therefore, the use of analysis techniques developed for the normal distribution can lead to erroneous conclusions. Probability distributions of batches B, C and D show a right tail (right-skewed distributions).
A skewness index was calculated in order to measure the probability distribution asymmetry. Table 5.5 reports the Pearson's skewness index (P.I.) calculated as:

$$\text{(Eq. 5.1)} \qquad \text{P.I.} = \frac{\text{mean} - \text{mode}}{\text{st.dev}}$$

Pearson's skewness index can be used to determine whether the distribution is symmetric or skewed. For a right-skewed distribution, P.I. is positive. By definition, the mean is the average of penetration depth values and, if the distribution is skewed, is located towards the tail because it's affected by extremes. The mode, instead, represents the value corresponding to peak point of the distribution and it's not affected by extremes.

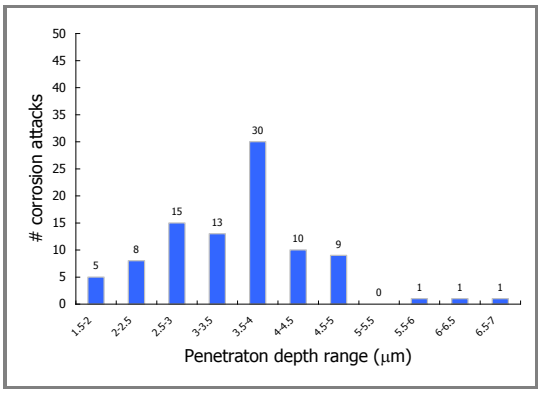

Figure 5.12 – Penetration depth measurements distribution of batch A

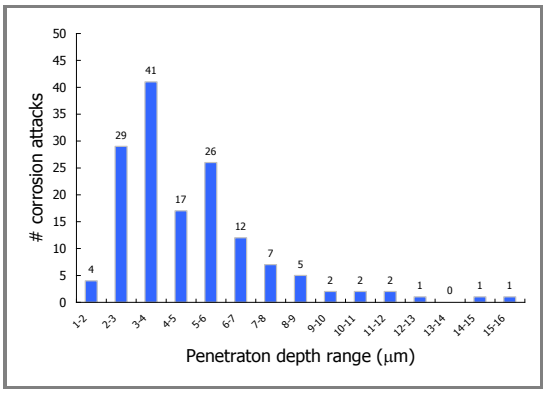

Figure 5.13 - Penetration depth measurements distribution of batch B

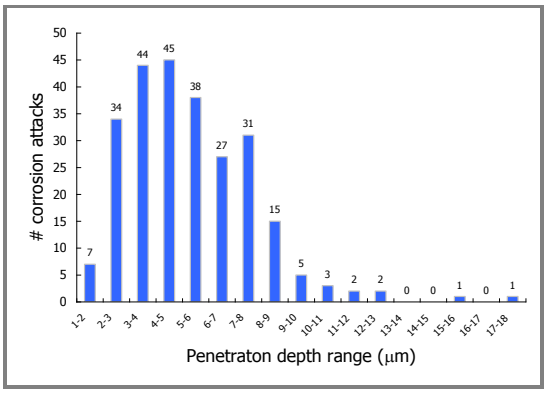

Figure 5.14 - Penetration depth measurements distribution of batch C

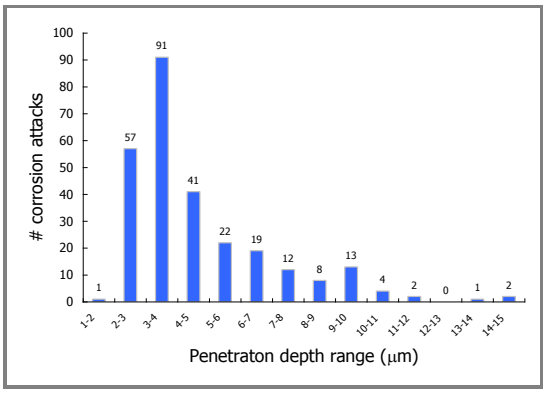

Figure 5.15 - Penetration depth measurements distribution of batch D

Table 5.5 – Pearson's skewness index of penetration depths distribution

Batch	# attacks	Mean (μm)	Mode (μm)	St. Deviation (μm)	Pearson index
A	93	3.5	3.7	0.9	-0.22
B	150	4.9	3.5	2.5	0.56
C	255	5.4	4.5	2.4	0.38
D	272	4.8	3.5	2.3	0.57

Table 5.6 – Penetration depth factor

Batch	# attacks	Mean (μm)	Maximum (μm)	P.D. factor
A	93	3.5	6.7	1.91
B	150	4.9	16.0	3.27
C	255	5.4	17.2	3.19
D	272	4.8	14.6	3.04

As reported by the standard guide [90], in order to evaluate corrosion propagation and to determine the probability of perforation by localized corrosion, the usual measures of distribution variability (as variance, standard deviation and coefficient of variation) aren't sufficient.
Even if the use of these measures can be useful in estimating confidence intervals and making prediction from observed data in several applications, a statistical treatment of data based only to these parameters could be too restrictive in order to estimating the maximum corrosion depth of a corroded steel pipe. In the case of localized corrosion, as AC corrosion, the failure is determined by the *extreme values* of the distribution, i.e. the maximum values of penetration depths which correspond to the upper tail of the distribution.
At a first analysis, corrosion penetration could be expressed in terms of the maximum pit depth and the average of the ten deepest pits, as reported by the standard guide [91] on the examination and evaluation of pitting corrosion (the most known localized corrosion form). Moreover, a *pitting factor* can also be calculated by the ratio between the deepest and the average corrosion penetration. A unitary pitting factor represents uniform corrosion.
Similarly, a *penetration depth factor* (P.D. factor) was calculated for every batch, considering all the penetration depth measurements. Table 5.6 shows that the number of corrosion attacks increases by increasing the time of AC interference while the P.D. factor, with the exception of batch A (samples interfered for one month), seems to be time-independent. For batch B, C and D, PD factor assumes a stable value of about 3, i.e. the maximum penetration depth is three times greater than the mean penetration depth.
This confirms that, in order to predict the service life of a pipeline in the presence of AC corrosion, a data analysis based exclusively on mean value is too hazardous and maximum values should be considered.

5.2.1 Extreme value statistics: theoretical background

Standard guidelines [90, 91] which dealt with corrosion data analysis report *extreme value analysis* as the most proper statistics to adopt in order to predict the remaining lifetime of a metal structure in the presence of localized corrosion.
Extreme value statistics has been successfully applied to maximum pit depth data analysis in order to estimate the maximum pit depth on a large area of material on the basis of the examination of small portion of it, for instance by a laboratory analysis. Generally, extreme value statistics considers the extreme deviations from the median of a probability distribution and is widely used in many fields, as structural engineering, finance, earth sciences, geological engineering. For instance, extreme value analysis is largely used in hydrology in order to estimate unusually floods by means of annual maximum values of daily rainfall and river discharge volumes. The generalized extreme value distribution is given by:

$$\text{(Eq. 5.2)} \qquad F_\gamma(z) = \exp\left\{-\left[1+\gamma\left(\frac{z-\mu}{\sigma}\right)\right]^{-\frac{1}{\gamma}}\right\} \quad \text{with} \quad 1+\gamma\left(\frac{z-\mu}{\sigma}\right) > 0 \qquad \gamma \neq 0$$

where μ is the location parameter, $\sigma\,(>0)$ is the scale parameter and γ is the shape parameter, which indicates the type of asymptotic distribution as follows:

Gumbel distribution (or Type I distribution)

(Eq. 5.3) $\gamma \to 0$ $$F(z) = \exp\left\{-\exp\left[-\frac{(z-\mu)}{\sigma}\right]\right\} \qquad -\infty < z < +\infty$$

Fréchet distribution (or Type II distribution)

(Eq. 5.4) $\gamma > 0$ $$F_\gamma(z) = \exp\left[-\left(\frac{z-\mu}{\sigma}\right)^{-\frac{1}{\gamma}}\right] \qquad z > \mu$$

Weibull distribution (or Type III distribution)

(Eq. 5.5) $\gamma < 0$ $$F_\gamma(z) = \exp\left\{-\left[-\left(\frac{z-\mu}{\sigma}\right)^{\frac{1}{\gamma}}\right]\right\} \qquad z < \mu$$

An exhaustive treatment of the statistical theory of extreme values was given by Gumbel [92], who showed examples of applications of extreme value statistics to various fields.

Type I distribution for the largest values and Type III distribution for the smallest values are most often observed in corrosion [93].
In particular, extreme value statistics using Gumbel distribution is recommended for estimating the maximum corrosion depth and its dependence on surface area [93]. For pitting corrosion, a standardized procedure was proposed in order to analyze the maximum pit depth distribution introducing the notion of *return period*.
Gumbel cumulative function distribution, F(z), is:

(Eq. 5.6) $$F(z) = \exp\left\{-\exp\left[-\frac{(z-\mu)}{\sigma}\right]\right\}$$

where z is the maximum penetration depth, μ is the location parameter, σ (>0) the scale parameter. The probability density function is:

(Eq. 5.7) $$f(z) = \frac{1}{\sigma}\exp\left\{-\left(\frac{z-\mu}{\sigma}\right) - \exp\left[-\left(\frac{z-\mu}{\sigma}\right)\right]\right\}$$

Introducing the normalized variable y:

(Eq. 5.8) $$y = \frac{z-\mu}{\sigma}$$

Gumbel's cumulative function (Eq. 5.6) becomes:

(Eq. 5.9) $$y = -\ln\{-\ln[F(z)]\} = \frac{z-\mu}{\sigma} = \frac{1}{\sigma}z - \frac{\mu}{\sigma}$$

The cumulative probability, F(z), can be plotted as a straight line on Gumbel probability plot, obtained with values of the associated cumulative probabilities (y) scaled on the vertical axis and with maximum penetration depths (z) on horizontal axis.
The cumulative probability can be calculated simply as:

(Eq. 5.10) $$F_i(z) = 1 - \frac{i}{1+N}$$

where i is the i_{th} position of the ordered value of z, in descending order, and N is the total number of samples. The scale parameter (σ) and the location parameter (μ) can be calculated by the slope and the intercept at y=0 of the straight line in the Gumbel probability plot (y-z).
Generally, maximum penetration depth measurements are taken from specimens with a surface area (a) smaller than the area of the metallic structure (A). The ratio A/a between the surface area of the structure and the specimen defines a size factor, called return period, T, calculated as:

(Eq. 5.11) $$T = \frac{1}{1 - F(z)}$$

The normalized variable y can be correlated to T as follows:

(Eq. 5.12) $$y = -\ln\{-\ln[F(z)]\} = -\ln\left\{-\ln\left[1 - \frac{1}{T}\right]\right\}$$

Mean (M_G) and standard deviation (SD_G) of Gumbel extreme values distribution are:

(Eq. 5.13) $$M_G = \mu + \beta\sigma$$

(Eq. 5.14) $$SD_G = \sqrt{\frac{\pi^2}{6}\sigma^2} = 1.28\sigma$$

where β is the Eulero-Mascheroni constant (0.58). The maximum corrosion penetration depth (z_{max}) is calculated for a given value of the cumulative function F(z). Considering F(z) = 0.99 (equal to a return period T of 100), z_{max} becomes:

(Eq. 5.15) $$y = -\ln\{-\ln[0.99]\} = 4.6$$

(Eq. 5.16) $$z_{max} = \mu + 4.6\sigma$$

z_{max} is the maximum penetration depth (calculated by means of Gumbel statistics) for a metallic structure with surface area 100 times greater than the surface area of the specimen on which penetration depths are measured.

5.2.2 Gumbel statistics for estimating AC corrosion penetration depth

An example of penetration depth data analysis by Gumbel statistics is reported for specimens of batch C, exposed for three months to AC stationary interference. Batch C consists of seven specimens (1.5 cm^2 surface area). Specimen C6 is excluded by statistical analysis because of experimental failure during the test.

As discussed, the cumulative probability, F(z), can be plotted as a straight line on Gumbel probability plot, constructed with values of the associated cumulative probabilities y as a function of maximum penetration depths (z), accordingly to Eq. 5.9. Penetration depths are ordered from the highest to the lowest in order to calculate the cumulative probability by Eq. 5.10. Maximum penetration depth varies in the range between 8.6 and 17.2 μm (Table 5.7). Figure 5.16 shows Gumbel probability plot for batch C. The fitting curve is obtained by means of the least square method:

(Eq. 5.17) $y = mz + q = 0.27z - 2.93 \qquad R^2 = 0.96$

By the slope and the intercept at y=0 of the regression line, the scale parameter (σ) and the location parameter (μ) can be calculated (Eq. 5.9) as:

(Eq. 5.18) $\sigma = \frac{1}{m} = \frac{1}{0.27} = 3.7\ \mu m$

(Eq. 5.19) $\mu = -\sigma \cdot q = 3.7 \cdot 2.93 = 10.9\ \mu m$

Mean (M_G) and standard deviation (SD_G) of Gumbel extreme values distribution are:

(Eq. 5.20) $M_G = \mu + 0.58\sigma = 10.9 + 0.58 \cdot 3.7 = 13.0\ \mu m$

(Eq. 5.21) $SD_G = \sqrt{\frac{\pi^2}{6}\sigma^2} = 1.28\sigma = 1.28 \cdot 3.7 = 4.8\ \mu m$

The maximum corrosion penetration depth of Gumbel distribution (z_{max}), calculated for F(z) = 0.99 which corresponds to a return period of 100, is:

(Eq. 5.22) $z_{max} = \mu + 4.6\sigma = 10.9 + 4.6 \cdot 3.7 = 28.0\ \mu m$

The same mathematical procedure described for batch C was applied for other batches. Data analysis by Gumbel statistics provides four values of maximum penetration depth, from one to four months of exposition to AC stationary interference (240 A/m^2). Table 5.8 reports mean and maximum values of penetration depth from experimental results and statistical analysis.

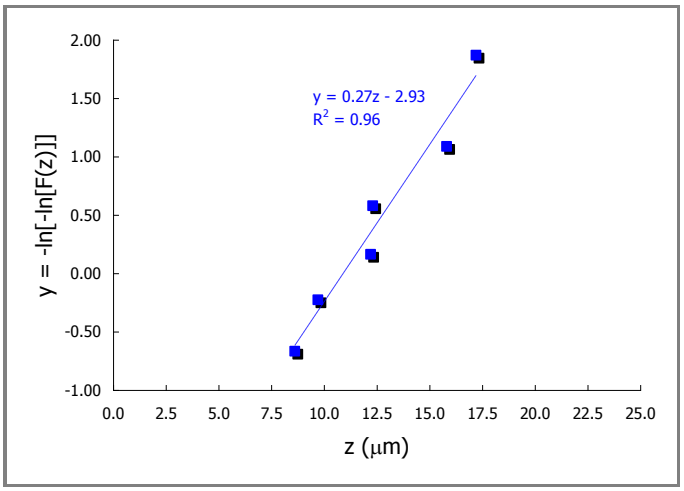

Figure 5.16 – Gumbel probability plot (batch C)

Table 5.7 – Maximum penetration depths and Gumbel cumulative probability (batch C)

Specimen	z (μm)	$F_i(z) = 1 - \frac{i}{1+N}$	$y = -\ln[-\ln[F_i(z)]]$
C5	17.2	0.8571	1.8698
C7	15.8	0.7143	1.0892
C4	12.3	0.5714	0.5805
C2	12.2	0.4286	0.1657
C3	9.7	0.2857	-0.2254
C1	8.6	0.1429	-0.6657

Table 5.8 – Mean and maximum penetration depth values (experimental and calculated by Gumbel statistics)

		Experimental		Gumbel statistics	
Batch	Time (months)	Mean (μm)	Maximum (μm)	Mean (μm)	Maximum (μm)
A	1	3.5	6.7	3.9	9.9
B	2	4.9	16.0	9.7	25.6
C	3	5.4	17.2	13.0	28.0
D	4	4.8	14.6	11.2	23.1

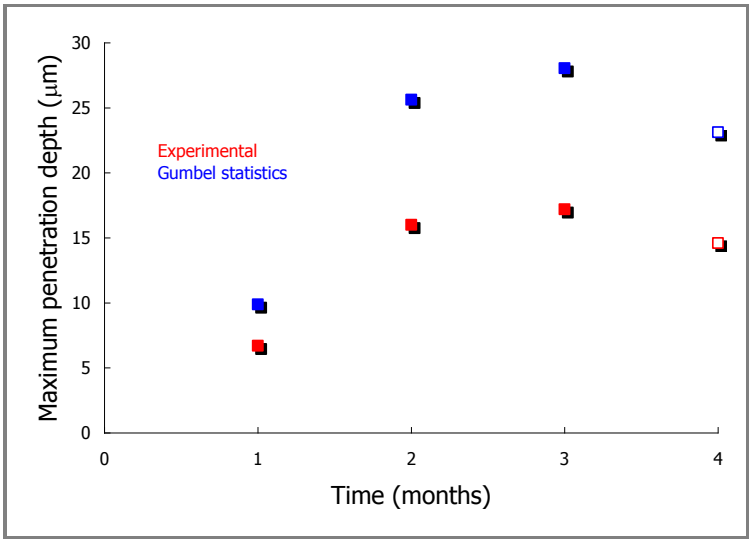

Figure 5.17 – Maximum penetration depth values (experimental and calculated by Gumbel statistics)

Maximum values calculated by Gumbel statistics are higher than experimental measurements providing a more accurate and safe approach to AC propagation study and service life prediction. Figure 5.17 compares maximum penetration depths obtained from both experimental analysis and Gumbel statistics. An odd behavior is observed for penetration depth value after four months (white markers in Figure 5.17) of AC interference which is lower than values calculated after two and three months. The trend shown in Figure 5.17 seems indicate that penetration depth increases initially and then tends to a steady value, i.e. penetration rate decreases with time.

Maximum penetration depths can be used to predict the remaining lifetime of a structure in corrosion condition due to the presence of AC interference.

Generally, in the case of localized corrosion (as AC corrosion) the limit state is defined by the perforation of the pipeline or by the achievement of a critical wall thickness reduction by the deepest corrosion attack. As discussed previously, the usual measures of variability distribution could not be sufficient to predict service (or remaining) life and extreme values analysis represents a proper and conservative analysis in order to predict corrosion lifetime. However, it could be too hazardous predicting the structure lifetime by fitting Gumbel penetration depths to a period about two orders of magnitude greater than the experimental time test. For instance, considering an expected corrosion lifetime of 30 years, a future

prediction by means of four months data is certainly too hazardous. Experimental restrictions limited experimental time to four months and a further investigation at medium-high time is forecast in order to investigate AC corrosion propagation law. However, some considerations can be pointed out.
As discussed previously, the standard guide [91] on pitting corrosion evaluation reports that corrosion penetration can be expressed in terms of a pitting factor given by the ratio of the deepest metal penetration to the average metal penetration. A penetration depth factor (P.D. factor) was calculated for penetration depths experimentally measured for every batch (Table 5.6). As discussed, with the exception of batch A (samples interfered for one month), P.D. factor assumes a stable value of about 3, i.e. the maximum penetration depth experimentally measured is three times greater than the mean penetration depth.
For comparative purpose, the P.D. factor was calculated by the ratio between the maximum penetration depth obtained by Gumbel statistics and the mean value of experimental measurements. Data are reported in Table 5.9.
The P.D. factor increases if Gumbel maximum values instead of those experimentally measured are considered. Indeed, the one calculated from experimental data doesn't take into account data variability in terms of deviation from the "most probable" extreme value. On the other hand, the one calculated from Gumbel maximum depth considers the distribution of maximum values (the extremes) and provides a more accurate statistical approach to localized corrosion.
Summarizing, if corrosion of a metallic structure is ongoing, a proper procedure should be adopted in order to evaluate corrosion propagation and to estimate the remaining lifetime of the structure, defined by a critical limit state. As discussed, extreme values statistics analysis could be helpful in the case of AC corrosion, being localized.
For new structures, the use of coupon test stations (CTS) is recommended. CTS are usually made of a steel plate with a known bare surface area in order to simulate a coating defect. They are buried close to the pipeline and connected to it through a test post. Generally, these coupons can either be used for measuring and/or for verifying local protection conditions. In order to measure corrosion rate, electrical resistance technique could be adopted. As discussed in Paragraph 1.8.2, corrosion rate is measured by means of the electric resistance variation measurement of a steel plate due to the metal loss caused by corrosion. Thickness variation is measured in time during the lifetime of the metallic structure.
Being AC corrosion localized, thickness variation measurement is the more appropriate in order to estimate corrosion propagation. Conversely, mass loss measurement could lead to an underestimation of corrosion, i.e. low corrosion rate by mass loss could correspond to high penetration rate. CTS should be buried at the same time of pipeline installation and connected to the metallic structure.

Table 5.9 – Penetration depth factor (experimental and calculated by Gumbel statistics)

Batch	Experimental mean (μm)	P.D. factor (experimental)	P.D. factor (Gumbel)
A	3.5	1.91	2.83
B	4.9	3.27	5.22
C	5.4	3.19	5.19
D	4.8	3.04	4.81

5.3 NUMBER AND SIZE OF CORROSION ATTACKS

Corrosion attacks of each specimen were counted by means of the procedure described in Paragraph 2.3.2.7. Corrosion attacks were divided in three dimensional classes, depending on the diameter of the attack (attacks with diameter smaller than 100 μm weren't considered):
- Class 1: 100 μm < d < 200 μm
- Class 2: 200 μm < d < 400 μm
- Class 3: d > 400 μm

Corrosion attacks were also divided in central or border attacks. In border attacks, the border line of corrosion attack is partially enclosed in the metal, due to the presence of the metal-resin interface. In central attacks, instead, the border line is completely included on the metal surface. Figure 5.18 reports the number of central attacks for unit area of carbon steel specimens of batches A, B, C and D, calculated as the mean of corrosion attacks number of each specimen. As expected, the number of corrosion attacks increases by increasing the time of exposure to AC interference (blue bars in Figure 5.18).
After one month (batch A) Class 1 attacks density is 26/cm^2. No attacks with diameter greater than 400 μm are observed. The number of Class 1 attacks grows with time up to 234/cm^2 after four months of interference. While new attacks appear by increasing the exposition time to AC interference indicating new corrosion initiation points on the metal surface, the attacks already formed grow: for instance, the amount of Class 2 attacks grows up to 38/cm^2 after three months of exposure, about one order of magnitude greater than Class 2 corrosion attacks after one month interference.
As for penetration depth measurements (Paragraph 5.2.2), an odd behavior is observed after four months (batch D): while Class 1 attacks number increases from 188 to 234/cm^2, the number of Class 2 and Class 3 attacks decreases compared to that measured after three months. It should be pointed out that protection and interference conditions are the same in each batch; nevertheless, such disagreement could be explained with the stochastic aspect associated to localized corrosion in its occurrence.
AC corrosion attacks were observed also corresponding to the interface between the metal and the resin, which acts as a polymer coating of a buried pipeline and creates a boundary line that's could promote corrosion initiation. Generally, localized corrosion initiation (as chlorides-induced corrosion) is favored by non-uniformities in the metal, in the environment or in the assembly between the metal and a different material (metallic or not). The number of border attacks wasn't determined for experimental restrictions due to the impossibility to identify clearly small point-shaped border attacks that tends with time to coalesce with the formation of clusters.
As discussed in Paragraph 5.1, AC corrosion starts preferably corresponding to discontinuities as the border line between the metal and the resin; then, corrosion propagates and corrosion attacks becomes more deep and extended on the metal surface.

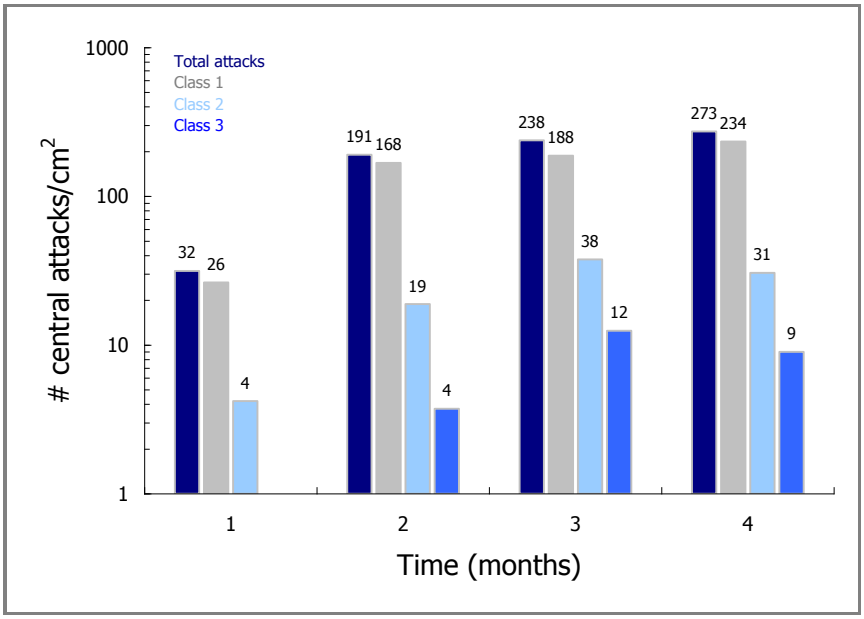

Figure 5.18 – Corrosion attacks number as a function of AC interference time

5.4 AC EFFECT ON MAGNESIUM ANODE CONSUMPTION

As discussed in Paragraph 2.3.2, experimental tests were carried out on carbon steel specimens, grade API 5L X52, cathodically protected by means of a galvanic magnesium alloy, grade AZ63D (UNS M11636) in order to investigate AC effect on corrosion propagation.
AC corrosion morphology and propagation was discussed previously. In this section, particular attention is focused on the effect of AC on the anodic consumption of the magnesium alloy used as galvanic anode in soil-simulating environment. The interest on this aspect is strictly related to the design of a CP system which must take into account the anodic consumption in order to assure protection against corrosion for all the designed lifetime of the structure. Two parameters, working potential and capacity, determine CP performance of a galvanic anode. The working potential determines the driving voltage and anode current output; the capacity, that is the charge per unit mass, defines anodic consumption and therefore the mass necessary to ensure protection for the entire service life of the structure.
Magnesium alloy anode was interfered by the same AC supplied to carbon steel specimens by means of the electrical circuit shown in Figure 2.24. However, while this interference current corresponds to 240 A/m^2 on carbon steel specimen, AC density on magnesium alloy is equal to 13 A/m^2, due to the different surface area. Indeed, anodes were over-sized to take into account the increase of the anodic consumption in the presence of AC interference measured in the first phase of the research [63]. The aim of this test is to confirm previous results and to provide a better understanding of AC effect on anodic behavior.
Anodic consumption was evaluated by means of mass loss measurement (accuracy ±0.1 mg). The metal mass loss of the anode is proportional to the charge it supplies to the cathode and is given by Faraday's law. Figure 5.19 to Figure 5.22 show metal loss rate expressed in mdd (mg/dm^2·day) for anodes of batches A, B, C and D, respectively. Table 5.10 reports mean value and standard deviation of corrosion rate data.
In the presence of 13 A/m^2 AC stationary interference, anodic metal loss increases with respect to the reference condition with zero AC. Obviously, a metal loss is measured even in the absence of AC interference, due to the galvanic coupling current that magnesium supplies to steel, which is electrochemically more noble. For control specimens (absence of AC), corrosion rate (CR_0) is in the range between 10 and 18 mdd. Generally, magnesium anode efficiency is not higher than 50% [2]. Experimental anode efficiency in the absence of AC interference was calculated as follows:

$$\eta_0 = 100 \cdot \frac{CR_{th}}{CR_0} \qquad \text{(Eq. 5.23)}$$

where CR_0 is the practical corrosion rate experimentally measured and CR_{th} is the theoretical corrosion rate, considering an anode efficiency of 100%, given by:

$$CR_{th} = \frac{C_{a,th} \cdot I_{CP,mean}}{S_a} \qquad \text{(Eq. 5.24)}$$

where $C_{a,th}$ is the theoretical anodic consumption (4 kg/Ay, as indicated by the electrochemical properties of the commercial magnesium alloy used), $I_{CP,mean}$ is the mean CP current supplied by the anode and S_a is the anodic surface area (0.28 dm^2).
$I_{CP,mean}$ was monitored during the test and data are reported in Table 5.11 with practical efficiency values in the absence of AC, calculated by Eq. 5.23. Experimental anode efficiency is about 30%, except for the anode of batch D which efficiency is 52%.
Corrosion rate increases of about one order of magnitude in the presence of AC: corrosion rate grows up to 169 mdd for batch D (Table 5.10). For all the interfered specimens, corrosion rate (CR_{AC}) is greater than the one measured in the absence of AC interference.

Nevertheless, strong corrosion rate data variability is observed, especially for batch C and batch D which show the highest standard deviation. For batch C (Figure 5.21), corrosion rate is in the range between 80 mdd (specimen C4) and 241 mdd (specimen C1).
Figure 5.23 show digital camera images of one anode for each batch after one to four months of AC interference. Images of anodes in the reference condition (only CP without AC) are also reported.

AC interference causes a strong increase of metal loss of the tested magnesium alloy. This could be due to two effects:

1. the increase of CP current density in the presence of AC interference;
2. the decrease of magnesium anode efficiency in the presence of AC interference.

In the following, these effects will be discussed separately.

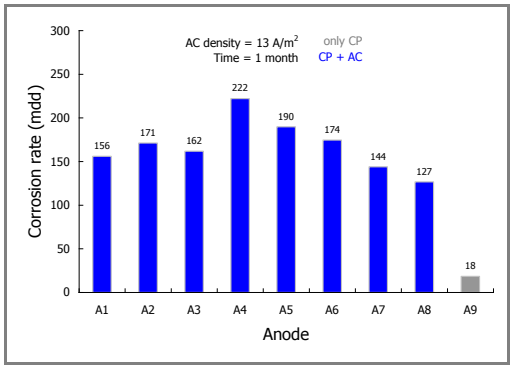

Figure 5.19 – Experimental mass loss rate of magnesium anodes (batch A)

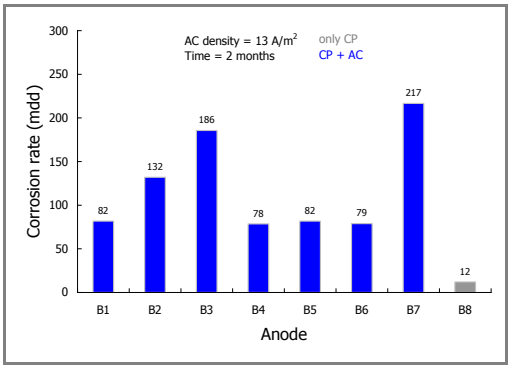

Figure 5.20 – Experimental mass loss rate of magnesium anodes (batch B)

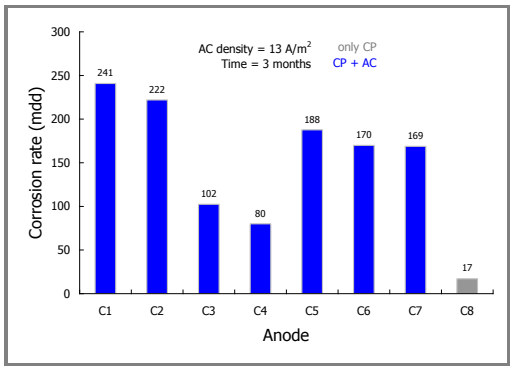

Figure 5.21 – Experimental mass loss rate of magnesium anodes (batch C)

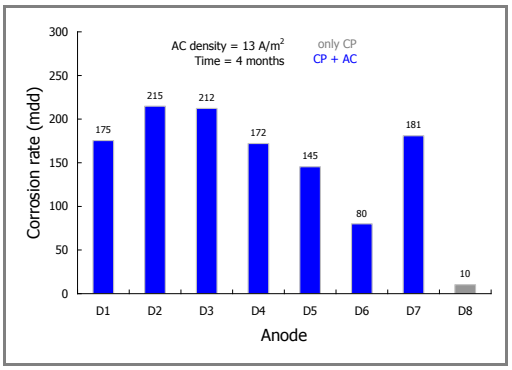

Figure 5.22 – Experimental mass loss rate of magnesium anodes (batch D)

Table 5.10 – Anodic corrosion rate by mass loss measurements

Batch	Time (months)	Corrosion rate (mdd)	
		Only CP (CR_0)	CP + 13 A/m^2 AC (CR_{AC})
A	1	18	168 ± 29
B	2	12	122 ± 58
C	3	17	167 ± 59
D	4	10	169 ± 46

Table 5.11 – Practical anode efficiency by experimental tests (no AC interference)

Batch	CP current density (mA/m^2)	η_0 (%)
A	53	31
B	40	36
C	48	31
D	49	52

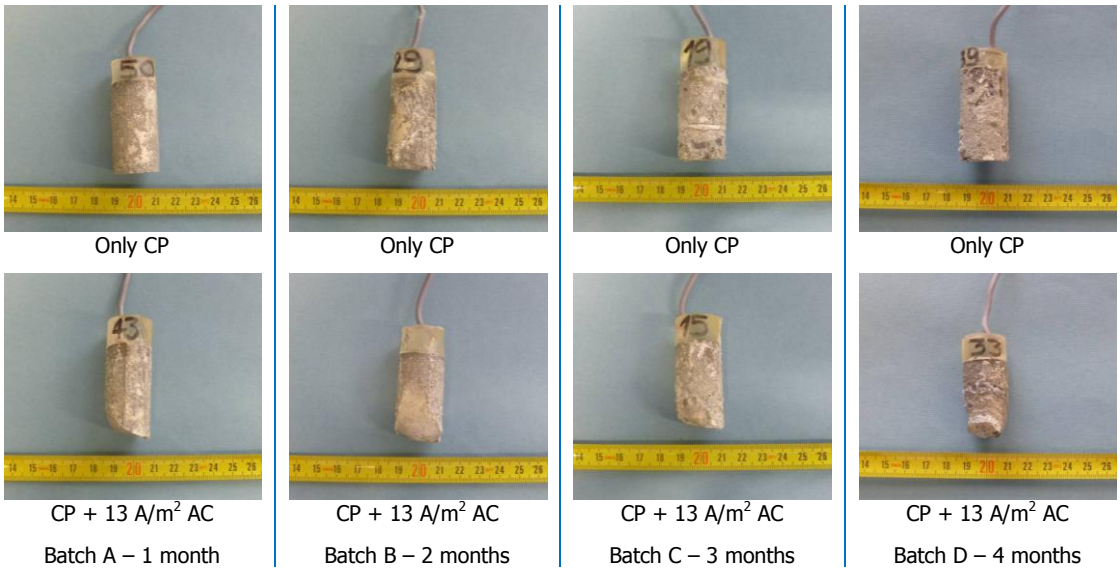

Figure 5.23 - Digital camera images of anodes after one to four months of AC interference compared with the reference condition

5.4.1 Anodic consumption: AC effect on CP current density

As discussed in Paragraph 3.2, CP current density increases by increasing AC density. As a result, the anodic consumption increases, accordingly to Faraday's law. At a first analysis, the experimental increase of anodic consumption (Table 5.10) could be explained by means of the higher CP current density supplied by the anode in order to protect steel from corrosion.
A dummy corrosion rate (CR^*) can be calculated considering the increase of CP current density as the only effect due to the presence of AC interference. Anodic efficiency in the presence of AC interference is considered equal to the efficiency calculated by experimental data for the reference condition (Table 5.11):

(Eq. 5.25) $$CR^* = \frac{\left(C_{a,th} / \eta_0\right) \cdot I_{CP,mean}}{S_a}$$

Figure 5.24 shows mass loss rate calculated by Eq. 5.25 as a function of the corresponding CP current density measured during the interference period at 13 A/m^2 on magnesium anodes (Table 5.12). Data are compared with anodic mass loss rate experimentally measured (CR_{AC}) and with the anodic mass loss rate in the absence of AC interference (CR_0).
Mass loss rates calculated assuming higher CP current densities are almost twice the mass loss experimentally measured for magnesium anodes in the absence of AC (Table 5.12). Nevertheless, even though the increase of CP current density leads to an increase of anodic consumption, it doesn't play the main role because of the strong difference between CR_{AC} and CR^*. Indeed, experimental corrosion rate (from 122 to 169 mdd, Table 5.10) is about four times greater compared to the corrosion rate calculated assuming the only effect of AC on CP current density (from 23 to 48 mdd).

Summarizing, AC interference affects the anodic consumption, causing an increase due to the higher cathodic current supplied by the anode in the presence of AC. Nevertheless, this contribution alone cannot explain the strong increase of anodic mass loss in the presence of AC interference.

Table 5.12 – Effect of CP current density (i_{CP}) increase on anodic corrosion rate

Batch	No AC interference (only CP)		13 A/m² AC density (CP + AC)		
	i_{CP} (mA/m²)	CR_0 (mdd)	i_{CP} (mA/m²)	CR^* (mdd)	CR_{AC} (mdd)
A	53	18	138 ± 4	48 ± 1	168 ± 29
B	40	12	115 ± 17	34 ± 5	122 ± 58
C	48	17	111 ± 13	39 ± 5	167 ± 59
D	49	10	108 ± 10	23 ± 2	169 ± 46

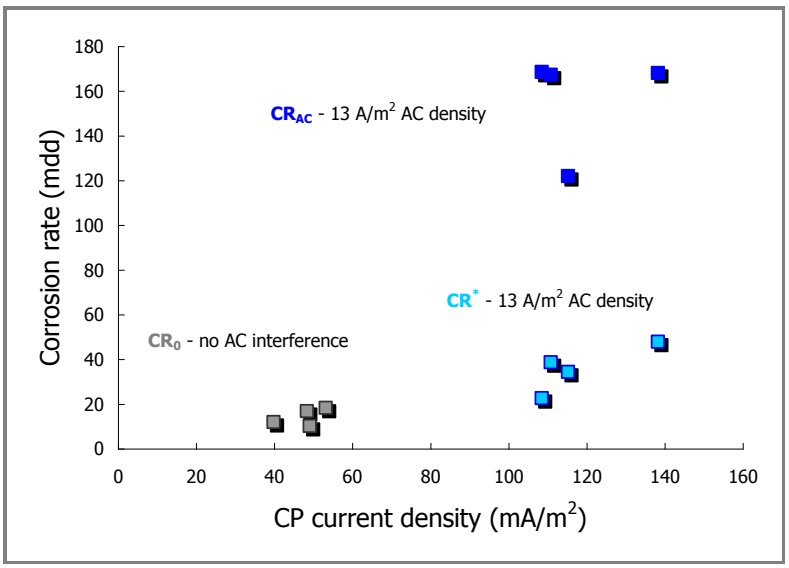

Figure 5.24 – Anodic corrosion rate: effect of CP and AC current density

5.4.2 Anodic consumption: AC effect on anodic efficiency

As discussed in Paragraph 5.4.1, the only effect of AC on CP current density cannot explain the experimental anodic mass loss. Hence, a detrimental effect of AC interference on anodic efficiency should be considered. Magnesium efficiency is related to magnesium self-corrosion in the environment in which is placed. In soil, efficiency is not higher than 50%, due to soil corrosiveness, regardless the presence of CP. Magnesium efficiency was calculated by the ratio between theoretical (Eq. 5.24) and experimental corrosion rate (CR_{AC}):

(Eq. 5.26) $$\eta_{AC} = 100 \cdot \frac{CR_{th}}{CR_{AC}}$$

where terms have the same meaning described previously. Magnesium alloy efficiency (Table 5.13) in the presence of 13 A/m² AC density is in the range between 7% and 10%. Conversely, in the absence of AC interference efficiency is always higher than 31%.
This means that anode self-corrosion increases in the presence of AC interference. The efficiency drop in the presence of AC interference could be explained considering polarization curves on the magnesium alloy, discussed in Paragraph 3.3 concerning the effect of AC on CP potential and current density. Figure 5.25 shows anodic and cathodic polarization curves obtained in the absence of AC and with 13 A/m² AC density to the metal.

Table 5.13 – Effect of AC on anodic efficiency

Batch	η_0 (%)	η_{AC} (%)	η_0/η_{AC}
A	31	9	3.4
B	36	10	3.6
C	31	7	4.3
D	52	7	7.4

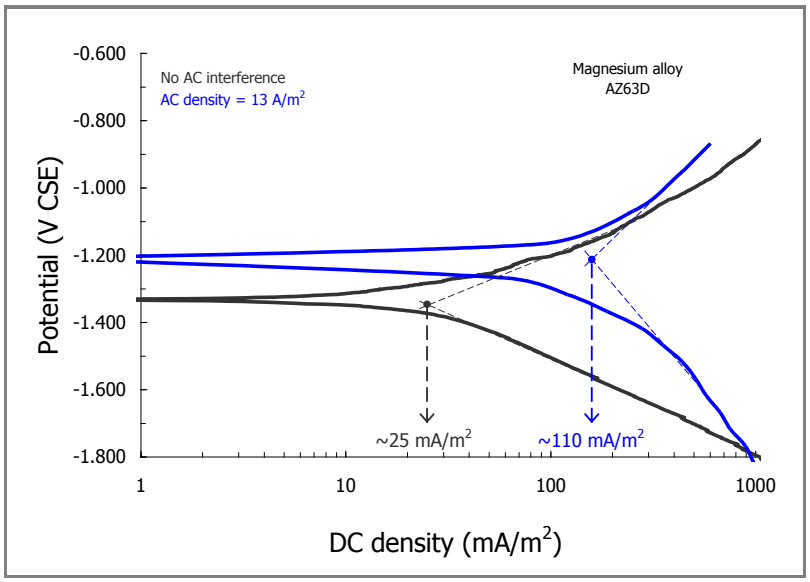

Figure 5.25 – Effect of AC interference on anodic and cathodic polarization curves

Corrosion potential and current density can be estimated by the intersection of the dotted lines that correspond to anodic and cathodic Tafel curves (Figure 5.25). The intersection point identifies the working point of the system, in which anodic and cathodic current are equal to the corrosion current.
In the absence of AC interference, corrosion current is about 25 mA/m^2. In the presence of 13 A/m^2 AC density, current density increases to about 110 mA/m^2. Faraday's law provides corrosion rate (CR, mm/y) from corrosion current density:

$$\text{(Eq. 5.27)} \quad CR = K \cdot \frac{i_{cor}}{\rho} \cdot EW$$

where K is a constant ($3.27 \cdot 10^{-3}$ mm·g/μA·cm·y), i_{cor} is the corrosion current in μA/cm^2, ρ is the metal density (1.74 g/cm^3) and EW is the adimensional equivalent weight (12.15). In the absence of AC, corrosion current density is about 25 mA/m^2 which corresponds to a corrosion rate of 57 μm/y, or 2.7 mdd. In the presence of 13 A/m^2 AC density, corrosion current density is about 110 mA/m^2 which corresponds to a corrosion rate of 251 mm/y, or 12 mdd.
By polarization curves extrapolation, in the presence of 13 A/m^2 AC density magnesium corrosion rate increases of about four times with respect to the no-AC condition. As shown in Table 5.13, the same ratio was calculated between anodic efficiency in the absence of AC interference and with 13 A/m^2 AC (η_0/η_{AC}).

Summarizing, AC has a harmful effect on magnesium anodic consumption, due to the increase of CP current density and to the strong decrease of anodic efficiency. The second effect plays the main role to increase anodic consumption.

5.5 SUMMARY

Experimental tests were carried out in soil-simulating environment on carbon steel specimens cathodically protected by means of galvanic magnesium anodes in the presence of 240 A/m^2 AC stationary interference. Penetration depth measurements were carried out in order to evaluate corrosion propagation in time (from one to four months).
AC corrosion morphology is localized. Corrosion penetration depth and corrosion attacks number increase with time. Extreme value statistics was applied to experimental penetration

depth data. Even if a service life prediction could be too hazardous, the Gumbel statistics provides a safe approach in order to assess corrosion risk, due to the localized nature of AC corrosion. Corrosion products are quite complex and characterized by the formation of agglomerate of sand and corrosion products that cover the sample. Moreover, AC has a harmful effect on magnesium anode consumption, due to the increase of CP current density and to the strong decrease of anodic efficiency. The second effect plays the main role to increase anodic consumption.

Conclusions

This work is part of a project of the research group PoliLaPP ("Laboratorio di Corrosione dei Materiali Pietro Pedeferri") of Politecnico di Milano which deals with the study of the effects of AC interference on corrosion of steel in cathodic protection (CP) condition.
The first phase of the research started in 2002 and was focused mainly on the set-up of a proper instrumentation in order to measure and to apply separately DC and AC signal, on the individuation of critical parameters of AC corrosion and on CP criteria assessment in the presence of AC. The second phase of the research is currently ongoing and aims to propose a corrosion mechanism of carbon steel in CP condition and in the presence of AC.

In this work a proposal of AC corrosion mechanism is discussed. Moreover, the effect of AC on protection potential and protection current as well as corrosion propagation are investigated. Experimental tests were carried out in the laboratories of the research group PoliLaPP of Politecnico di Milano and, during an internship period of four months, in collaboration with the AC corrosion group of the Metallurgical and Materials Engineering Department of Colorado School of Mines (Golden, CO, USA). The main conclusions are summarized in the following.

A AC effect on protection potential and protection current density

CP criteria are generally based on the value of the structure-to-electrolyte potential. Potential measurement is therefore necessary in order to assess CP effectiveness.
Galvanostatic and potentiostatic tests were carried out on carbon steel specimens in soil simulating environment in the presence of AC stationary interference, varying protection and interference conditions.
AC effects on protection potential and protection current can be summarized as follows:

- AC shifts protection potential towards more positive values (anodic shift);
- protection current increases in the presence of AC interference;
- protection potential and current variations increase by increasing AC density and depend on electrolyte chemical composition;
- AC influence on protection potential and current could be due to the AC effect on polarization curves (E-log(i)) of carbon steel in soil simulating environment;
- in the presence of AC stationary interference, anodic and cathodic curves shift towards high polarization current. AC acts by changing anodic and cathodic overpotentials and exchange current densities. However, these effects, widely studied in the previous phase of the research, weren't investigated;
- if CP is achieved by means of a galvanic anode system (magnesium alloy anode), protection potential and current increase simultaneously due to the effect on polarization curves of both carbon steel and magnesium anode.

B AC corrosion mechanism of carbon steel in CP condition

Cathodically protected steel corrosion can occur in the presence of AC interference, even if the -0.850 V CSE criterion is matched. Overprotection (potential lower than -1.1 V CSE) seems to be the most dangerous condition with respect AC corrosion risk.

A two-steps corrosion mechanism is proposed:

1) *Step 1: the film breakdown mechanism*. AC causes the electro-mechanical breakdown of the passive film formed on the metal surface in CP condition;
2) *Step 2: high pH corrosion*. After passive film breakdown, corrosion occurs if the pH at the metal-to-electrolyte interface is close to 14.

B.1 Step 1. The film breakdown mechanism

Cathodic reactions (oxygen reduction and hydrogen evolution at low potentials) can promote the formation of a passive film on carbon steel surface, due to the alkalization of the metal-to-electrolyte interface.

The characterization of the passive film on steel in CP condition is still ongoing and further investigations on the better understanding of protection mechanism (i.e. by immunity or by passivity) are scheduled. Nevertheless, the effect of a cathodic pre-polarization on linear polarization resistance (LPR) of carbon steel specimens was investigated. LPR is about one order of magnitude greater in the presence of a cathodic pre-polarization applied to the metal. Although such measurement doesn't provide directly information about the presence of a protective film formed on the metal surface, the increase of LPR in the presence of a cathodic pre-polarization could be associated to the presence of a passive film formed on the metal during the cathodic period. Some experimental evidences from literature about passive film formation on cathodically protected carbon steel were widely discussed.

In order to study the influence of AC on passive condition, experimental tests on passive metals (as stainless steels in neutral environment and carbon steel in alkaline solution) were carried out. Tests showed that AC has an harmful effect on passive condition, reducing the critical chlorides threshold and causing a depassivation of the metal (by the increase of the passive current density and the decrease of pitting potential). AC leads to the weakening of passive condition and, over a critical AC density threshold, the local breakdown of the oxide.
The proposed model deals with the passive film breakdown due to the presence of electro-mechanical stresses within the film. Accordingly, the presence of high alternating electric field could lead to film local breakdown. Electrostriction (i.e. the deformation of a dielectric body as the result of an applied electric field that polarizes the randomly-aligned electrical domains within the material) could be a possible explanation.
Electrostriction pressure depends on the electrical properties of the passive film (by means of the dielectric constant of the oxide) and on the square of the electric field. Film cracking occurs corresponding to the achievement of a critical electric field, in the order of MV/cm. In order to estimate the alternating breakdown electric field, alternating voltage measurements were carried out on stainless steels in neutral solution and on carbon steel in CP condition. Tests showed the existence of a critical alternating voltage beyond which film breakdown occurs. The corresponding electric fields are of the same order of magnitude of electrostriction breakdown fields reported in literature (MV/cm).

The application of this model, known in the field of localized corrosion, represents an absolute novelty in the AC corrosion mechanism description. The existence of critical levels of AC interference and the localized nature of AC corrosion find good explanation considering the proposed mechanism, in terms of a mechanical analogy.

B.2 Step 2. High-pH corrosion

The electro-mechanical cracking of the passive film that covers the metal in CP condition give direct assess of the solution to the unprotected metal. After film breakdown, corrosion occurs only if the pH inside the crack becomes very high, close to 14.

pH measurements were carried out varying CP current density: the pH of the solution in close proximity to the metal increases by increasing cathodic current density, as expected. Nevertheless, even in overprotection condition, pH doesn't reach the unsafe values regarding corrosion, i.e. in ordinary operative conditions and in the absence of stray currents, corrosion of cathodically protected steel doesn't occur.
As discussed previously, the presence of AC interference causes the increase of protection current density due to an effect on the cathodic polarization curve of steel; as a consequence, the superimposition of a stationary AC interference could have the indirect effect of increasing the pH of the electrolyte in contact with the metal.
These considerations are in good agreement with experimental AC corrosion risk diagram according to which overprotection (potential lower than -1.1 V CSE) is the most dangerous condition. Overprotection is achieved by means of large cathodic currents that produce a strong alkalization of the electrolyte close to the metal. As a consequence, just a few A/m^2 AC densities can be harmful because of the effect on CP current density and pH.
Moreover, a chemical dissolution mechanism (potential-independent corrosion) can be hypothesized.

This work represents only the first phase on the investigation about AC corrosion mechanism and further tests are required in order to validate the proposed mechanism. However, this model doesn't exclude the possibility that more than one theory can describe AC corrosion phenomenon. In the near future, a critical comparison between this model and the proposed corrosion mechanisms reported in literature will be carried out.

C AC corrosion propagation

Since AC corrosion is localized, mass loss measurement is not ordinarily recommended to assess corrosion propagation because it doesn't provide information about corrosion penetration depth. Therefore, corrosion was evaluated by means of penetration depth measurements on carbon steel specimens in CP condition through a magnesium alloy anode in soil-simulating environment. Penetration depth measurements were carried out in order to evaluate corrosion propagation with time (from one to four months). Furthermore, the effect on AC of magnesium anode consumption was investigated.

Corrosion penetration depth and corrosion attacks number increase with time. Extreme value statistics was applied to experimental penetration depth data. Even if a service life prediction could be too hazardous by experimental data, Gumbel statistics provides a safe approach and is recommended in order to assess AC corrosion risk, due to its localized morphology.
Corrosion products are quite complex and are characterized by the formation of an agglomerate of sand and corrosion products that cover the sample.
AC has a harmful effect on magnesium anode consumption, due to the increase of CP current density and to the strong anodic efficiency decrease. The second effect plays the main role to increase anodic consumption.

Future works

In this work, a proposal of AC corrosion mechanism of carbon steel in cathodic protection (CP) condition is discussed. Although the model seems in good agreement with experimental data, further laboratory tests are mandatory in order to confirm the proposed mechanism. Moreover, field tests are in progress and results are expected in the near future in order to validate laboratory results.

A Laboratory tests

Some aspects related to the proposed corrosion mechanism will be investigated further by means of laboratory tests, in particular:

- the characterization of the passive film formed on steel in CP condition;
- the measurement of the film breakdown electric field;
- the high-pH corrosion mechanism.

A.1 Characterization of the passive film formed on steel in CP condition

As widely discussed, CP of carbon steel is achieved by the potential lowering from the corrosion to the immunity domain. Nevertheless, a passive film may form on metal surface due to the alkalization of the electrolyte in close proximity to the metal cathodically polarized. As discussed in Paragraph 4.3, there is scarcity of data about the effective protection mechanism achieved by CP (i.e. by immunity or by passivity). This is mainly associated to the absence of corrosion cases in ordinary CP condition, with a consequent lack of interest on this specific topic. In the near future, a more accurate analysis will be carried out in order to characterize the passive film formed on steel in CP condition, varying protection condition. The main difficulty is related to the necessity to perform in-situ analysis during CP application, in that the interruption of CP may dissolve or change passive film properties.
In this work, linear polarization resistance (LPR) measurements on steel after a cathodic pre-polarization were carried out but a proper in-situ investigation is required.

Electrochemical impedance spectroscopy (EIS) and *spectroscopic ellipsometry* (SE) techniques may be helpful for a better understanding of the real protection mechanism.
Generally, EIS provides a description of the electrochemical system by means of an electrical equivalent circuit. EIS is conducted in the frequency domain and allows separating each electrical component representing the electrochemical behavior of the metal. For instance, EIS could provide the true polarization resistance of the metal in CP condition. Indeed, LPR as measured in this work provides the algebraic sum of the polarization resistance and the solution resistance. The last one represents a source of error which could be reduced by using EIS technique.
Moreover, in order to investigate optical and electrical properties of the thin passive film, SE could be adopted. Ellipsometry uses polarized light to characterize thin films. The light undergoes a change in polarization when it interacts with the sample. Through the analysis of the polarization of the light reflected by the sample, ellipsometry can yield information about layers thinner than the wavelength of the light. Ellipsometry can probe the complex refractive index or dielectric function tensor, which gives access to fundamental physical parameters and is related to a variety of electrical and optical properties of the passive film. Furthermore, SE could be helpful in order to measure film thickness and morphology.

A.2 Film breakdown electric field measurement

In this work (Paragraph 4.4.2), breakdown electric fields were estimated by means of alternating voltage measurements. Nevertheless, a more proper experimental set-up should be adopted, in order to measure the breakdown voltage minimizing all the contribution that fake the measurement, as discussed in Paragraph 4.4.2.
An investigation of the state-of-the-art on this topic is actually ongoing. For instance, an interesting work was carried out by Qin et al. [94]. Authors studied the dielectric breakdown of iron oxides (Fe_2O_3 and Fe_3O_4) by means of scanning tunneling microscopy (STM) technique under UHV conditions by increasing the bias voltage between the sample and the STM tip under constant current mode (Figure A1). Iron oxide films formed at 300 K (27 °C) were exposed to high electric fields by increasing the bias voltage between the STM tip and the sample in constant current feedback. In these conditions, the passive film breakdown was marked by a precipitous retreat of the tip from the sample surface (Figure A2). The possibility to perform this test in AC mode will be considered and evaluated. The test conducted in AC mode could provide the breakdown voltage in order to calculate the breakdown alternating electric field considering the film thickness calculated for instance by spectroscopic ellipsometry (SE) technique (Paragraph A.1).

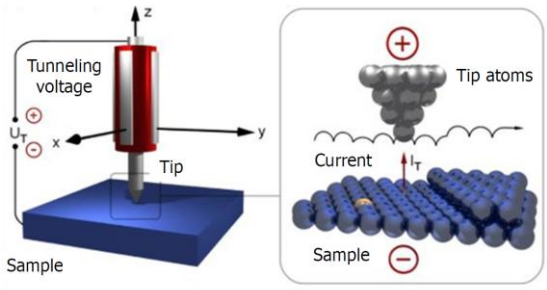

Figure A1 – Schematic representation of STM technique

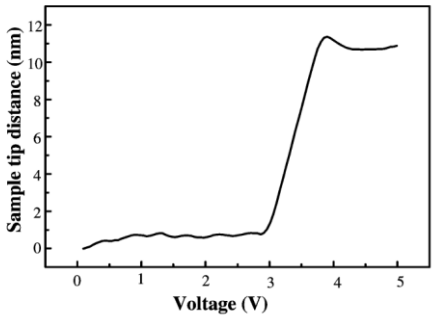

Figure A2 – Distance-voltage spectrum by STM technique for dielectric breakdown measurement of iron oxide at 300 K [94]

A.3 High-pH corrosion mechanism

High-pH corrosion mechanism of carbon steel in CP condition and in the presence of AC interference will be more investigated in order to identify anodic and cathodic reactions involved in the process. Paragraph 4.5 reports corrosion reactions, as indicated by iron potential-pH diagram. Nevertheless, depending on thermodynamic stability of ionic species, two equilibrium iron-water equilibrium diagrams should be considered (Figure 4.40 and Figure 4.41). The diagrams differ because of the "shape" of the high-pH corrosion domain. In particular, iron chemical dissolution (potential-independent corrosion) could represent a possible corrosion mechanism.
Experimental tests are scheduled but haven't yet been designed. Electrochemical tests, as EIS and voltammetry, could be taken into account. Tests will be performed on carbon steel specimens varying the pH of solution and protection potential in aerated o de-aerated condition.

B Field tests

From November 2008, field tests on carbon steel specimens in free corrosion and in CP condition are in progress in collaboration with the Experimental Institute of RFI (Rete Ferroviaria Italiana, Gruppo Ferrovie dello Stato Italiane Spa [8]).

Specimens were installed in an area located in correspondence to the km 91 of the Rome-Naples section of the high-speed Italian railway line (Rete Alta Velocità-Alta Capacità, AV/AC), that links Milan to Naples. The Italian AV/AC railway line uses a 2x25 kV AC electrification system at 50 Hz frequency. The power system is connected directly to the national grid at 380 kV; power substations are connected each other with the first and the last substation connected to two central national grids at 380 kV by means of a set of dedicate transformers that reduce the voltage to 150 or 132 kV (depending on the Italian geographic area). Electrical substations reduce AC voltage by means of transformers with the primary at 150 or 132 kV and the secondary connected to two terminals at +25 kV (contact line) and -25 kV (feeder). The resulting system is the so-called 2x25 kV–50 Hz AC electrical system.

Carbon steel specimens simulate coating defects of a buried pipeline that runs parallel to the high-speed railway line.
Three coating defect dimensions were adopted: 1 mm^2, 1 cm^2 and 10 cm^2 (Figure B1) to obtain different AC densities in the presence of AC interference current spreads by rails or induced by overhead high voltage line. Specimens were buried according to the electrical sketch reported in Figure B2 in order to reproduce the following conditions:

- free corrosion condition in the presence of AC interference;
- CP condition through a magnesium anode in the presence of AC interference;
- free corrosion and CP condition in the absence of AC interference (control tests).

It should be pointed out that field test interference condition differs from that reproduced in laboratory. Indeed, in field tests AC interference takes place only during the transit of the train (about every 15 minutes) and has a limited duration (non-stationary interference).

Potential and current are periodically monitored. Preliminary monitoring results are described elsewhere [95]. Actually, the maximum AC density on specimens with the smallest exposed area is not higher than 15 A/m^2, as Figure B3 reports. This value is lower than the expected one and this could be due to the too short parallelism between the high-speed railway and the pipeline, simulated by means of a copper cable between the grounding conductor and specimens (Figure B2). The parallelism length was restricted to 180 m, due to dimensional limitation of the area available. Specimens will be excavated in the near future in order to probe their corrosion state.

Obviously, it could be more interesting to investigate the corrosion behavior of steel specimens in CP condition in the most critical AC corrosion condition, for instance represented by the parallelism between a pipeline and a high-voltage transmission line (HVTL), because of the high electric field induced and the presence of a stationary interference which is maintained all the time. On the other hand, nowadays AC interference is mitigated in practical application in order to reduce AC corrosion likelihood if AC voltages are higher than 10 V, as reported by the technical specification CEN/TS 15280:2006 [12]. Similarly, in the U.S., AC voltage threshold is mostly driven by safety considerations and the standard NACE SP0177-2007 [9] reports that a steady-state touch AC voltage of 15 V or more with respect to local earth is considered to constitute a shock hazard. As a result, due to these restrictions, the individuation of a new site in which study AC corrosion phenomena by field tests in the most dangerous conditions is still ongoing.

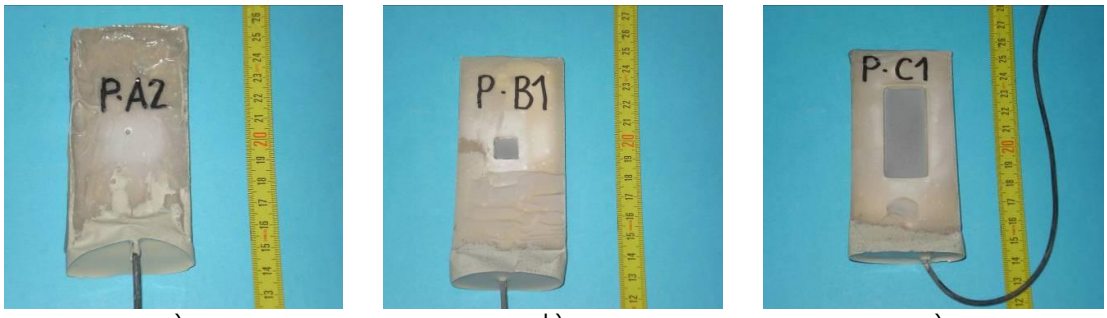

a) b) c)

Figure B1 – Carbon steel specimens installed in field tests: a) 1 mm^2, b) 1 cm^2, c) 10 cm^2

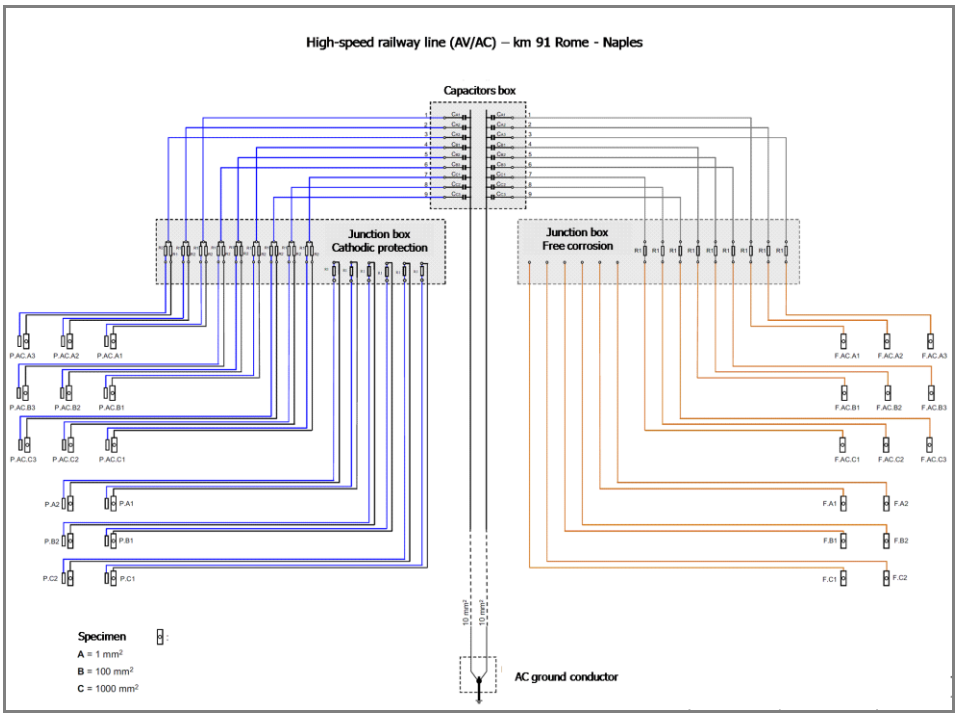

Figure B2 – Field tests: electrical circuit

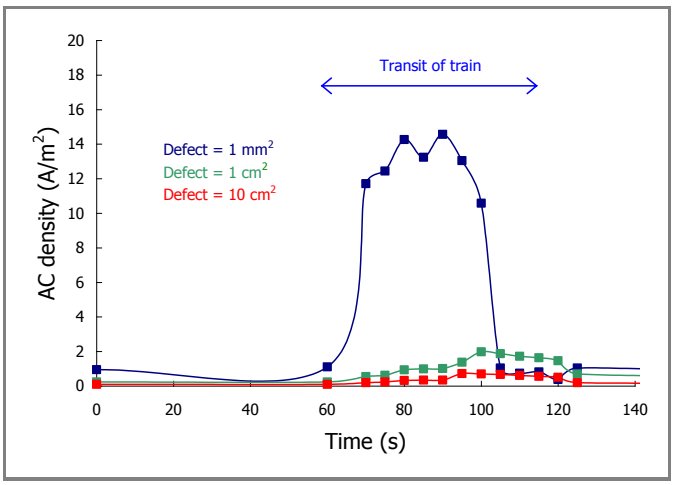

Figure B3 – Field tests: non-stationary AC interference

References

[1] L. Di Biase, "Interaction and stray-current corrosion", Shreir's Corrosion, Vol. 4, Chapter 4.22, pp. 2833-2838, ISBN: 978-0-444-52787-5, Elsevier, 2010.

[2] L. Lazzari, P. Pedeferri, "Cathodic protection", pp. 370, ISBN: 8873980201, Polipress, 2006.

[3] UNI EN 12954, "Cathodic protection of buried or immersed metallic structures - General principles and application for pipelines", UNI – Ente Nazionale Italiano di Unificazione, 2002.

[4] UNI EN 13509, "Cathodic protection measurement techniques", UNI – Ente Nazionale Italiano di Unificazione, 2004.

[5] UNI 11094, "Protezione catodica di strutture metalliche interrate – criteri generali per l'attuazione, le verifiche e i controlli ad integrazione della UNI EN 12954 anche in presenza di correnti disperse", UNI – Ente Nazionale Italiano di Unificazione, 2004.

[6] BSI BS EN 50162, "Protection against corrosion by stray current from direct current systems", BSI - British Standards Institution, 2005.

[7] NACE SP0169, "Control of external corrosion on underground or submerged metallic piping systems", NACE International Standard Practice, 2007.

[8] RFI website, "http://www.rfi.it/", RFI – Rete Ferroviaria Italiana, Gruppo Ferrovie dello Stato Italiane Spa.

[9] NACE SP0177, "Mitigation of alternating current and lightning effects on metallic structures and corrosion control systems", NACE International Standard Practice, 2007.

[10] R. D. Southey, F. P. Dawalibi, "Computer modelling of AC interference problems for the most cost-effective solutions", CORROSION/98, NACE International, San Diego, CA, USA, paper 98564, 1998.

[11] R. W. Bonds, "The effect of overhead AC power lines paralleling ductile iron pipelines", DIPRA publication, DIPRA - Ductile Iron Pipe Research Association, 1997.

[12] CEN/TS 15280, "Evaluation of a.c. corrosion likelihood of buried pipelines - Application to cathodically protected pipelines", Technical Specification, CEN - European Committee for Standardization, 2006.

[13] NACE Technical Committee Report 35110, "AC corrosion state-of-the-art: corrosion rate, mechanism, and mitigation requirements", NACE International Task Group 327 Publication, 2010.

[14] S.R. Pookote, D.T. Chin, "Effect of alternating current on the underground corrosion of steels", Materials Performance 17 (3), pp. 9-15, 1978.

[15] S. Goidanich, L. Lazzari, M. Ormellese, "AC corrosion. Part 2: parameters influencing corrosion rate", Corrosion Science 52, pp. 916-922, 2010.

[16] G. Helm, T. Helm, H. Heinzen, W. Schwenk, "Investigation of corrosion of cathodically protected steel subjected to alternating currents", 3R International 32 (5), pp. 246-249, 1993.

[17] D.T. Chin, T.W. Fu, "Corrosion by alternating current: a study of the anodic polarization of mild steel in Na_2SO_4 solution", Corrosion 35 (11), pp. 514-523, 1979.

[18] P. Carpentiers, A. Pourbaix, "Detection and assessment of AC induced corrosion", CEBELCOR publication, CEBELCOR - Belgian Centre for Corrosion Study, RT. 321, 1999.

[19] D.A. Jones, "Effect of alternating current on corrosion of low alloy and carbon steels", Corrosion 34 (12), pp. 428-433, 1978.

[20] M. Yunovich, N.G. Thompson, "AC corrosion: corrosion rate and mitigation requirements", CORROSION/2004, NACE International, New Orleans, LA, USA, paper 04206, 2004.

[21] P. Pedeferri, "Corrosione e protezione dei materiali metallici", pp. 336, ISBN: 9788873980322, Polipress, 2007.

[22] I. Ragault, "AC corrosion induced by V.H.V electrical lines on polyethylene coated steel gas pipelines", CORROSION/98, NACE International, San Diego, CA, USA, paper 98557, 1998.

[23] R.G. Wakelin, R.A. Gummow, S.M. Segall, "AC corrosion - case histories, test procedures, and mitigation", CORROSION/98, NACE International, San Diego, CA, USA, paper 98565, 1998.

[24] H. Song, Y. Kim, S. Lee, Y. Kho, Y. Park, "Competition of AC and DC current in AC corrosion under cathodic protection", CORROSION/2002, NACE International, Denver, CO, USA, paper 02117, 2002.

[25] L.V. Nielsen, F. Galsgaard, "Sensor technology for on-line monitoring of AC induced corrosion along pipelines", CORROSION/2005, NACE International, Houston, TX, USA, paper 05375, 2005.

[26] S.Z. Fernandes, S.G. Mehendale, S. Venkatachalam, "Influence of frequency of alternating current on the electrochemical dissolution of mild steel and nickel", Journal of Applied Electrochemistry 10 (5), pp. 649-654, 1980.

[27] M.L. Mateo, T. Fernandez Otero, D.J. Schiffrin, "Mechanism of enhancement of the corrosion of steel by alternating currents and electrocatalytic properties of cycled steel surfaces", Journal of Applied Electrochemistry 20 (1), pp. 26-31, 1990.

[28] W.W. Qiu, M. Pagano, G. Zhang, S.B. Lalvani, "A periodic voltage modulation effect on the corrosion of Cu-Ni alloy", Corrosion Science 37 (1), pp. 97-110, 1995.

[29] D-T. Chin, S. Venkatesh, "A study of alternating voltage modulation on the polarization of mild steel", Journal of Electrochemical Society 126 (11), pp. 1908-1913, 1979.

[30] K.V. Quang, F. Brindel, G. Laslaz, R. Buttoudin, "Pitting mechanism of aluminum in hydrochloric acid under alternating current", Journal of Electrochemical Society 130 (6), pp. 1248-1252, 1983.

[31] R.L. Ruedisueli, H.E. Hager, C.J. Sandwith, "An application of a state-of-the-art corrosion measurement system to a study of the effects of alternating current on corrosion", Corrosion 43 (6), pp. 331-338, 1987.

[32] M. Yunovich, N.G. Thompson, "AC corrosion: mechanism and proposed model", Proceedings of IPC (International Pipeline Conference), ASME (American Society of Mechanical Engineers) International, Calgary, Canada, paper IPC2004-0574, pp. 183-195, 2004.

[33] G. Camitz, C. Johansson, A. Marbe, "Alternating current corrosion on cathodically protected steel in soil - A long-term field investigation", CeoCor (Committee on the Study of Pipe Corrosion and Protection) International Congress, Bruxelles, Belgium, 2000.

[34] L.V. Nielsen, P. Cohn, "AC corrosion and electrical equivalent diagrams", CeoCor (Committee on the Study of Pipe Corrosion and Protection) International Congress, Bruxelles, Belgium, 2000.

[35] J.F. Williams, "Corrosion of metals under the influence of alternating current", Materials Protection 5 (2), pp. 52-53, 1966.

[36] P. Linhardt, G. Ball, "AC corrosion: results from laboratory investigations and from a failure analysis", CORROSION/2006, NACE International, San Diego, CA, USA, paper 06160, 2006.

[37] C.-H. Voûte, F. Stalder, "Influence of soil composition on the spread resistance and of A.C. corrosion on cathodically protected measuring probes", CeoCor (Committee on the Study of Pipe Corrosion and Protection) International Congress, Bruxelles, Belgium, 2000.

[38] L.V. Nielsen, K.V. Nielsen, B. Baumgarten, H. Breuning-Madsen, P. Cohn, H. Rosenberg, "AC-induced corrosion in pipelines: detection, characterization, and mitigation", CORROSION/2004, NACE International, New Orleans, LA, USA, paper 04211, 2004.

[39] L.V. Nielsen, "Role of alkalization in AC induced corrosion of pipelines and consequences hereof in relation to CP requirements", CORROSION/2005, NACE International, Houston, TX, USA, paper 05188, 2005.

[40] L.V. Nielsen, B. Baumgarten, P. Cohn, "On-site measurements of AC induced corrosion: effect of AC and DC parameters – A report from the Danish activities", CeoCor (Committee on the Study of Pipe Corrosion and Protection) International Congress, Dresden, Germany, 2004.

[41] S.B. Lalvani, X.A. Lin, "A theoretical approach for predicting AC-induced corrosion", Corrosion Science 36 (6), pp. 1039-1046, 1994.

[42] S.B. Lalvani, X. Lin, "A revised model for predicting corrosion of materials induced by alternating voltages", Corrosion Science 38 (10), pp. 1709-1719, 1996.

[43] H. Xiao, S.B. Lalvani, "A linear model of alternating voltage-induced corrosion", Journal of The Electrochemical Society 155 (2), pp. 69-74, 2008.

[44] U. Bertocci, "AC induced corrosion. The effect of an alternating voltage on electrodes under charge-transfer control", Corrosion 35 (5), pp. 211-215, 1979.

[45] R.W. Bosch, W.F. Bogaerts, "A theoretical study of AC-induced corrosion considering diffusion phenomena", Corrosion Science 40 (2-3), pp. 323-336, 1998.

[46] S. Goidanich, L. Lazzari, M. Ormellese, "AC corrosion - Part 1: effects on overpotentials of anodic and cathodic processes", Corrosion Science 52, pp. 491-497, 2010.

[47] Y. Hosokawa, F. Kajiyama, Y. Nakamura, "New CP criteria for elimination of the risks of AC corrosion and overprotection on cathodically protected pipelines", CORROSION/2002, NACE International, Denver, CO, USA, paper 02111, 2002.

[48] P. Carpentiers, R. Gregoor, A. Pourbaix, "AC corrosion: detection, investigations and mechanisms", EUROCORR - The European Corrosion Congress, Budapest, Hungary, paper 307, 2003.

[49] R.A. Gummow, R.G. Wakelin, S.M. Segall, "AC corrosion - A new challenge to pipeline integrity", CORROSION/98, NACE International, San Diego, CA, USA, paper 98566, 1998.

[50] L.V. Nielsen, K.V. Nielsen, "Differential ER-technology for measuring degree of accumulated corrosion as well as instant corrosion rate", CORROSION/2003, NACE International, San Diego, CA, USA, paper 03443, 2003.

[51] API SPEC 5L, "Specification for line pipe - FORTY-FOURTH EDITION", API - American Petroleum Institute, 2007.

[52] ASTM G1, "Standard practice for preparing, cleaning, and evaluating corrosion test specimens", ASTM International, 2003.

[53] ASTM G187, "Standard test method for measurement of soil resistivity using the two-electrode soil box method", ASTM International, 2005.

[54] UNI EN ISO 17475, "Corrosion of metals and alloys - Electrochemical test methods - Guidelines for conducting potentiostatic and potentiodynamic polarization measurements", UNI – Ente Nazionale Italiano di Unificazione, 2008.

[55] ASTM B843, "Standard specification for magnesium alloy anodes for cathodic protection", ASTM International, 2007.

[56] ASTM G59, "Standard test method for conducting potentiodynamic polarization resistance measurements", ASTM International, 1997 (R 2009).

[57] UNI EN 10088-1, "Stainless steels - Part 1: List of stainless steels", UNI – Ente Nazionale Italiano di Unificazione, 2005.

[58] CEN EN 10080, "Steel for the reinforcement of concrete - Weldable reinforcing steel - General", CEN - European Committee for Standardization, 2005.

[59] T. Reyes, D.L. Olson, S. Bhola, B. Mishra, "Study of corrosion of super martensitic stainless steel under alternating current in artificial sea water", CORROSION/2011, NACE International, Houston, TX, USA, paper 11341, 2011.

[60] A. Nysveen, H. Kulbotten, J. K. Lervik, A. H. Børnes, M. Høyer-Hansen, J.J. Bremnes, "Direct electrical heating of subsea pipelines - Technology development and operating experience", IEEE transactions on industry applications, vol. 43, No. 1, 2007.

[61] ASTM D1141, "Standard practice for the preparation of substitute ocean water", ASTM International, 1998 (R 2008).

[62] ASTM A967, "Standard specification for chemical passivation treatments for stainless steel parts", ASTM International, 2005.

[63] S. Goidanich, L. Lazzari, M. Ormellese, MP. Pedeferri, "Effect of AC on cathodic protection of carbon steel in soil simulated conditions", EUROCORR - The European Corrosion Congress, Maastricht, Netherland, proceeding on CD-Rom, 2006.

[64] F. Bolzoni, S. Goidanich, L. Lazzari, M. Ormellese, "Laboratory test results of AC interference on polarized steel", CORROSION/2003, NACE International, San Diego, CA, USA, paper 03704, 2003.

[65] Z. Ahmad, "Principles of corrosion engineering and corrosion control", pp. 656, ISBN: 9780750659246, Elsevier Ltd., 2006.

[66] F. Bolzoni, S. Goidanich, L. Lazzari, M. Ormellese, MP. Pedeferri, "Laboratory testing on the influence of alternated current on steel corrosion", CORROSION/2004, NACE International, New Orleans, LA, USA, paper 04208, 2004.

[67] S. Goidanich, L. Lazzari, M. Ormellese, MP. Pedeferri, "Influence of AC on corrosion kinetics for carbon steel, zinc and copper", CORROSION/2005, NACE International, Houston, TX, USA, paper 05189, 2005.

[68] M. Ormellese, L. Lazzari, S. Goidanich, V. Sesia, "CP criteria assessment in the presence of AC interference", CORROSION/2008, NACE International, New Orleans, LA, USA, paper 08064, 2008.

[69] M. Pourbaix, "Atlas of electrochemical equilibria in aqueous solutions", pp. 644, ISBN: 0915567989, NACE Cebelcor, 1974.

[70] M. Pourbaix, "Lectures on electrochemical corrosion", pp. 342, ISBN: 1877914916, NACE International publication, 1995.

[71] L.I. Freiman, E.G. Kuznetsova, "Model investigation of the peculiarities of the corrosion and cathodic protection of steel in the insulation defects on underground steel pipelines", Protection of Metals, Vol. 37, No. 5, pp. 484-490, 2001.

[72] M. Yunovich, L.I. Freiman, N.V. Alekseeva, "Active-passive corrosion macrocells on iron located underground", Protection of Metals, Vol. 26, No. 1, pp. 54-60, 1990.

[73] S.S. Leeds, R.A. Cottis, "An investigation into the influence of surface films on the mechanism of cathodic protection", CORROSION/2006, NACE International, San Diego, CA, USA, paper 06084, 2006.

[74] S.S. Leeds, R.A. Cottis, "The influence of cathodically generated surface films on corrosion and the currently accepted criteria for cathodic protection", CORROSION/2009, NACE International, Atlanta, GA, USA, paper 09548, 2009.

[75] B. MacDougall, M.J. Graham, "Growth and stability of passive films", in: "Corrosion mechanisms in theory and practice. Second edition, revised and expanded. Edited by P. Marcus", pp. 189-216, ISBN: 0824706668, Marcel Dekker, Inc., 2002.

[76] H. Böhni, "Localized corrosion of passive metals", in: "Uhlig's corrosion handbook. Second edition. Edited by R. Winston Revie", pp. 173-190, ISBN: 0471157775, John Wiley & Sons, Inc., 2000.

[77] H-H. Strehblow, "Mechanism of pitting corrosion", in: "Corrosion mechanisms in theory and practice. Second edition, revised and expanded. Edited by P. Marcus", pp. 243-285, ISBN: 0824706668, Marcel Dekker, Inc., 2002.

[78] Y.M. Kolotyrkin, "Pitting corrosion of metals", Corrosion, Vol. 19, No. 8, pp. 261-268, 1963.

[79] T.P. Hoar, D.C. Mears, G.P. Rothwell, "The relationships between anodic passivity, brightening and pitting", Corrosion Science 5, No. 4, pp. 279-289, 1965.

[80] K. J. Vetter, H-H. Strehblow, "Origin and form of corrosion pitting holes in the iron and theoretical implications for pitting corrosion", Journal of pharmaceutical science and mathematics, Vol. 74, No. 10, pp. 1024-1035, 1970.

[81] N. Sato, "A theory for breakdown of anodic oxide films on metals", Electrochimica Acta, Vol. 16, No. 10, pp. 1683-1692, 1971.

[82] Y. Tang, R. Ballarini, "A theoretical analysis of the breakdown of electrostrictive oxide film on metal", Journal of the Mechanics and Physics of Solids 59, pp. 178-193, 2011.

[83] J-F. Vanhumbeeck, J. Proost, "On the contribution of electrostriction to charge-induced stresses in anodic oxide films", Electrochimica Acta 53, pp. 6165-6172, 2008.

[84] Y.F. Cheng, J.L. Luo, "Electronic structure and pitting susceptibility of passive film on carbon steel", Electrochimica Acta 44, pp. 2947-2957, 1999.

[85] L. Bertolini, B. Elsener, P. Pedeferri, R.B. Polder, "Corrosion of steel in concrete. Prevention, diagnosis, repair", pp. 409, ISBN: 3527308008, Wiley-VCH, 2004.

[86] C. Alonso, C. Andrade, M. Castellote, P. Castro, "Chloride threshold values to depassivate reinforcing bars embedded in a standardized OPC mortar", Cement and Concrete Research 30, pp. 1047-1055, 2000.

[87] M.D. Tkalenko, D.A. Tkalenko, V.S. Kublanovs'kyi, "Change in the pH of solutions and the cathodic passivation of metals under the conditions of electrochemical protection in aqueous media", Materials Science, Vol. 38, No. 3, pp. 394-398, 2002.

[88] X. Chen, X.G. Li, C.W. Du, Y.F. Cheng, "Effect of cathodic protection on corrosion of pipeline steel under disbonded coating", Corrosion Science 51, pp. 2242-2245, 2009.

[89] F. Stalder, "Pipeline failures", Material Science Forum, Vol. 247, pp. 139-146, 1997.

[90] ASTM G16, "Standard guide for applying statistics to analysis of corrosion data", ASTM International, 1995 (R 2010).

[91] ASTM G46, "Standard guide for examination and evaluation of pitting corrosion", ASTM International, 1994 (R 2005).

[92] E.J. Gumbel, "Statistics of extremes", pp. 375, ISBN: 0486436047, Dover Publications, Inc., 2004 (originally published: New York Columbia University press, 1958).

[93] T. Shibata, "Corrosion probability and statistical evaluation of corrosion data", in: "Uhlig's corrosion handbook. Second edition. Edited by R. Winston Revie", pp. 367-392, ISBN: 0471157775, John Wiley & Sons, Inc., 2000.

[94] F. Qin, N.P. Magtoto, M. Garza, J.A. Kelber, "Oxide film growth on Fe(111) and scanning tunneling microscopy induced high electric field stress in Fe_2O_3/Fe(111)", Thin Solid Films 444, pp. 179-188, 2003.

[95] A. Brenna, A. Trombetta, M. Ormellese, L. Lazzari, "Effect of AC interference on corrosion and protection on carbon steel: field tests", Metallurgia Italiana, Vol. 102, No. 10, pp. 21-28, 2010.

In copertina:

"Sezione trasversale del traliccio di un elettrodotto ad alta tensione nel comune di Schlins (Austria)"
Di: Friedrich Böhringer
01 novembre 2007
Fonte: http://it.wikipedia.org/wiki/Elettrodotto

Ringrazio il gruppo di ricerca PoliLaPP del Dipartimento di Chimica, Materiali e Ingegneria Chimica ”Giulio Natta” del Politecnico di Milano con cui ho svolto la mia ricerca di dottorato, in particolare Marco e Luciano per la professionalità, la disponibilità e l’amicizia.
Ringrazio anche Max e Antonello per i preziosi consigli e per il tempo dedicatomi.

Ringrazio il prof. B. Mishra e la dott.ssa T. Reyes del “Metallurgical and Materials Engineering Department of Colorado School of Mines (Golden, CO, USA)” per l’ospitalità mostrata durante i quattro mesi trascorsi in Colorado.

Un sentito ringraziamento anche alla prof.ssa Chiara Castiglioni, Sara e Silvia del coordinamento del dottorato in Ingegneria dei Materiali del Politecnico di Milano.

Il ringraziamento più importante va a Valentina per la pazienza, il sostegno e più semplicemente perché è il mio “essere speciale”.

Grazie alla mia famiglia e a tutti gli amici.

Andrea